Improvements to the Assessment of Site-Specific Seismic Hazards

Ashly Margot Cabas Mijares

Dissertation submitted to the faculty of the Virginia Polytechnic Institute and State University in partial fulfillment of the requirements for the degree of

Doctor of Philosophy
In
Civil Engineering

Adrian Rodriguez-Marek (Chair)
Luis Fabian Bonilla
Martin C. Chapman
Russell A. Green
Roberto T. Leon

August 2nd, 2016
Blacksburg, VA

Keywords: site response analysis, amplification function, seismic hazard, attenuation of seismic waves, damping ratio

Improvements to the Assessment of Site-Specific Seismic Hazards

Ashly Margot Cabas Mijares

ABSTRACT

The understanding of the impact of site effects on ground motions is crucial for improving the assessment of seismic hazards. Site response analyses (SRA) can numerically accommodate the mechanics behind the wave propagation phenomena near the surface as well as the variability associated with the input motion and soil properties. As a result, SRA constitute a key component of the assessment of site-specific seismic hazards within the probabilistic seismic hazard analysis framework. This work focuses on limitations in SRA, namely, the definition of the elastic half-space (EHS) boundary condition, the selection of input ground motions so that they are compatible with the assumed EHS properties, and the proper consideration of near-surface attenuation effects. Input motions are commonly selected based on similarities between the shear wave velocity (V_s) at the recording station and the materials below the reference depth at the study site (among other aspects such as the intensity of the expected ground motion, distance to rupture, type of source, etc.). This traditional approach disregards the influence of the attenuation in the shallow crust and the degree to which it can alter the estimates of site response. A V_s-κ correction framework for input motions is proposed to render them compatible with the properties of the assumed EHS at the site. An ideal EHS must satisfy the conditions of linearity and homogeneity. It is usually defined at a horizon where no strong impedance contrast will be found below that depth (typically the top of bedrock). However, engineers face challenges when dealing with sites where this strong impedance contrast takes place far beyond the depth of typical V_s measurements. Case studies are presented to illustrate potential issues associated with

the selection of the EHS boundary in SRA. Additionally, the relationship between damping values as considered in geotechnical laboratory-based models, and as implied by seismological attenuation parameters measured using ground motions recorded in the field is investigated to propose alternative damping models that can match more closely the attenuation of seismic waves in the field.

Dedicated to my dear Sebastián and Celso,
and to my beloved family (Ingrid, José, Ayleen, Diana, Celso and Andrés)

AKNOWLEDGMENTS

It was the guidance of great professors and the support of my beloved family and friends what made this dissertation possible. My gratitude expands beyond these few words that cannot possibly do justice to all their contributions. First, I would like to thank my advisor, Dr. Adrian Rodriguez-Marek for being a source of inspiration and a role model, both professionally and personally. His guidance and friendship are invaluable to me and have nourished my passion for geotechnical earthquake engineering since I started pursuing my Ph.D. degree. I will be forever grateful for all the times he challenged me intellectually, and for providing me with diverse opportunities to learn. His genuine enthusiasm for research and teaching captivated me and led me to pursue a career in academia. Thanks for Tchaikovsky, the lovely stories from Bolivia and for Huracán.

I would also like to acknowledge the members of my committee for reviewing this dissertation and providing their valuable feedback. I am especially grateful for the guidance and support of Dr. Russell Green. His insightful comments during research meetings contributed greatly to this work. His thorough and well-organized lectures on soil dynamics and geotechnical earthquake engineering not only provided me with a strong academic background, but also sparked my curiosity. Our conversations always teach me something, from interesting historic facts about Terzaghi's life, to insightful assessments of geotechnical systems and theories. I am also thankful for Dr. Luis Fabian Bonilla's mentorship while I was a visiting researcher at the Institut Français des Sciences et Technologies des Transports, de l'Aménagement et des Réseaux (IFSTTAR), in Paris. His input to this work has been instrumental. Stimulating discussions with Dr. Martin Chapman also contributed ideas and direction. His lessons on strong motion seismology provided me

with tools to understand my research from different angles. Finally, feedback from Dr. Roberto Leon has broaden my perspectives on the practical applications of this work and improved the quality of this dissertation.

Additionally, I am very grateful for these years at Virginia Tech (VT) because I have had the opportunity to learn from other truly outstanding professors, such as Dr. J.M. Duncan, Dr. J.K. Mitchell, Dr. G. Filz, Dr. T. Brandon, and Dr. J. Dove. I would like to specially thank Dr. Dove for his support and everything he taught me during my first year in graduate school. Thanks are also extended to the professionals with whom I have had very interesting discussions that have ultimately improved the quality of this work: Dr. Julian Bommer, Dr. Izzat M. Idriss, Dr. Youssef Hashash, Dr. Gonzalo Montalva, Dr. Nico Kuehn, Dr. Brady Cox, Dr. Laurie Baise, Dr. Domniki Asimaki, and Dr. Albert Kottke. Likewise, the interesting discussions and guidance from the professionals I met at the IFFSTAR are truly appreciated.

The encouragement and guidance provided by Dr. Jesus M. de la Garza, Dr. Ioannis Koutromanos, Dr. Katerina Ziotopoulou, Dr. Tripp Shealy, Dr. Madeleine Flint, Dr. Jennifer Irish, and the wonderful staff of the Department of Civil Engineering at VT were also key in the completion of this dissertation. Special thanks to Sandy Simpkins and Kara Lattimer. Financial support was provided by the United States Geological Survey and the Électricité de France.

Thanks to my huge Blacksburg family, Luis Fargier, Betsy Vera, Nestor Suarez, Ana Milena Serrano, Nelie Loufakis, Polydefkis Bouratsis, Ana Elisa Valenciano, Karla Santacruz, Alex Reeb, Melis Sutman, Amber Reeb, Antonio Barbalace, Manisha Ray, Melis Brenes, Maria Elena Nieves, Pedro Bengochea, Valentina Stevenson, Kristobal

Gudenschwager, Vincent Legout, Erin and Adam Phillips, Lucy and Jody Priddy, Alfonso Rivera, Bernardo Castellanos, Lindy and Wes Cranwell, for being there for me and making my time in Blacksburg so memorable. I have inevitably failed to acknowledge all of those who have shared their friendship and support during these years. However, my gratitude does extend to all my classmates, friends, and former and current members of the geotechnical engineering program.

I would also like to thank Tina, Naira and Aliosha for making me feel a part of their wonderful family. I treasure every moment I have spent with them, and can only hope for many more in the future. Also, to Chris, Huey and Owen, for always being so kind and care about me and my family.

Finally, the words team work never had more meaning to me than during these past months. My deepest thanks go to my incredible family, for their sacrifices and their love. Without their help, this dissertation would have not been completed. Without their encouragement, I would not have found the strength to continue. I am so grateful for sharing this path with my husband and best friend Celso; it is his love what makes these adventures possible and what keeps us dreaming of many more. Lastly, I want to thank the other love of my life, Sebastián, for being my biggest motivation and for making me stronger and more determined. This dissertation is possible because of him. Everything is possible because of him.

TABLE OF CONTENTS

LIST OF FIGURES

CHAPTER 2

CHAPTER 3

CHAPTER 4

CHAPTER 5

LIST OF TABLES

CHAPTER 2

CHAPTER 3

CHAPTER 4

CHAPTER 5

CHAPTER 1

INTRODUCTION

1.1 Problem Description

Quantifying the influence of local soil conditions on the nature of earthquake damage has proven challenging. The early work of Seed and Idriss (1970), as well as observations from past earthquakes (e.g., Seed et al., 1972; Seed et al., 1987; Seed et al., 1991; Rathje et al., 2000) have led to an improved understanding of the role that site effects play on the intensity of ground shaking. Local site conditions are capable of amplifying or deamplifying ground motions in addition to changing their frequency content and duration. Advancing the understanding of these effects and the implementation of suitable modeling techniques constitute key steps towards mitigating seismic risk and creating more resilient communities.

Seismic site response analyses (SRA) can numerically accommodate the mechanics behind the seismic wave propagation phenomena near the surface, and provide a means of estimating surface motions that may directly affect the stability of structures. Typical engineering 1D SRA are conducted under the following assumptions: (a) the Earth can be modeled as a 1D structure, comprised of horizontal layers of lateral infinite extent overlying a half-space, (b) the seismic wavefield is composed of vertically propagated incident plane shear waves; under this simplifying assumption, no shear wave to compressional wave scattering can occur and general S-wave scattering is greatly simplified, (c) each layer in the model is defined by the material properties (e.g., shear

modulus, density and damping. Nonlinear stress-strain response of the materials are used to define shear modulus and damping as a function of shear strain), and (d) the seismic wavefield is assumed to be known at some point in the Earth model, which is hereafter referred to as the SRA *input motion*. In geotechnical engineering projects, the subsurface characterization of a site is limited and judgment is necessary to fully describe the site's profile and quantify its corresponding properties. Uncertain assumptions are commonly used in association with the attenuation characteristics in situ (i.e., damping) and the location of the elastic half space (EHS). Typical geotechnical damping models are developed empirically by testing different small-scale soil samples in the laboratory under dynamic loading. Hence, these procedures can only characterize intrinsic material damping and fail to capture other sources of seismic attenuation as they occur in the field (e.g., scattering effects). The EHS is a boundary condition set at the base of the profile to be modeled, and typically also the location where input ground motions are applied to. Given that geotechnical subsurface exploration techniques often stop shortly below the soil/bedrock boundary, the latter is generally used as the EHS boundary condition. However, when the EHS is placed at a depth that does not comply with the EHS assumptions (i.e., linearity and homogeneity), some site effects can end up being overlooked or simply not captured (e.g., amplification from a strong impedance contrast located deeper in the site profile) if the selected input motions do not properly reflect the bedrock conditions below the site. This is an issue for sites in Central and Eastern US (CEUS), where ground motions with the signature from characteristic deeper geologic structures are scarce.

Despite the proliferation of strong ground motion recordings worldwide, it can be hard to find recording stations with similar site properties to the assumed EHS at the study site.

Moreover, when the EHS boundary is placed at great depths in layers with high V_s (e.g., 3000 m/s for hard rocks in CEUS), the number of stations with similar characteristics is significantly reduced. Deconvolution techniques have traditionally provided a solution to the problem of predicting bedrock motions from surface recordings. However, the uncertainties in site properties as well as potential numerical issues (Kramer, 1996) impose a relevant constraint to the application of deconvolution techniques in practice.

1.2 Significance

Site-specific evaluations of site response are useful not only to define ground motions to be used in dynamic analyses of structures, but also to translate the estimated seismic hazard at the reference site (typically at rock conditions) to the surface while accounting for the response of shallow materials. The contribution of the site response also constitutes a key component of the stochastic method for simulating ground motions (Boore, 2003), along with the consideration of source and path effects. Ground motion prediction equations (GMPEs) that account for site effects parameterized by the average shear wave velocity in the top 30 m of the site (V_{s30}), can only provide average levels of site response; but their ergodic predictions could represent the actual response at a given site, if the site term was known or estimated (Stewart et al., 2014, Rodriguez-Marek et al., 2014). The predictions of the site term generally involve SRA.

The importance of properly characterizing site response is unequivocally large, but only a few studies have investigated the components of seismic attenuation that are not captured by typical geotechnical damping models used for SRA. Likewise, the degree to which the placement of the EHS boundary condition at a geologic unit that does not comply with the

EHS hypotheses introduces errors in the estimation of the site response has received rather limited attention to date. Finally, in spite of previous efforts to address the variability resulting from traditional input motion selection protocols, simple procedures that expand the catalog of earthquakes that can be used in SRA (such that compatibility with the EHS properties is ensured) are currently not available.

1.3 Research Objectives

The overarching goal of this research is to improve the assessment of site-specific seismic hazards by accounting for fundamental limitations in 1D SRA; particularly regarding alternative damping models that match the observed attenuation in the field more closely, and the definition of an appropriate EHS boundary condition and compatible input motions with its V_S profile and attenuation characteristics. In summary, the specific research objectives of this dissertation include:

1. Propose alternative damping models that combine typical geotechnical models with seismological attenuation descriptors.
2. Provide guidelines on the selection of appropriate EHS boundary conditions when conducting SRA at sites without a clear, shallow impedance contrast.
3. Develop simple but robust correction factors to render input ground motions compatible with the characteristics of the assumed EHS.

1.4 Organization of Dissertation

This dissertation consists of six chapters. The first chapter defines the need for improvements in the characterization of site response and describes the broader impacts of addressing the identified limitations in 1D SRA. The review of pertinent literature on the

topics of site response (specifically, on the EHS assumption and modeling techniques) and the attenuation of seismic waves (particularly, a concise background on seismological attenuation descriptors) is provided in Chapter Two.

Chapters Three, Four and Five are self-contained chapters that have been or will be submitted for publication in scholarly journals. Chapter Three will be submitted to the Bulletin of the Seismological Society of America, Chapter Four will be submitted to the Journal of Geotechnical and Geoenvironmental Engineering while Chapter Five is under review in Earthquake Spectra. Collectively, these chapters will serve as improvements towards a more rigorous and consistent assessment of site-specific seismic hazards:

Chapter Three – Cabas, A., Rodriguez-Marek, A., and Bonilla, L. F., (*to be submitted*), Estimation of Kappa (κ)-consistent Damping Values at KiK-net sites to Assess the Discrepancy between Laboratory-based Damping Models and Observed Attenuation (of seismic waves) in the Field, *Bulletin of the Seismological Society of America*.

Chapter Four – Cabas, A., Rodriguez-Marek, A. and Green, R. (*to be submitted*), The Importance of the Selection of the Elastic Half-Space in Site Response Analysis, *Journal of Geotechnical and Geoenvironmental Engineering.*

Chapter Five – Cabas, A. and Rodriguez-Marek, A. (*under review*), V_S-κ Correction Factors for Input Ground Motions used in Seismic Site Response Analysis, *Earthquake Spectra*.

Chapter Six presents a summary of the findings and a discussion of insights derived from this work. Recommendations for future research are also provided.

References

Boore, D., (2003). Simulation of Ground Motion Using the Stochastic Method, *Pure and Applied Geophysics* **160**(3-4), 635-676.

Kramer, S., (1996). *Geotechnical Earthquake Engineering*, Prentice Hall, Upper Saddle River, NJ.

Rathje, E.M., Idriss, I.M., and Somerville, P., (2000). Strong ground motion and site effects, *Earthquake Spectra* Special Volume on 1999 Kocaeli, Turkey, earthquake.

Rodriguez-Marek, A., Rathje, E. M., Bommer, J. J., Scherbaum, F., and Stafford, P. J., (2014). Application of Single-Station Sigma and Site-Response Characterization in a Probabilistic Seismic-Hazard Analysis for a New Nuclear Site. *Bull. Seism. Soc. Am.*, **104**, (4), doi: 10.1785/0120130196

Seed, H.B., and Idriss, I.M., (1970). *Soil Moduli and Damping Factors for Dynamic Response Analyses*, Report UCB/EERC-70/10, Earthquake Engineering Research Center, University of California, Berkeley, CA.

Seed, H.B., Romo, M.P., Sun, J.I., Jaime, A., and Lysmer, J., (1987). *Relationships between Soil Conditions and Earthquake Ground Motions in Mexico City in the Earthquake of September 19, 1985*, Report UCB/EERC-87/15, Earthquake Engineering Research Center, University of California, Berkeley, CA.

Seed, H.B., Whitman, R.V., Dezfulian, H., Dobry, R., and Idriss, I.M., (1972). Soil Conditions and Building Damage in 1967 Caracas Earthquake, *Journal of the Soil Mechanics and Foundations Division*, **98**(8), 787-806.

Seed, R.B., Dickenson, S.E., and Idriss, I.M., (1991). Principal Geotechnical Aspects of the 1989 Loma Prieta earthquake, *Soils and Foundations*, **31**(1), 1-26.

Stewart, J.P., Afshari, K. and Hashash, Y.M.A., (2014). *Guidelines for Performing Hazard-Consistent One-Dimensional Ground Response Analysis for Ground Motion Prediction*. PEER Report.

CHAPTER 2

LITERATURE REVIEW

2.1 Introduction

The subject of study of this research intersects with the geosciences, geotechnical engineering and the field of engineering seismology. All these disciplines are important for the assessment of seismic hazards. Certain limitations identified in 1D SRA methods are addressed in Chapters 3, 4 and 5. Hence, a review of the main modeling assumptions implemented by two of the most commonly used approaches for modeling the propagation of shear waves from the bedrock level through shallower deposits to the ground surface is provided in this chapter. A comparison of these approaches is not only relevant to the specific research objectives of this study, but also timely, given that recent seismic hazard studies have explored how conservative equivalent-linear (EQL) site response estimations are, relative to methods that account fully for the nonlinear dynamic behavior of soils. Analogously, the investigation of coupling models of geotechnical and seismological attenuation descriptors in Chapter 3 requires some background on the relationship among the selected parameters. Comprehensive descriptions of the origin and applications of each attenuation parameter are beyond the scope of this research work. However, relevant contributions towards that end have populated the literature recently and only a brief summary of key definitions will be provided herein.

2.2 Site Response

2.2.1 Overview

The Caracas 1967 earthquake provided some of the first demonstrations of the existence of a correlation between damaged structures and site effects. Particularly, structural damage to high buildings (10 to 12 story-high) was found to be more frequent in the municipal district of Los Palos Grandes, where alluvium soil deposits can reach up to 300 m and have V_s values lower than 500 m/s (Duval et al., 2001). Papageorgiou and Kim (1991) also commented on the pronounced effect that sedimentary deposits (e.g., sediment-filled valleys or basins such as the one in Caracas) have on the intensity of strong ground motion and provide other well-documented examples where the response of shallow sedimentary deposits has proven to be relevant.

The Mexico City 1985 earthquake (also known as the Michoacán earthquake) caused only moderate damage in the vicinity of its epicenter but extensive damage around 350 km away, in Mexico City. Recorded ground motions at different sites illustrated the relationship between local soil conditions (e.g., varying thickness of very soft clay layers) and damaging ground motions (Papageorgiou and Kim, 1991; Seed et al., 1987). Similar observations after the Loma Prieta and Kocaeli seismic events, further demonstrated how different levels of ground motion intensity are attributed to local site effects (Seed et al., 1991; Rathje et al., 2000). Even the South Napa earthquake which struck northern California on August 24, 2014, and registered on the moment magnitude scale (M_w) as M_w 6.0, is believed to have caused damage in Napa due to both directivity effects, and the presence of soft sediment deposits in the Napa valleys. According to the USGS, the river valley sediments likely contributed to the amplification of ground shaking around Napa.

More recent seismic events continue to provide evidence of the influence of local site conditions on the intensity of ground motions and structural damage. For instance, site effects (particularly, topographic effects) have been associated with the severe damage observed in the Kathmandu Valley after the Nepal (Gorkha) earthquake of April 25, 2015. Likewise, particular soil conditions (e.g., strong impedance contrast at depth) in the city of Concepción in Chile have been found to be partly responsible for the distinct response observed in recorded ground motions from the 2010 Chile (Maule) earthquake (Cabas et al., 2015).

Site effects can be estimated by means of different methodologies, from fully nonlinear models, 1D EQL models, to simpler linear approximations. Formulations for vertical propagation of horizontally polarized shear waves through horizontally layered near-surface materials are typically used in 1D SRA. All layers are assumed to have infinite lateral extent and both upward and downward propagating waves are considered in the estimation of the transfer function (TF). The constructive and destructive interference of vertically propagating seismic waves is taken into account in this type of SRA, which Boore (2013) called full resonance (FR) methods. However, actual field conditions may not allow these resonances to build over time, in which case they are considered spurious resonances (Kramer, 1996). Commonly used software such as SHAKE (Schnabel et al., 1972; Idriss and Sun 1992), STRATA (Kottke and Rathje, 2008a, b), or DEEPSOIL (Hashash et al., 2015) apply FR methods either using 1D EQL (e.g., SHAKE, STRATA, and DEEPSOIL) or fully nonlinear approaches (e.g., DEEPSOIL).

The square-root-impedance (SRI) method provides a transparent and simple alternative to estimate linear site amplifications. Unlike FR methods, the SRI approach is centered on

the influence of the impedance contrasts present in the profile under study, and it does not incorporate the effects associated with the resonance phenomena. Amplifications from either FR or the SRI methods can be misleading if an accurate model of the near-surface deposits and materials assumed to act as an elastic half-space are not used.

Joyner et al., (1981) proposed the application of ray theory (which expresses the amplitude of motion along a ray tube as a function of the seismic impedance) to the estimation of site amplification, *A*:

$$A = \left(\frac{Z_R}{\bar{Z}}\right)^{1/2} = \left(\frac{\rho_R * V_R}{\bar{\rho} * \bar{V}}\right)^{1/2} \quad (1)$$

where Z_R refers to the seismic impedance (i.e., the product of the density and seismic wave propagation velocity of the medium) at the reference rock, while $\bar{Z}$ is the average seismic impedance. The variables ρ_R and V_R are the density and the V_s at a reference depth, while $\bar{\rho}$ and $\bar{V}$ refer to the average density and V_s over a certain depth. When the depth of averaging is defined as a quarter wavelength for each frequency considered in the analysis, as also proposed by Joyner et al., (1981), this method is known as the quarter-wavelength method (QWL) and the specific details regarding its implementation can be found in Boore (2003).

The main difference between FR and SRI methods is shown in Figure 1, which was reproduced after Boore (2013). The site amplifications presented correspond to a simple one-layer model for which anelastic attenuation has not been considered. The density was assumed to be constant, with a value of 2.0 g/cm^3. The amplifications are relative to the motions at the surface of an effective half space formed by removing the material above 37.5 m. The SRI method does not show the effect of resonances in the system.

The amplitude of the resonant peaks for the FR model correspond to the ratio of the impedances (Z_2 and Z_1) of the layer and the assumed EHS, whereas the SRI amplitude is given by the square root of the impedance ratio. In this case, the SRI amplifications are exactly equal to the root mean square of the FR linear amplifications for frequencies greater than 1 Hz, which is the fundamental resonant frequency of the one-layer profile considered in Figure 1 (Boore, 2013).

2.2.2 The elastic half space

One of the fundamental decisions when conducting 1D SRA involves the determination of the depth and characteristics of the EHS. This boundary condition is usually defined at a horizon sufficiently stiff such that the assumption of linear behavior will likely hold and no strong impedance contrasts will be found below this depth. This premise is typically satisfied by the reference rock layer. However, the definition of reference rock remains a topic of debate in the literature (e.g., Cadet et al., 2010; Laurendeau et al., 2013), and its investigation is out of the scope of this study. Some characteristics associated with reference rock sites as found in scientific publications and official regulations around the world are presented in Table 1 to illustrate the heterogeneity of the concept.

The assumption of an EHS also implies that the downward propagating component of the wavefield that refracts into the half-space is never reflected upward back into the shallower layers. The amplitude of the incident wave is a function of the impedance contrast (α_z) at the interface between two adjacent layers as given by Kramer (1996):

$$\alpha_z = \frac{\rho_1 V_{s1}}{\rho_2 V_{s2}} \tag{2}$$

where ρ_1 and V_{s1} refer to the density and V_s of material 1 which is assumed to overly a different material 2 with density ρ_2 and V_s equal to V_{s2}. The incident layer is in material 2. The influence of α_z on the wave propagation phenomena is illustrated in Table 2, where the amplitude of the incident, reflected, and transmitted (or refracted) waves are presented as α_z increases from 0 to infinity. For instance, when α_z is less than 1, an incident wave can be thought of as approaching a softer material. For this case, the reflected wave will have a smaller amplitude (i.e., displacement amplitude) than the incident wave, and the transmitted wave will have a greater amplitude than the incident wave. If α_z is greater than 1 (e.g., a profile with V_s reversals, where low V_s layers are in between higher V_s layers, or simply down-going waves propagating through a profile where V_s monotonically increases with depth), the incident wave is approaching a stiffer material in which the amplitude of the transmitted wave will be lower than that of the incident wave and the amplitude of the reflected wave will also be less than the incident wave while having a change in signs (Kramer, 1996).

2.2.3 Site Response Methodologies (Equivalent-Linear versus Nonlinear Site Response Analysis)

The EQL total stress approach, as programmed in 1D SRA codes (e.g., SHAKE) has been the principal method used to evaluate the influence of local site conditions on earthquake design ground motions. However, this type of analysis has limitations. "If sediments were perfectly elastic, their response would be independent of incident-wave amplitudes. As with any real material, however, sediments begin to yield at some level of strain, and this violation of Hooke's law will give rise to a nonlinear response" (Field et al., 1998). Thus, the EQL approach although computationally easy to use and implement, should be

regarded as an approximation to the nonlinear cyclic response of soils (Hashash and Park, 2002).

Discrepancies between nonlinear (NL) and EQL SRA are typically associated with large shear strains over some depth interval within the profile (Stewart et al., 2014). Some authors have found that NL analyses are required when shear strains exceed 0.5-1.0 % (Stewart et al., 2014) while other studies suggest a smaller threshold: 0.1-0.4% (e.g., Kaklamanos et al., 2013). The EQL methods of analysis are more efficient than NL analysis, not only because of their shorter computation times but also due to the required input parameters (e.g., damping versus shear strain curves is the only damping input required for EQL SRA, whereas NL approaches need a backbone stress - shear strain curve and unloading/reloading rules). Consequently, an issue often found in practice is whether EQL analyses are sufficiently accurate or whether more comprehensive NL analyses should be used (Stewart et al., 2014).

A reasonable agreement between observed and predicted site response when using both, EQL and NL approaches in vertical arrays have been obtained by previous studies (e.g., Stewart et al., 2008; Kwok et al., 2008; Assimaki and Li 2012; and Kaklamanos et al., 2013). However, such studies were usually conducted for conditions resulting in relatively modest shear strain values (e.g., firm soils and/or low intensity ground shaking). Differences between EQL and NL ground motion predictions can be more effectively elucidated when the analyses use relatively strong motions with the potential to induce large strains (Stewart et al., 2014).

Other researchers have also provided insights on the relationships between EQL and NL SRA by comparing NL, EQL, and linear numerical evaluations of site responses with linear

empirical evaluations. For instance, Assimaki and Li (2012) found that the intensity of nonlinear effects at a given site during a specific ground motion is a function of $V_{s30,}$ the amplitude at the fundamental resonance (i.e., both of which are site parameters), and the characteristics of the incident-motion parameter (e.g., peak ground velocity). Régnier et al., (2013), using a statistical analysis of empirical data from the Kiban-Kyoshin (KiK-net) Japanese database showed that, regardless of the site, the probability that there is a significant departure from linear site response is greater than 20% for PGA values recorded at the downhole station between 30 to 75 cm/s^2.

Model differences impacting site response estimations

Time-invariant secant shear modulus (G) and damping (ξ) in each soil layer are used in EQL SRA. The EQL method assumes linear soil behavior to compute a closed form solution of the 1D differential wave equation in the frequency domain. Iterative calculations are performed so that the G and ξ used for each layer are compatible with the computed shear strain, γ. The EQL approximation can lead to errors. For example, large values of γ induced in the profile (e.g., by subjecting soft soils to strong ground shaking) produce high ξ levels which are applied over the duration of the entire ground motion; when in reality, those large values of ξ only occur during a limited time (i.e., with the arrival of the strongest S-waves) (Stewart et al., 2014).

On the other hand, the NL site response approach is framed in the time domain where an input motion is propagated through the soil column of interest such that the soil properties can vary with time as the severity of shaking changes (Kottke, 2010; Stewart et al., 2014). The latter is only possible due to time-stepping algorithms used to solve the equation of

motion, which results in a more realistic representation of the soil nonlinear dynamic behavior, especially for high-intensity input motions (Kottke, 2010).

The definition of the soil stress-strain behavior is also different within the NL SRA framework (Rodriguez-Marek, 2000). A backbone stress-strain curve and unloading/reloading rules (e.g., Masing rules) are used to define the hysteretic response of the soil subjected to cyclic loading. A commonly used backbone curve is the modified hyperbola proposed by Matasovic and Vucetic (1993), also known as the MKZ model. Nonlinear stress-strain models can be related to measured modulus reduction and damping curves (e.g., Darendeli, 2001; Menq, 2003) by converting the backbone curve (and its associated hysteresis loops at different strain levels) into equivalent G/G_{max} (where G_{max} is the maximum secant shear modulus) and ξ curves. This is typically required by NL SRA programs, such as DEEPSOIL (Hashash et al., 2015) and DMOD (Matasovic, 1992). Nonlinear fitting parameters are then chosen based on the best fit between the original and equivalent modulus reduction and damping curves (Kottke, 2010). An example is provided in Figure 2 (after Kottke, 2010) where damping curves from Darendeli (2001) model are compared with those resulting from the MKZ model. While a reasonable agreement is observed at smaller strains, the MKZ curve deviates from the empirical curve at larger strains. Kottke (2010) indicated that the cause for this common discrepancy with NL models was the shape of the modified hyperbolic stress-strain curve at large strains along with the implementation of the Masing rules to define the hysteresis loops.

DEEPSOIL, which is a site response program capable of conducting NL SRA, solves the equation of motion by means of the Newmark β method in time domain (Hashash et al., 2015). The model assumes an average acceleration within a time step which makes the

method unconditionally stable (Chopra, 2007), and beneficial for multi-degree-of-freedom systems. However, numerical errors associated with the time step of the input motion may result in errors of the high-frequency response (Hashash et al., 2015), frequency shortening (i.e., amplification peaks at high frequencies shift towards lower frequencies) and amplitude decay (Chopra, 2007).

In addition to the hysteretic damping that results from the application of Masing rules to a backbone curve, soils also have damping at very small strains, where Masing rules would predict near zero damping. Damping at low strains has been associated with viscous damping mechanisms in soils (Lanzo and Vucetic 1999). Low strain damping in NL formulations is generally modeled through Rayleigh damping formulations. Hashash and Park (2002) investigated the viscous damping formulation in NL SRA because it was found that it causes an underestimation of the site response at high frequencies for time domain methods. These authors proposed a new viscous damping formulation that represents more accurately the wave propagation for soil columns greater than 50 m thick and improves NL SRA at shorter periods. According to these authors, the use of this new formulation ensures that the computed ground motion response in time domain analysis is similar to that computed in the frequency domain when the soil behavior is linear. A frequency-independent viscous damping matrix which reduces the over-damping at high frequencies was later proposed by Phillips and Hashash (2009). A reduction factor that modifies the extended Masing loading/unloading strain–stress relationship to match measured modulus reduction and damping curves simultaneously over a wide range of shear strains was also introduced (Phillips and Hashash, 2009).

Case studies comparing EQL and NL SRA

Results from a survey conducted by Matasovic and Hashash (2012) showed that there was a consensus among practitioners regarding the conditions that required performing NL SRA (i.e., for shear strains larger than 1%). Ground motion intensity measures are typically used to evaluate the potential for soil nonlinearity (e.g., peak ground acceleration values above a certain threshold), disregarding the influence of material type on the dynamic behavior of soils. For instance, strain levels in soft soil deposits can be rather high even when subjected to low intensity ground motions (Kim et al., 2013).

Kaklamanos et al., (2013) identified critical parameters that most significantly contribute to uncertainty in estimations of site response by performing linear and EQL SRA using the KiK-Net downhole array data in Japan. Thresholds for selecting among linear, EQL and NL SRA were provided with respect to the maximum shear strain in the soil profile, the observed peak ground acceleration at the ground surface, and the predominant spectral period of the surface ground motion. The aforementioned parameters were found to be the best predictors of conditions where the site response evaluated models become inaccurate (Kaklamanos et al., 2013). The peak shear strains beyond which linear analyses become inaccurate in predicting surface pseudospectral accelerations were found to be between 0.01% and 0.1% for periods lower than 0.5 sec, whereas EQL SRA were deemed inaccurate at peak strains of approximately 0.4% within the same period range.

Kim et al., (2013) computed the ratio of spectral acceleration values resulting from EQL and NL SRA (what they referred to as Sa^{EL}/Sa^{NL}) to develop a model for quantifying the differences between both approaches (for multiple periods). Site response simulations were conducted for 510 incident motions and 24 sites. Then, regressions of Sa^{EL}/Sa^{NL} against

several ground motion and site parameters were conducted to test their predictive capabilities. The estimated strain (γ_{est}), defined as the ratio of the peak ground velocity (PGV) and V_{s30} provided the highest correlation with relative differences between Sa^{EL} and Sa^{NL}. Other important findings from this study are summarized below:

- EQL and NL results are similar for all periods for $\gamma_{est} \leq 0.1\%$. Hence, it was the proposed threshold below which soil nonlinearity can be equally represented by the EQL and NL approaches.

- EQL method can appropriately capture nonlinearity for long periods (i.e., T > 1 sec), regardless of the value of γ_{est}.

- For $\gamma_{est} > 0.4$ %, the differences between spectral accelerations from EQL and NL methods become relevant.

More recent work has replaced the outcomes from Kim et al., (2013) due to changes in now-preferred analysis protocols (i.e., Stewart et al., 2014) regarding the input motion selection process and specification of nonlinear soil properties. Kim et al. 2016 assessed the differences between EQL and NL models for a variety of site conditions and sets of input motions (i.e., using ground motions compatible with active crustal regions and stable continental regions). Site profiles and recorded ground motions from Western US (WUS) and Central and Eastern US (CEUS) were used to implement both approaches by means of the site response program DEEPSOIL (Hashash et al., 2015).

Ratios of Sa^{EL}/Sa^{NL} were also computed and plotted against the shear strain index, I_γ (i.e., same as the estimated strain, γ_{est}, defined by Kim et al., 2013) to investigate trends in the observed mismatch between EQL and NL SRA. In WUS, EQL analyses provided higher

predictions of spectral accelerations at the frequencies considered for most of the I_γ values. At lower I_γ values, the Sa^{EL}/Sa^{NL} ratios were close to the unity for all frequencies but deviated from it for I_γ>0.1%. Results corresponding to the CEUS were generally similar to the ones obtained for WUS. Another important contribution from this study is the comparison of recommendations from previous studies in terms of thresholds at which EQL SRA are no longer reliable. Other important concluding remarks from this study included the following:

- Near the resonant site frequency, EQL ordinates exceed NL due to EQL forming a stronger resonant response that is associated with the use of time-invariant soil properties.

- At high frequencies, EQL ordinates are lower than NL due to EQL overdamping. These differences are more evident for Fourier amplitudes ratios than for spectral acceleration ratios.

Recently published guidelines for performing hazard consistent SRA (Stewart et al., 2014) have also provided useful comparisons between EQL and NL site response methodologies. They presented case studies where low-to-moderate and high intensity motions were used to investigate differences in resulting spectral shapes from both types of analysis. For instance, EQL and NL spectral shapes at La Cienaga were found to be similar for an input motion that induced relatively low strains. However, spectral shapes differed significantly for the large amplitude synthetic motions. Stewart et al., (2014) noted that "for the large-strain simulation, the spectral shapes at low periods (T< ~0.2 sec) from EQL analyses are flatter and have less period-to-period fluctuations than those from NL analyses". Such flat response was deemed to be an indicator of unreliable EQL site response results, after

comparisons with spectral values provided by Campbell and Bozorgnia (2008) GMPE (See Figure 3). According to Stewart et al., (2014), the observed features of EQL analysis result from large strains being associated with high damping that is applied across the complete ground motion duration. Hence, portions of the time series and the spectrum are overdamped by the implementation of the EQL approach. Varying soil properties with time (as the strength of shaking changes) helps NL procedures overcome this issue.

Similar results were obtained by Kwok et al., (2008) in the blind prediction exercise conducted at the Turkey Flat vertical array in California. Spectral shapes resulting from EQL and NL analyses were found to be similar when using low intensity input motions. However, at stronger shaking levels and at periods below the site frequency, the spectral shapes from EQL analyses were flatter. This particular study compared six different site response programs; hence, useful insights were derived in terms of code-to-code variability. For example, they found that the results of the considered NL codes differed significantly from each other when using higher intensity input motions. More details on the reasons behind the mismatch observed for NL methods are provided in Kwok et al., (2008) and Stewart et al., (2008).

Finally, research on the difference in amplitude and phase of the transfer functions derived from EQL and NL SRA have also been conducted in recent years (e.g., Kottke, 2010). According to Kottke (2010), the instantaneous change in stiffness that occurs upon stress reversal in NL methods cause a phase incoherence and large peaks in the amplitude of the TF at high frequencies. These effects, along with the frequency shortening and amplitude decay were found to occur at frequencies exceeding 10 Hz. An increase in the amplitude of the TF at high frequencies is expected to produce larger spectral accelerations over the

same frequency range, but "the phasing of these frequencies is incoherent such that they destructively interfere with one another" (Kottke, 2010). In contrast, the computed amplitude and phase at low frequencies (<10 Hz) were found to be similar for both approaches.

2.3 Kappa

2.3.1 Early Work on the Description of the Attenuation of Seismic Waves

Seismic wave attenuation is an important topic for both, seismology and engineering. Its assessment constitutes the focus of various endeavors related to the prediction of ground motions, the differentiation of materials, and the evaluation of seismic hazards. There are four processes widely recognized to be responsible for the decrease of seismic wave amplitudes as they travel through the earth materials: geometric spreading, multipathing, scattering, and anelasticity. The latter is the only process where the kinetic energy of elastic wave motion is converted to heat due to permanent deformation of the medium (Stein and Wysession, 2003). The other processes can be thought of as elastic processes. Campbell (2010) and Ktenidou et al., (2013) also refer to the attenuation of seismic waves as a fractional loss of energy per cycle of harmonic oscillation and as the exponential decrease in wave amplitude in time or distance.

Early papers by Knopoff and MacDonald (1958) and Futtermann (1962) introduced a seismic quality factor into the wave equation to account for anelastic loss during wave propagation. The seismic quality factor, represented by Q, is a dimensionless quantity that is inversely proportional to the attenuation of elastic wave energy. The definition of Q was built upon electrical circuit theory (Knopoff, 1964; Futterman, 1962) using the following expression:

$$\frac{2\pi}{Q} = \frac{\Delta E}{E} \tag{3}$$

where E is the maximum energy stored in a certain volume during a cycle of harmonic oscillation and ΔE is the amount of energy dissipated in that same volume per cycle of harmonic excitation (Kramer, 1996; Barton, 2007; Knopoff, 1964; Futterman, 1962).

Knopoff (1964) worked with homogeneous materials in the laboratory and in the field to evaluate if the effects of anelastic attenuation were the same everywhere in the earth interior. He found "hints of a fine structure of Q in the upper mantle" envisioning the existence of other kinds of site effects that needed to be captured, perhaps by a finer discretization of Q.

The parameter Q is a dimensionless factor whose inverse represents a measure of the attenuation of seismic waves. This definition can be derived by looking into both, the expressions for the homogeneous solution of a single degree of freedom oscillator (for free vibrations):

$$x(t) = A_o e^{-\xi\omega t} sin\left(t\omega(1-\xi)^{\frac{1}{2}}\right) \tag{4}$$

where ω is the angular frequency and A_o is the amplitude of the wave when t=0, and the formulations for anelastic attenuation (i.e., dispersive wave equation) as defined by Knopoff (1964) and Futterman (1962):

$$A(\omega) = A_o e^{-\frac{\omega x}{2cQ}} \tag{5}$$

where ω is the frequency; x is the travel path length; c is the phase velocity of the wave and A_o is the wave amplitude at x=0. If we equate the terms that describe the decay of the

amplitude of the wave in each case, we obtain the widely known relationship between ξ and the Q:

$$e^{-\xi\omega t} = e^{\frac{-\omega x}{2cQ}} \tag{6}$$

Substituting the ratio of distance (x) and velocity (c) by the travel time of the wave (t):

$$-\xi\omega t = \frac{-\omega t}{2Q} \tag{7}$$

the relationship between material damping, ξ, and Q can be easily expressed by (Goodman, 1988; Silva, 1997):

$$\xi = \frac{1}{2Q} \tag{8}$$

Equations 3 and 8 are also consistent with the definition of material damping expressed in terms of the ratio between the energy dissipated per cycle and maximum stored energy per cycle (Kramer, 1996):

$$\xi = \frac{1}{4\pi}\frac{\Delta E}{E} \tag{9}$$

In addition to anelastic loss, wave scattering and geometrical spreading contribute to the observed attenuation of seismic waves with distance from the source (and travel time). The effect of anelastic loss is often very difficult to experimentally isolate from scattering effects for high frequency waves of engineering interest. Thus, measured values of Q usually reflect components of both anelastic loss and scattering. Attempts to decouple the various attenuation mechanisms in Q have been conducted (e.g., Dainty, 1981; Chapman et al., 2008) but reliable measurements of Q and their interpretation are still challenging due to the limitations of testing procedures in the laboratory and in the field. Thus, the attenuation of seismic waves is a complex phenomenon precisely because of the difficulty

in decoupling the effects of the multiple mechanisms responsible for the overall attenuation being observed or measured (Dainty, 1981; Barton, 2007; Assimaki et al., 2008).

2.3.2 The Road to κ

When developing his original stochastic method, Boore (1983) included a high-cut filter that accounted for the decay of the acceleration spectra in the higher frequencies; suggesting that the whole-path attenuation within the crust could not entirely explain the sharp decrease of the spectrum with increasing frequency (Boore, 1983; Campbell 2009; Ktenidou et al., 2013). Accordingly, besides the path attenuation term affected by Q, he added to his model the effect of f_{max}, which was the filter resulting from the attenuation near the recording site, as proposed by Hanks (1982). Even though there were other studies that suggested the high-cut filter was primarily a result of source effects (e.g., Papageorgiou and Aki, 1983), Boore indicated that his model only intended to show that the diminution of high frequency motions (D (f)) could be accounted for by a simple multiplicative filter (Boore, 2003):

$$D(f) = \left[1 + \left(\frac{f}{f_{max}}\right)^8\right]^{-\frac{1}{2}} \tag{10}$$

Additionally, in the early 1980s, κ's predecessor, t^*, was introduced by Cormier (1982) to represent the path-integrated effect of Q. Attenuation was defined based on the rate of high-frequency spectral decay above the corner frequency. The parameter t^* was derived from a similar expression to the exponential term used by Futterman (1962) and Knopoff (1964) (equation 5); but expected to represent not only intrinsic attenuation but also scattering effects:

$$t^* = \int_{path} Q^{-1}(r) V_s^{-1}(r) dr = \kappa \quad (11)$$

where V_s is the shear wave velocity and r represents the distance traveled by the waves. A few years later, Anderson and Hough (1984) and Hough and Anderson (1988) introduced the widely-used spectral decay factor κ which is equivalent to t^* in equation 11. Anderson and Hough (1984) assumed a frequency-independent seismic quality factor and defined κ as the slope of the acceleration Fourier amplitude spectrum over a subjectively chosen range of frequencies (where the decay of the spectrum can be considered linear). Thus, κ is not a material property, but an observable parameter that quantifies total path frequency dependent attenuation. The assumption of a frequency-independent Q has created a lot of controversy in the literature. However, it is not the purpose of this study to validate any of the theories that try to explain the behavior of Q over a certain range of frequencies (e.g., Knopoff, 1964; Dainty, 1981; Cormier, 1982; Anderson and Hough, 1984; Barton, 2007; Chapman et al., 2008), but to briefly present the rationale behind them.

Knopoff (1964) based his work on laboratory tests on nonmetals, metals, rocks (i.e., all relatively homogeneous seismic media) and a few field measurements. He found that a frequency independent Q was a valid assumption for most solids. On the contrary, two decades later, the scattering model developed by Dainty (1981) was able to capture the effect of the heterogeneities within the earth materials. Consequently, Dainty's model included a frequency-dependent component of Q corresponding to the scattering effects. Likewise, Cormier (1982) found a frequency dependency of Q from spectral studies of attenuation. Anderson and Hough (1984) explicitly expressed the need for their model to show consistency with other studies that indicated a potential frequency dependency of Q at the time (e.g., Dainty, 1981). Acknowledging that their analysis could not possibly allow

for the detection of a frequency dependency on Q, if any, Anderson and Hough (1984) commented on the implications of such hypothesis on their model: first, if Q were frequency dependent, their method would only account for the intrinsic or anelastic attenuation. Secondly, if only the attenuation in the shallow crust (i.e., depths not greater than five km) was found to be frequency independent, then t^* would be almost the same as κ.

More recent studies still reflect the same controversy around this topic. For instance, Barton (2007) indicated that the frequency dependency of Q can be explained by the range of scales in which the different attenuation mechanisms act upon. On the one hand, in the presence of micro cracks, joints and water saturation, the attenuation is likely to increase due to the inertial forces of the fluids in the joints and due to scattering (Barton, 2007). On the other hand, there are other researchers that believe that Q might be frequency independent for the frequency range of engineering concern (Chapman et al., 2008; Campbell, 2009).

Considering that the path term based on Q does not completely account for the observed attenuation of high frequencies (Boore, 1983, and 2003), the investigation of other parameters such as κ has become more attractive. Even though Boore (2003) included κ in his stochastic model to account for the path-independent loss of high-frequency in ground motions, he did not particularly support any of the theories that tries to explain the origins of such parameter (e.g., Papageorgiou and Aki, 1983; Hanks, 1982; Anderson and Hough, 1984). The usefulness of κ has also been found in its superior fit to strong motion data (Campbell, 2009) and because it has become a key input parameter to create and calibrate GMPEs for regions lacking a comprehensive catalog of strong ground motions. The latter

application is particularly relevant to establish theoretical constraints to extrapolations made in regions with insufficient data.

While κ can be measured directly, it cannot be interpreted without some knowledge of the velocity and Q (damping) structure, along the path between source and receiver (as expressed in equation 11). In other words, to make use of the information contained in measurements of κ, it is required to translate (actually, mathematically invert) such measurements into a velocity and Q (or damping) versus depth model of the Earth at a site of engineering interest.

2.3.3 Methodologies to Compute κ

The high-frequency decay parameter κ was first introduced by Anderson and Hough (1984) as a site and distance dependent parameter. It can be determined empirically by computing the slope of the decay portion of the Fourier amplitude spectrum (FAS) corresponding to a particular ground motion recording (Figure 4b):

$$A(f)=A_o\, e^{-\pi \kappa f} \quad for\ f > f_E \tag{12}$$

where A_o is a source-and path-dependent parameter, f_E is the frequency above which the spectral decay of log $A(f)$ versus frequency can be considered approximately linear, and κ is the spectral decay parameter. More than three decades after being introduced to the scientific community, κ has proven to be a useful parameter not only in the prediction of ground motions (e.g., used as a high-frequency filter in stochastic models for the generation of synthetic motions) but also as a key parameter to make host-to-target adjustments to ground motion prediction models (GMPEs) (Campbell, 2009; Ktenidou et al., 2014; Al

Atik et al., 2014). Comprehensive descriptions of the origins of κ and the existent methodologies to compute it can be found in Campbell (2009) and Ktenidou et al. (2014).

The parameter κ can be partitioned into a distance-independent component and a distance-dependent component. The former is known as the site-specific kappa (κ_0) and captures the attenuation of seismic waves as they travel through shallower material (Ktenidou et al., 2014):

$$\kappa_r = \kappa_0 + \kappa_R * R \quad (13)$$

where R refers to the distance from the source to the station where the ground motion was recorded, κ_R reflects the attenuation of horizontally polarized shear waves as they propagate through the crust, and κ_0 can be obtained by extrapolating the κ_r trend to zero epicentral distance (i.e., for $R = 0$). An example of the computation of κ_0 and κ_r is illustrated in Figure 4a. It allows for the visualization of the relationship between individual estimations of κ for different recordings at the same station (i.e., blue circles) and the linear regression (red line) based on equation 4 which leads to the estimation of κ_0. It is important to note that equation 3 is only valid under the assumption that the quality factor (Q), which represents regional attenuation, is frequency-independent (Anderson and Hough, 1984; Ktenidou et al., 2013).

Most current studies consider κ_0 as a parameter predominantly controlled by site conditions (i.e., surficial geology) while having variable influence from the source and the path depending on the region under study (Van Houtte et al., 2011, Ktenidou et al., 2014). Estimates of κ_0 can be further subdivided if the contributions of the near-surface materials and the base rock are considered separately in the characterization of the attenuation directly below the site. The contribution of the intrinsic material damping within the rock

mass can be represented by $\kappa_{bedrock}$, whereas the low strain hysteresis damping of the shallower strata can be denoted as $\kappa_{profile}$ (L. Al Atik, 2014, personal communication):

$$\kappa_0 = \kappa_{profile} + \kappa_{bedrock} \quad (14)$$

Other methodologies to compute κ_0 values or estimate them based on other site parameters such as V_{s30} have populated the literature recently (e.g., Silva and Darragh, 1995; Chandler et al. 2006; Drouet et al., 2010; Van Houtte et al., 2011). Consequently, as suggested by Ktenidou et al. (2014), it is necessary to understand the differences among the resulting κ_0 values from each method before using them for SRA purposes. For instance, Drouet et al. (2010) measured a site-specific (i.e., independent of distance) κ value directly on the high frequency portion (i.e., frequencies higher than 10 Hz) of a site's TF. Source-path-site inversions using weak to moderate earthquakes recorded by the French Accelerometric Network were used to estimate the TF at 76 stations. Values of κ_0 derived from this methodology are called κ_{0_TF} (Ktenidou et al., 2014). Laurendeau et al., (2013) related κ to the spectral shape of the normalized response spectrum. This method uses stochastically generated acceleration response spectra (where κ_0 is one of the point-source seismological model input parameters and is applied to the entire frequency range) coupled with the site amplification computed from the site profile. These authors computed κ_{0_RESP} as a function of the frequency corresponding to the maximum response spectral acceleration (f_{amp1}).

References

Al Atik, L., Abrahamson, N., Bommer, J., Scherbaum, F., Cotton, F., and Kuehn, N., 2010. The variability of ground-motion prediction models and its components, *Seismological Research Letters*, **81**(5), 794-801.

Anderson, J.G., and Hough, S.E., (1984). A model for the shape of the Fourier amplitude spectrum of acceleration at high frequencies, Bulletin of the Seismological Society of America **74**(5), 1969-1993.

Assimaki D., Li W., (2012). Site- and ground motion-dependent nonlinear effects in seismological model predictions, *Soil Dyn. Earthq. Eng*., **32**(1): 143–151.

Assimaki, D., Li, W., Steidl, J. H., and Tsuda, K., (2008). Site Amplification and Attenuation via Downhole Array Seismogram Inversion: A Comparative Study of the 2003 Miyaki-Oki Aftershock Sequence, *Bulletin of the Seismological Society of America*, **98**(1), 301-330.

Barton, N., (2007). *Rock Quality, Seismic Velocity, Attenuation and Anisotropy*, Taylor and Francis Group, London, UK.

Boore, D., (1983). Stochastic simulation of high-frequency ground motions based on seismological models of the radiated spectra, *Bulletin of the Seismological Society of America*, **73**(6), 1865–1894.

Boore, D., (2003). Simulation of Ground Motion Using the Stochastic Method, *Pure and Applied Geophysics*, **160**(3-4), 635-676.

Boore, D., (2013). The Uses and Limitations of the Square-Root-Impedance Method for Computing Site Amplification, *Bulletin of the Seismological Society of America*, **103**(4), 2356-2368.

Boore, D., and Joyner, W., (1997). Site amplifications for generic rock sites, *Bulletin of the Seismological Society of America*, **87**(2), 327–341.

Building Seismic Safety Council, (2000). *The 2000 NEHRP recommended provisions for new buildings and other structures: Part I (Provisions) and Part II (Commentary)*, Technical report, FEMA 368/369, Federal Emergency Management Agency, Washington, D.C.

Cabas, A., Rodriguez-Marek, A. and Montalva, G. (2015), V_s-κ Consistent Input Ground Motions for Site Response Analyses, Case Studies in Concepción and San Pedro, Chile, Proc. of the XV Pan-American Conference on Soil Mechanics and Geotechnical Engineering, Buenos Aires, Argentina, November 15-18, 2015.

Cadet, H., Bard, P.-Y., and Rodriguez-Marek, A., (2010). Defining a Standard Rock Site: Propositions based on the KiK-net Database, *Bulletin of Earthquake Engineering* **100**(1), 172-195.

Campbell K.W., Bozorgnia Y. (2008). NGA ground motion model for the geometric mean horizontal component of PGA, PGV, PGD, and 5%-damped linear elastic response spectra for periods ranging from 0.01 to 10 s, *Earthquake Spectra*, **24**(1), 139–171.

Campbell, K. W., (2010). *Proposed Site Kappa (κ0) for a Reference Hard-Rock Site in Eastern North America*, NGA-East White Paper, EQECAT, Inc. Beaverton, Oregon.

Campbell, K.W., (2009). Estimates of shear-wave Q and kappa(0) for unconsolidated and semi-consolidated sediments in eastern North America, *Bull. Seism. Soc. Am.*, **99**, 2365–2392.

Chandler, A.M., Lam, N.T.K., and Tsang, H.H., (2006). Near-surface attenuation modelling based on rock shear-wave velocity profile, *Soil Dynamics and Earthquake Engineering*, **26**(11), 1004-1014.

Chapman, M., Beale, J. N., and Catchings, R. D., (2008). Q for P waves in the Sediments of the Virginia Coastal Plain, *Bulletin of the Seismological Society of America*, **98**(4), 2022–2032.

Chopra, A.K., (2007). *Dynamics of Structures: Theory and Applications to Earthquake Engineering*. Prentice Hall, Upper Saddle River, New Jersey, third edition, 2007.

Cormier, V., (1982). The effect of attenuation on seismic body waves, *Bulletin of the Seismological Society of America,* **72**(6), S169-S200.

Dainty, A. M., (1981). A scattering model to explain seismic Q observations in the lithosphere between 1 and 30 Hz, *Geophys. Res. Lett.*, **8**, 1126–1128.

Darendeli, M. (2001). Development of a new family of normalized modulus reduction and material damping curves. Ph.D. Thesis, Dept. of Civil Eng., Univ. of Texas, Austin.

Drouet S., Cotton, F., and Gueguen, P., (2010). V_{s30}, κ, regional attenuation and Mw from accelerograms: application to magnitude 3-5 French earthquakes, *Geophysical Journal International*, **182**(2), 880-898.

DS. No. 61, (2011). *Regulation determined seismic design of buildings and repeals,* Decree No. 117 of 2010, Ministerio de Vivienda y Urbanismo. Official Journal of 13/12/2011.

Duval, A.M., Vidal, S., Meneroud, J.P., Singer, A., De Santis, F., Ramos, C., Romero, G., Rodriguez, R., Pernia, A., Reyes, N., and Griman, C., (2001). Caracas, Venezuela, Site Effect Determination with Microtremors, *Pure and Applied Geophysics*, **158**, 2513-2523.

Eurocode 8 (2004). *Design of structures for earthquake resistance, part 1: General rules, seismic actions and rules for buildings*, EN 1998-1, European Committee for Standardization (CEN), http://www.cen.eu/ cenorm/homepage.htm.

Field, E.H., Kramer, S., Elagamal, A.-W., Bray, J.D., Matasovic, N., Johnson, P.A., Cramer, C., Roblee, C., Wald, D.J., Bonilla, L.F., Dimitriu, P.P. and Anderson, J.G. (1998). *Nonlinear Site Response: Where We're At* (A report from a SCEC/PEER seminar and workshop). *Seismological Research Letters*, **69** (3).

Futterman, W., (1962). Dispersive Body Waves, *Journal of Geophysical Research*, **67**(13), 5279-5291.

Hanks, T.C., (1982). f_{max}, *Bulletin of the Seismological Society of America*, **72**(6), 1867-1879.

Hashash, Y.M.A. and D. Park (2002). Viscous damping formulation and high frequency motion propagation in nonlinear site response analysis, *Soil Dynamics and Earthquake Eng*., **22**(7), 611–624.

Hashash, Y.M.A., Musgrove, M.I., Harmon, J.A., Groholski, D.R., Phillips, C.A., and Park, D., (2015). DEEPSOIL 6.0, User Manual 116 p.

Hough, S.E., and Anderson, J.G., (1988). High-frequency spectra observed at Anza, California: Implications for Q structure, *Bulletin of the Seismological Society of America*, **78**(2), 692-707.

Idriss, I. M. and Sun, J. I. (1992). User's Manual for SHAKE91, A computer Program for Conducting Equivalent Linear Seismic Response Analyses of Horizontally Layered Soil Deposits Program Modified based on the Original SHAKE Program Published in December 1972 by Schnabel, Lysmer and Seed.

Japan Road Association (1980). *Specifications for highway bridges*, Part V, Seismic Design, Maruzen Co., LTD.

Japan Road Association (1990). *Specifications for highway bridges*, Part V, Seismic Design, Maruzen Co., LTD.

Joyner, W.B., Warrick, R.E., and Fumal, T.E., (1981). The effect of quaternary alluvium on strong ground motion in the Coyote Lake, California, earthquake of 1979, *Bulletin of the Seismological Society of America*, **71**(4), 1333-1349.

Kaklamanos J., Bradley B.A., Thompson E.M., Baise L.G., 2013, Critical parameters affecting bias and variability in site-response analyses using KiK-net downhole array data, Bull. Seismol. Soc. Am., 103(3): 1733-1749.

Kim B, Hashash Y.M.A., Kottke A., Assimaki D., Li W., Rathje E.M., Campbell K.W., Silva W.J., Stewart J.P. (2013). A predictive model for the relative differences between nonlinear and equivalent-linear site response analyses, Transactions, SMiRT-22, Division IV, San Francisco, CA.

Kim, B., Youssef M. A. Hashash, Jonathan P. Stewart, Ellen M. Rathje, Joseph A. Harmon, Michael I. Musgrove, Kenneth W. Campbell, and Walter J. Silva (2016). Relative Differences between Nonlinear and Equivalent-Linear 1D Site Response Analyses. *Earthquake Spectra* (In-Press.)

Knopoff, K., (1964). Q, *Reviews of Geophysics*, **2**(4), 625-660.

Knopoff, K., and MacDonald, G. J. F., (1958). Attenuation of small amplitude stress waves in solids, *Reviews of Modern Physics*, **30**(4), 1178-1192.

Kottke, A. (2010). A Comparison of Seismic Site Response Methods, Ph.D. Thesis, Dept. of Civil Eng., Univ. of Texas, Austin.

Kottke, A. R., and Rathje, E.M., (2008a). *Strata*, Version alpha, Revision 381, University of Texas, Austin, TX.

Kottke, A. R., and Rathje, E.M., (2008b). *Technical Manual for Strata, Report 2008/10*, Pacific Earthquake Engineering Research (PEER) Center, University of California, Berkeley, CA.

Kramer, S., (1996). *Geotechnical Earthquake Engineering*, Prentice Hall, Upper Saddle River, NJ.

Ktenidou, O.J., Cotton, F., Abrahamson, N.A., and Anderson, J.G., (2014). Taxonomy of κ: A Review of Definitions and Estimation Approaches Targeted to Applications, *Seismological Research Letters*, **85**(1), 135-146.

Ktenidou, O.J., Gélis, C., and Bonilla, L.F., 2013. A study on the variability of kappa (κ) in a borehole: Implications of the computation process, *Bulletin of the Seismological Society of America*, **103**(2A), 1048–1068.

Kwok A.O.L., Stewart J.P., Hashash Y.M.A (2008). Nonlinear ground-response analysis of Turkey Flat shallow stiff-soil site to strong ground motion, *Bull. Seismol. Soc. Am.*, **98**(1), 331-343.

Lanzo, G. and Vucetic, M., (1999). Effect of Soil Plasticity on Damping Ratio at Small Cyclic Strains, *Soils and Foundations*, **39**(4), 131-141.

Laurendeau, A., Cotton, F., Ktenidou, O.J., Bonilla, L.F, and Hollende, F., (2013). Rock and Stiff-Soil Site Amplification: Dependency on V_{S30} and Kappa (κ_0), *Bulletin of the Seismological Society of America*, **103**(6), 3131-3148.

Matasovic N. (1992). Seismic Response of Composite Horizontally-Layered Soil Deposits, Ph.D. Thesis, Department of Civil and Environmental Engineering, University of California, Los Angeles, CA.

Matasovic, N. and M. Vucetic (1993). Cyclic Characterization of Liquefiable Sands, *J. of Geotech. Eng.*, ASCE, **119**(11), 1805-1822

Menq F.Y. (2003). Dynamic Properties of Sandy and Gravelly Soils, Ph.D. Thesis, Department of Civil Engineering, University of Texas, Austin, TX.

Matasovic, N. and Y. Hashash (2012). *NCHRP428: Practices and procedures for site-specific evaluations of earthquake ground motions (A synthesis of highway practice).* National Cooperative Highway Research Program, Transportation Research Board: 78 pages. Washington, D.C.

Papageorgiou, A., and Kim, J., (1991). Study of the propagation and amplification of seismic waves in Caracas valley with reference to the 29 July 1967 earthquake: SH waves, *Bulletin of the Seismological Society of America* **81**(6), 2214-2233.

Papageorgiou, A.S., and Aki, K., (1983). A specific barrier model for the quantitative description of inhomogeneous faulting and the prediction of strong ground motion. I. Description of the model, *Bulletin of the Seismological Society of America***, 73**(3), 693-722.

Phillips, C. and Hashash, Y., (2009). Damping formulation for non-linear 1D site response analyses, *Soil Dynamics and Earthquake Engineering*, **29**, 1143–1158.

Rathje, E.M., Idriss, I.M., and Somerville, P., (2000). Strong ground motion and site effects, *Earthquake Spectra* Special Volume on 1999 Kocaeli, Turkey, earthquake.

Régnier, J., Cadet, H., Bonilla, L.F., Bertrand, E., and Semblat, J.-F. (2013). Assessing Nonlinear Behavior of Soils in Seismic Site Response: Statistical Analysis on KiK-net Strong-Motion Data, *Bulletin of the Seismological Society of America*, **103**(3), 1750–1770.

Rodriguez-Marek, A., (2000). Near-Fault Seismic Site Response, Ph.D. Thesis, Department of Civil Engineering, University of California, Berkeley.

Schnabel, P. B., Lysmer, J., and Seed, H. B. (1972). *SHAKE: A computer program for earthquake response analysis of horizontally-layered sites*, Report No. EERC-72/12. Earthquake Engineering Research Center, University of California at Berkeley, Berkeley, CA.

Seed, H.B., Romo, M.P., Sun, J.I., Jaime, A., and Lysmer, J., (1987). *Relationships between Soil Conditions and Earthquake Ground Motions in Mexico City in the Earthquake of September 19, 1985*, Report UCB/EERC-87/15, Earthquake Engineering Research Center, University of California, Berkeley, CA.

Seed, R.B., Dickenson, S.E., and Idriss, I.M., (1991). Principal Geotechnical Aspects of the 1989 Loma Prieta earthquake, *Soils and Foundations*, **31**(1), 1-26.

Silva, W., and Darragh, R., (1995). *Engineering characterization of earthquake strong ground motion recorded at rock sites*, Report TR-102261, Electric Power Research Institute (EPRI), Palo Alto, California.

Stein, S., and Wysession, M., (2003). *Introduction to seismology, earthquakes, and earth structure*, Blackwell Publishing, UK.

Stewart J.P., Kwok A.O., Hashash Y.M.A., Matasovic N., Pyke R., Wang Z., Yang Z. (2008). *Benchmarking of nonlinear geotechnical ground response analysis procedures*,

PEER Report No. 2008/04, Pacific Earthquake Engineering Research Center, University of California, Berkeley, CA.

Stewart, J.P., Afshari, K. and Hashash, Y.M.A., (2014). Guidelines for Performing Hazard-Consistent One-Dimensional Ground Response Analysis for Ground Motion Prediction. *PEER Report*.

Van Houtte, C., Drouet, S., and Cotton, F., (2011). Analysis of the origins of κ (Kappa) to compute hard rock to rock adjustment factors for GMPEs, *Bulletin of the Seismological Society of America*, **101**(6), 2926–2941.

Table 1: Main properties of reference rock sites.

Reference	Definition of Reference Rock Conditions
National Earthquake Hazard Reduction Program (NEHRP) (Building Seismic Safety Council, 2000)	V_{s30} > 760 m/s - rock sites V_{s30} > 1500 m/s - very hard rock sites
European Regulations (Eurocode 8, 2004)	V_{s30} > 800 m/s - rock sites
Japanese regulations (Japan Road Association, 1980, 1990)	V_{s30} > 600 m/s - rock sites
Recommendation from Cadet et al. (2010)	750 < V_{s30} < 850 m/s and f_0 > 8 Hz - "standard reference rock site"
Boore and Joyner (1997) generic rock sites	V_{s30} > 620 m/s and κ_0 = 0.04 sec - rock sites (mostly in western North America) V_{s30} > 2000 m/s and κ_0 < 0.01 sec - very hard rock sites (mostly in eastern North America)
Chilean regulations (DS. No. 61, 2011)	V_{s30} > 500 m/s - soft rock or fractured rock V_{s30} > 900 m/s - rock sites, cemented soils
Hashash et al. (2014)	2700 m/s < V_s < 3300 m/s and κ_0 = 0.006 sec (for Central and Eastern North America)

Table 2: Influence of α_z on the wave amplitudes (after Kramer, 1996). Ai refers to the displacement amplitude of the incident wave.

Impedance Ratio	Wave Amplitudes		
α_z	Incident	Reflected	Transmitted
0	A_i	A_i	$2A_i$
0.25	A_i	$3A_i/5$	$8A_i/5$
0.5	A_i	$A_i/3$	$4A_i/3$
1	A_i	0	A_i
2	A_i	(-) $A_i/3$	$2A_i/3$
4	A_i	(-) $3A_i/5$	$2A_i/5$
infinite	A_i	(-) A_i	0

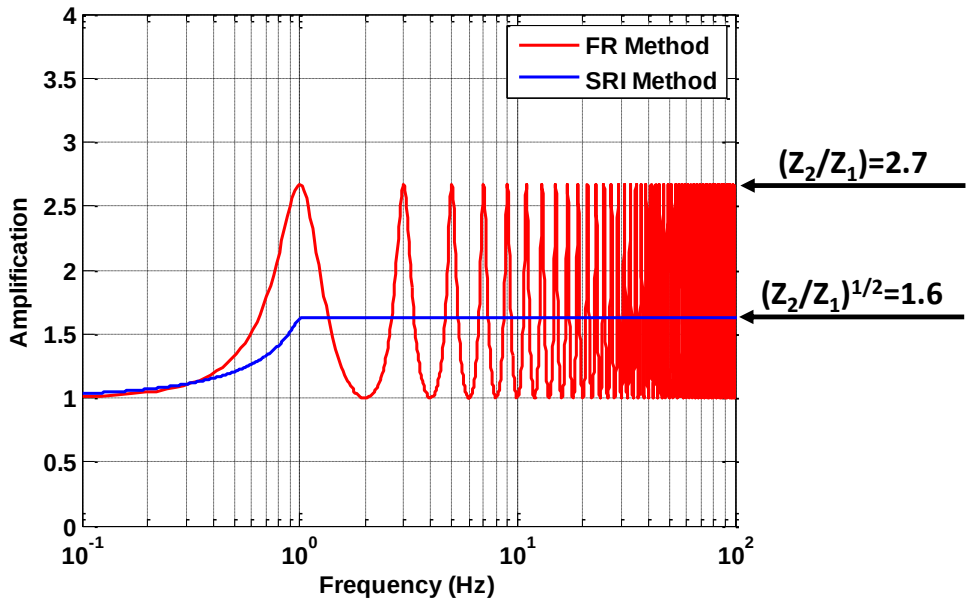

Figure 1: Site amplifications from FR and SRI methods for a one-layer undamped site model (after Boore, 2013).

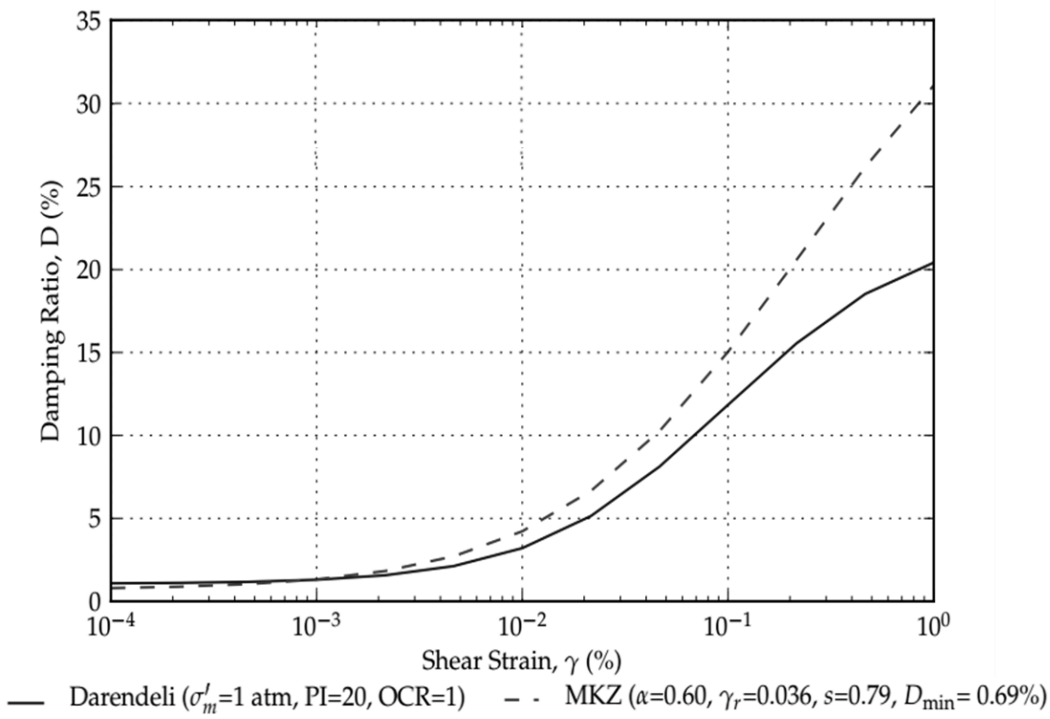

Figure 2: Differences in damping curves as obtained from Darendeli (2001) and MKZ models (modified after Kottke, 2010).

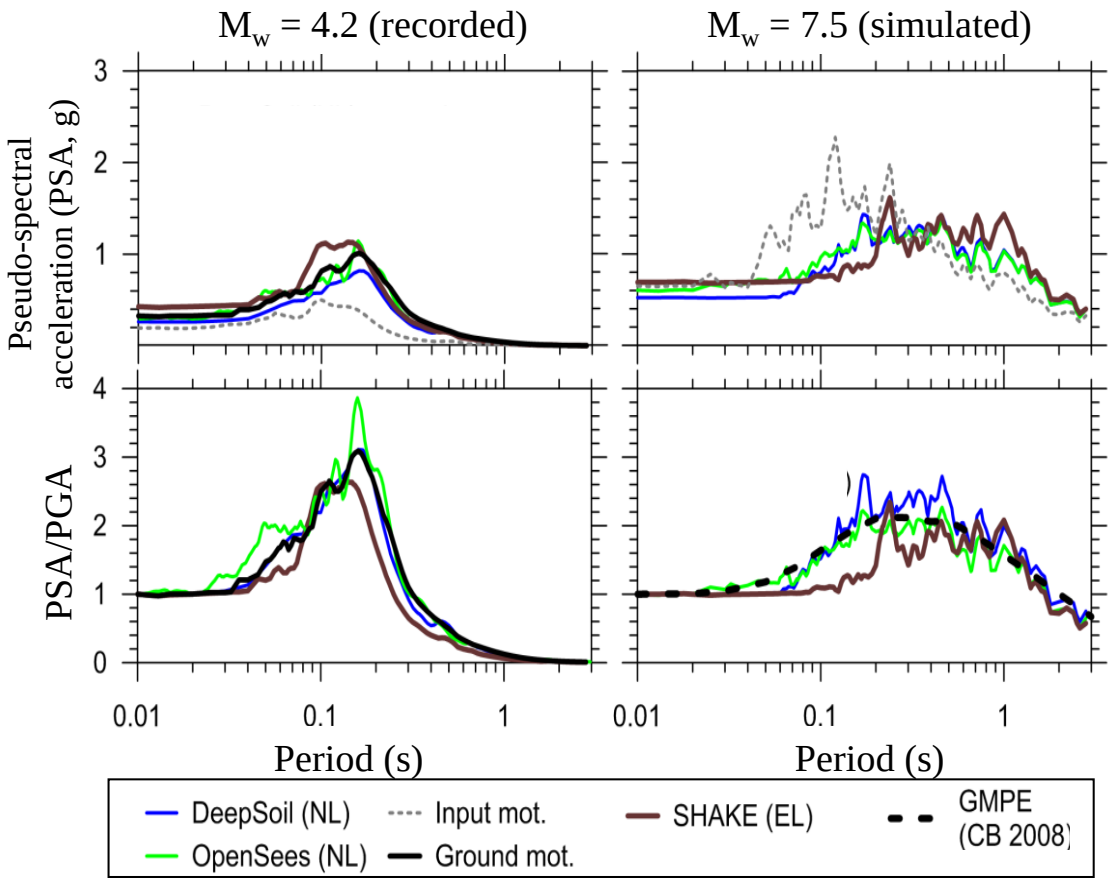

Figure 3: Comparison of estimated response spectra at La Cienaga site when conducting equivalent-linear and nonlinear site response analyses for a small and a large magnitude earthquakes (adapted from Stewart et al., 2014).

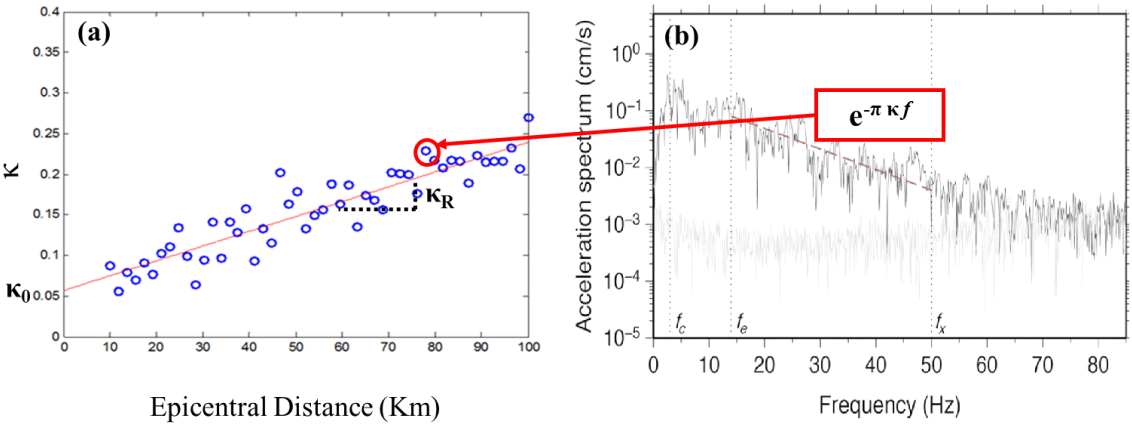

Figure 4: (a) κ_r versus epicentral distance, and (b) Individual measure of κ in the Fourier Amplitude Spectrum (modified after Ktenidou et al., 2013). The slope of the dashed line in (4b) is $-\pi*\kappa$.

CHAPTER THREE

ESTIMATION OF KAPPA (κ)-CONSISTENT DAMPING VALUES AT KIK-NET SITES TO ASSESS THE DISCREPANCY BETWEEN LABORATORY-BASED DAMPING MODELS AND OBSERVED ATTENUATION (OF SEISMIC WAVES) IN THE FIELD

Abstract

In this paper we use selected stations from the KiK-net database to compare field estimates of the attenuation of seismic waves, through measurements of site-specific κ (i.e., κ_0), with laboratory-based values of minimum shear strain damping (ξ_{min}). Combined models of κ_0 and ξ_{min} are proposed and found to provide an upper limit for low-strain damping profiles when compared to laboratory-based models used in geotechnical site response analysis. The latter can only quantify intrinsic material damping. Other attenuation mechanisms, such as scattering of the wavefield, are impossible to capture when testing small-scale samples. In addition, we evaluate the difference in damping at the surface and at borehole stations to determine the contribution of shallow layers to attenuation as captured by κ_0 values at the surface of the study sites. Thus, values of κ_0 are computed at the surface and at the downhole instrument depth, and their difference, $\Delta\kappa$, is found to correlate well with the averaged shear wave velocity (V_s) over the top 30 m of the profile, V_{s30}, and also with the depth to bedrock. Estimates of κ_0 for hard rock and stiff sites in Japan are also examined

and compared to other regional κ_0 values proposed for high V_{s30} materials in New Zealand, Greece, and Switzerland. Two values of κ_0 are deemed potential descriptors of hard rock conditions in Japan, and both values are lower than the corresponding estimates for the other regions.

3.1 Introduction

The main purpose of this study is to determine kappa (κ)-consistent damping values at selected stations from the Japanese database, KiK-net (NIED, 1996) and evaluate potential inconsistencies between field estimates of attenuation of seismic waves and laboratory-based damping models. Our second objective is to assess the contribution of shallow layers to attenuation, as captured by site-specific kappa (κ_0) values at the surface, by quantifying the difference in damping estimates at surface and downhole recording stations. Attenuation of seismic waves is considered a topic of major interest in both, seismology and engineering. It plays a key role in studies on the simulation of ground motions (e.g., Boore, 2003), seismic hazard assessment (e.g., Rodriguez-Marek et al., 2014; SSHAC 1997), adjustment of ground motion prediction equations (GMPEs) (e.g., Al Atik et al., 2014; Laurendeau et al., 2013; Cotton et al., 2006) and site response analysis (e.g., Stewart et al., 2014; Rathje et al., 2010).

Different parameters can be used as measures of seismic attenuation; some of them can be obtained empirically while others are derived mathematically. The seismic quality factor, Q (Knopoff, 1964), and the high-frequency spectral decay parameter, κ (Anderson and Hough, 1984) are more common in engineering seismology. Material damping, ξ, is customarily used in geotechnical and structural engineering. The concept of κ was originally introduced by Anderson and Hough (1984) as a site and distance dependent low-

pass filter. It was based on the observation that in log-linear space, the acceleration Fourier amplitude spectrum (FAS) can be assumed to decay linearly for high frequencies above a certain value. The zero-distance intercept of κ is known as site-specific κ or κ_0. Most recent studies identify it as "an observed site characteristic" (Edwards et al., 2015) because it captures the attenuation of seismic waves as they travel vertically through the subsurface geological structure underneath the site (Anderson & Hough, 1984). Estimates of ξ are usually expressed in terms of the ratio between the energy dissipated per cycle and maximum stored energy per cycle (Kramer, 1996). Both, Q and ξ are comparable fundamental material properties, whereas κ is a measure of total path attenuation. The latter can be measured directly from linear ground motions recorded in the field. The value of ξ is strain dependent and results from geotechnical damping models developed empirically in the laboratory. Only intrinsic material damping can be captured when testing small-scale soil elements in the laboratory. This means that other sources of attenuation (e.g., scattering effects, geometric spreading and multipathing) cannot be quantified. Additionally, sample disturbance may affect stress-strain loops obtained in the laboratory (Stewart et al., 2014). A few recent studies have provided evidence that laboratory-based damping cannot capture the more complex energy dissipation phenomena involved in seismic wave propagation as it occurs in the field (Stewart et al., 2014). Afshari and Stewart (2015), Tsai and Hashash (2009) and Elgamal et al. (2001) used vertical array data from California and Taiwan to show that higher damping was observed in the field when compared to laboratory estimates. Yee et al. (2013) evaluated data from a vertical array in Japan using relatively weak ground motions, and found that the minimum shear strain damping (ξ_{min}) should be increased by 2% to 5% for site response results to agree with field observations. Combining

geotechnical and seismological attenuation descriptors can provide insights on the portion of the attenuation being ignored when only relying on dynamic laboratory testing. Integrating knowledge from different ways of characterizing attenuation may prove to be a key step towards obtaining better predictions of site response, improved evaluations of site-specific seismic hazards and potentially more stable GMPEs (Ktenidou et al., 2015). Ktenidou et al. (2015) and Afshari and Stewart (2015) explored alternatives to combine κ_0 estimates (from direct measurements of linear surface ground motions and relationships with V_s, respectively) and ξ_{min} values. While these studies provided examples of how to combine κ and ξ, their work was based on rather small databases which still leaves the critical need for more accurate estimations of damping unresolved. In fact, Stewart et al. (2014) cautioned that further analysis of weak motion data on vertical arrays is still necessary. This study utilizes a large database to investigate how much attenuation should be added to laboratory-based damping models (i.e., $\Delta\xi_{min}$), so that a better compatibility with the field attenuation is achieved.

The second objective of this study is to assess the contribution of shallow layers to the measured κ_0 values at the surface. Recent studies refer to the depth of influence of κ_0 rather vaguely because there is still a need to elucidate the actual portion of the profile beneath the site that contributes to κ_0. The weak correlation between κ_0 and the time-averaged shear wave velocity (V_s) over the top 30 m of the profile (V_{s30}) found by several authors (e.g., Silva et al., 1998; Chandler et al., 2006; Edwards et al., 2011; Van Houtte et al., 2011; Poggi et al., 2013) hints that κ_0, although linked to the attenuation of shallower layers, may have a deeper origin. Ktenidou et al. (2015) found equally strong correlations of κ_0 with shallow geology (i.e., upper 30 m.) and the deeper geologic structure (down to 400m.).

These authors proposed a new conceptual model for κ_0-V_s dependence where a minimum value of κ_0, corresponding to high V_s values, is associated with a regional characteristic of the rock. Earlier studies (e.g., Campbell, (2009), Van Houtte et al., (2011) and Ktenidou et al., (2013)) have also suggested a deeper origin for κ_0, implying that it may be affected not only by near-surface materials down to a few hundreds of meters but geologic formations as deep as a few kilometers. The current study adds to the aforementioned efforts by investigating how intrinsic damping within the rock mass and the attenuation in near-surface deposits contribute to the overall attenuation as characterized by κ_0 values at the surface. This paper presents a description of the database and selected study sites, along with the method implemented to compute κ_0 and ξ_{min} values. The comparison of alternative combinations of κ, Q and ξ is then provided; followed by the discussion of results and insights on the discrepancy between field estimates of attenuation and laboratory-based damping models.

3.2 Database and Study Sites

In this study we use the Kiban-Kyoshin network (KiK-net), which has collected a large database of unprecedented volume and quality (Van Houtte et al., 2011) that offers a unique coverage of Japan. The use of a large database is deemed necessary to avoid bias in κ estimates (Edwards et al., 2015). The KiK-net database is composed of 660 pairs of surface-downhole recording stations located on weathered rock sites or on shallow sediment deposits (Aoi et al., 2004; Fujiwara et al., 2004). The sensor located at depth is typically between 100 m to 200 m below the surface, but some stations have downhole instruments positioned at a depth of 2000 m (Fujiwara et al., 2004). Also, V_s data (from

downhole logging) and boring logs are available for most stations at the KiK-net database website (kyoshin.bosai.go.jp).

Each ground motion recording in the database was systematically processed using an automated protocol thoroughly described in Dawood et al. (2016), which complies with recommendations on record processing by Ktenidou et al. (2013) (e.g., baseline correction and adequate noise windows). Then, appropriate records for κ calculations are selected based on recommendations also presented by Ktenidou et al. (2013): shallow crustal seismic events (which were identified by means of Garcia et al. (2012) method) that do not trigger nonlinear behavior and for which the assumption of a unique and frequency-independent Q could be valid. The ability to trigger nonlinearity has been typically defined in κ studies by setting thresholds to peak ground acceleration (PGA) values (e.g., PGA<10 cm/sec^2, Ktenidou et al., 2013). However, there is no consensus in the literature regarding what defines weak motions for κ calculations. In this study, shear strain index values (I_γ, defined as the ratio of the peak ground velocity (PGV) and V_{s30} of the site profile (Chandra et al., 2014; Chandra et al., 2016; Kim et al., 2016) are used. Recent studies on the nonlinear dynamic behavior of soils and methods for site response analysis (e.g., Kim et al., 2013; Kim et al., 2016; Stewart et al., 2014; Gueguen, 2015) have indicated that I_γ has a stronger correlation to the significance of nonlinearity, than other parameters such as PGA. Thus, only ground motions with I_γ values lower than 0.1% have been selected. Ktenidou et al. (2012) indicated that event-station azimuths were not found to affect κ estimations in their study. However, we consider source-to-site paths for all records in our database because Japan has zones with different regional attenuation characteristics (i.e., different Q values; Pei et al., 2009 and Nakano et al., 2015). A tomography study from Pei et al. (2009)

indicated that low Q values were more common in the central Japanese islands and correlated with the volcano distribution in that region. Likewise, high Q values were identified between the front of Japan's volcanic belt and their east coast. Results from Nakano et al. (2015), although more detailed, were in agreement with the aforementioned findings. Thus, source-to-site paths are used in the current study to filter out ground motions whose ray paths may have crossed the Japanese volcanic belt. In addition, only ground motions with epicentral distances lower than 150 km were selected in order to avoid capturing multiple ray paths. Finally, only recording stations with thirty or more suitable ground motions were deemed appropriate to estimate κ_0 values. The implementation of the aforementioned criteria resulted in 94 appropriate sites for this study.

3.3 Methodology

3.3.1 Estimation of κ_0

The traditional approach originally introduced by Anderson and Hough (1984) is implemented in this study to compute individual κ values for all suitable records at the selected sites. These individual κ values measured on the acceleration spectrum (AS) are referred to as $\kappa_{r\_AS,}$ according to the taxonomy of existing approaches to estimate κ proposed by Ktenidou et al. (2014).

The linear trend of the amplitude decay on the high-frequency portion of the acceleration FAS in a log-linear space is computed using a robust linear regression for each horizontal component. The slope of this line is equal to $-\pi\,\kappa_{r\_AS}$. In this study, Ktenidou et al. (2013) recommended practices to yield more consistent κ_{r_AS} values are followed. The frequency range, f_1 to f_2, over which κ_{r_AS} is measured is selected by visual inspection, ensuring that

f_1 lies above the corresponding corner frequency (f_c). Estimates of f_c values were obtained from correlations to seismic moment (Brune, 1970, 1971):

$$f_c = 4.9x10^4\beta\left(\frac{\Delta\sigma}{M_0}\right)^{\frac{1}{3}} \quad (1)$$

where f_c is in Hz, β is the V_s in the vicinity of the source (in km/s), $\Delta\sigma$ is the stress drop in MPa, and M_0 is the seismic moment in N.m. Estimates of β for sources in Japan can be found in Pei et al. (2009), while estimates of $\Delta\sigma$ are presented in Nakano et al. (2015). When picking f_1, available empirical transfer functions for KiK-net stations (Régnier, 2013) are also used to avoid resonant peaks resulting from site effects at the selected stations. These peaks can introduce bias in κ_{r_AS} estimates (Parolai and Bindi, 2004). Values of f_2 are selected within a frequency band where the instrument's response is considered to be flat, so that it has no influence on κ_{r_AS} calculations. According to Kinoshita, (1998) and Fujiwara et al. (2004), KiK-net instrument's response can be compared to that of a three-pole Butterworth filter with a cutoff frequency of 30 Hz. Hence, the analysis should be restricted to frequencies below 30 Hz (Laurendeau et al., 2013). Signal to noise ratios greater than 3 are also considered when selecting f_2, as well as a minimum Δf (i.e., f_1 - f_2 range) of 10 Hz to ensure robustness of the regressions. Other studies have set similar constraints to Δf (e.g., Ktenidou et al., 2013; Van Houtte et al., 2014 and Edwards et al., 2015). The selected frequency range in each case varies according to the event's magnitude, empirical transfer function at the site, noise level and spectral shape (Ktenidou et al., 2015), but on average, our κ_{r_AS} values are measured within the 11 Hz – 25 Hz frequency band. Additional performance criteria have customarily been used in other κ studies. For example, Ktenidou et al. (2013) recommended to report and use

average values of κ_{r_AS} measured on two horizontal components only when the difference between individual values is lower than 20%. This criterion is adopted in our study.

We use the whole FAS instead of only selecting the corresponding S-wave window to compute κ_{r_AS}. Douglas et al. (2010) showed that manual picking of the arrival of P- and S-waves might add such a degree of uncertainty to the κ_{r_AS} calculations, that it is preferred to use the whole spectrum instead. Furthermore, negative κ_{r_AS} values, if apparent from the data, are not rejected. Estimates of κ_0 at the surface (i.e., κ_{0_surf}) and at depth (i.e., κ_{0_down}) are obtained by linearly regressing the individual κ_{r_AS} values with epicentral distance at each station. This constitutes the original model proposed by Anderson and Hough (1984), which assumes a unique and frequency-independent Q:

$$\kappa_{r\_AS} = \kappa_0 + \kappa_R * R \quad (2)$$

κ_{r_AS} is in units of time, R is the epicentral distance, κ_R reflects the attenuation of shear waves as they propagate through the crust, and κ_0 is obtained by extrapolating the κ_R trend to zero epicentral distance. Regional attenuation is represented by the slope of equation 2, (Ktenidou et al., 2013 and 2015; Edwards et al., 2015). Hence, we constrain it to be the same for surface and borehole stations at the same site. This approach provides robustness to the regressions and reflects a more consistent physical interpretation (Douglas et al., 2010; Ktenidou et al., 2013). The constant difference across epicentral distances between the linear model fitting surface data and the one corresponding to borehole data will be hereafter referred to as $\Delta\kappa$ (Figure 1a).

Additionally, the geographic location of the selected stations is used to identify sites that may share the same regional attenuation characteristics. The latter is based on independent studies of Q values in Japan, such as Pei et al. (2009) and Nakano et al. (2015). Specifically,

Figure 2 in Pei et al. (2009) has been used to group stations with the same Q values in clusters. Values of κ_{0_surf} and κ_{0_down} are then estimated for these clusters, by constraining the slopes of all the corresponding surface and borehole regressions of stations in that cluster, to be the same (Figure 1b). This approach allows for the comparison of our estimates of regional attenuation (i.e., κ_R per cluster) with values in the literature for the same region. When calculating κ_{0_down}, we ignore the effects of downgoing waves resulting from potential strong reflections from above the borehole instrument location.

3.3.2 Towards More Robust Estimates of κ_0

A protocol to categorize stations according to the quality of their data is proposed as a simple procedure to filter out sites that may obscure true trends in the attenuation characteristics of a given region. The protocol accounts for three key steps in κ_{r_AS} calculations, which are responsible for adding significant uncertainty to the ultimate results: (1) selection of f_1 and f_2, (2) consistency between components, and (3) number of records available per regression. The selection of the frequency range to measure individual κ_{r_AS} values is related to the spectral shape of records. Recordings having a sharp amplitude decay over a short frequency range (sometimes linked to site effects) or without a linear decay at high frequencies (e.g., having a flat response or resulting in a negative kappa) make it harder to select f_1 and f_2 unambiguously. This in turns, adds uncertainty and variability to the resulting κ_{r_AS}. Edwards et al. (2015) provides a detailed study on the selection of an appropriate frequency range for κ_{r_AS} calculations. We introduce the concept of the consistency ratio, c, as a measure of how many κ_{r_AS} values were measured consistently in both horizontal components. Thus, it is the ratio of the number of final recordings with a difference lower than 20% between horizontal components, and the

original number of available ground motions for estimating κ_{r_AS}. The former is selected as the minimum value between surface and borehole records at the site of interest. Sometimes, only surface records would have issues, but because we are fixing the slope of the regression based on data from both, surface and downhole instruments, reporting poor quality data at any depth is necessary. The value of *c* does not depend on V_{s30} and it is not biased by the mean value of $\Delta\kappa$. Finally, the actual number of records utilized for the linear regression (equation 2) is used as a measure of how robust the model is. A description of these components and their role within the proposed categorization scheme is shown in Table 1. In this study, we only use stations ranked 1 and 2, which reduces our original dataset of 94 sites to 60.

3.3.3 Estimation of κ_0 for the Sedimentary Column

Campbell (2009) proposed a modification of a relationship originally introduced by Hough and Anderson (1988), and later used by Chapman et al. (2003), to relate spectral decay parameters to Q structure. While Hough and Anderson (1988) integrated the Q effects over the whole ray path (analogously to κ's predecessor, t*, proposed by Cormier (1982)), Campbell (2009) suggested to isolate the contribution to κ_0 due to the sediments:

$$\kappa_0 = \int_0^H \frac{1}{Q_{ef}(z)V_s(z)}\,dz \tag{3}$$

where $Q_{ef}(z)$ is the effective seismic quality factor at a depth *z* within the sedimentary column, and it is assumed to be independent of frequency (which is a basic assumption in equivalent linear site response analysis as well). $V_s(z)$ is the shear wave velocity at a depth *z* within the profile, and H is the total depth of the profile of interest Hough and Anderson (1988) indicated that their relationship between κ and Q only considered the frequency-independent contribution to Q (which they referred to as Q_i), instead of the total Q. The

latter was defined by Dainty (1981) as the contribution of both, frequency-independent and frequency-dependent attenuation mechanisms. Campbell (2009) presents a summary of previous studies that provide evidence to the validity of assuming frequency-independent Q values in sediments. In this study, we do not examine whether attenuation in sediments is frequency-independent or not, because any frequency-dependent attenuation effects that might take place in situ are not accounted for when implementing equation 3 (Campbell, 2009).

If a finer discretization of Q values near the surface is considered (Knopoff, 1964), and assumed to be frequency-independent, Q can be directly related to soil damping (Goodman, 1988; Silva, 1997):

$$Q = \frac{1}{2\xi} \tag{4}$$

where, ξ is the damping ratio in decimal units. Equation 4 can also be used to establish a relationship between material damping as defined in geotechnical engineering and κ_0 values (Silva, 1997; Ktenidou et al., 2015; Afshari and Stewart, 2015). We use equations 3 and 4 to compute κ_0 values corresponding to the profile at the selected sites from the surface down to the downhole instrument depth, which we hereafter refer to as $\kappa_{damping}$. Because κ_0 is related to the low deformations, elastic regime only, ξ_{min} from geotechnical damping models are used when estimating $\kappa_{damping}$ values.

The information available to us for the site profiles at KiK-net stations did not allow for a precise definition of the ξ_{min} corresponding to the soils in situ. Hence, we use a variety of soil properties (e.g., different values of the plasticity index, PI, and the over-consolidation ratio, OCR for clays, as well as the coefficient of uniformity, c_u and the grain diameter corresponding to 50% passing by weight, D_{50} for sands) to predict a reasonable range of

ξ_{min} using Darendeli (2001) and Menq (2003) models at each site. A binary classification system is used to differentiate soil materials from rocks based on their reported V_s value on the KiK-net database website. Two classification schemes for rocks are implemented (i.e., materials with $V_s \geq 500$ m/s and $V_s \geq 800$ m/s (after Cadet et al., 2010)). Darendeli (2001) and Menq (2003) formulations of ξ_{min} are assigned to materials classified as soils, while two different models are used for rocks: (a) a constant ξ_{min}=0.33% (which is similar to the ξ_{min} proposed by EPRI (1993) curves for the 150 m to 300 m depth range), and (b) Darendeli (2001) model for PI=0% and OCR=1.

3.3.4 Relationship between Δκ, $\kappa_{damping}$, and ξ_{min}

Campbell (2009) postulated that the value of κ_0 can be partitioned such that the contributions of the sedimentary column and the underlying rock mass are accounted for independently. The basis for his postulation was the strong correlation found between κ_0 and the thickness of sediments in eastern North America (ENA). This partition is useful in hazard analyses. For example, when applying host-to-target conversions in GMPEs, the reference rock must be characterized by both its V_{s30} and its κ_0 values (Laurendeau et al., 2013; Al Atik et al., 2014; Ktenidou et al., 2015). Similarly, input motions for site response analyses should also be selected with consideration of the rock κ_0 values (Ktenidou et al., 2015; Cabas and Rodriguez-Marek, 2016).

In this study, we use $\Delta\kappa$ values obtained from the linear regression of measured κ_{r_AS} at the surface and at depth (hereafter referred to as $\Delta\kappa_{meas}$) to quantify the contribution to overall attenuation from the strata between the ground surface and the depth of the downhole sensor. Hence, we compare $\Delta\kappa_{meas}$ values with estimates of $\kappa_{damping}$ obtained by assuming different models for ξ_{min} as described in the previous section.

3.3.5 Combining κ, Q, and ξ

Afshari and Stewart (2015) showed that laboratory-based damping values were lower than ξ_{min} estimates derived from κ_0. However, only estimates of κ_0 (from Campbell (2009) and a V_{s30}-κ_0 relationship by Van Houtte et al. (2011)) were used instead of direct measurements on actual recordings. Ktenidou et al. (2015) used measured κ_0 values in the EUROSEISTEST network, to compare them with predicted κ_0 values at the surface. Field measurements of Q in shallow layers were also used in their study. Predicted κ_0 values at the surface resulted from adding the contribution of the shallow layers, obtained in a similar fashion to equation 3, to the measured κ_0 at downhole depth. These authors also showed discrepancies between κ_0 values based on ξ_{min} and the measured difference of κ_0 at the surface and at depth (which is equivalent to our definition of $\Delta\kappa_{meas}$). However, comparisons between their measured and predicted κ_0 values were only conducted for two stations. The study presented herein, not only investigates alternative models that combine κ, Q and ξ, but also overcomes limitations in previous studies by using a larger database with available surface and downhole data that allows direct measurement of κ_0 values.

Two functional forms for estimating new ξ_{min} values are used:

$$(\xi_{min})_{new} = \psi * (\xi_{min})_{lab} \tag{5a}$$

$$(\xi_{min})_{new} = (\xi_{min})_{lab} + \Delta\xi_{min} \tag{5b}$$

where ψ, hereafter referred to as the correction factor, is defined as the ratio of $\Delta\kappa_{meas}$ and $\kappa_{damping}$, while $\Delta\xi_{min}$ results from the following models based on $\Delta\kappa_{meas}$, $\kappa_{damping}$, and Q-V_s relationships:

$$\Delta\kappa_{meas} = \int_0^H \frac{2*((\xi_{min})_{lab}(z)+\Delta\xi_{min}(z))}{100} \frac{1}{V_s(z)} dz \tag{6}$$

where H refers to the depth of the profile of interest (in this case, the portion of the profile from the ground surface down to the depth of the downhole instrument).The maximum likelihood method is used to constrain the values of the free parameters in equation 6. Accurate estimates of ξ_{min} for the KiK-net stations are not available. Hence, minimum and maximum ξ_{min} values from laboratory-based damping models and different soil and rock properties, as described in previous sections, are used in equation 6 to capture a range for $\Delta\xi_{min}$ values. Two approaches to compute $\Delta\xi_{min}$ values following equation 6 are also tested; one considering a depth-independent $\Delta\xi_{min}$ and another assuming V_s-dependent $\Delta\xi_{min}$. The latter is based on the functional form derived by Afshari and Stewart (2015):

$$\Delta\xi_{min} = d_0 \left(\frac{V_s}{200}\right)^{-0.3} \tag{7}$$

where d_0 is a constant obtained from the regression and V_s is the shear wave velocity in m/s for each layer.

In addition, $\Delta\kappa_{meas}$ can be used to define Q by computing the constant of proportionality, γ:

$$\Delta\kappa_{meas} = \int_0^H \frac{1}{\gamma\, V_s{}^2(z)}\, dz \tag{8}$$

where H refers to the depth of the profile of interest. The proportionality constant, γ, (from $Q = \gamma V_s$) is based on the observation that Q and V_s both increase with depth and depend on similar rock material properties (Silva and Darragh, 1995). Estimates of ξ_{min} are then obtained by using equation 4. It is not the purpose of this study to recommend specific values of $\Delta\xi_{min}$ for design purposes, but rather to investigate the compatibility of ξ_{min} from the laboratory with measurements in the field as captured by κ_0.

3.4 Results and Discussion

3.4.1 Measured κ_0 and κ_R Values

To avoid confusion in what is meant by the multiple terms used in this study to describe different estimates of κ and ξ_{min}, Table 2 presents a summary of the main symbols and their corresponding definitions. Measured values of Δκ, κ_{0_surf}, and κ_{0_down} are shown in Table 3, as well as the standard deviation (σ) of the corresponding regressions, mean $\kappa_{damping}$ values, V_{s30} and site class corresponding to each one of the sixty selected stations. Our estimates of κ_0 are in good agreement with previous studies that have also used the KiK-net database. A comparison with κ_0 values from Van Houtte et al. (2011) is presented in Figure 2. Laurendeau et al. (2013) indicated that "particularly for the lower κ_0 value sites, the method used by Van Houtte et al. (2011) will lead to overestimated κ_{0_AS}" given that the instrument response was not accounted for in their κ calculations. Such trend is observed in Figure 2 precisely for lower values of κ_0. Van Houtte et al. (2011) used hypocentral distances and computed data-driven κ_R values (instead of constraining the slope to be the same for surface and downhole records), while only considering measurements of κ from borehole instruments.

Additionally, we compare inferred regional Q values from κ_R estimates (for selected clusters) with Q values for Japan found in the literature (e.g., Pei et al., 2009; Nakano et al., 2015) in Table 4. The former are obtained from a relationship derived by Ktenidou et al. (2015):

$$Q = \frac{1}{\beta\, \kappa_R} \tag{9}$$

where β refers to an average crustal shear wave velocity. Clusters 1 to 4, shown in Table 4, were defined based on high and low Q zones provided by Pei et al. (2009). An example

of the linear regressions performed for one of these clusters is shown in Figure 1b. The stations grouped per cluster, as well as their geographic coordinates are provided in Appendix B. Pei et al. (2009) presented lateral variations of Q values at 1 Hz (i.e., Q_0). We estimate Q between f_1 = 11 Hz and f_2 = 25 Hz, which is the frequency band where our κ_{r_AS} calculations are conducted, and convert these values to 1 Hz using:

$$Q(f) = Q_0 f^{\alpha} \tag{10}$$

where f is the desired frequency and α is a regional parameter, assumed to be 0.88 for Japan (Tsuda et al., 2006). As shown in Table 4, our estimates of Q from κ_R per cluster and the average of Q values from κ_R at the stations in each cluster, generally lie in between Q values at computed for 11 Hz and 25 Hz. Frequency-dependent Q models developed by Nakano et al. (2015) are only valid for frequencies up to 10 Hz in the zones considered herein, hence our estimates could not be directly compared with their models.

3.4.2 Difference between Laboratory Models and Field Measurements of Damping

Mean $\kappa_{damping}$ estimates and $\Delta\kappa_{meas}$ values are shown in Figure 3. The former, which are based on ξ_{min} values from geotechnical damping models are much lower than $\Delta\kappa_{meas}$ from linear regressions on measured κ_{r_AS}. This difference is significantly larger than the standard deviation of $\Delta\kappa_{meas}$ estimated from the regressions. Errors in the V_s profile are a plausible cause for the underprediction, but the uncertainty in V_s alone cannot explain the large discrepancy between laboratory and field estimates of damping. As suggested by recent studies (e.g., Ktenidou et al., 2015), it is more likely that the observed discrepancy between $\Delta\kappa_{meas}$ and $\kappa_{damping}$ is due to the different attenuation mechanisms they capture.

New estimates of ξ_{min} (equations 5a and 5b) based on models presented in equations 6, and 8 are compared to laboratory-based ξ_{min} values at the sixty selected KiK-net stations. Figure 4 shows damping profiles corresponding to four selected stations. Figure 4 includes: (a) traditional laboratory-based ξ_{min}, and $(\xi_{min})_{new}$ estimates based on the additive model in equation 5b using (b) $\Delta\kappa_{meas}$-based depth-independent $\Delta\xi_{min}$, (c) $\Delta\kappa_{meas}$-based V_s-dependent $\Delta\xi_{min}$, and (d) $\Delta\kappa_{meas}$-based γ. Profiles of $(\xi_{min})_{new}$ based on the multiplicative model in equation 5a are also provided in Figure 4 using a mean value of ψ equal to 13.2.

Profiles of traditional laboratory-based ξ_{min} shown in Figure 4 assume rock layers to have $V_s \geq 800$ m/s (after Cadet et al., 2010) and use Darendeli (2001) model with PI=0% and OCR=1. This characterization for rocks provides a fair representation of their attenuation characteristics, however, other alternatives have also been tested as described in previous sections (i.e., rock layers having $V_s \geq 500$ m/s, and constant damping equal to 0.33%). Results from all considered alternatives are consistent with the damping profiles shown in Figure 4. This ξ_{min} for rock layers is also used in equation 6 to compute $\Delta\xi_{min}$ values. Variations for ξ_{min} in soils are considered, but only minimum and maximum values of resulting damping profiles are shown in Figure 4.

In general, laboratory-based models provide lower estimates of ξ_{min} than combined models considered herein; a trend that has also been observed in recent studies (Afshari and Stewart, 2015 and Ktenidou et al., 2015). Similar results are obtained for all the selected sites (see Appendix C). Laboratory-based measures of attenuation capture only material damping, which explains why they result in the smallest estimates of damping.

New profiles of ξ_{min} based on the multiplicative model in equation 5a provide the highest estimates of ξ_{min}, which are usually above 5%.

Profiles of ξ_{min} based on $\Delta\kappa_{meas}$ result in intermediate values between the lower bound represented by laboratory-based models, and the upper bound defined by ξ_{min} from corrected $\kappa_{damping}$ values. When using an additive model for ξ_{min}, the resulting damping profile is independent of the original ξ_{min}. Thus, just one estimate of new ξ_{min} values from equation 6 is depicted in Figure 4. Additionally, the depth-independent and V_s-dependent models for $\Delta\xi_{min}$ result in similar damping profiles, as also found by Afshari and Stewart (2015) in California sites. Although the V_s-dependent model results in slightly lower damping values. In the current study, a depth-dependency for $\Delta\xi_{min}$ at the selected sites cannot be defined rigorously. Afshari and Stewart (2015) did explore such option, but found that it resulted in fairly similar ξ_{min} estimates to the depth-independent and V_s-dependent options. The resulting $\Delta\xi_{min}$ values based on $\Delta\kappa_{meas}$ when assuming depth-independency, vary between 2.2% to 2.8%. These results now provide a wealth of data to support earlier studies that suggested an increase in ξ_{min} by 2% to 5% (e.g., Yee et al., 2013; Stewart et al., 2014).

Finally, the value of γ obtained from Equation 8 is equal to 0.0417 sec/m and provides intermediate results, generally in accordance with the upper bound ξ_{min} estimates from laboratory-based measurements. Models based on Q which were tested by Afshari and Stewart (2015) for California sites also provided intermediate values of ξ_{min} when compared to laboratory and κ_0-based models. We use our $\Delta\kappa_{meas}$-based γ value to obtain Q estimates and compare them with Campbell (2009) Q-V_s model in Figure 5. Campbell (2009) indicated that there was a need to validate his proposed Q-V_s models because they were loosely derived from low-intensity ground motion data and mostly based on the expert opinions of a few seismologists (e.g., Boore and Joyner, 1991; Cramer et al., 2004). Our

model is based upon V_s data that expands from 90 m/s to 3220 m/s and V_{s30} values from 106 m/s to 904 m/s. For intermediate V_s values (between 300 m/s and 800 m/s) our model shows a reasonable agreement with Campbell (2009) Model 1. The compatibility between both models significantly improves for higher V_s values (> 1000 m/s), where our Q estimates are closer to the values from Campbell (2009) Model 3.

3.4.3 Contribution of Shallow Layers to κ_0

Recording stations FKSH07, NGNH29, IBRH13, and IBRH10, whose V_s and damping profiles are depicted in Figure 4, are classified as sites B, C, D and E, respectively (according to classification system by the National Earthquake Hazard Reduction Program, NEHRP (Building Seismic Safety Council, 2000)). The corresponding linear regressions of κ_{r_AS} values with epicentral distance at these KiK-net stations are shown in Figure 6. Their $\Delta\kappa_{meas}$ increase with decreasing V_{s30}, from 0.023 sec at FKSH07 to 0.061 sec at IBRH10. Values of $\Delta\kappa_{meas}$ obtained at all the selected sites are plotted against V_{s30} in Figure 7. Estimates of $\Delta\kappa_{meas}$ decrease with increasing V_{s30}. In this study, $\Delta\kappa_{meas}$ values are also found to depend on the depth of the profile, hence the trends of $\Delta\kappa_{meas}$ and V_{s30} for profiles less than 150 m deep and more than 150 m are plotted separately. A better correlation between $\Delta\kappa$ and V_{s30} for shallower sites was expected because V_{s30} is a more adequate proxy for site characterization of near-surface materials. However, both linear correlations are similar.

Mean values of $\Delta\kappa_{meas}$ are computed per site class and presented in Table 5, along with their standard deviation. Mean $\Delta\kappa_{meas}$ values increase with decreasing V_{s30}, from 0.024 sec for site class C to 0.060 sec for site class E. However, the large scatter in $\Delta\kappa_{meas}$ for site class B resulted in a higher mean than the corresponding to site class C and D.

The relationship between $\Delta\kappa_{meas}$ values and the depth to bedrock (H_{800}), as inferred from the depth to a layer with V_s> 800 m/s (Cadet et al., 2010), is also examined. Values of $\Delta\kappa_{meas}$ increase as H_{800} increases, as shown in Figure 8. A similar correlation was found by Campbell (2009) when investigating the relationship between the sediment thicknesses of ENA site profiles and κ_0 values calculated using equation 3.

The correlation between κ_0 and V_{s30} is also investigated to further assess the influence of the shallow geology (i.e., top 30 m in this case) on κ_0 estimates. Both, κ_{0_surf} and κ_{0_down} are plotted in Figure 9 against their corresponding V_{s30} values. We obtain a decreasing linear trend of κ_0 with increasing V_{s30} following the classical functional form also observed by other researchers in the past. Ktenidou et al. (2015) proposed a new conceptual model for κ_0 - V_s dependence where κ_0 first decreases as the material stiffness increases, but then reaches an asymptotic value for rock. These authors then proposed that the difference between high-V_{s30} asymptotic κ_0 values might be associated with a regional characteristic of the rock. For instance, at high values of $V_{s30,}$ κ_0 for Volvi in Greece, was found to be equal to 0.021 sec (Ktenidou et al., 2015), for New Zealand κ_0 = 0.03 sec (Van Houtte et al., 2014), while data from Swiss rock sites (Edwards et al., 2015) revealed a κ_0 = 0.012 sec (Figure 9). Estimates of κ_0 at the borehole are plotted against the V_s value at the downhole instrument depth. Two asymptotic values at high V_{s30} seem reasonable from the data in Figure 9, one at κ_0 = 0.01 sec and another one at κ_0 = 0.0015 sec. Potential causes for such gap include differences in material type at the bottom of the borehole (e.g., differences in rock hardness, degree of fracturing and erosion, and type of rock), rock quality and geologic times. Other potential contributors, such as the influence of the

geographic location and complex geology that results in significant 2D site response (e.g., Van Houtte et al., 2014) were tested with our data set and were not found to be significant. Our data support previous studies showing that only using V_{s30} as a proxy for κ_0 cannot lead to accurate estimations of κ_0 and its variability (e.g., Van Houtte et al., 2014; Laurendeau et al., 2013; Edwards et al., 2015). In addition, it has been shown that the shallow layers do have a significant contribution toward the overall attenuation capture by κ_0 at the surface.

3.5 Conclusions

Values of κ-consistent damping were estimated at multiple recording stations from the large Japanese database, KiK-net to evaluate the discrepancy between field measurements of attenuation and laboratory-based damping models. Models integrating geotechnical and seismological descriptors of attenuation (i.e., κ_0, Q and ξ_{min}) were proposed and compared at all the selected sites. Typical laboratory-based damping models were found to provide the lowest estimates of minimum shear strain damping, while Δκ-based estimates result in the largest ones. Intermediate values of damping were obtained from our Q-based models. The latter was found to be in good agreement with Campbell (2009) Q-V_s models. Proposed additive models based on measured Δκ values showed that increasing minimum shear strain damping values from typically used laboratory-based models by 2% to 3%, can provide low strain damping profiles, which are more compatible with the measured κ_0 at the site. However, it is not the purpose of this paper to propose specific values of minimum shear strain damping to be added to laboratory-based estimates in order to improve the compatibility with field measurements. The κ and ξ_{min} integrated models proposed herein aim to contribute towards finding a better characterization of the

attenuation of seismic waves in the field. The latter constitutes a key step on the path to obtaining better predictions of site response, improved evaluations of site-specific seismic hazards and potentially more stable GMPEs.

The contribution of shallow layers to κ_0 estimates was also investigated. The difference between κ_0 at the surface and at depth was quantified (i.e., $\Delta\kappa$) and its correlation to shallow geologic structures explored. Values of κ_0 measured at the surface were found to have a significant contribution from the attenuation in the shallow layers; as demonstrated in plots of $\Delta\kappa$ values versus V_{s30}. Hence, we support κ models where the contributions of the attenuation in the rock mass and the overlying sediments are accounted for separately. This effective separation can also prove to be useful for site response analyses and site-specific seismic hazard assessments. An alternative definition of the κ_0 associated with the sedimentary column and based on minimum shear strain damping from geotechnical models was also examined. It underestimated the actual attenuation in the sedimentary column when compared to measured $\Delta\kappa$ values. The latter, proved to correlate well with the depth to bedrock for the sites considered in this study.

Finally, when assessing the relationship between κ_0 and V_{s30}, it was found that V_{s30} alone cannot provide accurate estimates of κ_0. Regardless of the wealth of data used in this and other studies on κ, a lot of scatter is still found on κ_0-V_{s30} relationships. In the context of the conceptual model for κ_0-V_s dependence proposed by Ktenidou et al. 2015 (where asymptotic values of κ_0 at high V_s values are associated with regional characteristics of the rock), we found that Japan data lead to two distinct asymptotic values of κ_0. Some hypotheses to explain the observed gap between κ_0 estimates were explored, but further research is necessary to fully understand the potential causes. Additionally, the

quantification of the effects of downgoing propagating seismic waves resulting from potential strong reflections from above the borehole instrument location should be assessed in future research involving the estimation of κ values at depth within vertical arrays.

References

Afshari, K. and Stewart, J.P. (2015). Effectiveness of 1D ground response analyses at predicting site response at California vertical array sites, Proc. SMIP2015 Seminar on Utilization of Strong Motion Data, California Strong Motion Instrumentation Program, Sacramento, CA (electronic file).

Al Atik, L., Kottke, A., Abrahamson, N., and Hollenback, J. (2014). Kappa (κ) Scaling of Ground-Motion Prediction Equations Using an Inverse Random Vibration Theory Approach, *Bull. Seism. Soc. Am.* **104** (1), 336-346.

Anderson, J.G., and Hough, S.E., (1984). A model for the shape of the Fourier amplitude spectrum of acceleration at high frequencies, *Bull. Seism. Soc. Am.* **74** (5), 1969-1993.

Aoi, S., Kunugi, T., and Fujiwara, H., (2004). Strong-Motion Seismograph Network Operated by NIED: K-NET and KiK-net, *Journal of Japan Association for Earthquake Engineering* **4** (3), 65-74.

Boore, D. M., and Joyner W. B., (1991). Estimation of ground motion at deep-soil sites in eastern North America, *Bull. Seism. Soc. Am.* **81**, 2167–2185.

Boore, D., (2003). Simulation of Ground Motion Using the Stochastic Method, *Pure and Applied Geophysics* **160**(3-4), 635-676.

Brune, J.N., (1970). Tectonic stress and the spectra of seismic shear waves from earthquakes, Journal of Geophysical Research **75**, 4997-5009.

Brune, J.N., (1971). Correction, Journal of Geophysical Research **76**, 5002.

Building Seismic Safety Council (2000). The 2000 NEHRP recommended provisions for new buildings and other structures: Part I (Provisions) and Part II (Commentary), *Tech. rep., FEMA 368/369*, Federal Emergency Management Agency, Washington, D.C.

Cabas A. (2016). Improvements to the Assessment of Site-Specific Seismic Hazards, *Ph.D. Thesis*, Department of Civil and Environmental Engineering, Virginia Tech, Blacksburg, VA.

Cabas, A. and Rodriguez-Marek, A. (2016), V_s-κ Correction Factors for Input Ground Motions used in Seismic Site Response Analysis, *Earthquake Spectra* (under review)

Cadet, H., P.-Y. Bard, and A. Rodriguez-Marek (2010). Defining a standard rock site: Propositions based on the KiK-net database, *Bull. Seism. Soc. Am.* **100** (1), 172–195.

Campbell, K.W., (2009). Estimates of shear-wave Q and kappa(0) for unconsolidated and semi-consolidated sediments in eastern North America, *Bull. Seism. Soc. Am.* **99**, 2365–2392.

Chandler, A.M., Lam, N.T.K., and Tsang, H.H., (2006). Near-surface attenuation modelling based on rock shear-wave velocity profile, *Soil Dynamics and Earthquake Engineering* **26** (11), 1004-1014

Chapman, M. C., P. Talwani, and R. C. Cannon (2003). Ground-motion attenuation in the Atlantic Coastal Plain near Charleston, South Carolina, *Bull. Seism. Soc. Am.* **93**, 998–1011.

Cormier, V. F. (1982). The effect of attenuation on seismic body waves, *Bull. Seism. Soc. Am.* **72**, S169–S200.

Cotton, F., F. Scherbaum, J. J. Bommer, and H. Bungum (2006). Criteria for selecting and adjusting ground-motion models for specific target regions: Application to Central Europe and rock sites, *J. Seismol*. **10** (2), 137–156.

Cramer, C. H., J. S. Gomberg, E. S. Schweig, B. A. Waldron, and K. Tucker (2004). The Memphis, Shelby Country, Tennessee, seismic hazard maps, *U.S. Geol. Surv. Open-File Rept. 04-1294.*

Chandra, J., Guéguen, P., Steidl, J.H., and Bonilla, L.F. (2015). In Situ Assessment of the G–γ Curve for Characterizing the Nonlinear Response of Soil: Application to the Garner Valley Downhole Array and the Wildlife Liquefaction Array, *Bull. Seism. Soc. Am.*, **105**, (2A), 993-1010.

Chandra, J., Guéguen, P., and Bonilla, L.F. (2016). PGA-PGV/Vs considered as a stress–strain proxy for predicting nonlinear soil response, *Soil Dyn. Earthq. Eng.*, **85**, 146–160

Dainty, A. M. (1981). A scattering model to explain seismic Q observations in the lithosphere between 1 and 30 Hz, *Geophys. Res. Lett*. **8**, 1126–1128.

Darendeli M.B. (2001). Development of a New Family of Normalized modulus reduction and material damping curves, *Ph.D. Thesis*, Department of Civil Engineering, University of Texas, Austin, TX

Dawood, H. M., Adrian Rodriguez-Marek, Jeff Bayless, Christine Goulet, and Eric Thompson (2016). A Flatfile for the KiK-net Database Processed Using an Automated Protocol. *Earthquake Spectra*, **32**, (2), 1281-1302.

Douglas, J., Gehl, P., Bonilla, L.F., and Gélis,C., (2010). A κ Model for Mainland France, *Pure appl. Geophys*., **167**, 1303–1315.

Edwards, B. & Fäh, D., (2013). Measurements of stress parameter and site attenuation from recordings of moderate to large earthquakes in Europe and the middle east, *Geophys. J. Int.*, **194**, 1190–1202.

Edwards, B., F¨ah, D. & Giardini, D., (2011). Attenuation of seismic shear wave energy in Switzerland, *Geophys. J. Int.,* **185**, 967–984.

Edwards, B., Ktenidou, O.-J., Cotton, F., Abrahamson, N.A., Van Houtte, C. & Fäh, D., (2015). Epistemic uncertainty and limitations of the κ0 model for near-surface attenuation at hard rock sites, *Geoph. J. Int.,* **202**, 1627–1645.

Elgamal A., Lai T., Yang Z., He L. (2001). Dynamic soil properties, seismic downhole arrays and applications in practice, *Proceedings, 4th International Conference on Recent Advances in Geotechnical Earthquake Engineering and Soil Dynamics*, S. Prakash, ed., San Diego, CA.

Electric Power Research Institute (1993). Guidelines for Determining Design Basis Ground Motions, *Final Report, EPRI TR-102293*, Palo Alto, CA, November.

Fujiwara, H., S. Aoi, T. Kunugi, and S. Adachi (2004). Strong-motion Observation Networks of NIED: K-NET and KiK-net, Technical report, Consortium of Organizations for Strong-Motion Observation Systems (COSMOS). http://www.cosmos-eq.org/events/wkshop_records _processing/presentations/Fujiwara.pdf.

García D., Wald D.J., Hearne M.G. (2012). A global earthquake discrimination scheme to optimize ground-motion prediction equation selection, *Bull. Seismol. Soc. Am.* **102**(1): 185–203.

Goodman, L.E. (1988). *Material damping and slip damping*, Chapter 36 in C.M. Harris, ed., Shock and Vibration Handbook, 3rd ed., McGraw-Hill, New York.

Guéguen P. (2015). Predicting nonlinear site response using spectral acceleration vs. PGV/Vs30: A case history using the Volvi-test site, *Pure and Applied Geophysics*. doi: 10.1007/s00024-015-1224-5

Hough, S.E. & Anderson, J.G., 1988. High-frequency spectra observed at Azna, California: implications for Q structure, *Bull. Seism. Soc. Am.* **78**, 692–707.

Kim B, Hashash Y.M.A., Kottke A., Assimaki D., Li W., Rathje E.M., Campbell K.W., Silva W.J., Stewart J.P., (2013). A predictive model for the relative differences between nonlinear and equivalent-linear site response analyses, *22nd Conference on Structural Mechanics in Reactor Technology (SMiRT22)*. San Francisco. August 18-23.

Kim, B., Youssef M. A. Hashash, Jonathan P. Stewart, Ellen M. Rathje, Joseph A. Harmon, Michael I. Musgrove, Kenneth W. Campbell, and Walter J. Silva (2016) Relative Differences between Nonlinear and Equivalent-Linear 1D Site Response Analyses. *Earthquake Spectra* (In-Press.)

Kinoshita, S. (1998). Kyoshin net (K-NET), *Seismol. Res. Lett.* **69**, (4), 309–332.

Knopoff, K., (1964). Q, *Reviews of Geophysics* **2**(4), 625-660.

Knopoff, K., and MacDonald, G. J. F., (1958). Attenuation of small amplitude stress waves in solids, *Reviews of Modern Physics* **30**(4), 1178-1192.

Kramer, S., (1996). *Geotechnical Earthquake Engineering*, Prentice Hall, Upper Saddle River, NJ.

Ktenidou, O.J., Abrahamson, N.A., Drouet, S., and Cotton, F., (2015). Understanding the Physics of Kappa (K): Insights from a downhole array. *Geophysical Journal International* **203**(1), 678-691.

Ktenidou, O.J., Cotton, F., Abrahamson, N.A., and Anderson, J.G., (2014). Taxonomy of κ: A Review of Definitions and Estimation Approaches Targeted to Applications, *Seismological Research Letters* **85**(1), 135-146.

Ktenidou, O.J., Gélis, C., and Bonilla, L.F., (2013). A study on the variability of kappa (κ) in a borehole: Implications of the computation process, *Bull. Seism. Soc. Am.* **103**(2A), 1048–1068.

Laurendeau, A., F. Cotton, O.-J. Ktenidou, L.-F. Bonilla, and F. Hollender (2013). Rock and stiff soil site amplification: Dependency on VS30 and kappa (κ0), *Bull. Seism. Soc. Am.* **103**, (6), 3131–3148.

Menq F.Y. (2003). Dynamic Properties of Sandy and Gravelly Soils, Ph.D. Thesis, Department of Civil Engineering, University of Texas, Austin, TX.

Nakano, K., Shinichi Matsushima, and Hiroshi Kawase, (2015). Statistical Properties of Strong Ground Motions from the Generalized Spectral Inversion of Data Observed by K-NET, KiK-net, and the JMA Shindokei Network in Japan, *Bull. Seism. Soc. Am.* **105**, (5), 2662–2680.

National Research Institute for Earth Science and Disaster Prevention (NIED), 1996. Strong Motion Seismograph Networks (K-NET, KiK-net), <http://www.kyoshin.bosai.go.jp/> (Oct. 9, 2014).

Parolai, S., and D. Bindi (2004). Influence of soil-layer properties on k evaluation, *Bull. Seism. Soc. Am.* **94**, 349–356.

Pei, S., Cui, Z., Sun, Y., Toksöz, M. N., Rowe,C.A., Gao, X., Zhao, J., Liu, H., He, J., and Morgan, F.D., (2009). Structure of the Upper Crust in Japan from S-Wave Attenuation Tomography. *Bull. Seism. Soc. Am.* **99**, (1), 428–434.

Poggi, V., Edwards, B., and Fäh, D., (2013). Reference S-wave velocity profile and attenuation models for ground-motion prediction equations: application to Japan, *Bull. Seism. Soc. Am.* **103**, 2645–2656.

Rathje, E., Kottke, A., and Trent, W., (2010). Influence of Input Motion and Site Property Variabilities on Seismic Site Response Analysis, *Journal of Geotechnical and Geoenvironmental Engineering* **136**(4), 607-619.

Régnier, J., (2013). Variability of Seismic Response: Classification of Sites Based on the Non-Linear Behavior of Soils, Ph.D. Dissertation, Université Paris-Est, Paris, France (in French).

Rodriguez-Marek, A., Rathje, E. M., Bommer, J. J., Scherbaum, F., and Stafford, P. J., (2014). Application of Single-Station Sigma and Site-Response Characterization in a Probabilistic Seismic-Hazard Analysis for a New Nuclear Site. *Bull. Seism. Soc. Am.* **104**, (4), doi: 10.1785/0120130196

Silva, W., and R. B. Darragh (1995). Engineering characterization of strong ground motion recorded at rock sites, Technical report, Electric Power Research Institute, El Cerrito, California. *EPRI Report TR- 102262.*

Silva, W., Darragh, R., Gregor, N., Martin, G., Abrahamson, N. & Kircher, C., (1998). Reassessment of site coefficients and near-fault factors for building code provisions, *technical report program element II: 98-HQGR- 1010*, Pacific Engineering and Analysis, El Cerrito, USA.

Silva, W.J., (1997). Characteristics of vertical strong ground motions for applications to engineering design, in Proceedings of the FHWA/NCEER Workshop on the National

Representation of Seismic Ground Motion for New and Existing Highway Facilities, eds Friedland, I.M., Power,M.S. & Mayes, R.L., *Technical Report NCEER-97-0010*.

SSHAC, (1997). Recommendations for probabilistic seismic hazard analysis: Guidance on uncertainty and use of experts *(NUREG/CR-6372)*, US Nuclear Regulatory Commission Washington, DC.

Stewart, J.P., Afshari, K. and Hashash, Y.M.A., (2014). Guidelines for Performing Hazard-Consistent One-Dimensional Ground Response Analysis for Ground Motion Prediction. *PEER Report*.

Tsai C.C., Hashash Y.M.A. (2009). Learning of dynamic soil behavior from downhole arrays, ASCE, *J. Geotech. Eng.*, **135**(6): 745–757.

Tsuda, K., Steidl, J., Archuleta, R., Assimaki, D., (2006). Site-Response Estimation for the 2003 Miyagi-Oki Earthquake Sequence Considering Nonlinear Site Response, *Bull. Seism. Soc. Am.* **96**, (4A), 1474–1482.

Van Houtte, C., Drouet, S., and Cotton, F., (2011). Analysis of the origins of κ (Kappa) to compute hard rock to rock adjustment factors for GMPEs, *Bull. Seism. Soc. Am.* **101**, 2926–2941.

Van Houtte, C., Ktenidou, O.-J., Larkin, T. & Holden, C., (2014). Hard-site κ0 (kappa) calculations for Christchurch, New Zealand, and comparison with local ground motion prediction models, *Bull. Seism. Soc. Am.* **104**, 1899–1913.

Yee E., Stewart J.P., Tokimatsu K. (2013). Elastic and large-strain nonlinear seismic site response from analysis of vertical array recordings, ASCE, *J. Geotech. Eng.*, **139**(10): 1789–1801.

Table 1: Proposed categorization scheme for defining appropriate sites for κ_0 calculations.

Station Ranking	Selection of f_1 & f_2	Consistency ratio [c]	# of records per regression*
1	Unambiguous, consistent across ground motions	c >65%	>30
2	Generally easy. Less than 50% of the ground motions have problematic spectral shapes	30%< $c \leq$ 65%	≥20
3	Challenging. More than 50% of the ground motions have problematic spectral shapes	15%< $c \leq$ 30%	<20
4	Hard and ambiguous. Debatable for most ground motions	$c \leq$ 15%	<20

**for either surface or depth conditions*

Table 2: Nomenclature used in this study and their definitions.

Symbol	Definition
κ or κ_r	individual measurement of κ
κ_{r_AS}	individual κ values measured specifically on the acceleration Fourier spectrum (after Ktenidou et al., 2014)
κ_R	slope of the linear regression on κ_r with epicentral distance
κ_0	site-specific, distance-independent κ
κ_{0_surf}	estimates of κ_0 at the surface
κ_{0_down}	estimates of κ_0 at the downhole instrument depth
$\Delta\kappa$ or $\Delta\kappa_{meas}$	constant difference across epicentral distances between linear regressions of surface and downhole values of κ_r
$\kappa_{damping}$	κ_0 for the sedimentary column (calculated in this study based on ξ_{min}, V_s and the thickness of each layer in the profile)
ξ_{min}	minimum shear strain damping
$\Delta\xi_{min}$	Estimates of ξ_{min} to be added to original laboratory-based values
ψ	Proposed correction factor for ξ_{min}
Q or Q_{ef}	seismic quality factor or efective seismic quality factor
γ	proportionality constant in Q-V_s relationships

Table 3: Measured κ values along with the corresponding V_{s30} and site class at each selected station. The standard deviations from the regressions and the proposed correction factor, ψ, are also provided.

Station Name	V_{s30} (m/s)	Site Class	κ_{0_down}	$\Delta\kappa$	κ_{0_surf}	κ_R	σ	Mean $\kappa_{damping}$	ψ
YMTH13	577.0	C	0.0087	0.017	0.0253	0.0002	0.009	0.0017	9.9
FKSH01	703.6	C	0.0094	0.021	0.0300	0.0002	0.009	0.0012	17.7
FKSH03	349.7	D	0.0013	0.033	0.0343	0.0005	0.014	0.0032	10.3
FKSH05	596.0	C	0.0028	0.018	0.0213	0.0003	0.012	0.0016	11.8
NIGH08	326.9	D	0.0017	0.031	0.0329	0.0004	0.013	0.0055	5.7
FKSH06	680.2	C	0.0019	0.020	0.0214	0.0003	0.011	0.0014	14.1
FKSH07	828.9	B	0.0021	0.023	0.0254	0.0002	0.011	0.0015	15.9
TCGH08	723.2	C	0.0074	0.017	0.0245	0.0002	0.011	0.0020	8.7
FKSH21	364.9	C	0.0008	0.037	0.0377	0.0002	0.013	0.0027	13.8
TCGH12	343.7	D	0.0319	0.033	0.0653	0.0001	0.016	0.0030	11.3
FKSH12	448.5	C	0.0005	0.049	0.0492	0.0003	0.023	0.0016	30.6
IBRH18	558.6	C	0.0109	0.048	0.0586	0.0002	0.013	0.0034	14.1
IBRH14	829.1	B	0.0005	0.073	0.0739	0.0002	0.014	0.0011	68.9
IBRH13	335.4	D	0.0006	0.055	0.0557	0.0003	0.021	0.0019	29.6
TCGH16	213.2	D	0.0292	0.042	0.0708	0.0001	0.009	0.0040	10.3
TCGH10	371.5	C	0.0208	0.020	0.0405	0.0002	0.015	0.0030	6.7
FKSH10	487.0	C	0.0023	0.015	0.0177	0.0003	0.012	0.0030	5.2
IBRH12	485.7	C	0.0192	0.015	0.0345	0.0001	0.009	0.0026	5.9
IBRH17	300.8	D	0.0011	0.028	0.0293	0.0002	0.015	0.0080	3.5
IBRH15	450.4	C	0.0025	0.006	0.0088	0.0002	0.007	0.0022	2.9
TCGH13	573.6	C	0.0118	0.006	0.0176	0.0002	0.010	0.0017	3.3
IBRH11	242.5	D	0.0019	0.024	0.0256	0.0002	0.011	0.0024	9.7
IBRH19	692.3	C	0.0025	0.011	0.0131	0.0001	0.010	0.0017	6.2
NIGH18	311.1	D	0.0016	0.028	0.0292	0.0005	0.028	0.0027	10.2
GIFH19	744.1	C	0.0167	0.023	0.0395	0.0003	0.011	0.0013	18.1
GIFH15	369.2	C	0.0196	0.036	0.0554	0.0002	0.012	0.0025	14.1
GIFH13	592.6	C	0.0109	0.037	0.0480	0.0002	0.010	0.0023	16.0
ISKH09	635.8	C	0.0152	0.021	0.0365	0.0002	0.012	0.0017	12.6
NIGH17	383.4	C	0.0526	0.025	0.0772	-0.0001	0.013	0.0032	7.8
NIGH13	461.1	C	0.0712	0.016	0.0875	0.0000	0.014	0.0020	8.2
NGNH29	464.9	C	0.0219	0.042	0.0639	0.0001	0.012	0.0022	19.1
NIGH14	437.6	C	0.0227	0.041	0.0634	-0.000002	0.010	0.0043	9.6
NIGH15	685.8	C	0.0014	0.020	0.0217	0.0002	0.011	0.0015	13.4
NIGH11	375.0	C	0.0511	0.011	0.0621	-0.00001	0.012	0.0039	2.8

Table 3 (continued)

Station Name	V_{s30} (m/s)	Site Class	κ_{0_down}	$\Delta\kappa$	κ_{0_surf}	κ_R	σ	Mean $\kappa_{damping}$	ψ
AKTH18	431.0	C	0.0306	0.012	0.0421	0.0001	0.010	0.0024	4.8
AKTH03	320.2	D	0.0006	0.031	0.0318	0.0005	0.011	0.0028	11.1
AKTH04	458.7	C	0.0151	0.020	0.0347	0.0003	0.014	0.0018	11.0
AICH07	428.1007	C	0.0019	0.0137	0.0156	0.0002	0.0101	0.0020	6.8
CHBH10	252.3711	D	0.0398	0.0328	0.0726	0.0000	0.0145	-	-
CHBH13	234.5178	D	0.0204	0.0189	0.0393	0.0001	0.0142	-	-
FKIH06	395.6044	C	0.0181	0.0402	0.0582	0.0002	0.0122	0.0023	17.3
FKOH08	535.7787	C	0.0192	0.0380	0.0572	0.0003	0.0107	0.0016	23.6
FKSH09	584.6235	C	0.0016	0.0522	0.0538	0.0002	0.0152	0.0018	29.8
FKSH14	236.5613	D	0.0425	0.0235	0.0659	0.0001	0.0108	0.0037	6.3
GIFH11	904.1519	B	0.0019	0.0304	0.0323	0.0002	0.0117	0.0009	32.2
GNMH07	647.482	C	0.0057	0.0098	0.0155	0.0002	0.0145	0.0019	5.0
IBRH07	106.8345	E	0.0165	0.0589	0.0754	0.0000	0.0114	-	-
IBRH10	144.1379	E	0.0019	0.0617	0.0636	0.0000	0.0211	0.0114	5.4
IBRH20	243.871	D	0.0334	0.0102	0.0436	0.0001	0.0146	0.0112	0.9
IWTH27	670.3125	C	0.0222	0.020	0.0424	0.0000	0.012	0.0013	16.0
KMMH01	574.631	C	0.0203	0.047	0.0674	0.0003	0.011	0.0014	32.9
MYGH09	358.2453	D	0.0225	0.034	0.0568	0.0001	0.013	0.0024	14.3
MYGH10	347.5373	D	0.0201	0.040	0.0596	0.0001	0.011	0.0039	10.2
NIGH06	336.1373	D	0.0206	0.047	0.0679	0.0001	0.013	0.0026	18.1
NIGH07	528.1931	C	0.0014	0.030	0.0318	0.0003	0.012	0.0016	18.6
NIGH09	462.9349	C	0.0198	0.021	0.0406	0.0001	0.009	0.0020	10.2
TCGH06	371.25	C	0.0004	0.011	0.0113	0.0002	0.015	-	-
TCGH07	419.4915	C	0.0187	0.018	0.0368	0.0001	0.007	0.0018	10.3
TCGH09	468.4015	C	0.0240	0.009	0.0327	0.0001	0.014	0.0019	4.5
TCGH14	849.0051	B	0.0240	0.004	0.0279	0.0001	0.010	0.0011	3.6

Table 4: Comparisons between κ-based estimates of Q and values from the literature.

		Pei et al. (2009)			
Cluster #	Average Q from κ_R per station	Q from κ_R per cluster	Q_0	Q (f=11 Hz)	Q (f=25Hz)
1	1084	1190	105	866	1784
2	1819	2226	280	2310	4757
3	1471	2584	105	866	1784
4	1675	1291	105	866	1784

Table 5: Mean $\Delta\kappa_{meas}$ values and standard deviations per site class.

Site Class	Mean $\Delta\kappa_{meas}$ (sec)	σ (sec)
B	0.033	0.025
C	0.024	0.013
D	0.032	0.010
E	0.060	0.001

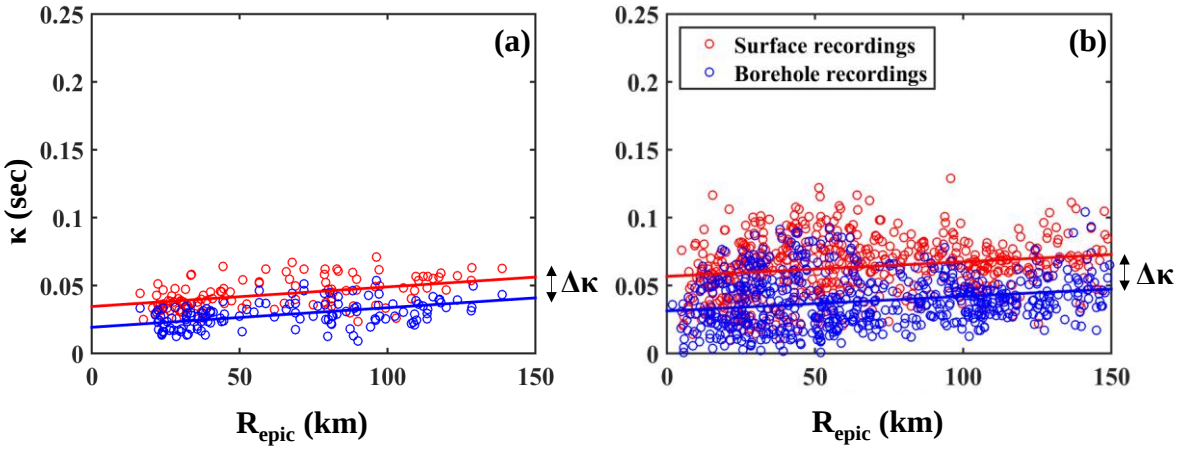

Figure 1: Linear regressions of individual measurements of κ against epicentral distances at (a) station IBRH12, and (b) Cluster #3.

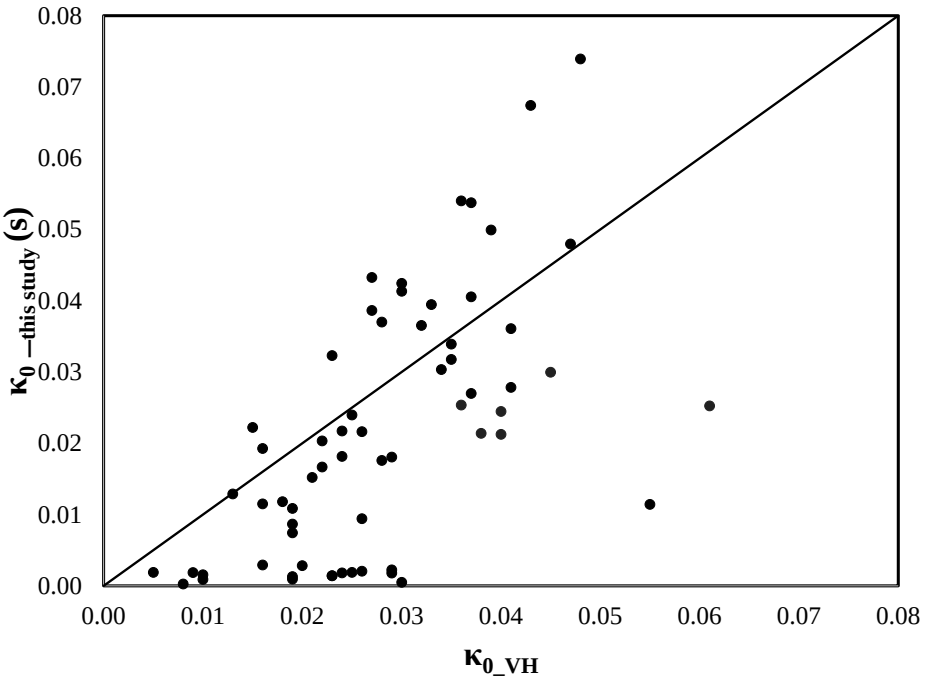

Figure 2: Comparison of κ_0 values from Van Houtte et al. (2011) and the estimates presented in this study. The black line depicts a 1:1 relationship.

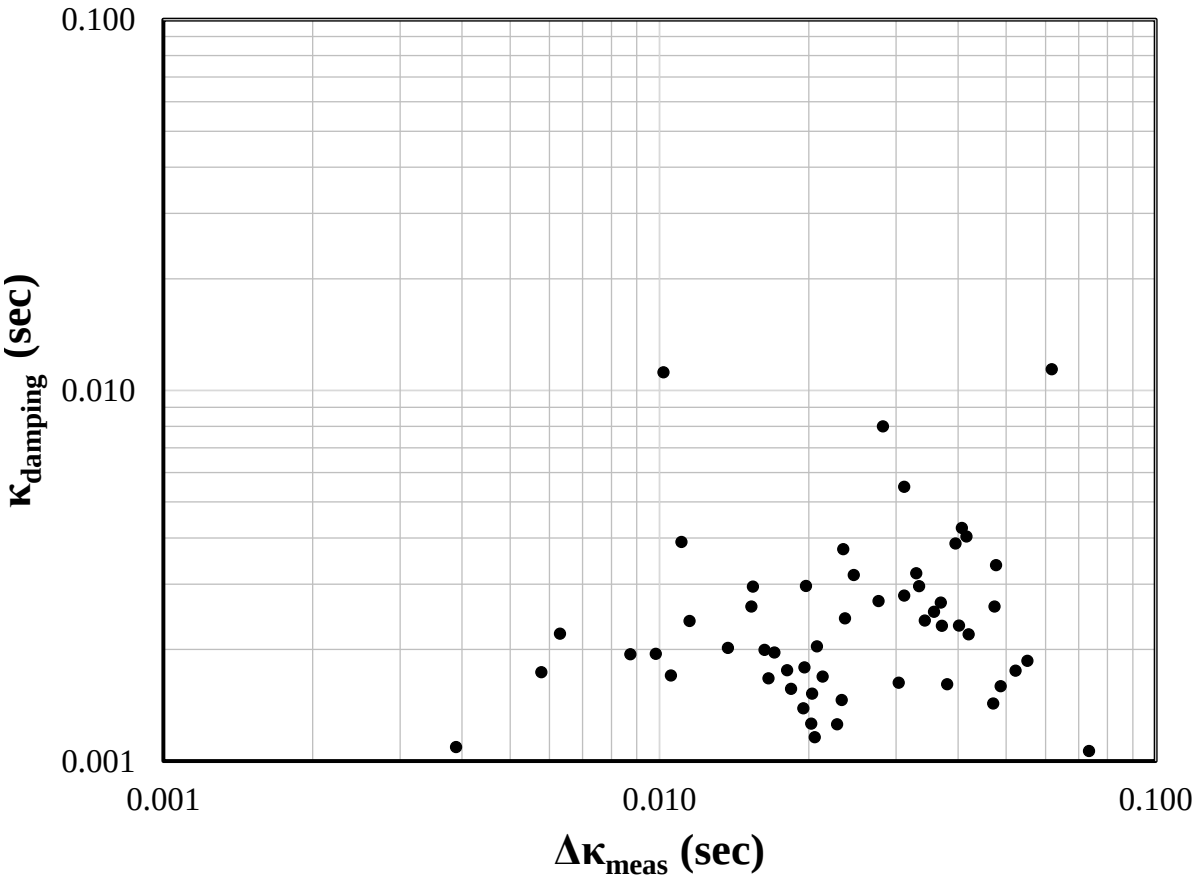

Figure 3: Values of $\kappa_{damping}$ and $\Delta\kappa$ measured from linear regressions at the sixty study sites.

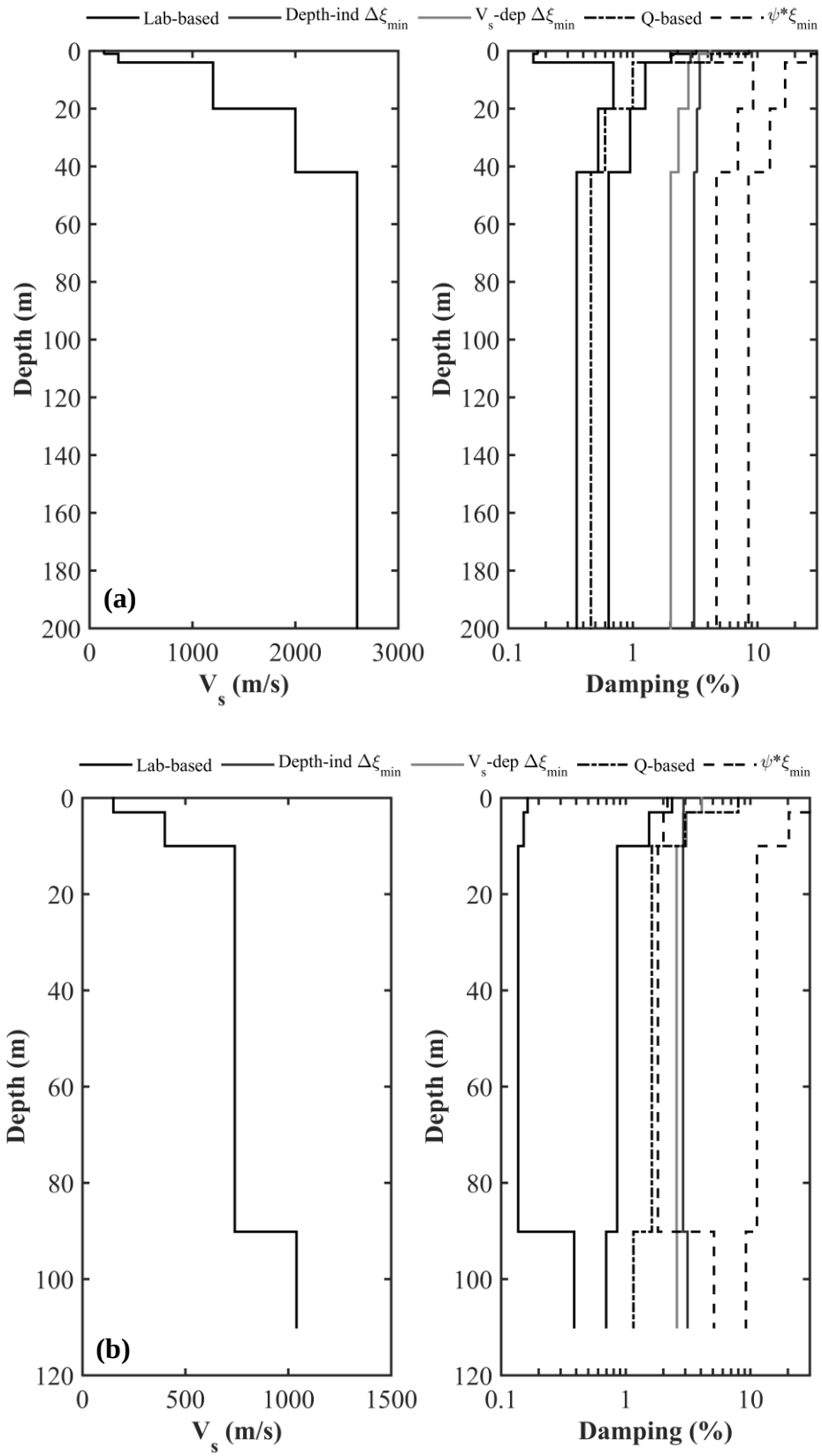

Figure 4: Shear wave velocity and minimum shear strain damping profiles at (a) FKSH07, (b) NGNH29, (c) IBRH13, and (d) IBRH10.

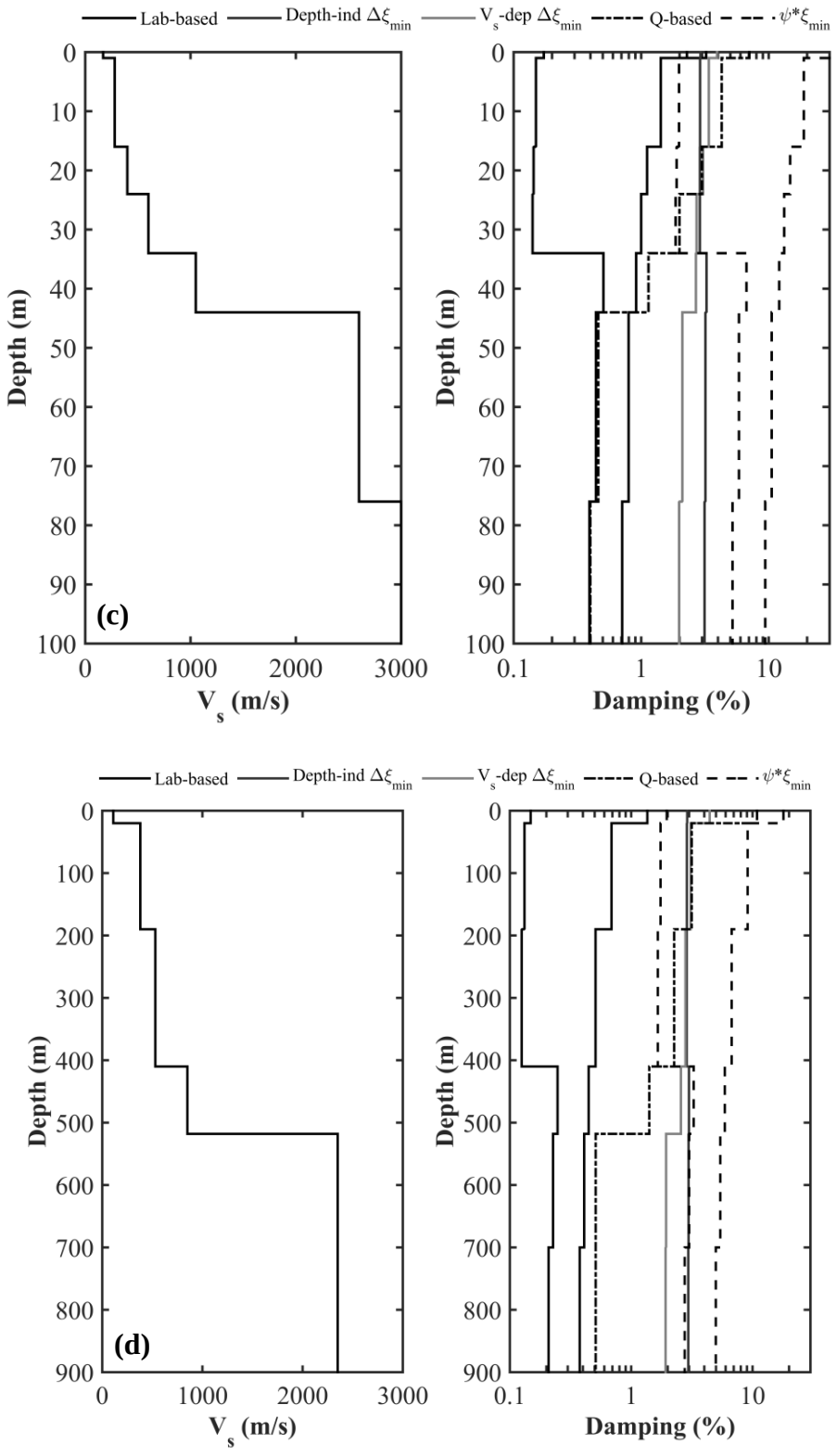

Figure 4 *(cont.)***:** Shear wave velocity and minimum shear strain damping profiles at (a) FKSH07, (b) NGNH29, (c) IBRH13, and (d) IBRH10.

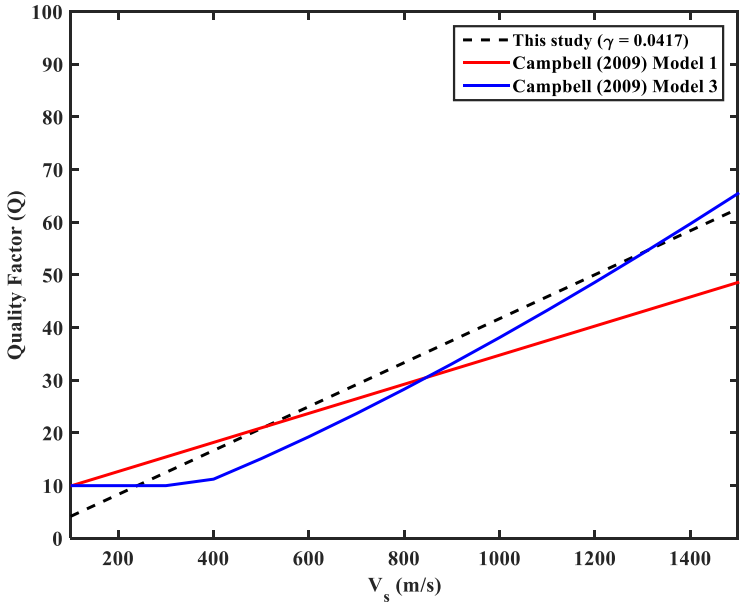

Figure 5: Comparison of Q-V_s models from this study and Campbell (2009).

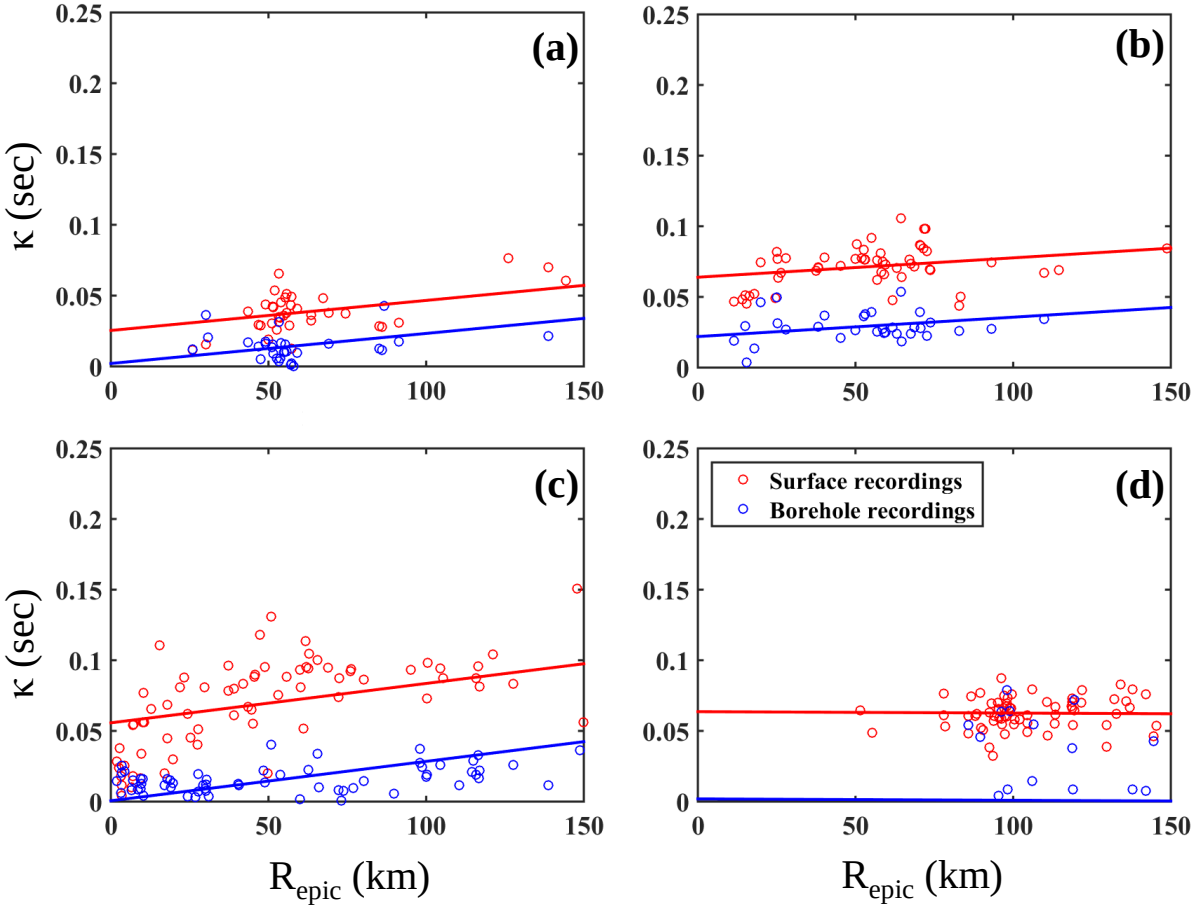

Figure 6: Linear regressions of individual measurements of κ at (a) FKSH07, (b) NGNH29, (c) IBRH13, and (d) IBRH10.

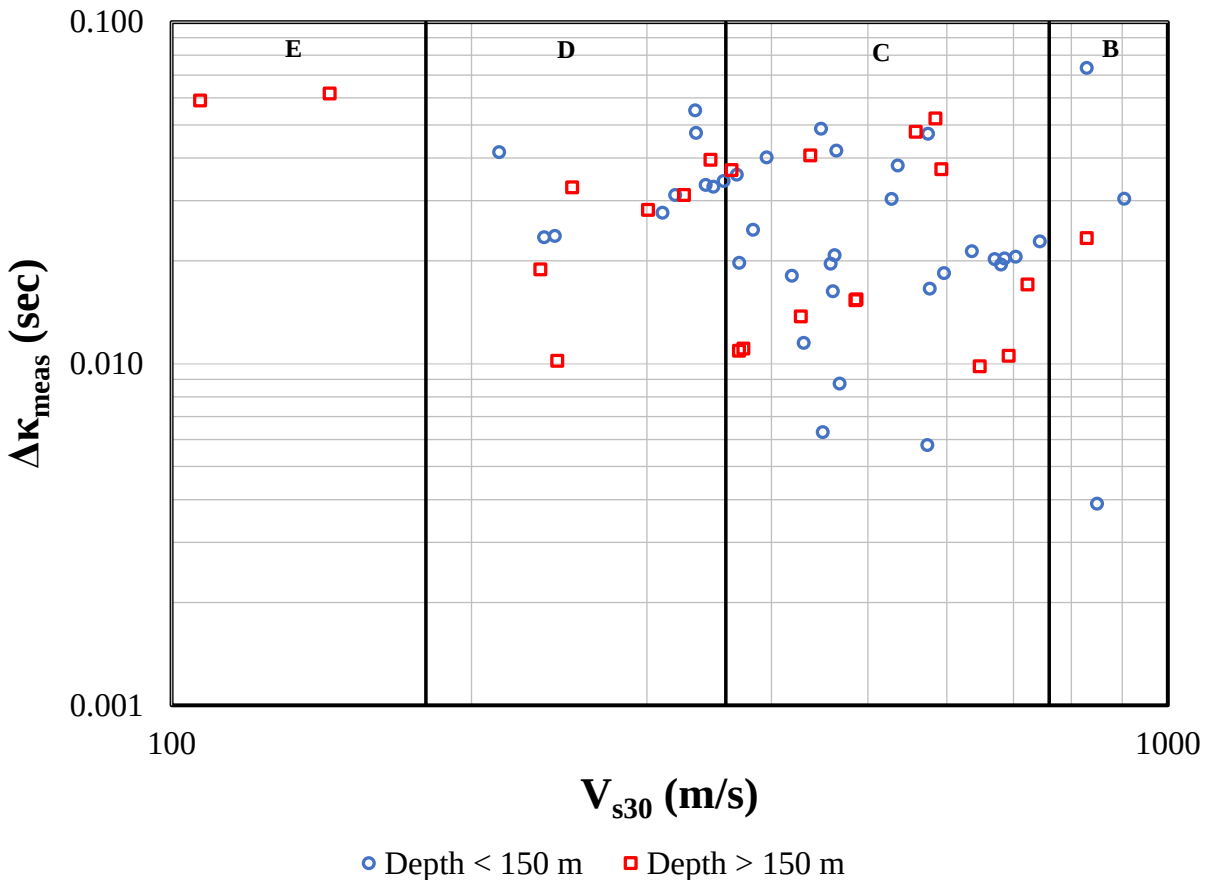

Figure 7: Measured Δκ values at the selected sites versus the corresponding V_{s30}.

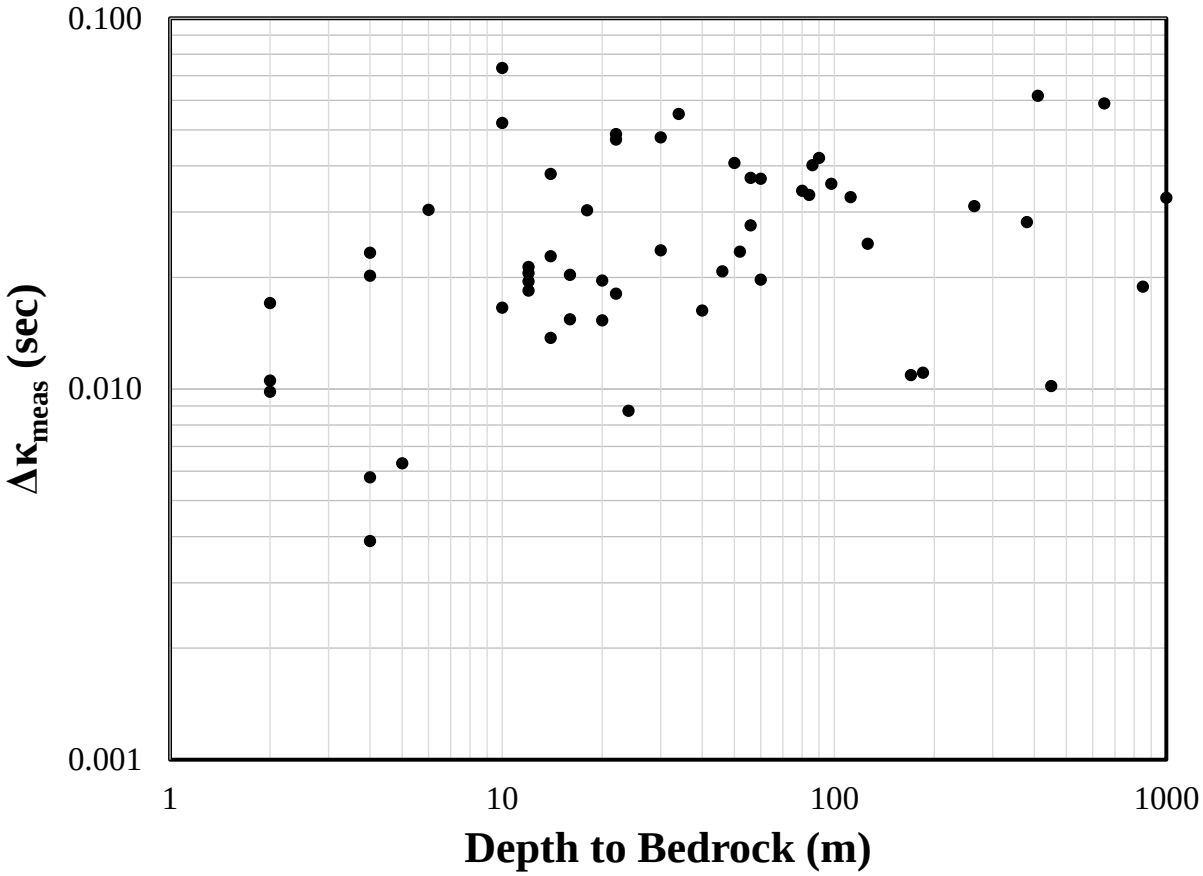

Figure 8: Measured Δκ values at the selected sites versus the corresponding depth to bedrock (as inferred from the depth to a layer with V_s> 800 m/s).

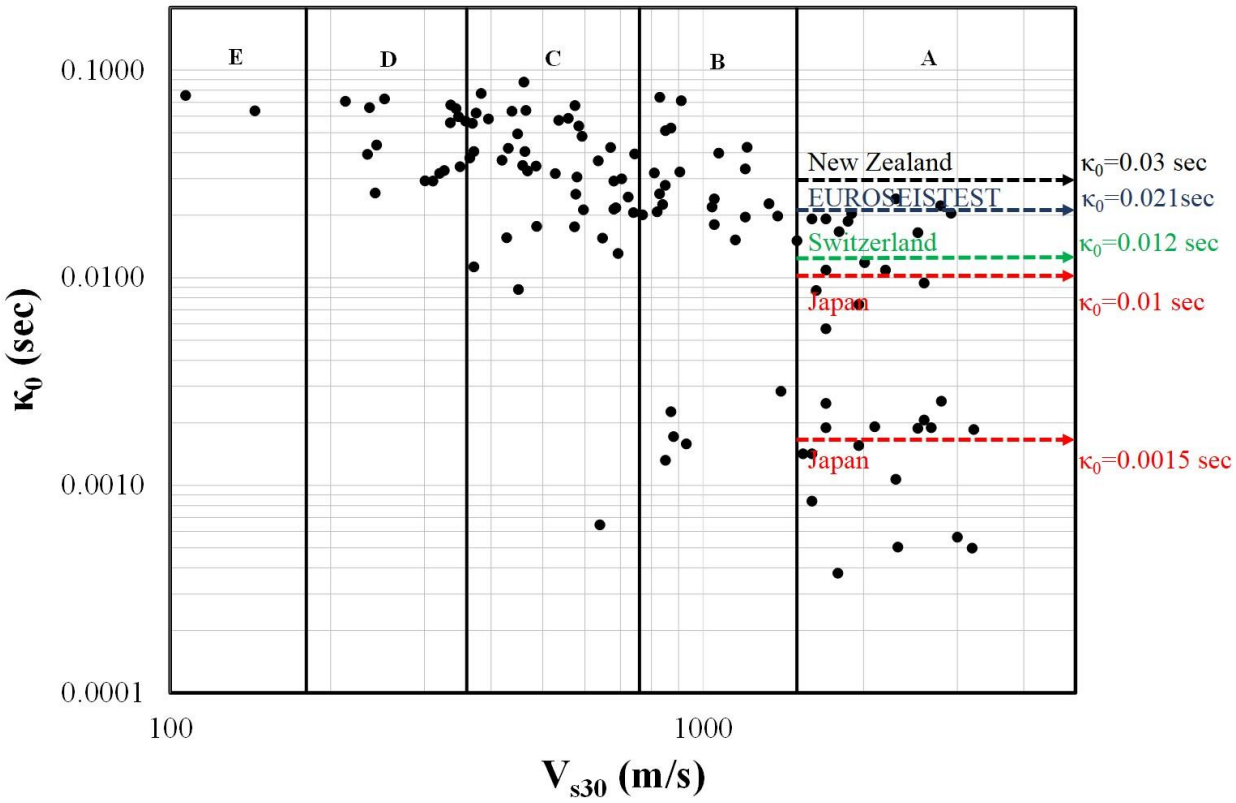

Figure 9: Estimates of κ_0 at the selected study sites versus V_{s30}. Regional asymptotic values proposed by previous studies in New Zealand, Switzerland, and Greece are provided along with two potential κ_0 values for hard rock and stiff sites in Japan.

CHAPTER FOUR

THE IMPORTANCE OF THE SELECTION OF THE ELASTIC HALF-SPACE IN SITE RESPONSE ANALYSIS

Abstract

One of the fundamental decisions when conducting one-dimensional site response analyses (SRA) involves the selection of the depth and characteristics of the elastic half-space (EHS). This boundary condition assumes linear and homogenous material for an infinite depth, and as a result, waves that are potentially reflected from deeper material boundaries in the actual geologic profile are not considered in the numerical site response. If a strong soil-rock impedance contrast is present at the site of interest, the EHS boundary is typically set at this depth. However, for many profiles, the selection of the EHS depth and characteristics is not intuitive and can lead to significant errors in site response. A parametric study is conducted on a three-layer model and shows that the presence of a strong impedance contrast is not enough to define the EHS location. The shear wave velocity and thickness of the shallow soil deposits are also influential factors. Two case histories of sites where the selection of the EHS impacts the accuracy of SRA are presented. For instance, the presence of soft interbeds below the assumed location of the EHS can introduce strong errors. Conversely, a case in which a stronger impedance contrast is located at much greater depths (such as in study sites in Charleston, NC), the EHS can be assumed to be at the shallower impedance contrast.

4.1 Introduction

The objective of this study is to quantify the effects of the strata that lie below the assumed location of the elastic half-space (EHS) boundary in site response analyses (SRA). The assumptions inherent to EHS boundary condition are not always met when a geologic profile is modeled numerically, hence the associated error and implications on estimates of site response are investigated herein. An EHS implies linear and homogenous material for an infinite depth, and as a result the EHS absorbs a portion of the downward-propagating seismic waves in the overlying profile. These conditions are typically satisfied by hard rock materials with high shear wave velocity (V_s), which are often located at great depths so that there are no significant impedance contrasts below them.

Selecting the appropriate depth and properties of EHS boundary for one-dimensional (1D) SRA often requires engineers to overcome hurtles related to the subsurface characterization of a site. These hurtles, which can arise from budgetary and/or technological constraints, can prevent the proper identification of layers that meet the EHS assumptions. Selection of the depth and properties of the EHS can prove challenging even if adequate data about the profile under study is available, if the profile has particularities such as velocity reversals. Furthermore, the correct identification of the EHS boundary condition at a site must be accompanied by the selection of input ground motions that are compatible with the assumed EHS properties. However, the lack of motions recorded on hard rock (e.g., V_{s30} > 1500 m/s) conditions imposes yet another challenge.

This paper examines cases where the selection of the EHS boundary impacts the accuracy of 1D SRA. To this end, the effects of different profiles and layer properties for assumed EHS boundary are investigated. Case studies of profiles for which the selection of the EHS

boundary is not obvious are also presented. Then, based on the discussion of the results from the analyses conducted, we provide insights regarding the importance of the EHS selection in estimating site response.

4.2 Background

4.2.1 The Elastic Half-space Assumption

One of the fundamental decisions when conducting one-dimensional (1D) SRA involves the selection of the depth and characteristics of the EHS. This boundary is usually defined at a horizon sufficiently stiff such that the assumption of linear behavior will likely hold and no subsequent strong impedance contrast is expected below this depth. However, there is still no consensus on the specific properties of the EHS (e.g., Cadet et al., 2010; Laurendeau et al., 2013). Some characteristics associated with reference rock sites as found in the literature and official regulations around the world are presented in Table 1, where the reference rock is analogous to the EHS.

Selection of bedrock as the EHS implies that bedrock is fully elastic and that a portion of the energy of downward-propagating seismic waves will be completely absorbed by the rock mass. This latter condition is not satisfied if the bedrock is not homogeneous. In this case, some of the energy of downward-traveling waves at depth below the assumed EHS boundary will be reflected upward from deeper impedance boundaries in the actual geologic profile. These waves are not considered in the numerical site response analyses. If the EHS conditions are satisfied, the ratio of the absorbed and reflected waves is a function of the impedance contrast between the materials at either side of the EHS boundary (Kramer, 1996).

4.2.2 Reference Rock and Decoupling in Site Response Analysis

The effects of wave propagation in material below the selected depth of the EHS boundary are not captured in numerical analyses of site response; hence, these effects must be inherent in the selected motions for use in the SRA. Thus, all SRA imply decoupling, where the site is truncated at the reference depth (i.e., the EHS boundary) and the effects of deeper strata on site response are decoupled from the assessment of shallower layers. Despite the proliferation of strong ground motion recordings worldwide, it can be difficult to find recording stations with similar V_s profiles and attenuation characteristics to the assumed EHS at the site of interest. Also, when the EHS boundary is placed at great depths within layers with high V_s values, the number of compatible recording stations is significantly reduced. Additionally, decoupled SRA can be representative of a two-step process, where the response of a certain portion of the profile is first assessed up to a horizon of interest, and then the rest of the profile is analyzed. This can occur in practice when the subsurface characterization of a site is known only up to a certain horizon. If shallower deposits vary significantly across that site, and will be characterized later on in the project, it might be desirable to conduct SRA up to such horizon where sufficient information is available first. Results from those analysis could be then combined with the response of the shallower deposits, once more details on their properties become available.

Decoupled analyses are common practice, but the degree to which they introduce errors in the estimation of site response has received rather limited attention to date. Likewise, the epistemic uncertainty they add to the analysis of seismic hazards is usually overlooked. A schematic representation of decoupled site response models as compared to a full column analysis is shown in Figure 1. Comprehensive information on the V_s profile for the simple

three-layer model depicted in Figure 1 would allow for the positioning of the EHS boundary condition at the soft rock/hard rock horizon (i.e., point C). However, V_s data is often limited only to the first strong impedance contrast, in which case the EHS boundary condition is often assumed to lie at the interface between soil and the softer rock (i.e., point B). The assumption of the location of the EHS at either interface is not an issue for site response analyses, as long as the selected input motions are compatible with the corresponding properties of the assumed EHS in each case. However, the lack of ground motions recorded at sites with high V_s values, often leads to selecting ground motions recorded at soft rock sites to be applied to a much harder reference rock profile. Moreover, the profile below the assumed EHS boundary at the site under analysis can be significantly different from the profile at the recording station.

4.3 Methodology

The comparison between full column and decoupled SRA cannot be made directly because of the difference in input motions inherently required for each analysis. Hence, our methodology is mainly based on the comparison of the transfer function (TF) for the complete profile (what we hereafter refer to as full column analysis) and the TF for the decoupled model. By comparing the resulting amplifications for each case, we can estimate the error associated with selecting the depth and properties of the EHS in a numerical SRA that are not in accord with implied characteristics of an EHS. In this study, we only conduct linear elastic SRA, so that the impact of the EHS boundary can be assessed without being obscured by nonlinear effects.

4.3.1 Full Resonance Methods and the Square-Root Impedance Method

We conduct linear elastic SRA by using theoretical formulations for wave propagation in layered media (hereafter referred to as full resonance or FR methods) as well as the square-root impedance method (SRI). Full resonance method is an approach to 1D SRA based on the vertical propagation of horizontally polarized shear waves through horizontally layered near-surface materials. All layers are assumed to be of infinite lateral extent and both upward and downward propagating waves are considered in the estimation of the TF. However, the necessary conditions to experience the full effects of constructive and destructive interference of seismic waves (i.e., resonance effects) stem from assumptions of uniformity and homogeneity of the site and the synchronized times of arrival of sequential reverberations. Field conditions, such as lateral variations in the V_s or deviations from horizontal layering, may not allow resonances to build over time, in which case such resonances are considered spurious (Kramer, 1996; Boore, 2013). Commonly used software such as SHAKE (Schnabel et al., 1972; Idriss and Sun 1992), STRATA (Kottke and Rathje, 2008a, b), or DEEPSOIL (Hashash et al., 2015) apply FR methods either using 1D equivalent-linear, EQL (e.g., SHAKE, STRATA, and DEEPSOIL) or nonlinear approaches (e.g., DEEPSOIL).

The SRI method was proposed by Joyner et al. (1981) who applied ray theory to estimate site amplification. The method is based on the influence of the impedance contrasts in a profile and it does not account for the effects associated with the resonance. As indicated by Boore (2013), amplifications resulting from procedures that account for resonance are sensitive to changes in the EHS properties.

4.3.2 Full Column versus Decoupled Analyses

The three-layer profile shown in Figure 1 is used subsequently to introduce the mathematical formulation of the TF for the full column and decoupled model. The TF for the full column is equal to the ratio of the acceleration Fourier amplitudes of the motions at the surface and Rock I – Rock II interface:

$$(TF)_{FULL} = \frac{FAS_{Surface}}{FAS_{Rock\ II}} \tag{1}$$

where FAS refers to the acceleration Fourier amplitude spectrum of outcrop ground motions for the depth indicated by the subscript. The TF for the decoupled model is obtained by multiplying the amplifications for each decoupled profile, *DI* and *DII*, as presented in Figure 1:

$$(TF)_{DECOUPLED} = \frac{FAS_{Rock\ I}}{FAS_{Rock\ II}} \frac{FAS_{Surface}}{FAS_{Rock\ I}} \tag{2}$$

The SRI method provides a transparent and simple way of estimating linear site amplifications, *A*:

$$A = \left(\frac{Z_R}{\bar{Z}}\right)^{1/2} = \left(\frac{\rho_R V_R}{\bar{\rho}\,\bar{V}}\right)^{1/2} \tag{3}$$

where Z_R refers to the seismic impedance (i.e., the product of the density and seismic wave propagation velocity of the medium) at the reference rock, while $\bar{Z}$ is the average seismic impedance. The variables ρ_R and V_R are the density and the shear wave velocity of the reference rock, and $\bar{\rho}$ and $\bar{V}$ are the average density and shear wave velocity over a certain depth. When the depth of averaging is defined as a quarter wavelength for each frequency considered in the analysis, as also proposed by Joyner et al. (1981), this method is also known as the quarter-wavelength (QWL) method. The specific details regarding the

implementation of the SRI method can be found in Boore (2003). Using the SRI method, the Equations 1 and 2 can be formulated as:

$$(A)_{FULL} = \sqrt{\frac{\rho_{RockII}\, V_{RockII}}{\bar{\rho}_{full}\, \bar{V}_{full}}}\; e^{-\pi\kappa_0 f} \tag{4}$$

$$(A)_{DECOUPLED} = \sqrt{\frac{\rho_{RockII}\, V_{RockII}}{\bar{\rho}_{DI}\, \bar{V}_{DI}}}\; e^{-\pi\kappa_{RockI} f} \sqrt{\frac{\rho_{RockI}\, V_{RockI}}{\bar{\rho}_{DII}\, \bar{V}_{DII}}}\; e^{-\pi\kappa_{surf} f} \tag{5}$$

where the subscript *full* (in the denominator of Equation 4) indicates that the average properties should be computed over the full column profile, whereas *DI* and *DII* refer to the decoupled profiles shown in Figure 1 for a three-layer model. The operator exp(-$\pi\kappa_0 f$) corresponds to the attenuation model used in the SRI method. The site-specific or distance-independent spectral decay parameter κ_0 was first introduced by Anderson and Hough (1984) as a site parameter that represents the attenuation in shallow geologic structures below the site. Comprehensive descriptions of the origins and applications of κ_0 can be found in Ktenidou et al. (2013 and 2014) and Campbell (2009). The values of κ_{RockI} and κ_{surf} correspond to the equivalent κ_0 measured at the top of each decoupled profile, *DI* and *DII*, respectively.

The transfer function ratio (TFR) is the parameter we define as the ratio of the TF for the full column and the decoupled models. This parameter represents a measure of the error introduced in 1D SRA when the location of the EHS is not in accord with inherent assumptions:

$$TFR_{FR} = \frac{(TF)_{FULL}}{(TF)_{DECOUPLED}} \tag{6}$$

The equivalent expression for TFR in terms of SRI amplifications has the form:

$$TFR_{SRI} = \frac{\sqrt{\frac{\rho_{RockII} V_{RockII}}{\bar{\rho}_{full} \bar{V}_{full}}}\; e^{-\pi\kappa_0 f}}{\sqrt{\frac{\rho_{RockII} V_{RockII}}{\bar{\rho}_{DI} \bar{V}_{DI}}} \sqrt{\frac{\rho_{RockI} V_{RockI}}{\bar{\rho}_{DII} \bar{V}_{DII}}}\; e^{-\pi(\kappa_{surf}+\kappa_{RockI}) f}} \tag{7}$$

Adding up the attenuation corresponding to the propagation of seismic waves through the soil deposit (i.e., κ_{surf}) and the soft rock layer (i.e., κ_{RockI}) results in the total attenuation experienced by the full site profile (i.e., κ_0). Hence, the attenuation terms cancel when computing TFR values in terms of SRI amplifications:

$$TFR_{SRI} = \sqrt{\frac{(\bar{\rho}_{DI}\bar{V}_{DI})(\bar{\rho}_{DII}\bar{V}_{DII})}{(\bar{\rho}_{full}\bar{V}_{full})(\rho_{RockI}V_{RockI})}} \quad (8)$$

Finally, the quantification of the effects of selecting an EHS for a numerical model that is not in accord with the inherent assumptions of an EHS is also expressed in terms of response spectra. Spectral ratios (for 5% damping) corresponding to the full column (i.e., SR_{FULL}) and decoupled (i.e., $SR_{DECOUPLED}$) models are defined similarly to Equations 1 and 2. The spectral ratios ratio (*SRR*) is defined as:

$$SRR = \frac{(SR)_{FULL}}{(SR)_{DECOUPLED}} \quad (9)$$

Spectral ratios are computed by dividing 5% damped spectral accelerations estimated at the surface and at the assumed EHS boundary in each case. The spectral ratio corresponding to the decoupled model is defined as the product of the spectral ratios at each decoupled profile (i.e., *DI* and *DII*), analogously to Equation 2.

4.4 Parametric Study on Three-layer Model

The parametric study presented herein is based on the three-layer model depicted in Figure 1. Variations in soil properties such as the V_s, thickness, and minimum shear strain damping values (ξ_{min}) are used to investigate their influence on resulting differences between full column and decoupled models. The range of values we consider for each property is shown in Table 2. Values of TFR are shown in Figure 2, where linear elastic site amplifications are estimated by means of FR methods.

The mismatch computed between the full column and decoupled SRA is frequency dependent. Values of TFR decrease overall for softer soils (i.e., darker curves in Figure 2a). This means that as the impedance contrast of the soil/soft rock boundary becomes more significant, the presence of a strong impedance contrast deeper within the profile becomes less influential on the site response results. In fact, for the simple model investigated herein, if the impedance contrast between the soft rock (Rock I) and the soil deposit (i.e., $V_r \rho_r$ / $V_s \rho_s$) is larger than 6.25, the TFR approximates 1. This observation raises the question of how strong the soil-rock impedance contrast needs to be, so that potential changes in the properties of strata located deeper in the profile do not affect the estimated site response.

As the V_s corresponding to the soft rock (Rock I) increases (i.e., lighter curves in Figure 2b), approaching the V_s of the hard rock, the error becomes less significant. When both velocities reach the same value, TFR is equal to one. Lower values of V_s in the Rock I layer leads to larger impedance contrasts at the interface with the hard rock layer. Such condition generates increasingly significant differences between the full column and the decoupled models. Changes in the V_s of Rock I result in TFR values as high as 1.7, which is the largest error quantified when compared to the ones produced by the variation of the other parameters considered herein.

An increase in the V_s of the hard rock (Rock II) produces significant differences between the full column and decoupled models, for frequencies lower than the fundamental frequency of the site (Figure 2c). When the V_s of Rock I and Rock II are the same, a TFR equal to one is obtained over all the frequencies considered in the analysis.

The increase of the thickness of the soil deposit is accompanied by a reduction of the thickness corresponding to the soft rock layer, such that the site's complete profile has a

fixed depth. The variation of these thicknesses does not produce a clear pattern in the TFR (Figure 2d), other than the change in the fundamental frequency of the site along with a shift in the corresponding resonant peaks. An increase in the maximum TFR value with increasing soil layer thickness is also apparent from the data. Unlike the aforementioned parameters, attenuation plays a small role when comparing full column and decoupled approaches. Varying the corresponding damping value of the soil deposit, the soft rock and hard rock layers does not affect significantly the results in terms of the variation of the TFR with frequency.

In general, resonance effects can be observed over the whole range of frequencies shown in Figure 2. As discussed earlier, resonance effects are not always likely to occur, in particular for higher resonance modes. Therefore, we also develop a comparison of TFR values when using linear amplifications from the SRI method (Figure 3). Our objective is to identify first order effects of the EHS assumption, which include the effects of impedance and the effects of first mode resonance. The SRI method can capture both of them.

The same three-layer profile and ranges of properties provided in Table 2 are used to conduct the parametric study in terms of the SRI method. As seen in Figure 3, the SRI method does not reflect the peaks and valleys typically observed when using FR methods. In general, results from SRI amplifications indicate that for frequencies higher than around 20 Hz, the full column and decoupled models produce the same results. Likewise, TFR values also approach one for very low frequencies (e.g., < 0.01 Hz).

Stiffer soil deposits lead to a decrease in TFR (Figure 3a). This trend contradicts the observations from FR methods, shown in Figure 2a. However, a closer look reveals that

the SRI method only captures the decrease of the peak corresponding to the first resonant frequency but fails to reflect the second mode effects where a difference between the full column and decoupled models appears to be still very significant. The frequency where the TFR based on SRI amplifications starts being exactly equal to one is the fundamental frequency of the *DI* profile.

Figure 3b is in good agreement with Figure 2b because they both show that as the V_s of the Rock I layer increases, the TFR decreases. Eventually, when the velocities are the same for both materials, the TFR equals one over all frequencies. Increasing the V_s of Rock II causes a more significant mismatch between the full column and decoupled models (Figure 3c). This trend is expected since the stronger the impedance contrast at depth, the larger the error when ignoring the true location and properties of the EHS.

The increase of the soil layer thickness leads to an increase in TFR values and broadens the range of frequencies over which TFR values are greater than one (Figure 3d). The fundamental frequency of the soil deposit (i.e., the *DII* profile) decreases, and the fundamental frequency of the *DI* profile increases. Finally, the variation of the damping ratio corresponding to the soil deposit and Rock I does not alter the results because the SRI method allows attenuation in the decoupled analysis to be consistent with the corresponding attenuation model for the full column analysis.

In general, the SRI method provides a more transparent means to assess the influence of the impedance contrasts in the profile without having resonances obscuring the results. This method also facilitates the identification of a specific range of frequencies where the decoupled approach underestimates the site response when compared to the full column analysis.

4.5 Case Studies

4.5.1 Charleston, SC: Profile with a Strong Impedance Contrast at Great Depth

The presence of a strong impedance contrast in sites located in Charleston, SC (Figure 4) is characteristic of hard rock conditions in Central and Eastern US, with mean hard rock V_s values of 3000 m/s (Hashash et al., 2014). This type of V_s profile facilitates the selection of the EHS boundary condition exactly at the location of the strong impedance contrast. However, because this contrast occurs at a great depth (>800 m), often only the upper portion of the profile is analyzed in geotechnical SRA (e.g., upper 75 m of the profile). The strong impedance contrast between the sedimentary formation and rock is ignored as well as the influence of the deeper strata on the site response.

The assessment of nine Charleston's profiles presented herein aims to investigate the influence of the thickness of sediments and the selected input motions on the importance of the EHS assumption. As shown in the plan view provided in Figure 5, the sites of interest are close to the coast on the southeast region of South Carolina. Seismic cone penetration test (SCPT) data are available at the sites and reveal profiles with varying thicknesses of soil deposits and marl before the same geological formations are reached (Table 3). In general, the soil composition is similar across sites; mainly sands and clays are present. However, the V_s profiles at each site differ, especially in the upper 80 m.

Both, the SRI and FR methods are used to conduct 1D linear elastic SRA. Full column and decoupled approaches are implemented to compute the corresponding TFR and SRR values for each study site. A decoupling depth equal to 72 m is selected because a significant impedance contrast takes place between the soil deposits and the sedimentary formations

below which a rather uniform V_s profile exists. Thus, the effect of the strong impedance contrast at depth can be examined.

The estimated TFR values from the SRI method are shown in Figure 6. The maximum value of TFR reaches 1.35 and corresponds to a frequency equal to 0.20 Hz, which is very close to the fundamental frequency of the study sites. Values of TFRs at this frequency are presented in Table 4. Additionally, Figure 6 shows that for frequencies higher than 6 Hz, the full column and decoupled models produce the same results. Values of TFR also approach one for frequencies lower than 0.02 Hz. The critical frequency range where decoupled SRA underestimate at least by 20% the actual site amplifications, as estimated by the full column SRA, lies between 0.18 Hz and 0.22 Hz.

To perform the 1D linear elastic SRA for the SRR approach, forty ground motion recordings (i.e., horizontal components) selected from the Pacific Earthquake Engineering Research Center (PEER) database (http://peer.berkeley.edu). These input motions correspond to shallow crustal earthquakes with moment magnitudes between 5 and 9, recorded at stations with V_{s30} values between 750 m/s and 1500 m/s. The epicentral distances range from 2 km to 103 km. It should be noted that the estimation of spectral accelerations to compute SRR values is highly dependent on the choice of input motions. In this case study, only ground motions recorded at rock sites were considered (i.e., V_s >760 m/s; according to the classification system by the National Earthquake Hazard Reduction Program, NEHRP (Building Seismic Safety Council, 2000)), but none of them corresponds to hard rock conditions (i.e., V_s > 1500 m/s). Therefore, the resulting values of SRR can only serve as a reference to evaluate patterns in the data rather than definitive measures of the error when conducting decoupled SRA at the sites of interest.

Using spectral factors to obtain the SRR for all the selected sites results in a smoothing effect, as illustrated in Figure 7. All the study sites provide fairly similar results in terms of SRR, and the mean measured error is always less than 30%. The largest SRR values at each site are provided in Table 4. These values occur at a frequency of 0.7 Hz for all the sites. The lowest TFR and SRR values over all the frequencies considered herein correspond to Site 8, which has no soil overlying the marl formations. Figure 8 presents the trends between maximum error, as measured by TFR and SRR values, and the thickness of the soil deposits, h_s, for the sites under study. Even though, a weak linear correlation seems possible, an expanded database, both in terms of the range of h_s and the number of sites, is required to confirm the observed patterns presented herein. Such patterns confirm previous observations from the parametric study on the three-layer model, where the estimated error associated with the EHS assumption increases with increasing thickness of soil deposits. One potential cause is the fact that the period of the overlying soil and the rock column get closer, so the difference between full column and decoupled approaches becomes larger.

An example of the variability in SRR calculations as a result of the selected input motions is shown for Site 1 in Figure 9. Even though mean SRR values oscillate closely to one over all frequencies, as seen in Figure 9, certain ground motions result in higher SRR values than others, which introduces more epistemic uncertainty to the analyses. For example, at Site 1 (Figure 9), mean SRR values do not exceed 1.2, but depending on the input motion selected for the analysis, SRR values can reach a value of 2 at a certain frequency. This means that the full column amplifications can be twice as big as those estimated by the decoupled model.

4.5.2 Hanford, WA: Profile with Strong Velocity Reversals

This study site is located in Hanford, WA on a sequence of sedimentary units that overlie the Columbia River Basalt Group (CRBG). The presence of velocity reversals in the profile serves as an ideal example of the implications of applying the EHS boundary condition at a depth that is not geologically justified. The CRBG is a sequence of basalt flows that erupted between 17 and 6 millions of years ago, forming broad plateaus. The upper four basalt flows are known as the Saddle Mountains Basalt. These basalt layers were laid down over a period of time that allowed sediments to accumulate in between (Rohay and Brouns, 2007); the sedimentary interbeds are collectively known as the Ellensburg formation. Consequently, as shown in Figure 10, the profile has significant V_s contrasts between layers of basalt flow (with a V_s from 2400 to 2900 m/s) and sedimentary interbeds (with a V_s from 800 to 1500 m/s). The V_s data at the site were obtained by means of downhole logging of shear and compression wave velocities. The measurements extended through the Saddle Mountain Basalt and the Ellensburg formations (Youngs, 2007).

This case study focuses on the effects of velocity reversals on the importance of the EHS assumption. Full column and decoupled SRA are conducted at the site to investigate how the wave propagation phenomenon in the basalt-sedimentary interbed sequence affects the estimated site response. The decoupling depth is selected at the top of the Saddle Mountain Basalt formation (i.e., ~117 m) because it is a high V_s horizon, similar to deeper basalt layers in the profile, and it is located at a reasonable depth for typical geotechnical SRA. This EHS assumption is illustrated in Figure 10. Values of TFR based on amplifications from a 1D linear elastic FR method are presented in Figure 11. Full column analyses can lead to larger amplifications than those obtained from the decoupled approach for

frequencies between 0.2 Hz and 1 Hz. Values of TFR greater than one are also obtained at higher frequencies, as a result of the considered resonances in the profile. Differences between the full column and decoupled models are larger than 10% for frequencies between 0.4 Hz and 0.8 Hz. Estimates of SRR are not computed for this study site given the lack of recorded ground motions compatible with an EHS boundary of V_s approximately equal to 3000 m/s. Deconvolution techniques could be used to generate such motions, but they are highly sensitive to model assumptions such as the V_s profile and attenuation models (Cadet et al. 2011; Kramer 1996). Generating synthetic motions using the stochastic method (Boore, 2003) for example, would be the best alternative because specific source, path and site characteristics could be taken into consideration.

Amplifications resulting from the full column and decoupled approaches at the Hanford site are presented in Figure 12. The decoupled approach has more energy than the full column analysis at the first resonant mode, as evidenced by the larger amplification peak. The full column analysis introduces more flexibility, which results in stronger dissipation of the energy at the first resonant mode. Perhaps, destructive interferences when considering the full column prevent the energy to build up at that specific frequency. The presence of strong velocity reversals in deep layers within the profile can cause reflected waves traveling back to the surface which may create such destructive interferences. Another possible explanation is that a portion of the energy of propagating seismic waves may get trapped within the sedimentary interbeds, so that it never reaches the upper layers in the profile. In addition, there is a narrow banded peak (between 5 Hz and 6 Hz) resulting from the decoupled approach, that is damped out when conducting full column SRA. The randomization process of soil properties, typically carried out in probabilistic seismic

hazard analyses, can also smooth out this peak. Finally, there is not a significant difference between the full column and decoupled analyses at high frequencies.

In this case study, the decoupling assumption based on an EHS boundary condition with V_s equal to 2400 m/s is not valid due to the presence of the basalt-sedimentary interbeds sequence below such target horizon. Ignoring the complex wave propagation phenomena among those layers with strong impedance contrasts highly affects the estimated site response.

4.6 Conclusions

All site response analyses imply decoupling the effects of deeper strata from the response of shallower layers. This study examined the potential systematic errors introduced in the analysis when the reference depth selected at the site does not comply with the assumptions of an ideal elastic half-space. The latter includes that all of the energy of the downwards propagating seismic wave transmitted into the half-space is radiated away from the surface layers. The appropriate choice of the EHS boundary condition in site response models is relevant because it also implies that the input motions applied to such horizon should be recorded at a site with an equivalent site response to that below the assumed EHS.

The consideration of the entire profile as well as its decoupled representation is used to estimate the error introduced in site response analysis when positioning the elastic half-space at a horizon that is not geologically justified. Theoretical formulations for wave propagation in layered media (or full resonance methods) and the square-root impedance methods were used to compute the corresponding amplifications from each approach (i.e., full column versus decoupled analysis).

A parametric study conducted at a three-layer profile to investigate the most influential factors on the error introduced by the EHS assumption in SRA revealed that the presence of a strong impedance contrast is not enough to define the EHS location. The shear wave velocity and thickness of the shallow soil deposits proved to be influential factors on the estimated error. Likewise, the shear wave velocities of underlying soft and hard rock layers also affect the estimates of site response over a specific range of frequencies of engineering interest.

Two case studies of challenging profiles at sites located in Charleston, SC and Hanford, WA were presented to show that the error associated with the EHS assumption on site response is not negligible for certain geologic conditions. For example, the presence of a strong impedance contrast located at depth or shear wave velocity reversals. These conditions represent a significant departure from the hypotheses behind an ideal EHS, and consequently can lead to errors in the estimation of the response at the site.

References

Anderson, J.G., and Hough, S.E., 1984. A model for the shape of the Fourier amplitude spectrum of acceleration at high frequencies, *Bulletin of the Seismological Society of America* **74**(5), 1969-1993.

Boore, D., 2003. Simulation of Ground Motion Using the Stochastic Method, *Pure and Applied Geophysics* **160**(3-4), 635-676.

Boore, D., 2013. The Uses and Limitations of the Square-Root-Impedance Method for Computing Site Amplification, *Bulletin of the Seismological Society of America* **103**(4), 2356-2368.

Boore, D., and Joyner, W., 1997. Site amplifications for generic rock sites, *Bulletin of the Seismological Society of America* **87**(2), 327–341.

Building Seismic Safety Council, 2000. *The 2000 NEHRP recommended provisions for new buildings and other structures: Part I (Provisions) and Part II (Commentary)*, Tech. rep., FEMA 368/369, Federal Emergency Management Agency, Washington, D.C.

Cadet, H., P.-Y. Bard, and A. Rodriguez-Marek (2010). Defining a standard rock site: Propositions based on the KiK-net database, *Bull. Seism. Soc. Am*. **100** (1), 172–195.

Campbell, K.W., (2009). Estimates of shear-wave Q and κ_0 for unconsolidated and semi-consolidated sediments in eastern North America, *Bull. Seism. Soc. Am.* **99**, 2365–2392.

DS. No. 61, 2011. *Regulation determined seismic design of buildings and repeals* Decree No. 117 of 2010, Ministerio de Vivienda y Urbanismo. Official Journal of 13/12/2011.

Eurocode 8, 2004. Design of structures for earthquake resistance, part 1: General rules, seismic actions and rules for buildings, EN 1998-1, *European Committee for Standardization (CEN)*, http://www.cen.eu/ cenorm/homepage.htm.

Hashash, Y. M. A., A. R. Kottke, J. P. Stewart, K. W. Campbell, B. Kim, C. Moss, S. Nikolaou, 368 E. M. Rathje and W. J. Silva (2014). Reference rock site condition for central and Eastern 369 North America. *Bulletin of the Seismological Society of America* **104**, 684-701.

Hashash, Y.M.A., Musgrove, M.I., Harmon, J.A., Groholski, D.R., Phillips, C.A., and Park, D., 2015. *DEEPSOIL 6.0, User Manual* 116 p.

Idriss, I. M. and Sun, J. I. (1992). *User's Manual for SHAKE91,* A computer Program for Conducting Equivalent Linear Seismic Response Analyses of Horizontally Layered Soil Deposits Program Modified based on the Original SHAKE Program Published in December 1972 by Schnabel, Lysmer and Seed.

Japan Road Association, 1980. *Specifications for highway bridges, Part V, Seismic Design*, Maruzen Co., LTD.

Japan Road Association, 1990. *Specifications for highway bridges, Part V, Seismic Design*, Maruzen Co., LTD.

Joyner, W.B., Warrick, R.E., and Fumal, T.E., 1981. The effect of quaternary alluvium on strong ground motion in the Coyote Lake, California, earthquake of 1979, *Bulletin of the Seismological Society of America* **71**(4), 1333-1349.

Kottke, A. R., and Rathje, E.M., 2008a. *Strata*, Version alpha, Revision 381, University of Texas, Austin, TX.

Kottke, A. R., and Rathje, E.M., 2008b. *Technical Manual for Strata*, Report 2008/10, Pacific Earthquake Engineering Research (PEER) Center, University of California, Berkeley, CA.

Kramer, S., 1996. *Geotechnical Earthquake Engineering*, Prentice Hall, Upper Saddle River, NJ.

Ktenidou, O.J., Cotton, F., Abrahamson, N.A., and Anderson, J.G., 2014. Taxonomy of κ: A Review of Definitions and Estimation Approaches Targeted to Applications, *Seismological Research Letters* **85**(1), 135-146.

Ktenidou, O.J., Gélis, C., and Bonilla, L.F., 2013. A study on the variability of kappa (κ) in a borehole: Implications of the computation process, *Bulletin of the Seismological Society of America* **103**(2A), 1048–1068.

Laurendeau, A., F. Cotton, O.-J. Ktenidou, L.-F. Bonilla, and F. Hollender (2013). Rock and stiff soil site amplification: Dependency on VS30 and kappa (κ_0), *Bull. Seism. Soc. Am.* **103**(6), 3131–3148.

Rohay, A.C., and Brouns, T.M. *Site-Specific Velocity and Density Model for the Waste Treatment Plant, Hanford, Washington*, Pacific Northwest Laboratory, prepared for U.S. DOE, June 2007.

Schnabel, P. B., Lysmer, J., and Seed, H. B. (1972). *SHAKE: A computer program for earthquake response analysis of horizontally-layered sites*, Report No. EERC-72/12. Earthquake Engineering Research Center, University of California at Berkeley, Berkeley, CA.

Youngs, R. R. *Updated Site Response Analyses for the Waste Treatment Plant, DOE Hanford Site, Washington*, Pacific Northwest Laboratory, prepared for U.S. DOE, June 2007.

Table 1: Main properties of reference rock sites.

Reference	Definition of Reference Rock Conditions
National Earthquake Hazard Reduction Program (NEHRP) (Building Seismic Safety Council, 2000)	V_{s30} > 760 m/s - rock sites V_{s30} > 1500 m/s - very hard rock sites
European Regulations (Eurocode 8, 2004)	V_{s30} > 800 m/s - rock sites
Japanese regulations (Japan Road Association, 1980, 1990)	V_{s30} > 600 m/s - rock sites
Recommendation from Cadet et al. (2010)	750 < V_{s30} < 850 m/s and f_0 > 8 Hz - "standard reference rock site"
Boore and Joyner (1997) generic rock sites	V_{s30} > 620 m/s and κ_0 = 0.04 sec - rock sites (mostly in western North America) V_{s30} > 2000 m/s and κ_0 < 0.01 sec - very hard rock sites (mostly in eastern North America)
Chilean regulations (DS. No. 61, 2011)	V_{s30} > 500 m/s - soft rock or fractured rock V_{s30} > 900 m/s - rock sites, cemented soils
Hashash et al. (2014)	2700 m/s < V_s < 3300 m/s and κ_0 = 0.006 sec (for Central and Eastern North America)

Table 2: Range of values considered for the parametric study on the three-layer model

Site Property	Layer	Range
V_s	Soil	150 m/s - 760 m/s
	Rock I	760 m/s - 2700 m/s
	Rock II	2000 m/s - 3000 m/s
ξ_{min}	Soil	2 % - 10 %
	Rock I	1 % - 5 %
	Rock II	0.5 % - 3 %
Thickness	Soil	60 m - 300 m

Table 3: General characteristics of the selected sites in Charleston, SC.

Site #	Depth to Marl (m)	Depth to Common Sedimentary Formation (m)
1	19.2	20.0
2	12.6	20.0
3	6.4	20.0
4	28.6	28.6
5	20.0	20.0
6	25.6	25.6
7	7.3	20.0
8	0.0	0.0
9	11.0	20.0

Table 4: TFR at 0.2 Hz from SRI amplifications, along with SRR values at each study site. h_s refers to the soil deposit thickness and f' to the fundamental frequency of the site.

Site #	h_s (m)	Max TFR $_{(SRI)}$	Max SRR	f' (Hz)
1	19.20	1.36	1.15	0.22
2	12.65	1.36	1.14	0.22
3	6.40	1.33	1.15	0.22
4	28.65	1.36	1.19	0.22
5	19.99	1.36	1.15	0.22
6	25.60	1.36	1.20	0.22
7	7.32	1.35	1.15	0.22
8	0.00	1.17	1.12	0.23
9	11.00	1.33	1.15	0.22

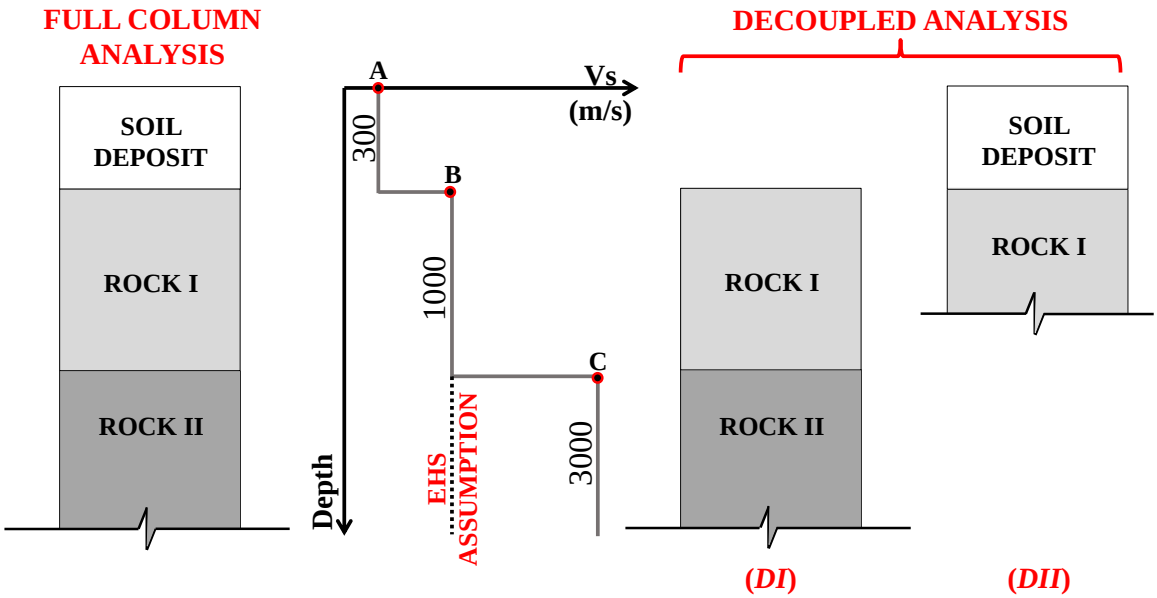

Figure 1: Full column profile shown on the left with its corresponding decoupled representation on the right (*DI* and *DII* profiles) and shear wave velocity profile.

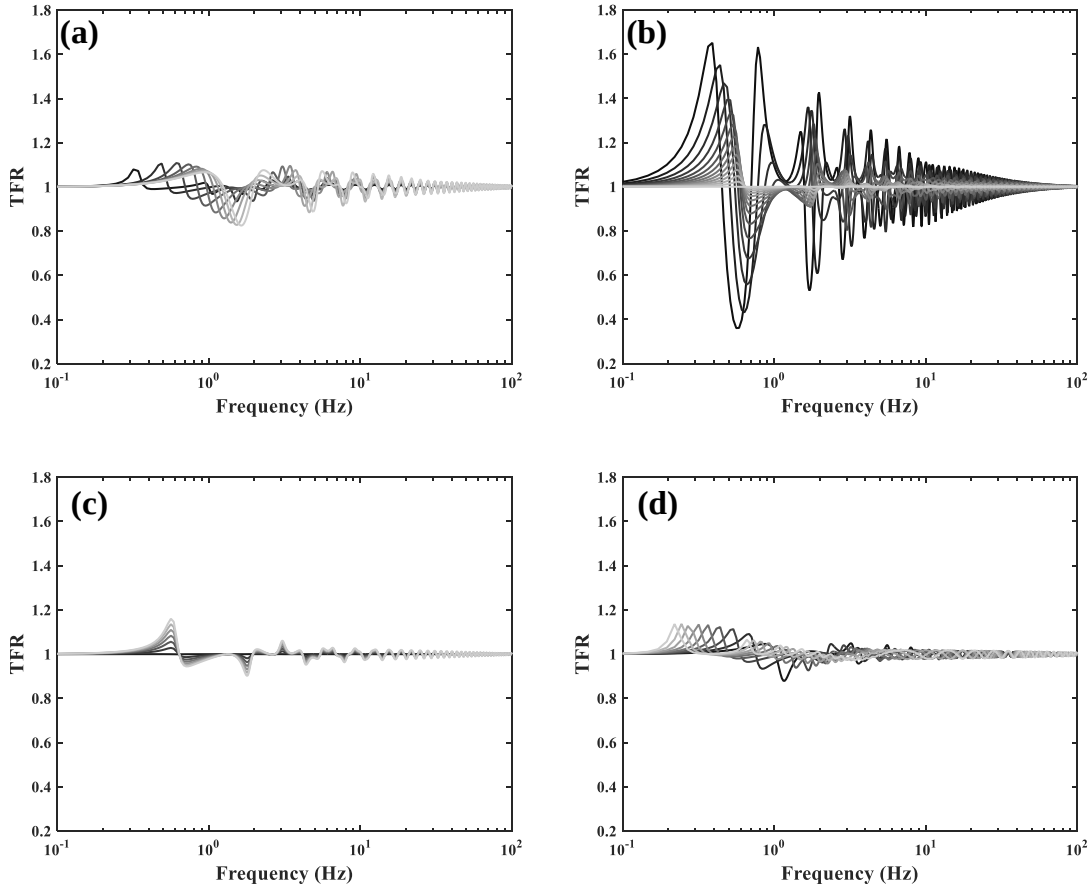

Figure 2: Results from a parametric study conducted in a three-layer model where the following properties are varied as indicated in Table 2: (a) the V_s of the soil deposits (with increments of V_s equal to 75 m/s), (b) the V_s of Rock I layer (with increments of V_s equal to 150 m/s), (c) the V_s of Rock II layer (with increments of V_s equal to 150 m/s), and (d) the thickness of the soil deposits (with increments of 30 m). Lighter curves indicate increasingly stiffer materials in (a), (b), and (c); and thicker soil deposits in (d).

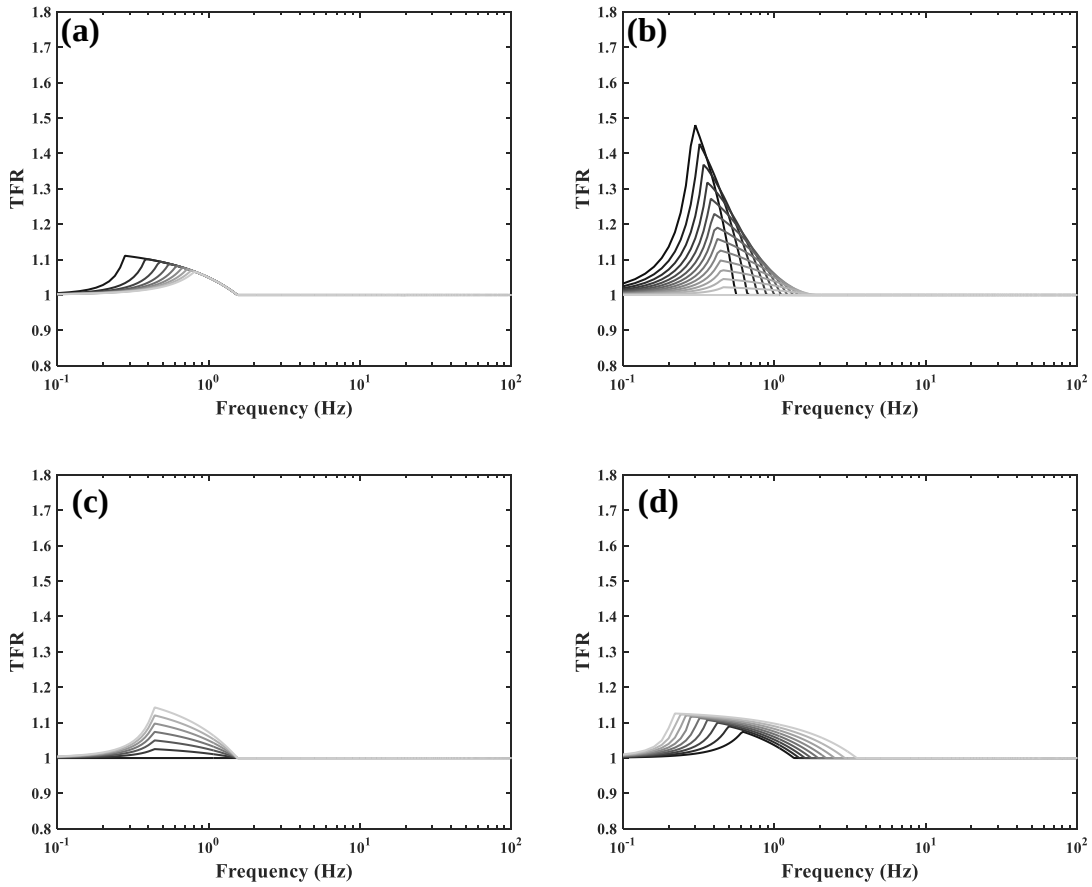

Figure 3: Results from a parametric study using the SRI method for a three-layer model while varying the following properties as indicated in Table 2(a) the V_s of the soil deposits (with increments of V_s equal to 75 m/s), (b) the V_s of Rock I layer (with increments of V_s equal to 150 m/s), (c) the V_s of Rock II layer (with increments of V_s equal to 150 m/s), and (d) the thickness of the soil deposits (with increments of 30 m). Lighter curves indicate increasingly stiffer materials in (a), (b), and (c); and thicker soil deposits in (d).

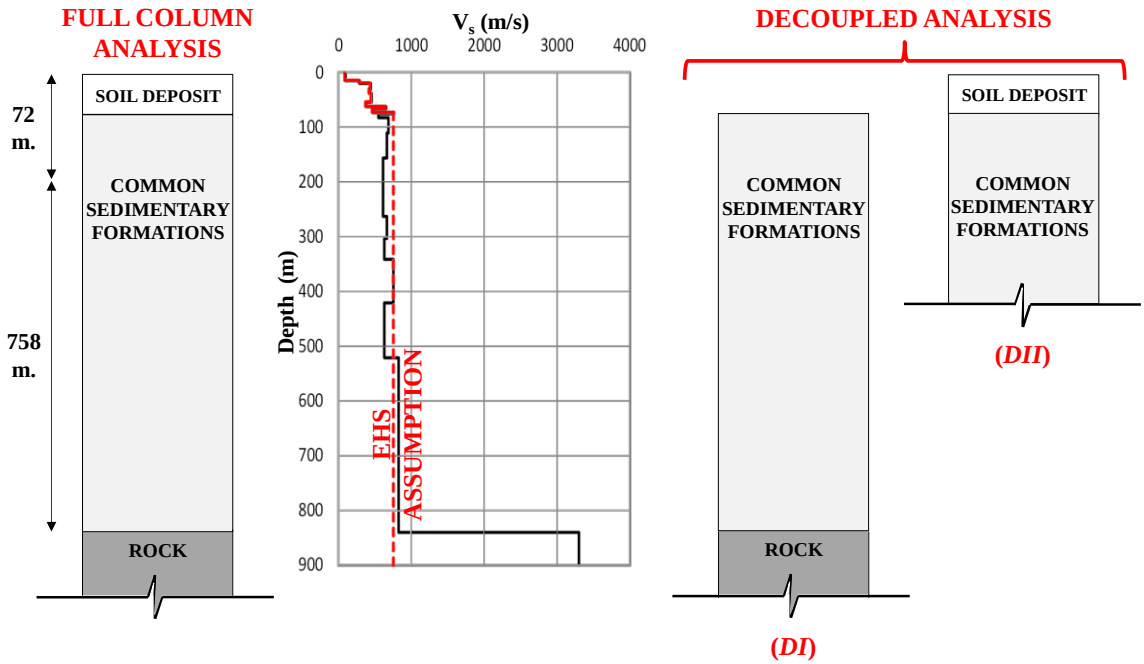

Figure 4: Full column profile corresponding to an idealized representation of the sites located in Charleston, SC on the left with a typical V_s profile of sites in the area. A typical assumption for the location of the EHS (in absence of sufficient V_s data) is also presented. *DI* and *DII* shown on the right refer to the corresponding decoupled profiles.

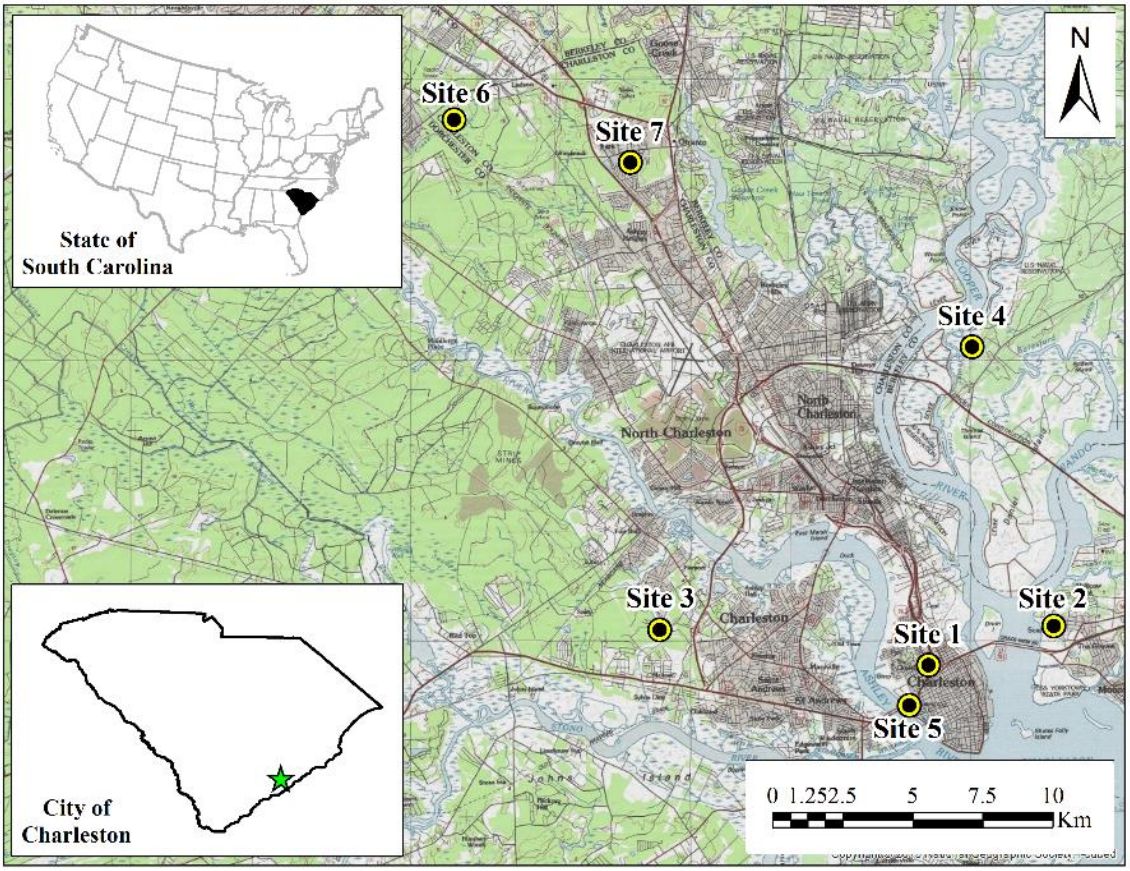

Figure 5: Plan view of the study area (data from USGS Topographic Maps 2012). The location of seven of the nine sites used in this study is shown. The specific coordinates for sites 8 and 9 are not available.

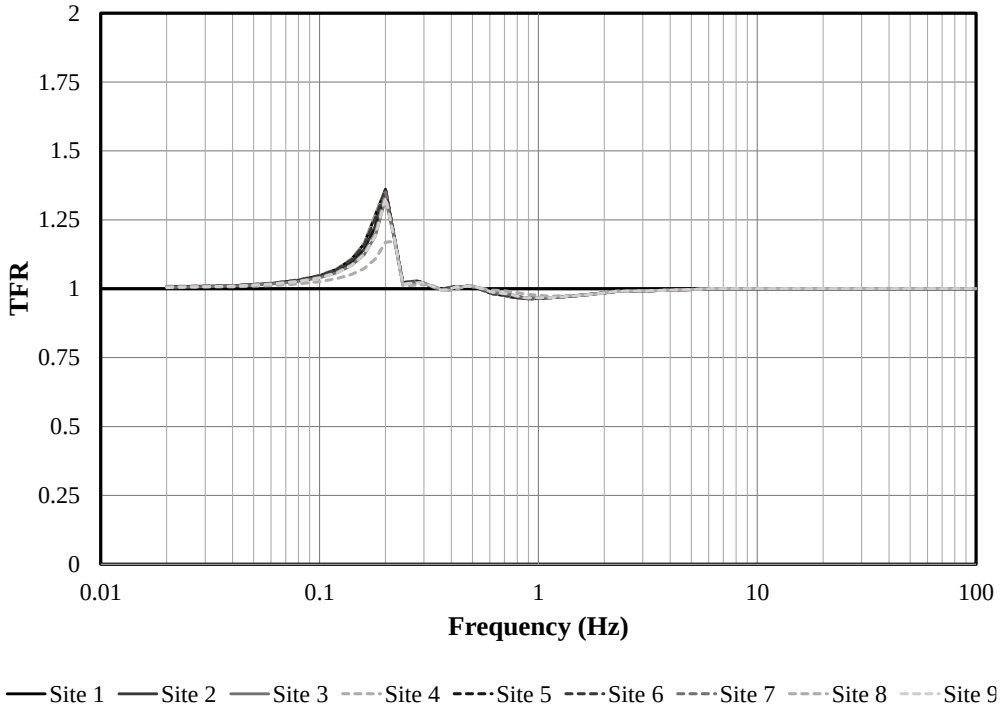

Figure 6: Transfer Function Ratios (TFR) when using site amplifications as estimated by the square-root impedance method at the selected study sites.

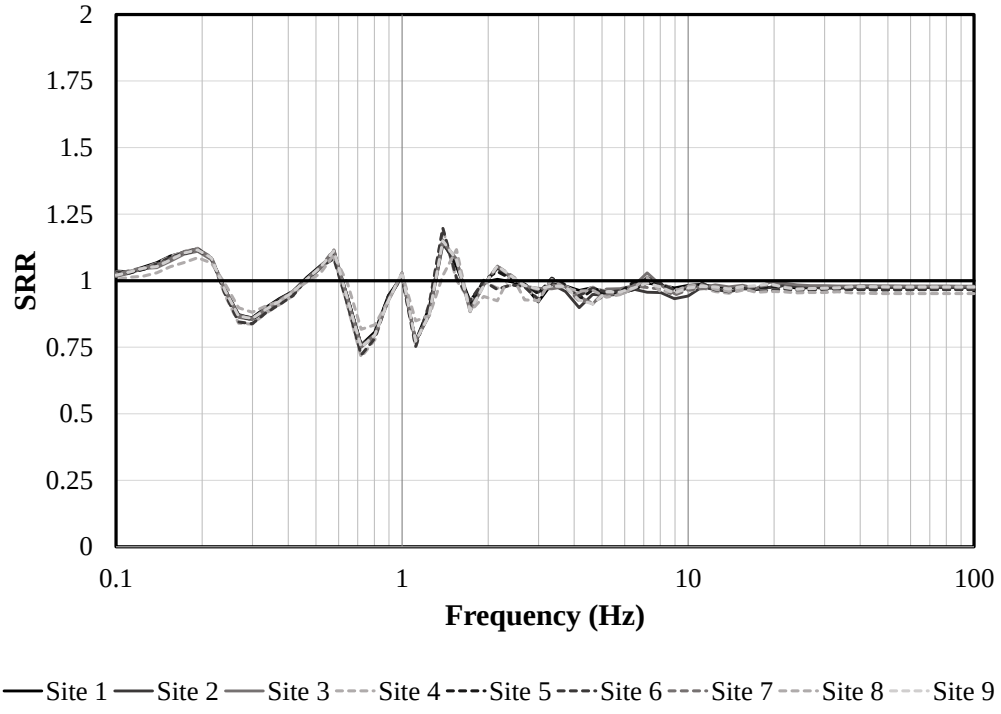

Figure 7: Values of mean Spectral Ratios Ratio (SRR) corresponding to all the sites under study.

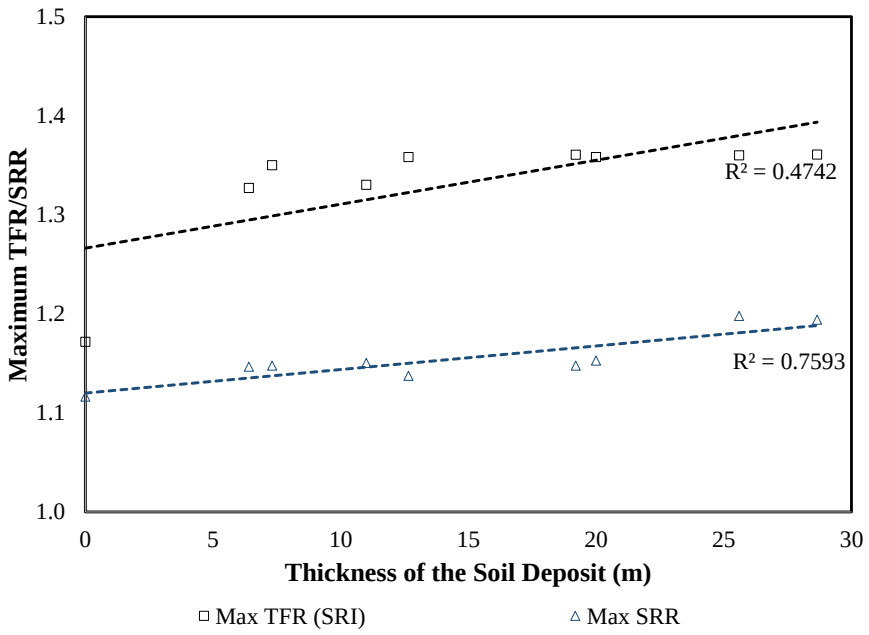

Figure 8: Maximum Transfer Function Ratio, TFR, at 0.2 Hz and maximum Spectral Ratios Ratio (SRR) values computed at each site under study, plotted against their corresponding thickness of soil deposit.

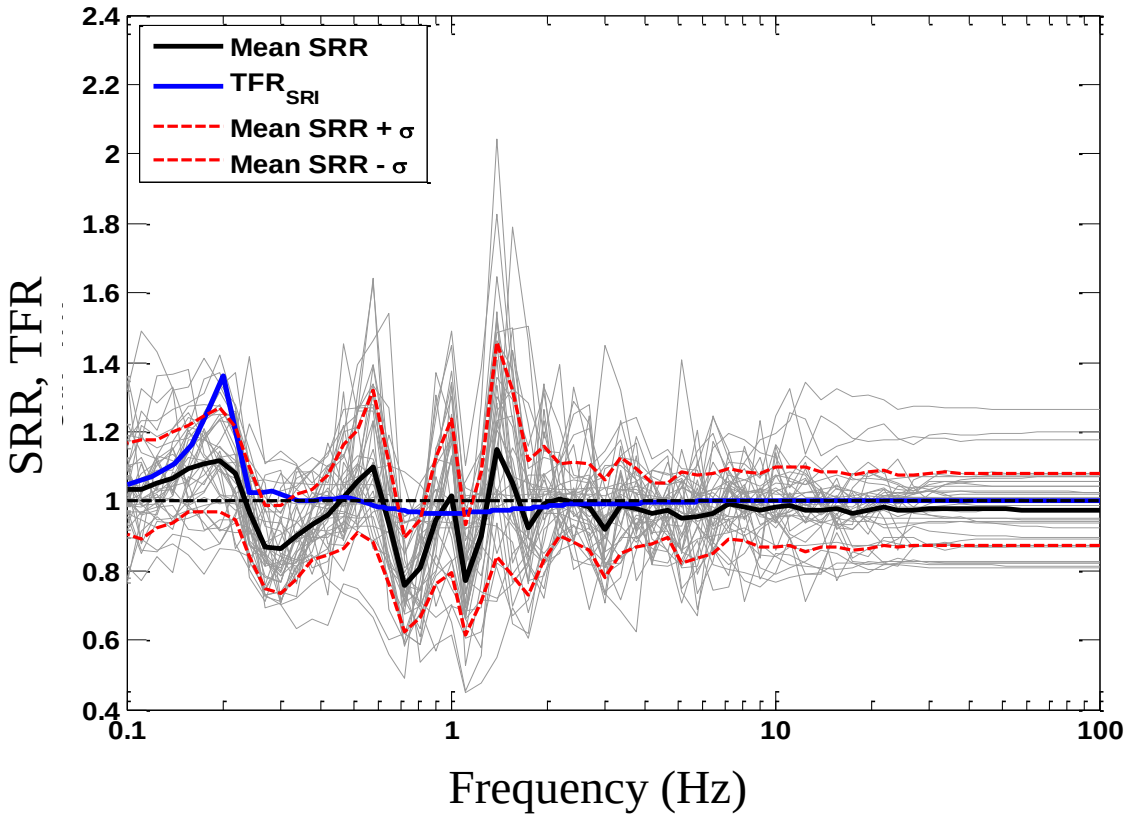

Figure 9: Spectral Ratios Ratio (SRR) for each selected input motion, mean SRR, and Transfer Function Ratio, TFR based on square-root impedance (SRI) amplifications, for Site 1 in Charleston, SC.

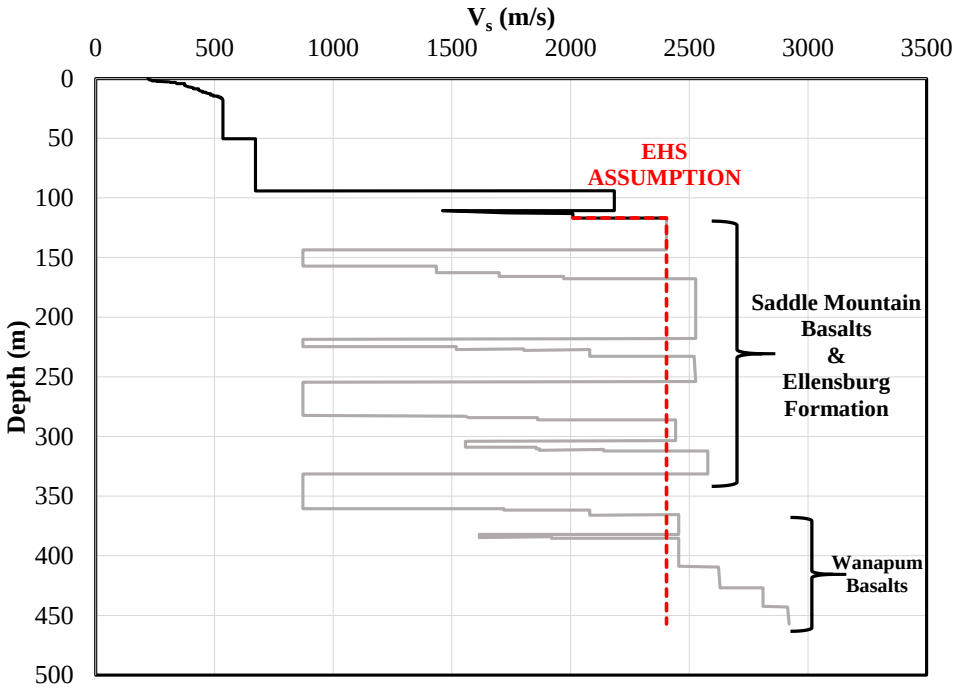

Figure 10: V_s profile at the study site located in Hanford, WA. A typical assumption for the location of the EHS boundary is shown in red. The V_s values of the soil deposit are shown in black while the V_s data not included in site response models when assuming such EHS are shown in gray.

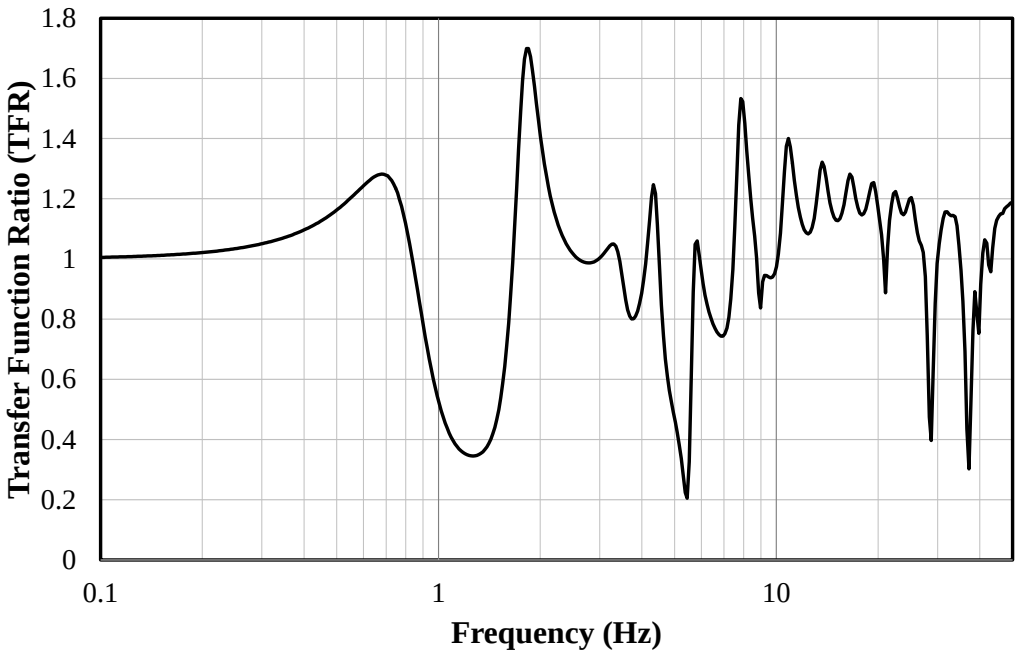

Figure 11: Transfer Function Ratios computed at the study site in Hanford, WA based on a linear-elastic 1D full resonance (FR) method.

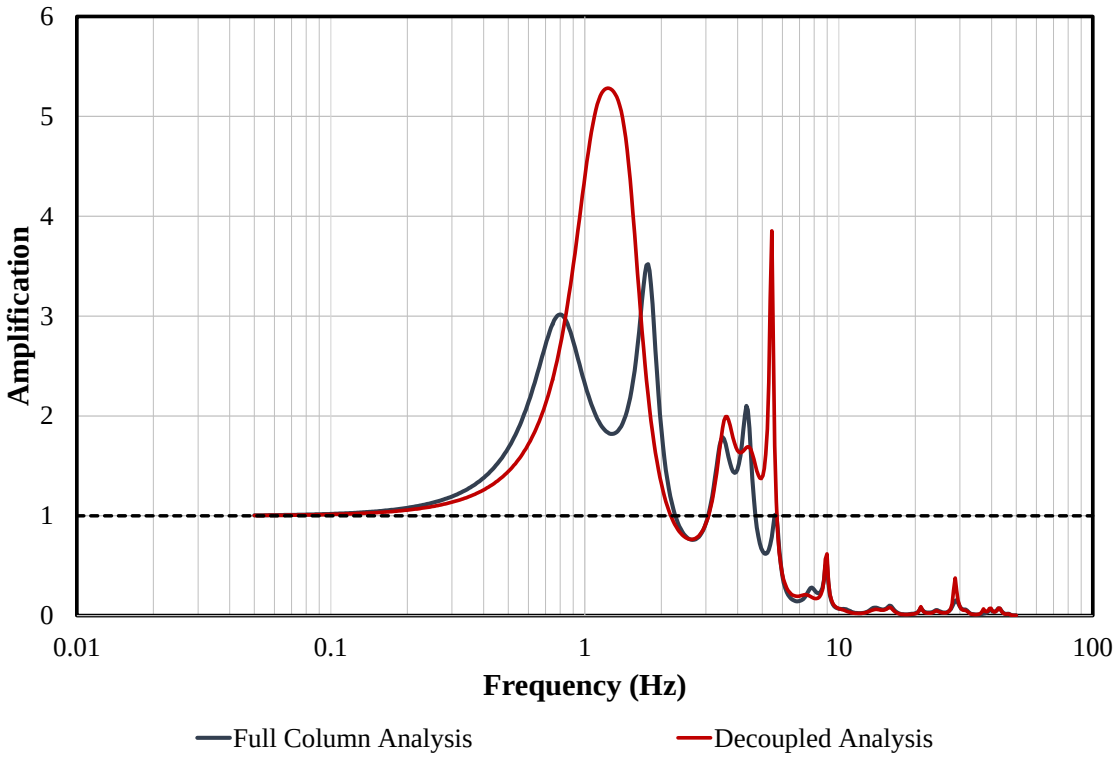

Figure 12: Site Amplification values obtained for the full column and decoupled site response analyses (as computed from full resonance methods) at the site located in Hanford, WA.

CHAPTER FIVE

V_S-κ CORRECTION FACTORS FOR INPUT GROUND MOTIONS USED IN SEISMIC SITE RESPONSE ANALYSES

Abstract

Input motions used in seismic site response analyses are commonly selected based on similarities between the shear wave velocity (V_s) at the recording station, and the reference depth at the site of interest (among other aspects such as the intensity of the expected ground motion). This traditional approach disregards the influence of the attenuation in the shallow crust on site response. Given that this attenuation (damping) can be characterized by the high-frequency attenuation parameter kappa (κ), a V_s-κ correction framework for input motions is proposed to render them compatible with the assumed properties of the reference depth at the site. The proposed correction factors were applied to a subset of recordings from the KiK-net database, and compared to traditional deconvolution. Results indicate that V_s-κ corrected motions outperform deconvolved motions in the characterization of the spectral energy in the high-frequency range. However, motions recorded at sites with soft deposits are not good candidates for the V_s-κ correction approach. V_s-κ corrections also affect amplification functions which can be important in the assessment of site-specific seismic hazards.

5.1 Introduction

The influence of local geologic conditions on strong ground motions and structural damage has been recognized by seismologists and engineers for many decades. The early work of Seed and Idriss (1970), as well as the observations after the 1967 Caracas (Seed et al. 1972), 1985 Mexico City (Seed et al. 1987), and 1989 Loma Prieta (Seed et al. 1991) earthquakes, have led to a better understanding of the role that site response plays on ground shaking. Such studies showed that local site conditions are capable of amplifying or deamplifying ground motions, in addition to changing their frequency content and duration. Seismic site response analyses (SRA) assess these effects and provide a means of estimating surface motions that may directly affect the stability of structures. Hence, this type of analysis constitutes a key component of the seismic design process (Rathje et al. 2010).

The criterion for selecting input motions for SRA varies depending on the application. When conducting one-dimensional (1D) equivalent linear SRA, an input ground motion is assumed to reflect the effects of deeper geologic structures within the site profile of the station where it was originally recorded. The use of a recording as an input motion to a profile that is truncated at a certain depth (typically, the depth at which the elastic half-space (EHS) assumption is believed to apply) implicitly assumes that the effects of deeper layers on site response are decoupled from the effects of shallower layers. The EHS is a boundary condition usually defined at a horizon sufficiently stiff such that no strong impedance contrasts will be found below this depth. This assumption implies that the portion of the energy of downward-propagating seismic waves that are refracted into the EHS will be completely absorbed by the rock mass, with the remaining portion of waves being reflected back up through the profile. As a result, the effects of wave propagation

below the depth of the assumed EHS are not captured in SRA, which means that these effects must be carried by the selected input ground motions.

The decoupled nature of SRA highlights the importance of selecting input ground motions recorded at a station with similar shear wave velocity (V_s) profile to the layers assumed to act as the EHS at the site of interest (Schnabel et al. 1972). In fact, current approaches for selecting input ground motions (e.g., Stewart et al. 2014) are based on such similarity of V_s profiles, but only consider the influence of the attenuation in the shallow crust in an indirect way. This attenuation (or damping) is typically characterized by the site kappa (κ_0), which was originally introduced as the high-frequency attenuation parameter (Anderson and Hough 1984). The consideration of κ_0 allows for a better constraint of the site effects at rock and stiff soils sites. Other site proxies, such as the time-averaged V_s over the top 30 m of the profile ($V_{s,30}$), are only roughly correlated to the near-surface attenuation, and therefore, may not correlate well with the high-frequency spectral content of ground motions. The latter might prove more relevant for regions in which the seismic hazard is dominated by nearby, large magnitude earthquakes, or where the surface geology is mostly composed of hard, unweathered rocks and very stiff soils (e.g., Central and Eastern US (CEUS)). In these cases, structures sensitive to high-frequency shaking might be designed non-conservatively when overlooking the effects of near-surface attenuation on input ground motion selection. The combination of V_s and κ_0 offers a more comprehensive approach that is applicable to a wider range of situations.

To illustrate the importance of accounting for the joint effect of V_s and κ_0, consider the scenario described in Figure 1 in which the site κ_0 at the station where the motion was recorded is relatively high (i.e., $(\kappa_0)_1$ at Site 1), while the rock underlying the site being

analyzed (below point B at Site 3) has a lower κ_0 value (i.e., $\kappa_{2,bedrock}$). Applying a ground motion recorded at Site 1 (point D) as an input motion at point B to conduct SRA at the site would imply that a significant portion of the high-frequency energy is being removed from the analyses due to the damping in Rock I (i.e., $\kappa_{profile}$). The removal of the high frequency energy will change the predicted spectral accelerations at Site 3 for short periods, and due to soil nonlinearity, it may also affect spectral accelerations estimated at long periods.

Despite the proliferation of strong ground motion recordings worldwide, the task of finding recording stations with similar V_s profiles and κ_0 to the assumed EHS at the study site can be rather challenging. For instance, when layers located at large depths with high V_s values are assumed to act as the EHS boundary for the site, the number of recording stations with similar characteristics is significantly reduced. The present study addresses this problem by proposing a framework for implementing simple but robust adjustments to ground motion recordings to render them compatible with the assumed properties of the EHS boundary condition. Correction factors are proposed to account for the variability on SRA that results from differences in V_s profiles and κ_0 between the recording station and the assumed EHS. Furthermore, the use of κ_0 (as part of the suggested methodology) will explicitly consider the differences in shallow-crust attenuation to properly characterize the high-frequency content of input motions specified at bedrock level.

The proposed V_s-κ correction factors are inspired partly on the work by Campbell (2003), Cadet et al. (2011), and Al Atik et al. (2014). The former introduced host-to-target correction factors to adjust ground motion prediction equations (GMPEs) from a region where strong motion recordings are abundant to a region where the data are sparse. Cadet

et al. (2011) proposed depth and impedance corrections to site amplification factors that were biased by the use of reference motions different from what they defined as a standard outcropping rock motion. Al Atik et al. (2014) developed a κ-scaling approach applicable to GMPEs to account for differences in site-specific κ estimates.

It is envisioned that the framework outlined herein will contribute towards simplifying current practices for obtaining bedrock motions from surface recordings; an approach conventionally referred to as deconvolution (Schnabel et al. 1972; Kramer, 1996). The latter is highly sensitive to model assumptions such as the V_s and attenuation models (Cadet et al. 2011; Kramer 1996). Simple but robust corrections embedded in the proposed methodology might prove preferable to account for impedance and attenuation differences in ground motion recordings. Moreover, the incorporation of the V_s-κ correction factors into existing selection and scaling protocols for input motions in SRA will expand, in a more physically correct basis, the catalog of suitable recordings for a given site.

After providing details on the development of the V_s-κ correction factors, a validation effort using ground motions from the Kiban-Kyoshin (KiK-net) Japanese database will be presented along with comparisons to a more conventional deconvolution approach. Finally, the practical implications of the proposed methodology on SRA are evaluated by comparing spectral acceleration values estimated at the surface and amplification factors resulting from using as recorded and V_s-κ corrected input motions at multiple sites.

5.2 Methodology

The proposed V_s-κ correction factors are based on the square-root-impedance (SRI) method introduced by Joyner et al. (1981), which is a linear method that only captures

impedance and attenuation effects. Hence, the correction is assumed to be linear, which is consonant with the intent of the V_s-κ correction of capturing only general trends in site response. The framework considered in this study for implementing the V_s-κ correction factors is presented in the flowchart shown in Figure 2. As depicted therein, the methodology includes two components, namely, an impedance and an attenuation correction factors.

The impedance correction factor (CF_{imp}) can be defined by estimating the linear amplification (i.e., the transfer function, *TF*) between the ground surface and the selected reference depth at the station where the surface motion to be adjusted was recorded. Such reference depth should be conveniently chosen as a common horizon between the station and the site of interest (e.g., Rock II in Figure 1). The required TF will be computed using the SRI method (Boore, 2013):

$$TF = \left(\frac{Z_R}{\bar{Z}}\right)^{1/2} = \left(\frac{\rho_R V_R}{\bar{\rho}\bar{V}}\right)^{1/2} \quad (1)$$

where *Z* refers to the seismic impedance contrast, ρ_R and V_R are the density and the V_s at a reference depth, respectively, while $\bar{\rho}$ and $\bar{V}$ refer to the average density and V_s over a certain depth. When the depth of averaging is defined as a quarter wavelength (QWL) for each frequency considered in the analysis, as proposed by Joyner et al. (1981), this approach is also known as the QWL method and the specific details regarding its implementation can be found in Boore (2003).

The SRI method neglects the effects of resonances that may develop in 1D analyses. However, field conditions, such as spatial variability or non-horizontal layering, may not allow these resonances to build over time, in which case these are considered spurious

resonances (Kramer 1996). In particular, this is true for high-frequency resonances that could develop in rock sites, where they may act as scatterers to the wave field depending on the scale of the heterogeneities. Thus, the proposed CF_{imp} can be expressed as follows:

$$CF_{imp} = \frac{1}{TF} \tag{2}$$

where *TF* is computed using Equation 1.

The proposed modification of recorded ground motions at the surface will serve two purposes. First, it will render ground motions consistent with the V_s profile below the reference depth at the site of interest (i.e., the EHS boundary condition assumed for SRA), and secondly, it will preserve the free surface effects of ground motions given that outcropping motions are preferable for conducting SRA.

The attenuation correction factor (CF_{atn}) has the original form proposed by Anderson and Hough (1984) in their definition of kappa (κ). Even though the physical meaning of c remains a subject of debate in the field of engineering seismology, most current studies consider it as a parameter predominantly controlled by site conditions (i.e., surficial geology) while having variable influence from the source and the path depending on the region under study (Ktenidou et al. 2014). Comprehensive descriptions of the origins of κ_0 and the existent methodologies to compute it can be found in Campbell (2009) and Ktenidou et al. (2014 and 2015).

The parameter κ can be partitioned into a distance-independent component (known as site-specific kappa) and a distance-dependent component (associated with regional attenuation). Site-specific kappa values (or simply site kappa, κ_0) represent the attenuation of shear waves as they travel through the shallow crust (Ktenidou et al. 2014), in other

words, as they travel through the geological structures right beneath the recording station (Ktenidou et al. 2015). This parameter can be further subdivided if the contributions of the near-surface materials ($\kappa_{profile}$) and the base rock ($\kappa_{bedrock}$) are considered separately in the characterization of the attenuation directly below the site (Al Atik, personal communication):

$$\kappa_0 = \kappa_{profile} + \kappa_{bedrock} \quad (3)$$

A similar expression to Equation 3 has been presented in a recent study by Ktenidou et al. (2015). These authors relate κ_0 values obtained from surface recordings with both, the κ_0 associated with recordings from a downhole instrument in a vertical array and the contributions from the sedimentary deposits up to the surface.

The proposed CF_{atn} accounts for the attenuation that seismic waves experience between the selected reference depth and the ground surface where the input motion was originally recorded. Thus, $\kappa_{profile}$ represents the additional attenuation at the recording station, which needs to be removed in order to use the recording as an input motion at the site. The CF_{atn} is essentially a filter used to increase the high frequency content of the input motion to compensate for high-frequency energy that was absorbed by the shallow stratigraphy at the recording station.

The definition of CF_{atn} requires the computation of $\Delta\kappa_0$ as the difference between estimates of $\kappa_{0\text{-bedrock}}$ and $\kappa_{0\text{-site}}$ at the recording station. Few, if any, measurements of κ_0 exist for ground motion stations. Consequently, values of κ_0 can be also estimated using available correlations with $V_{s,30}$ (e.g., Chandler et al. 2006). The same correlation must be used to obtain $\kappa_{0\text{-bedrock}}$ and $\kappa_{0\text{-site}}$ estimates in order to guarantee consistent values of $\Delta\kappa_0$. When using $V_{s,30}$-κ_0 relationships, the value of $\kappa_{0\text{-bedrock}}$ should correspond to the V_s profile below

the selected reference depth. The value of $\kappa_{0\text{-site}}$ should be computed considering the complete V_s profile at the recording station. Once $\Delta\kappa_0$ is estimated, the CF_{atn} can be computed using:

$$CF_{atn} = e^{-\pi\Delta\kappa_0 f} \tag{4}$$

The acceleration Fourier amplitude spectrum (FAS) corresponding to the recorded ground motion at the surface is then multiplied by both CF_{imp} and CF_{atn}; and the inverse fast Fourier transform (IFFT) is used to convert V_s-κ scaled FAS to an adjusted acceleration time history. The proposed V_s-κ correction factors modify only the amplitude of the FAS of the selected recording. Additionally, it should be noted that $\Delta\kappa_0$ will be a negative quantity, which means that the CF_{atn} adds energy to the high-frequency portion of the spectrum. If $\Delta\kappa_0$ is large (in absolute value), then a significant amount of energy is added to the motion. At high frequencies this is not realistic, hence a low-pass filter (e.g., Butterworth filter) or a cap can be applied if the reasonableness of the high frequencies obtained (as judged by the analyst) is questionable. It is also recommended to integrate the resulting acceleration time history to make sure the velocity and displacement time histories are appropriate (Kramer 1996).

5.3 Validation Efforts

5.3.1 *Data Selection*

In addition to developing analytical functions for the impedance and attenuation correction factors, one of the main objectives of this study is to demonstrate their effectiveness in adjusting the high-frequency content of input ground motions so that they are compatible with the reference depth at the site of interest. Eight close-by recording stations at rock

sites from the KiK-net database (NIED 1996) were used for validation purposes, and comparing the proposed framework to the outcome of traditional deconvolution techniques. These close-by rock sites were chosen based on the selection criteria described by Cadet et al. (2011).

The KiK-net database is composed of more than 600 pairs of surface-downhole recording stations which are located on weathered rock sites or on shallow sediment deposits (Aoi et al. 2004). Downhole recordings are inappropriate for comparison purposes because destructive interferences influence the motion recorded at depth. Surface recordings, on the other hand, are free surface motions which are deemed more suitable for the intended validation efforts. The main characteristics of the selected paired sites and the seismic events common to each pair are provided in Table 1. The V_s values shown in bold, highlight the $V_{s,30}$ and the V_s at the downhole depth ($V_{s,down}$) that were considered to be comparable by Cadet et al. (2011). Also, stations used as reference are indicated with the letter "R", while the rest correspond to stations where recordings were modified by the V_s-κ correction approach.

5.3.2 *Parameter Estimation*

Different $V_{s,30}$-κ_0 relationships have been recently proposed (e.g., Van Houtte et al. 2011, Chandler et al. 2006, Silva et al. 1998, Poggi et al 2013). In this study, we selected the generic relationship derived by Chandler et al. (2006) to estimate $\Delta\kappa_{0\text{-}CH}$. Alternatively, following the suggestion that the effects of kappa are additive over the ray path (Hough and Anderson, 1988) or over a profile (Anderson 1991; Campbell 2009), kappa can also be related to material damping if the value of the quality factor (Q) is assumed to be frequency-independent:

$$\kappa^{*}_{damping} = \sum_{i=1}^{N} \frac{H_i}{Q_i V_{si}} \quad (5)$$

where H is the thickness of each layer and the contributions are added up over N layers of the profile. In this study, independent Q measurements were not available for the recording stations of interest, but this parameter can be obtained from the decimal damping ratio values (ξ):

$$Q = \frac{1}{2\xi} \quad (6)$$

Values of $\kappa^{*}_{damping}$ (which can be considered equivalent to $\Delta\kappa_0$) were obtained based on small strain damping (ξ_{min}) estimates from Darendeli (2001) and are presented in Table 1 for comparison purposes. There is a significant level of uncertainty in ξ_{min} values which map into uncertainty in estimated $\kappa^{*}_{damping}$ values. Likewise, the significant variability observed in recently published $V_{s,30}$-κ_0 relationships has an impact on estimates of $\Delta\kappa_0$.

Another measure of $\Delta\kappa_0$, namely κ_{0_TF} (following the nomenclature suggested by Ktenidou et al. 2013) is also provided in Table 1. Estimates of κ_{0_TF} can be computed as the slope corresponding to the decay of the TF at the site of interest (Drouet et al. 2010). Different measures of $\Delta\kappa_0$ will lead to different shapes of the ultimate V_s-κ correction. The values of $\Delta\kappa_{0\text{-}CH}$ are consistently lower than κ_{0_TF} at all the stations considered in this study, except for TKYH12 from Pair 8 (TKYH13 - TKYH12) as shown in Table 1. Likewise, $\kappa^{*}_{damping}$ values were found to be the lowest kappa estimates, which may indicate that the attenuation inferred from typical soil damping models (used in geotechnical SRA) provides a lower bound of the actual attenuation characteristics of the site. This discrepancy, also observed between seismological (e.g., Q or κ) and geotechnical (e.g., ξ) descriptors of attenuation

has been highlighted by other recent studies (e.g., Ktenidou et al. 2015, Afshari and Stewart 2015).

Finally, the computation of CF_{imp} requires information about the V_s and densities at the recording station of interest. The V_s data as well as the boring logs corresponding to the sites shown in Table 1 are available at the KiK-net database website (kyoshin.bosai.go.jp). Densities for the materials identified in situ are estimated by means of the empirical relationship based on compressional wave velocities (V_p) proposed by Brocher (2005). As an example, the values of CF_{imp} and CF_{atn} are shown in Figures 3a and 3b, respectively, as computed for station ABSH05 from Pair 1 (see Table 1) using the recorded motion at ABSH04 as the reference motion. The net V_s-κ correction is also provided in Figure 3c.

5.3.3 Validation and Comparison to Traditional Deconvolution

As a validation exercise, we compare the response spectra of the reference outcropping rock motion and the V_s-κ corrected motions (which are obtained by modifying the as-recorded motions using Equations 2 and 4 with $\Delta\kappa_{0\text{-}CH}$). The V_s-κ corrected motions are expected to have a similar spectral shape to the outcropping motion at the reference station. A comparison of the aforementioned response spectra is provided in Figure 4a for the motions recorded at stations ABSH04 (reference) and ABSH05. The resulting acceleration time histories are also provided in Figure 4b along with the original surface ground motion recorded at station ABSH05. After the V_s-κ correction is implemented, a Butterworth filter with six poles and a cut-off frequency around 20 Hz is used. The spectral shape corresponding to the V_s-κ corrected motion (Figure 4a) provides a better agreement with the response spectrum of the reference outcropping rock motion (black dashed line in Figure 4a) than the original surface recording.

An alternative approach to modify surface motions are traditional deconvolution techniques. A deconvolution using linear elastic analyses (by means of the site response program Strata (Kottke and Rathje 2008a, b)) is compared with the proposed V_s-κ correction approach. The response spectra corresponding to the V_s-κ corrected motions and the deconvolved motions (when using Darendeli's (2001) model), for all study sites, are shown in Figure 5. Deconvolved motions provide in general, a lower response spectrum (dashed curve in Figure 5). Their agreement with the response spectrum associated with the reference outcropping rock motion improves for sites with softer (i.e., low $V_{s,30}$) shallow deposits, such as OITH07 (Pair 5), and SRCH09 (Pair 6), while V_s-κ corrected motions perform poorly at these stations (i.e., pairs 2, 5, and 6). On the other hand, V_s-κ corrected motions outperform deconvolved motions in the characterization of the spectral energy in the high-frequency or low-period range (e.g., pairs 1, 7a, 7c, and 7d).

The use of SRI to capture amplification effects ignores the potential of amplification due to resonances. These effects are particularly strong at soft sites. Hence the implementation of the proposed approach should be limited to motions recorded on weathered rock sites or very stiff soil deposits. In more general terms, records from sites with low $V_{s,30}$ or soft near surface deposits should not be used as input motions in SRA because they introduce mid- and long-period narrow-banded peaks that are not representative of an outcropping rock motion. Horizontal to vertical spectral ratios (H/V) may assist in identifying suitable input ground motions for SRA that can be adjusted with the V_s-κ correction framework.

5.4 Practical Implications

The implementation of V_s-κ corrections to input ground motions in SRA will affect the computed spectral accelerations at the surface. For sites underlain by hard rock (e.g., in

CEUS), the corrected input motions will have a much stronger high-frequency content. This is relevant in particular for structural systems sensitive to high-frequency motions. Spectral accelerations at the ground surface are not the only outcome from SRA. Amplification factors (typically defined as a function of ground shaking intensity) also result from SRA and constitute one of the major inputs to site-specific seismic hazard analysis. In this section, we explore the implications of the proposed correction framework on both, the spectral acceleration at the surface and on amplification functions (AFs). 1D equivalent-linear SRA at ten sites are performed (by means of the site response program Strata (Kottke and Rathje 2008a, b)) using as-recorded and V_s-κ corrected input motions.

5.4.1 Selection of Study Sites

Developing a rigorous protocol to identify cases where V_s-κ corrections are necessary would require a statistically significant dataset, where a diverse group of sites and several input ground motions are considered. As a first attempt, we assess ten sites (i.e., two site class C, six site class D and two site class E) and consider seven input ground motions from the KiK-Net database. The selected sites should comply with the assumptions behind 1D site response modeling. Moreover, the sites should preferably have hard rock at the reference depth to test the efficiency of V_s-κ corrections in producing compatible input motions at conditions where actual recordings are scarce (or not even available).

Thompson et al. (2012) developed a classification scheme for downhole arrays to identify recording stations where common 1D wave propagation assumptions apply. These authors analyzed data from 100 recording stations from the KiK-Net database and found 16 sites with a low inter-event variability along with a good fit to the theoretical TF obtained assuming 1D vertically propagating SH-waves through horizontally layered media. Out of

the aforementioned 16 sites, only eight (shown in Table 2) have a V_s value at the reference depth (i.e., soil-rock boundary) greater than 1500 m/s. Hence, those eight sites are considered for this study along with two more sites (not within the KiK-Net database): a site located in a park along the north side of the Charles River Basin, just west of the Boston University Bridge, in Boston, Massachusetts, USA and a generic soft clay site defined by Rodriguez-Marek (2000). The geotechnical characterization of the Boston site is obtained by compiling V_s measurements from Thompson et al. (2014) and an extensive literature review of the geology of the area (e.g., Johnson, 1989, Brankman and Baise, 2008, Berry et al. 2015-in review).

Seven ground motion recordings from the KiK-Net database are used as input motions for conducting SRA at the selected study sites (Table 3). Linear scaling of the pre-selected 7 ground motions (14 horizontal components) is applied to broaden the intensity range of these motions.

5.4.2 Implementation of V_s-κ Corrections

Correction factors for impedance and attenuation effects are applied to each input motion using the $\Delta\kappa_{0\_CH}$ estimates from Chandler et al. (2006). A uniform cap to the CF_{atn} is incorporated in order to limit the increase of high-frequency spectral energy to reasonable values and avoid contamination of the corrected records with high-frequency noise. The limits for the cap are selected based on the frequency range over which surface to borehole ratios decay with frequency. A linear transition from the highest frequency in the identified range up to 30 Hz is incorporated, so that after 30 Hz, the CF_{atn} equals one. Recordings from the KiK-Net database have a cutoff frequency at around 30 Hz. Hence, high-

frequency noise is not being amplified by the proposed correction, avoiding unrealistic FAS and response spectra.

Some of the corrections implemented (i.e., corrections vary according to the site conditions at each recording station) led to a decrease in the high-frequency energy content of the original input motion, while the rest slightly incremented it. This reduction occurs at recording sites with high $V_{s,30}$ where the $\Delta\kappa_0$ is relatively small and the impedance effects dominate the correction. For a subset of stations with low $V_{s,30}$ at the surface (i.e., NGNH08, NGNH34 and NGNH33), the attenuation correction dominates; hence the net V_s-κ correction resulted in an increase in high-frequency motions. In the next sections, we explore the effect of this increase in high-frequency content on spectral accelerations at the ground surface and on AFs.

5.4.3 Differences in Spectral Accelerations at the Ground Surface

Thirty as-recorded and thirty V_s-κ corrected input ground motions (i.e., original and linearly scaled motions) are used to conduct SRA at the selected study sites. The correlation between the ratio of surface spectral accelerations obtained from the as-recorded and V_s-κ corrected sets of input motions (i.e., $Sa,s^o/Sa,s^{Vs\text{-}\kappa}$) and different site and ground motion parameters is investigated. The latter include: (a) the difference between the $V_{s,30}$ value of the assumed elastic half-space at the site of interest and the $V_{s,30}$ at the recording station, ΔV_s; (b) the fundamental frequency of the site, *f'*; and (c) the shear strain index, I_γ (Idriss, 2011), also known as the estimated strain, γ_{est} (Kim et al. 2013) which is defined as the ratio of the peak ground velocity of the input motion and the $V_{s,30}$ of the site of interest ($PGV_{in}/V_{s,30}$). A correlation with *f'* is not found, while $Sa,s^o/Sa,s^{Vs\text{-}\kappa}$ decreases for smaller I_γ only at very short periods. At periods greater than 0.4 seconds, $Sa,s^o/Sa,s^{Vs\text{-}\kappa}$ ratios

approach unity regardless of the I_γ value. The strongest correlation across all periods considered (i.e., from 0.01 sec to 10 sec) is provided by ΔV_s values.

Differences between spectral accelerations computed at the surface when using as-recorded and V_s-κ corrected input motions are more significant for short periods (T) and high values of ΔV_s, especially for 0.03 sec < T < 0.2 sec and ΔV_s > 1500 m/s. Even though larger differences with increasing ΔV_s values are expected, the contours of $Sa,s^o/Sa,s^{Vs\text{-}\kappa}$ ratios shown in Figure 6 demonstrate that there is a specific range of periods where using as-recorded input ground motions may result in unconservative spectral accelerations at the surface. Very high values of ΔV_s can easily result from selecting ground motion recordings from Western US (WUS) as input for SRA conducted at sites overlying a very hard rock (e.g., in CEUS, where the V_s for bedrock is 3000 m/s (Hashash et al. 2014)).

Longer periods (i.e., T > 0.4 sec) are less affected by V_s-κ corrections. Hence, the implementation of the proposed correction framework might not be strictly necessary if the system of interest is known to respond primarily to dynamic loading in such period range. Likewise, when ΔV_s is less than 1000 m/s, as-recorded input ground motions result in spectral accelerations only 10% lower than V_s-κ corrected input motions. Additional efforts required to implement the proposed correction methodology may not be justified by the increased accuracy of the results in that case.

Contours of $Sa,s^o/Sa,s^{Vs\text{-}\kappa}$ corresponding to three site classes are presented in Figure 7. The effects of nonlinearity expected to be more significant for softer sites (i.e., site class E) seem to obscure the influence of V_s-κ corrections. The contours for site class E are noticeably narrower and predict higher values of $Sa,s^o/Sa,s^{Vs\text{-}\kappa}$ ratios than those for site classes C and D. The patterns observed for site class D mimic more closely the contours

presented in Figure 6 because six out of the ten selected study sites are categorized as class D. Contours for Site class C are more sensitive to variations in ΔV_s values, and for a very narrow range of short periods, this site class provide the lowest $Sa^o/Sa^{Vs-\kappa}$ ratios (reaching 0.3 for periods between 0.03 sec and 0.07 sec and ΔV_s values larger than 2500 m/s).

The influence of the input motion intensity on $Sa,s^o/Sa,s^{Vs-\kappa}$ ratios is also investigated. Results from a multivariate linear regression on $Sa,s^o/Sa,s^{Vs-\kappa}$ ratios as a function of both, ΔV_s and the spectral acceleration of the input motion at the period of interest are shown in Figure 8 (for T=0.01 sec and T=1.0 sec). The corresponding mean and standard deviation are provided along with data points from the SRA analyses conducted using Strata (Kottke and Rathje 2008a, b)). The latter are depicted as circles where lighter gray colors correspond to lower intensity motions. Over the short period range (i.e., T < 0.5 sec), $Sa,s^o/Sa,s^{Vs-\kappa}$ ratios become less conservative (i.e., lower than 1) for low intensity motions (e.g., Figure 8a); with the effect being more significant for high ΔV_s values. Lower $Sa,s^o/Sa,s^{Vs-\kappa}$ ratios than unity also result from high ΔV_s values at longer periods (i.e., T > 0.8 sec), but they only reach a value of approximately 0.9 and are not as significantly affected by the intensity of the input motions. At T=1 sec, stronger ground shaking is associated with lower $Sa,s^o/Sa,s^{Vs-\kappa}$ ratios (Figure 8b), however a consistent pattern is not observed for longer periods.

5.4.4 Differences in Amplification Functions

A regression fit (either a linear or a nonlinear relationship) of the amplification as a function of the spectral acceleration of the rock ($S_{a,rock}$) at the same oscillator period is typically used to define the trend of computed amplifications from SRA with input motion amplitude (e.g., see Stewart et al. 2014). We computed these functions for two separate cases, when

using as-recorded input motions (AF^{o}), and when using V_s-κ corrected input motions ($AF^{Vs\text{-}\kappa}$). The trends of the $AF^{o}/AF^{Vs\text{-}\kappa}$ ratios correlate well with site class as shown in Figure 9. For instance, curves corresponding to site class C for T=0.01 sec and T=0.1 sec (Figure 9a and 9b, respectively), show that V_s-κ corrected ground motions result in higher AFs for weak motions (i.e., for spectral accelerations in rock lower than 0.2 g), whereas site class E shows the opposite effect. However, sites categorized as site class E, have $AF^{o}/AF^{Vs\text{-}\kappa}$ ratios around 0.9 for stronger levels of ground shaking. The $AF^{o}/AF^{Vs\text{-}\kappa}$ ratios of all the selected study sites start to converge for longer periods. Some differences are still noticeable in Figure 9b (for T=0.1 sec), but for periods longer than 0.7 seconds, $AF^{o}/AF^{Vs\text{-}\kappa}$ ratios oscillate very closely around the unity for weaker motions and less so for stronger ground shaking (with site class D providing ratios lower than 1 for high intensity motions). At periods between 0.07 seconds and 0.3 seconds, sites categorized as site class D lead to $AF^{o}/AF^{Vs\text{-}\kappa}$ ratios lower than 1 more consistently for low intensity ground shaking, while for very short periods, these sites show more variability (e.g., Figure 9a).

Consequently, $AF^{o}/AF^{Vs\text{-}\kappa}$ ratios are also correlated to the level of intensity of the input ground motion. In fact, these ratios can be expressed as:

$$\frac{AF^{o}}{AF^{Vs-\kappa}} = \frac{\dfrac{Sa,s^{o}}{Sa,r^{o}}}{\dfrac{Sa,s^{Vs-\kappa}}{Sa,r^{Vs-\kappa}}} = \frac{Sa,s^{o}}{Sa,s^{Vs-\kappa}} \cdot \frac{Sa,r^{Vs-\kappa}}{Sa,r^{o}} \tag{7}$$

where *Sa,s* refers to spectral accelerations at the ground surface and *Sa,r* at the bedrock level (i.e., the reference depth at the site), while superscripts *o* and *V_s-κ* indicate the type of input motions used for conducting the SRA (e.g., *o* for original or as-recorded motions). The ratios $Sa,s^{o}/Sa,s^{Vs\text{-}\kappa}$ are shown in Figure 8 as a function of ΔV_s and $S_{a,rock}$. The ratio

$Sa,r^{Vs\text{-}\kappa}/Sa,r^{o}$ corresponds to the proposed V_s-κ correction as it would apply in the response spectral domain; and it is a function of ΔV_s while weakly correlated to $S_{a,rock}$. We use the $AF^{o}/AF^{Vs\text{-}\kappa}$ ratios (as computed using Equation 7) to identify cases where the proposed V_s-κ correction can affect the computed AFs. Mean values and their corresponding standard deviations for T=0.01 sec and T=1.0 sec are shown in Figure 10 across different ΔV_s values. Additionally, $AF^{o}/AF^{Vs\text{-}\kappa}$ data points obtained by the multiplication of empirical values of $Sa,s^{o}/Sa,s^{Vs\text{-}\kappa}$ and $Sa,r^{Vs\text{-}\kappa}/Sa,r^{o}$ ratios from SRA using Strata (Kottke and Rathje 2008a, b)) are provided as circles whose color is associated with the intensity of the ground shaking (i.e., $S_{a,rock}$). All sites and input ground motions were considered and plotted in accordance with their corresponding ΔV_s and $S_{a,rock}$ values.

At T=0.01 sec (Figure 10a) $AF^{o}/AF^{Vs\text{-}\kappa}$ ratios increase as ΔV_s values increase, while the intensity of the ground motion (i.e., $S_{a,rock}$) has only a minor influence. Overall, lower intensity motions lead to lower $AF^{o}/AF^{Vs\text{-}\kappa}$ ratios, which in some cases reach values lower than the unity. There is an increasing influence of the intensity of shaking on $AF^{o}/AF^{Vs\text{-}\kappa}$ ratios between 0.04 sec < T < 0.1 sec. Weaker motions (i.e., $S_{a,rock}$ < 0.15 g) result in lower $AF^{o}/AF^{Vs\text{-}\kappa}$ ratios than stronger ground motions and they also lead to $AF^{o}/AF^{Vs\text{-}\kappa}$ ratios lower than the unity. However, the influence of $S_{a,rock}$ is reduced for T > 0.1 sec.

For periods between 0.15 sec and 0.5 sec, $AF^{o}/AF^{Vs\text{-}\kappa}$ ratios do not change significantly with ΔV_s values, but at longer periods (e.g., Figure 10b), $AF^{o}/AF^{Vs\text{-}\kappa}$ ratios start decreasing as ΔV_s values increase. Interestingly, it is the stronger ground motions the ones leading to lower $AF^{o}/AF^{Vs\text{-}\kappa}$ ratios than the lower intensity motions within this period range.

These preliminary results indicate that AFs are less affected by V_s-κ corrections than computed spectral accelerations at the surface. However, given the dependency on site

class observed in Figure 9, future research should focus on investigating the impact of the proposed corrections on different site profiles. Stiffer sites subjected to low intensity input motions are likely to be more influenced by the change in high-frequency content of input motions used in SRA.

5.5 Conclusions

A V_s-κ correction framework has been proposed (as an alternative to traditional deconvolution techniques) to modify recorded motions on rock and soft rock such that these are compatible with the reference depth velocity and site kappa at a site where SRA are conducted. The key components of this methodology, namely the impedance and attenuation correction factors, are consistent with similar scaling approaches for GMPEs (e.g., Campbell 2003, Al Atik et al. 2014). Their implementation will allow for the expansion of the range of stations from which ground motions can be selected as input for SRA.

A validation exercise using a subset of close-by rock site pairs from the KiK-net database was conducted. The proposed methodology was found to depend heavily on the difference in κ_0 between the recording station and the reference rock at the site. In this study, we used estimates of κ_0 from Chandler et al. (2006). The V_s-κ corrected motions provided a reasonable agreement with the reference outcropping rock motions and deconvolved motions. However, motions recorded at sites with very soft near-surface deposits or with strong resonances are poor candidates for the V_s-κ correction approach. Our recommendation reinforces current practices in which ground motions affected by site resonances or recorded at low $V_{s,30}$ (i.e., soft deposits) sites are not considered a suitable input to SRA.

Finally, the impact of the proposed correction framework on spectral accelerations at the surface and AFs was investigated. Spectral accelerations at the ground surface were found to be highly affected by V_s-κ corrections, which can be relevant for dynamic analyses of new and existing infrastructure. As expected, the difference between V_s values at the reference depth at the site of interest, and at the recording station plays a major role in how influential (and necessary) the proposed corrections may be. Contours showing this dependency were provided so that a specific range of periods where unconservative estimates of spectral accelerations are expected could be identified. Additionally, stiffer sites (e.g., site class C) subjected to low intensity ground shaking levels can potentially be more influenced by changes in the high-frequency content of input motions (resulting from the proposed methodology) than softer sites (e.g., site class E). Consequently, V_s-κ corrections seem to have varying effects on spectral accelerations at the surface and AFs depending on the site class. Further investigation including a larger set of site profiles and input ground motions is needed to better understand which parameters control the observed behavior. Such study would be key to clarifying the potential implications of the V_s-κ correction framework on site-specific seismic hazards assessments and dynamic analyses of critical infrastructure.

References

Afshari, K. and Stewart, J.P., (2015). *Effectiveness of 1D ground response analyses at predicting site response at California vertical array sites*, Proc. SMIP2015 Seminar on Utilization of Strong Motion Data, California Strong Motion Instrumentation Program, Sacramento, CA (electronic file).

Al Atik, L., Kottke, A., Abrahamson, N., and Hollenback, J., (2014). Kappa (κ) Scaling of Ground-Motion Prediction Equations Using an Inverse Random Vibration Theory Approach, *Bulletin of the Seismological Society of America*, **104**(1), 336-346.

Anderson, J.G., (1991). A preliminary descriptive model for the distance dependence of the spectral decay parameter in southern California, *Bulletin of the Seismological Society of America*, **81**, 2186–2193.

Anderson, J.G., and Hough, S.E., (1984). A model for the shape of the Fourier amplitude spectrum of acceleration at high frequencies, *Bulletin of the Seismological Society of America* **74**(5), 1969-1993.

Aoi, S., Kunugi, T., and Fujiwara, H., (2004). Strong-Motion Seismograph Network Operated by NIED: K-NET and KiK-net, *Journal of Japan Association for Earthquake Engineering*, **4**(3), 65-74.

Berry, B.M, Baise, L.G., and Thompson, E.M., (under review). Regional stratigraphy and velocity models for soil amplification with a strong impedance contrast: Boston, Massachusetts, *Engineering Geology.*

Boore, D., (2003). Simulation of Ground Motion Using the Stochastic Method, *Pure and Applied Geophysics*, **160**(3-4), 635-676.

Boore, D., (2013). The Uses and Limitations of the Square-Root-Impedance Method for Computing Site Amplification, *Bulletin of the Seismological Society of America*, **103**(4), 2356-2368.

Brankman, C.M., and Baise, L.G., (2008). Liquefaction susceptibility mapping in Boston, Massachusetts: *Environmental and Engineering Geoscience*, **14**, 1–16.

Brocher, T.M., (2005). Empirical Relations between Elastic Wavespeeds and Density in the Earth's Crust, *Bulletin of the Seismological Society of America*, **95**(6), 2081-2092.

Cadet, H., Bard, P.Y., and Rodriguez-Marek, A., (2011). Site effect assessment using KiK-net data: Part 1. A simple correction procedure for surface/downhole spectral rations, *Bulletin of Earthquake Engineering*, **10**(2), 421-448.

Campbell, K. W., (2003). Prediction of Strong Ground Motion Using the Hybrid Empirical Method and Its Use in the Development of Ground-Motion (Attenuation) Relations in Eastern North America, *Bulletin of the Seismological Society of America*, **93**(3), 1012-1033.

Campbell, K. W., (2009). Estimates of Shear-Wave Q and κ_o for Unconsolidated and Semiconsolidated Sediments in Eastern North America, *Bulletin of the Seismological Society of America*, **99**(4), 2365-2392.

Chandler, A.M., Lam, N.T.K., and Tsang, H.H., (2006). Near-surface attenuation modelling based on rock shear-wave velocity profile, *Soil Dynamics and Earthquake Engineering*, **26**(11), 1004-1014

Darendeli, M.B., (2001). *Development of a New Family of Normalized Modulus Reduction and Material Damping Curves*, Ph.D. Dissertation, University of Texas, Austin, TX.

Drouet S., Cotton, F., and Gueguen, P., (2010). Vs30, κ, regional attenuation and Mw from accelerograms: application to magnitude 3-5 French earthquakes, *Geophysical Journal International*, **182**(2), 880-898.

Hashash, Y. M. A., A. R. Kottke, J. P. Stewart, K. W. Campbell, B. Kim, C. Moss, S. Nikolaou, 368 E. M. Rathje and W. J. Silva (2014). Reference rock site condition for central and Eastern 369 North America. *Bulletin of the Seismological Society of America,* **104**: 684-701.

Hough, S.E. and Anderson, J.G., (1988). High-frequency spectra observed at Azna, California: implications for Q structure, *Bulletin of the Seismological Society of America,* **78**, 692–707.

Idriss, I. M. (2011). Use of Vs30 to represent local site conditions. 4th LASPEI/IAEE 375 International Symposium Effects of Surface Geology on Strong Ground Motions. Santa 376 Barbara, California.

Johnson, E.G., (1989). Geotechnical characteristics of the Boston area: *Civil Engineering Practice-Journal of the Boston Society of Civil Engineers Section/ASCE,* **4**(1), 53–64.

Joyner, W.B., Warrick, R.E., and Fumal, T.E., (1981). The effect of quaternary alluvium on strong ground motion in the Coyote Lake, California, earthquake of 1979, *Bulletin of the Seismological Society of America,* **71**(4), 1333-1349.

Kim B, Hashash Y.M.A., Kottke A., Assimaki D., Li W., Rathje E.M., Campbell K.W., Silva W.J., Stewart J.P., (2013). A predictive model for the relative differences between nonlinear and equivalent-linear site response analyses, 22nd Conference on Structural Mechanics in Reactor Technology (SMiRT22). San Francisco. August 18-23.

Kottke, A. R., and Rathje, E.M., (2008a). *Strata, Version alpha, Revision 381*, University of Texas, Austin, TX.

Kottke, A. R., and Rathje, E.M., (2008b). *Technical Manual for Strata*, Report 2008/10, Pacific Earthquake Engineering Research (PEER) Center, University of California, Berkeley, CA.

Kramer, S., (1996). *Geotechnical Earthquake Engineering*, Prentice Hall, Upper Saddle River, NJ.

Ktenidou, O.J., Abrahamson, N.A., Drouet, S., and Cotton, F., (2015). Understanding the Physics of Kappa (K): Insights from a downhole array. *Geophysical Journal International* **203**(1), 678-691.

Ktenidou, O.J., Cotton, F., Abrahamson, N.A., and Anderson, J.G., (2014). Taxonomy of κ: A Review of Definitions and Estimation Approaches Targeted to Applications, *Seismological Research Letters*, **85**(1), 135-146.

National Research Institute for Earth Science and Disaster Prevention (NIED), (1996). *Strong Motion Seismograph Networks (K-NET, KiK-net)*, <http://www.kyoshin.bosai.go.jp/> (Oct. 9, 2014).

Poggi, V., Edwards, B., and Fäh, D., (2013). Reference s-wave velocity profile and attenuation models for ground-motion prediction equations: application to Japan, *Bulletin of the Seismological Society of America*, **103**, 2645–2656.

Rathje, E., Kottke, A., and Trent, W., (2010). Influence of Input Motion and Site Property Variabilities on Seismic Site Response Analysis, *Journal of Geotechnical and Geoenvironmental Engineering*, **136**(4), 607-619.

Rodriguez-Marek, A., (2000). Near-Fault Seismic Site Response, Ph.D. Thesis, Department of Civil Engineering, University of California, Berkeley.

Schnabel, P.B., Lysmer, J., and Seed, H.B, (1972). *SHAKE: A Computer Program for Earthquake Response Analysis of Horizontally Layered Sites*, Report UCB/EERC-72/12, Earthquake Engineering Research Center, University of California, Berkeley, CA.

Seed, H.B., and Idriss, I.M., (1970). *Soil Moduli and Damping Factors for Dynamic Response Analyses*, Report UCB/EERC-70/10, Earthquake Engineering Research Center, University of California, Berkeley, CA.

Seed, H.B., Romo, M.P., Sun, J.I., Jaime, A., and Lysmer, J., (1987). *Relationships between Soil Conditions and Earthquake Ground Motions in Mexico City in the Earthquake of September 19, 1985*, Report UCB/EERC-87/15, Earthquake Engineering Research Center, University of California, Berkeley, CA.

Seed, H.B., Whitman, R.V., Dezfulian, H., Dobry, R., and Idriss, I.M., (1972). Soil Conditions and Building Damage in 1967 Caracas Earthquake, *Journal of the Soil Mechanics and Foundations Division*, **98**(8), 787-806.

Seed, R.B., Dickenson, S.E., and Idriss, I.M., (1991). Principal Geotechnical Aspects of the 1989 Loma Prieta earthquake, *Soils and Foundations* **31**(1), 1-26.

Silva, W., Darragh, R., Gregor, N., Martin, G., Abrahamson, N., and Kircher C., (1998). Reassessment of site coefficients and near-fault factors for building code provisions, Technical Report Program Element II: 98-HQGR-1010, Pacific Engineering and Analysis, El Cerrito.

Stewart, J.P., Afshari, K. and Hashash, Y.M.A., (2014). *Guidelines for Performing Hazard-Consistent One-Dimensional Ground Response Analysis for Ground Motion Prediction*. PEER Report.

Thompson, E. M., Baise, L.G., Tanaka, Y., and Kayen, R.E., (2012). A taxonomy of site response complexity, *Soil Dynamics and. Earthquake Engineering,* **41**, 32–43.

Thompson, E.M., Carkin, B., Baise, L.G., and Kayen, R.E., (2014). Surface wave site characterization at 27 locations near Boston, Massachusetts, including 2 strong-motion stations: U.S. Geological Survey Open-File Report 2014–1232, 27 p., http://dx.doi.org/10.3133/ofr20141232.

Van Houtte, C., Drouet, S., and Cotton, F., (2011). Analysis of the origins of κ (Kappa) to compute hard rock to rock adjustment factors for GMPEs, *Bulletin of the Seismological Society of America*, **101**, 2926–2941.

Table 1: Characteristics of the close-by rock sites pairs selected by Cadet et al. (2011).

Pair no.	Couple [(1)]	# of Events (Date)	Sensor depth (m)	$V_{s,30}$ (m/s)	$V_{s,down}$ (m/s)	κ_{0_TF}	$\Delta\kappa_{0\text{-}CH}$	$\kappa^*_{damping}$
1	ABSH04 (R)	1 (9/26/03)	200	**1136**	3100			
	ABSH05		106	624	**1800**	*0.060*	*0.008*	*0.001*
2	KGWH03 (R)	1 (9/5/04)	100	**1410**	2590			
	KGWH01		117	255	**1287**	*0.040*	*0.024*	*0.002*
3	KGWH03 (R)	1 (9/5/04)	100	**1410**	2590			
	KGWH04		105	407	**1760**	*0.049*	*0.006*	*0.002*
4	OITH05 (R)	1 (10/6/00)	100	**1269**	1900			
	OITH04		230	459	**960**	*0.024*	*0.006*	*0.002*
5	OITH05 (R)	1 (10/6/00)	100	**1269**	1900			
	OITH07		101	276	**1600**	*0.049*	*0.043*	*0.003*
6	SRCH10 (R)	1 (9/26/03)	200	**1027**	1600			
	SRCH09		122	241	**780**	*0.047*	*0.040*	*0.004*
7	TKYH13 (R)	4 [(2)]	100	**1110**	2500			
	KNGH18		100	388	**1200**	*0.062*	*0.050*	*0.002*
8	TKYH13 (R)	4 [(2)]	100	**1110**	2500			
	TKYH12		147	326	**1800**	*0.019*	*0.054*	*0.003*

[(1)] R denotes the reference station
[(2)] event (a): 10/23/04, event (b): 9/5/04, event (c): 10/23/04 and event (c): 10/24/04

Table 2: Sites used to investigate influence of V_s-κ corrected motions on spectral accelerations at the surface and AFs.

Site	$V_{s,30}$ (m/s)	$V_{s,down}$ (m/s)	Site Class
IWTH02	390	2300	C
IWTH27	670	2790	C
IBRH13	335	3000	D
IBRH17	301	2300	D
IWTH08	305	2120	D
KSRH10	213	1700	D
TKCH08	353	2800	D
909BUB	295	1500	D
Generic E	135	1500	E
IBRH10	144	2350	E

Table 3: Ground motion recordings used in this study to estimate spectral accelerations at the surface and AFs at the selected study sites.

Station Name	Recording	Mw	R_{rup} (km)	$V_{s,30}$ (m/s)	$V_{s,down}$ (m/s)
NGNH08	RSN5219_CHUETSU_NGNH08EW RSN5219_CHUETSU_NGNH08NS	6.8	131.0	432.69	900
NGNH31	RSN5241_CHUETSU_NGNH31EW RSN5241_CHUETSU_NGNH31NS	6.8	141.6	526.87	1100
NGNH34	RSN5244_CHUETSU_NGNH34EW RSN5244_CHUETSU_NGNH34NS	6.8	106.5	489	970
TCGH09	RSN5355_CHUETSU_TCGH09EW RSN5355_CHUETSU_TCGH09NS	6.8	120.7	649.05	1050
AOMH15	RSN5538_IWATE_AOMH15EW RSN5538_IWATE_AOMH15NS	6.9	145.1	577.54	1200
FKSH08	RSN6520_NIIGATA_FKSH08EW RSN6520_NIIGATA_FKSH08NS	6.63	110.4	562.5	1470
NGNH33	RSN6721_NIIGATA_NGNH33EW RSN6721_NIIGATA_NGNH33NS	6.63	111.1	435.4	1100

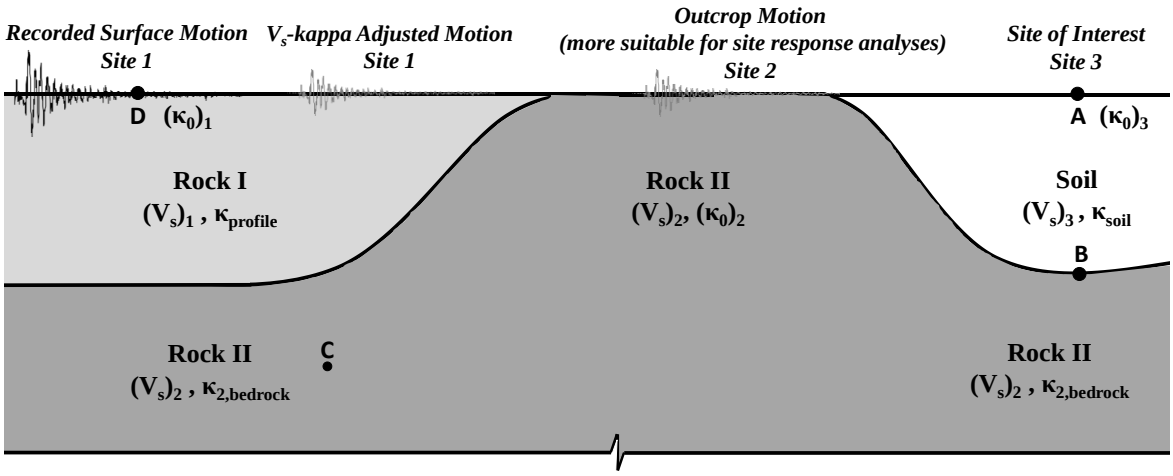

Figure 1: Representation of V_s-κ corrected motions in the context of SRA.

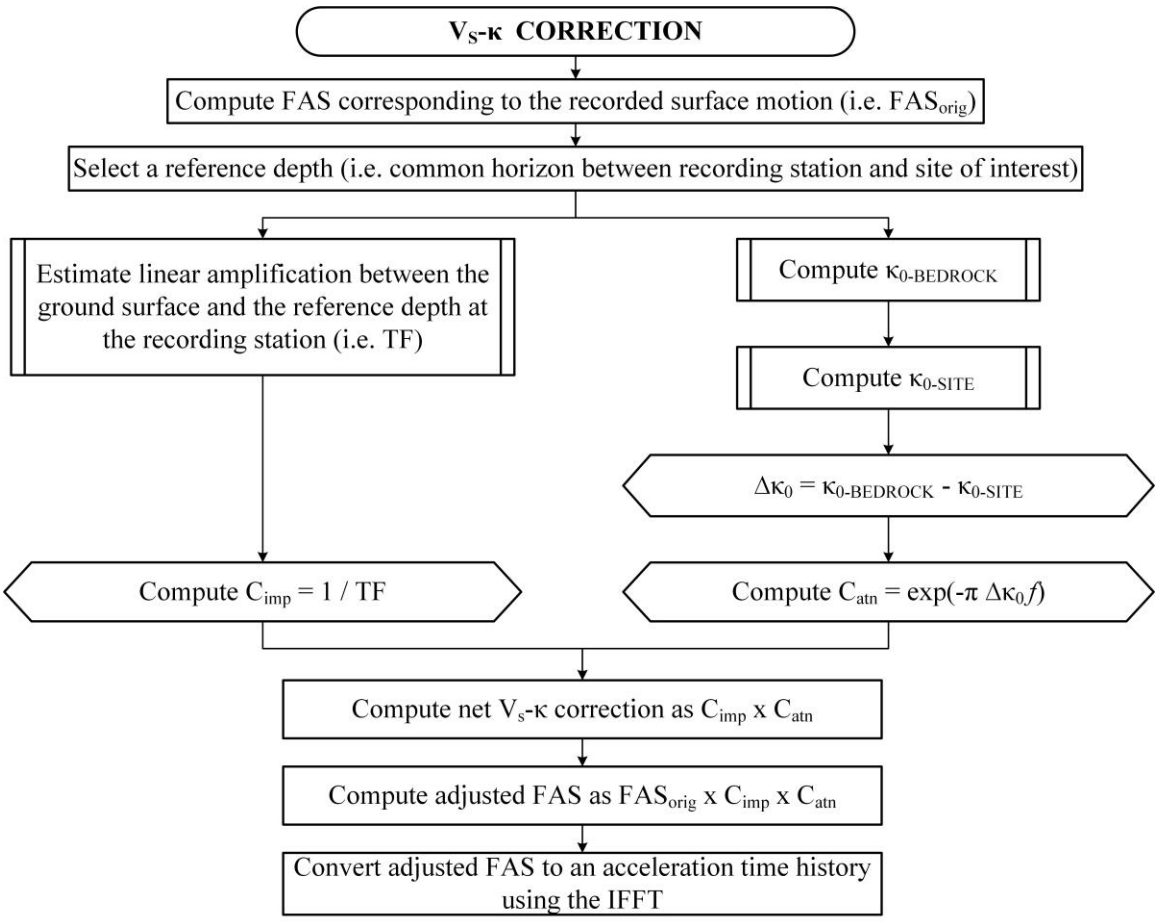

Figure 2: Steps for deriving V_s-κ correction factors and obtaining the adjusted input ground motion.

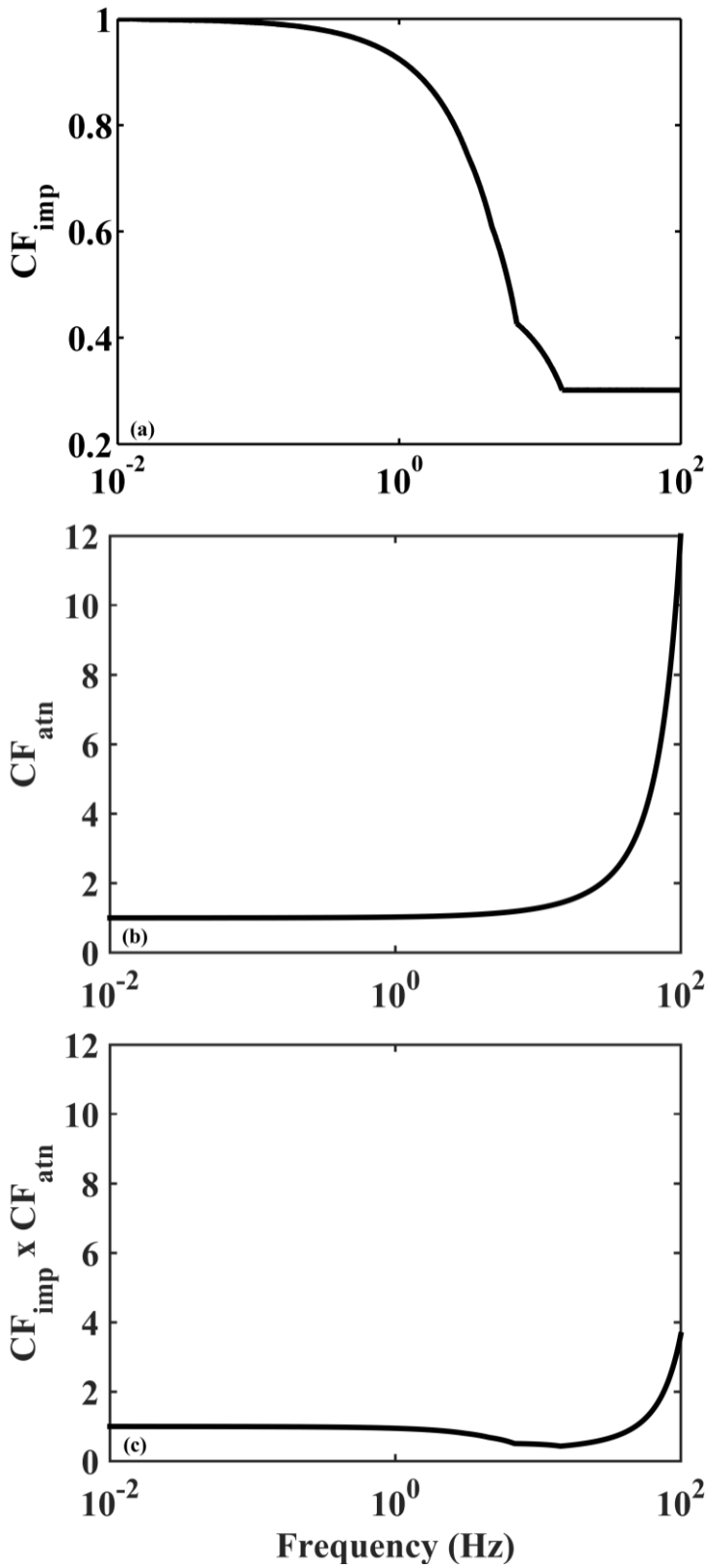

Figure 3: (a) Impedance and (b) attenuation correction factors, as well as (c) their net effect as calculated for station ABSH05.

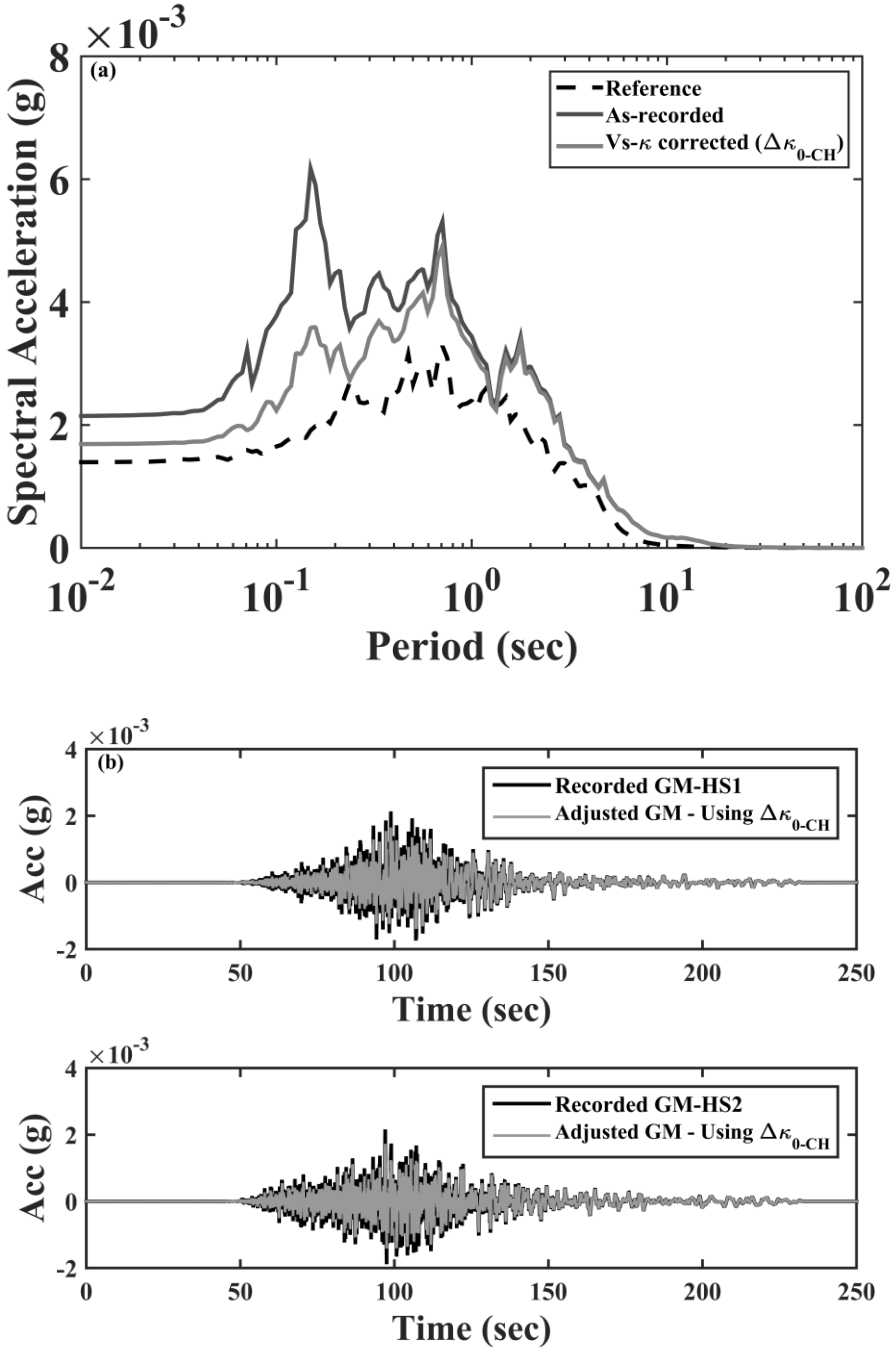

Figure 4: (a) Response spectra (geometric mean) corresponding to the V_s-κ corrected, as-recorded and reference motions, and (b) V_s-κ corrected time histories using $\Delta\kappa_{0\text{-CH}}$, along with the as-recorded acceleration time histories at ABSH04.

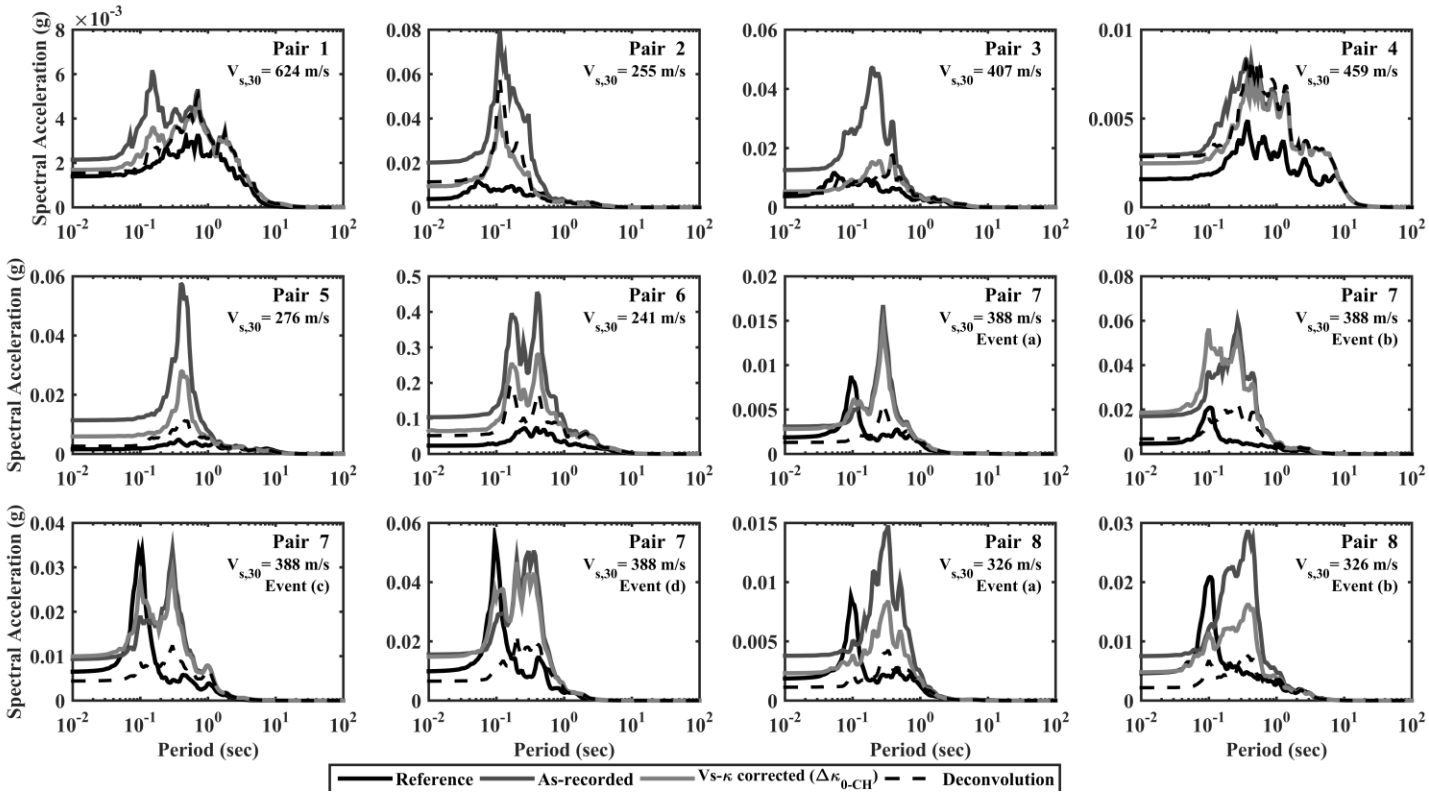

Figure 5: Response spectra corresponding to V_s-κ corrected and deconvolved motions.

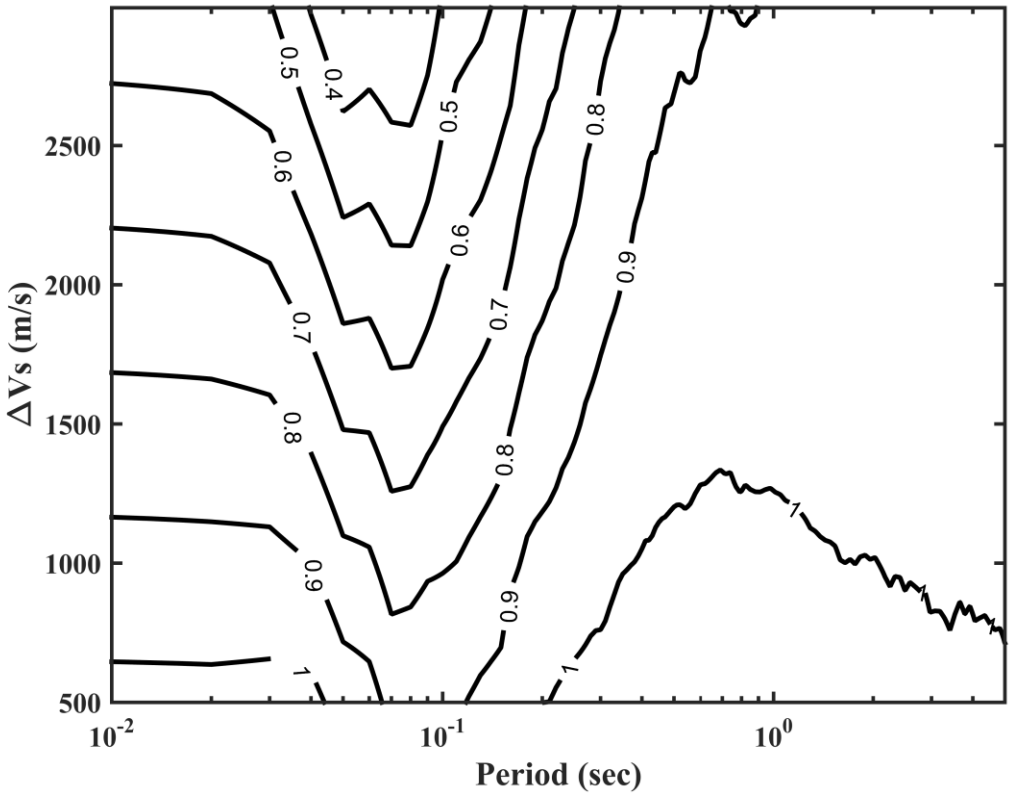

Figure 6: Contours of $Sa,s^{o}/Sa,s^{Vs\text{-}\kappa}$ ratios as a function of ΔV_s values (all sites considered).

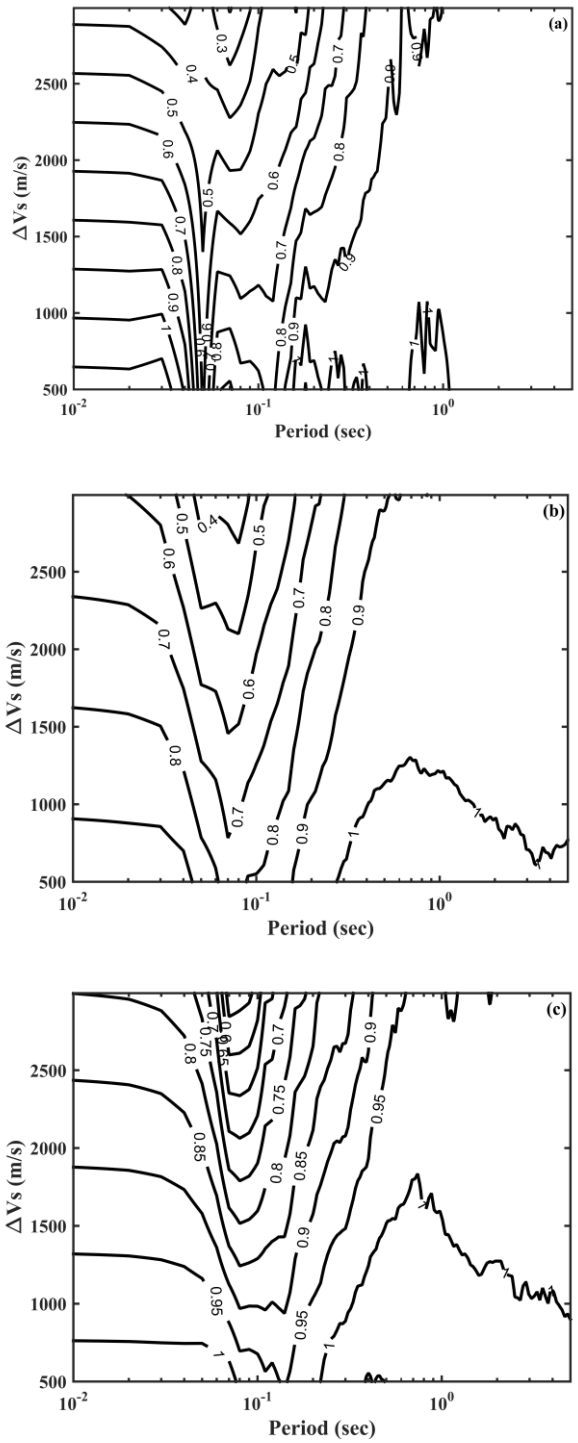

Figure 7: Contours of $Sa,s^{o}/Sa,s^{Vs\text{-}\kappa}$ ratios as a function of ΔV_s values across periods and per site class: (a) Site class C, (b) Site class D, and (c) Site class E.

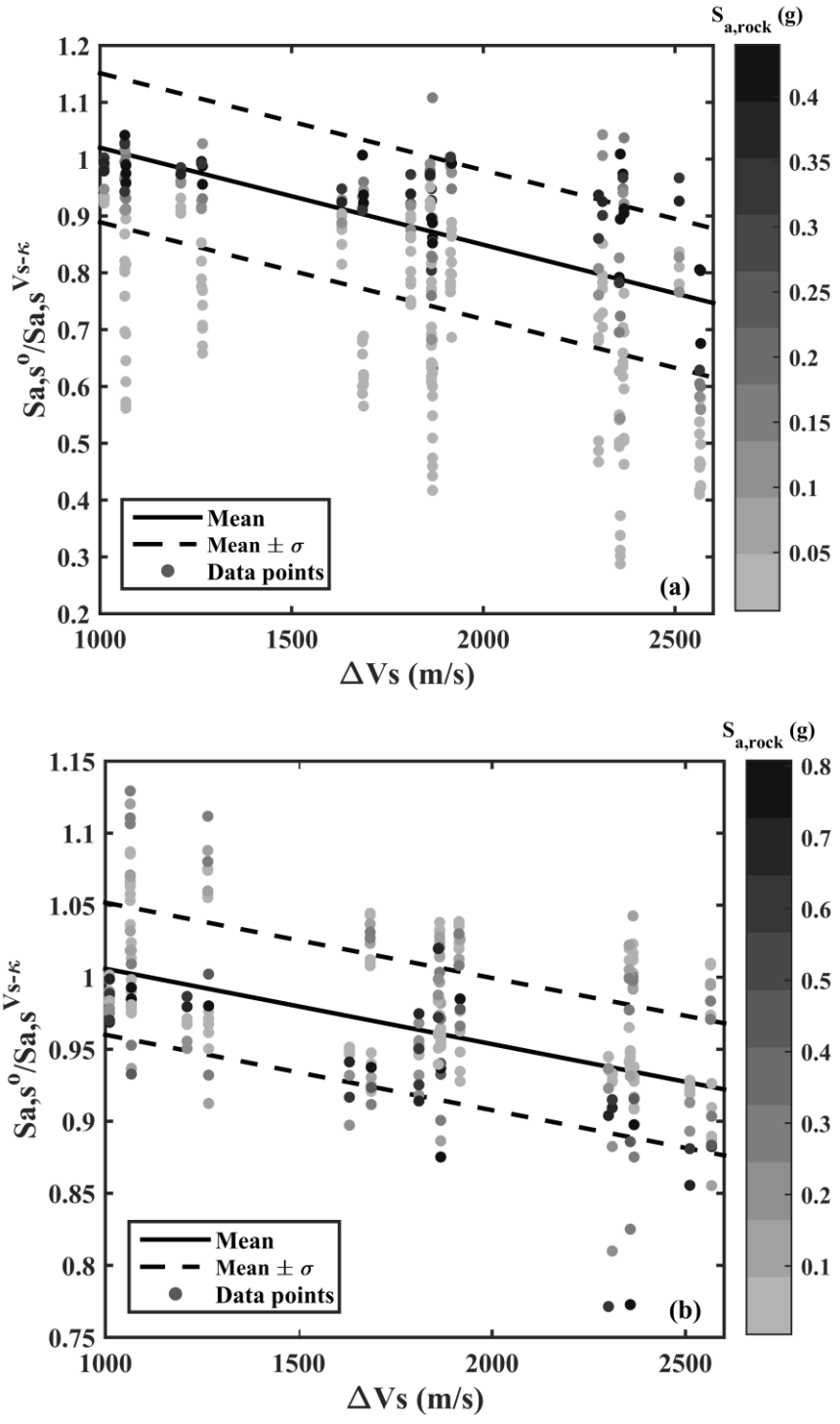

Figure 8: $Sa,s^{o}/Sa,s^{Vs-\kappa}$ ratios for (a) T = 0.01 sec and (b) T = 1.0 seconds.

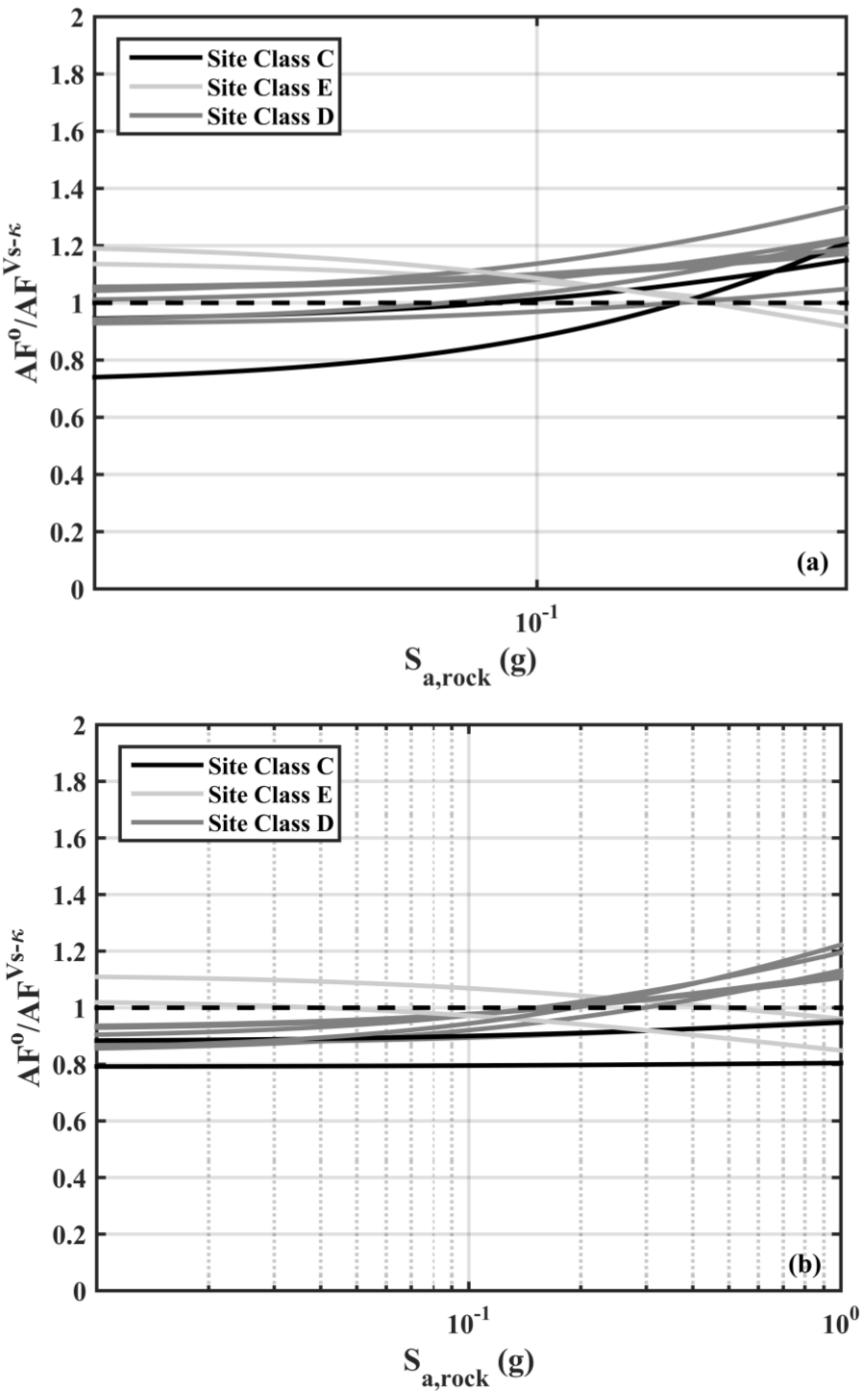

Figure 9: $AF^{o}/AF^{Vs\text{-}\kappa}$ ratios per site class corresponding to (a) T=0.01 sec and (b) T=0.1 sec.

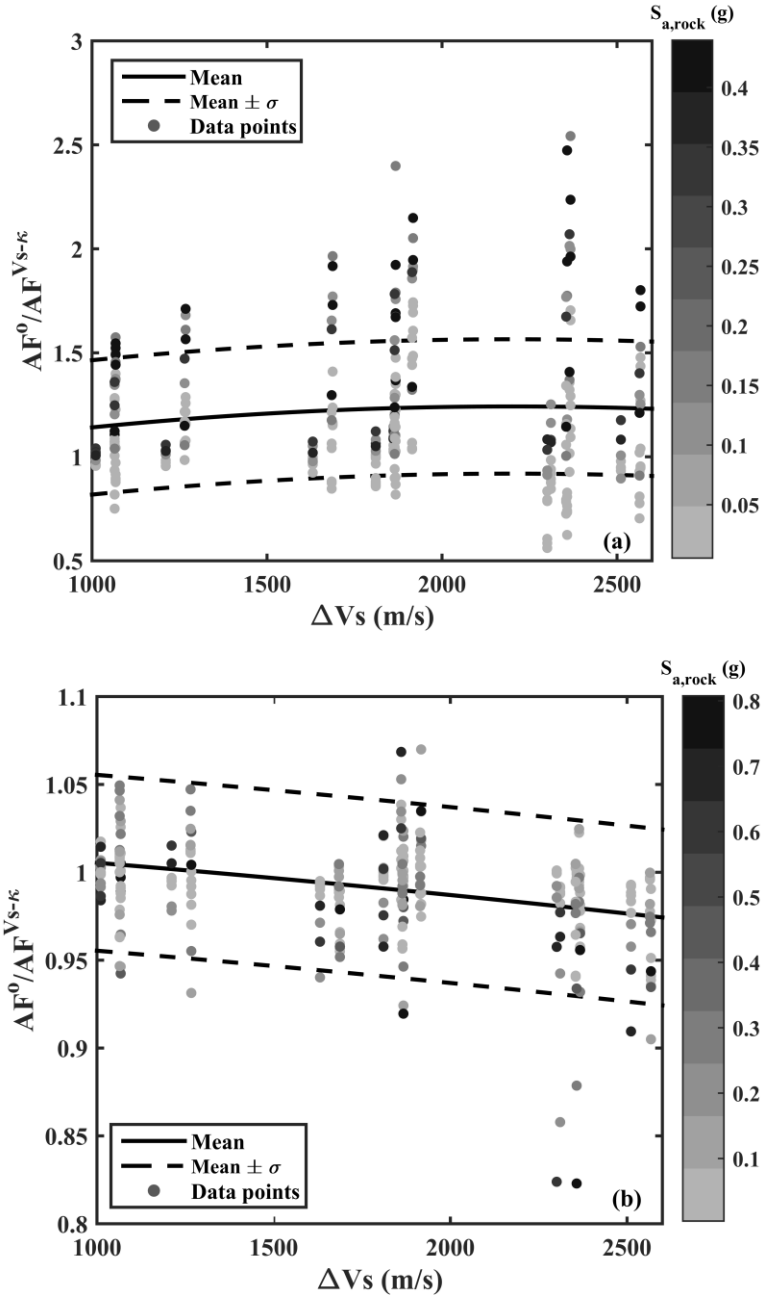

Figure 10: $AF^{o}/AF^{Vs-\kappa}$ ratios for (a) T=0.01 sec and (b) T=1 sec.

CHAPTER SIX

CONCLUSIONS

6.1 Summary

This research work presented improvements to the assessment of site-specific seismic hazards with a primary focus on overcoming some of the limitations in site response analysis (SRA). The main contributions of this research are listed as follows:

- Minimum shear strain damping values consistent with κ_0, an attenuation descriptor often used in engineering seismology, have been computed at multiple recording stations from the large Japanese database, KiK-net. Combined models of geotechnical and seismological attenuation descriptors were proposed.
- The contribution of the shallow layers to κ_0 estimates was investigated. The difference between κ_0 at the surface and at depth was quantified for several KiK-net stations and its correlation to shallow geologic structures was examined.
- The errors introduced in SRA when the reference depth, and the materials below it, at the site of interest do not comply with the assumptions of an ideal elastic half-space (EHS) were assessed. Geologic conditions leading to significant errors associated with the elastic half-space assumption were identified.
- A V_s-κ correction framework for input motions used in SRA has been proposed as an alternative to traditional deconvolution techniques, when only generic

knowledge of the profiles is known. Correction factors can modify recorded motions on rock and soft rock, such that these are compatible with impedance and attenuation characteristics of the assumed elastic half-space at the site.

6.2 Findings

6.2.1 Estimation of Kappa (κ)-consistent Damping Values

Values of κ_0 were computed at multiple stations from the KiK-net database. Minimum shear strain damping values consistent with the attenuation of seismic waves in the field, as captured by measured κ_0 values, were then estimated. The correlation of κ_0 estimates with shallow geology was also investigated. The key findings can be summarized as follows:

- Values of laboratory-based minimum shear strain damping when compared to the proposed κ_0-consistent estimates were found to provide a lower bound to the characterization of the attenuation in situ. Only intrinsic material damping can be captured when testing small-scale soil elements in the laboratory, which hinders the quantification of other sources of attenuation as they occur in the field (e.g., scattering effects and multipathing).
- Increasing minimum shear strain damping values from typical laboratory-based models by 2% to 3%, provided low strain damping profiles which are compatible with the measured κ_0 at the selected study sites.
- The difference between κ_0 values at the surface and at the downhole depth was found to be correlated with V_{s30} and the depth to bedrock. Such difference, referred

to as $\Delta\kappa$, decreases for stiffer, shallower sites. This implies that $\Delta\kappa$ can encapsulate the attenuation in near-surface materials. Also, this means that the contributions of the attenuation in the rock mass and the overlying sediments can be considered independently.

- Two estimates of κ_0 were deemed possible as regional hard rock κ_0 for Japan. Both values lie below regional estimates found by other researchers for New Zealand, Greece and Switzerland. This implies that Japanese hard rocks and stiff sites dissipate less energy than their counterparts in the aforementioned regions.

6.2.2 The Elastic Half-Space Assumption in Site Response Analysis

This study examined the potential systematic errors introduced in SRA when the selected reference depth, and the strata below it at the site of interest, do not comply with the assumptions of an ideal elastic half-space. Selecting an appropriate EHS boundary condition is relevant, because it also implies that the input motions applied at such horizon should be recorded at a site with an equivalent site response to that of the assumed EHS. The main outcomes from this research are outlined below:

- The ratio of transfer functions as obtained from the analysis of the full soil column and its corresponding decoupled representation was proposed as a measure of the error associated with the EHS assumption.
- A parametric study conducted at a three-layer profile investigated the most influential factors on the error introduced by the EHS assumption in SRA. This study revealed that the presence of a strong impedance contrast is not the only

condition that should be considered when defining the EHS location. Both, the shear wave velocity and thickness of the shallow soil deposits proved to be influential factors on the estimated error. Likewise, the shear wave velocities of underlying soft and hard rock layers also affect the estimates of site response over a specific range of frequencies of engineering interest.

- Case studies of unusual profiles found at sites in Charleston, SC and Hanford, WA were presented to show that the error associated with the EHS assumption on site response is not negligible for certain geologic conditions. The presence of a strong impedance contrast located at depth or shear wave velocity reversals represent a significant departure from the hypotheses behind an ideal EHS. Hence, they can lead to nontrivial errors in the estimation of the response at the site.

6.2.3 V_s-κ Correction Factors for Input Ground Motions used in Seismic Site Response Analysis

A V_s-κ correction framework has been proposed as an alternative to traditional deconvolution techniques. Impedance and attenuation differences between the recording and the study sites are addressed so that input motions are compatible with the velocity and site κ of the assumed EHS at the site of interest. This correction framework, although inspired by scaling approaches for ground motion prediction equations, represents an important contribution towards expanding the range of stations from which ground motions can be selected as input for SRA. The main findings are summarized as follows:

- The V_s-κ corrected motions provided a reasonable agreement with the reference outcropping rock motions and deconvolved motions. Deconvolved motions provided in general, a lower response spectrum than V_s-κ corrected motions. Their agreement with the response spectrum of the reference outcropping rock motion improved for sites with softer, shallower deposits. V_s-κ corrected motions outperformed deconvolved motions in the characterization of the spectral energy in the high-frequency range at most of the study sites.
- The proposed methodology was found to depend heavily on the difference in κ_0 between the recording station and the reference rock at the site.
- Motions recorded at sites with very soft near-surface deposits or with strong resonances are poor candidates for the V_s-κ correction approach. This finding reinforces current practices in which ground motions affected by site resonances or recorded at low $V_{s,30}$ sites are not deemed suitable inputs to SRA.
- Spectral accelerations at the ground surface were found to be highly affected by V_s-κ corrections, which can be relevant for dynamic analyses of new and existing infrastructure.
- The difference between V_s values of the assumed EHS at the site of interest, and at the recording station plays a major role in assessing the need for the proposed corrections.
- The amplification functions for stiffer sites subjected to weak ground shaking are more influenced by V_s-κ corrections. Nonlinearity obscures V_s-κ correction effects.

6.3 Recommendations for Future Research

The definition of an appropriate EHS, along with using compatible input motions with such EHS and damping values which more closely match the attenuation in the field address some of the limitations in SRA. In addition, the research presented herein has identified other issues that require further investigation:

- The main outcomes of this study (i.e., the V_s-κ corrections, recommendations for the location of the EHS and combined damping models) should be implemented at sites with vertical arrays so that the effectiveness of the proposed solutions can be tested against recorded ground motions. The variability in the resulting estimates of site response can be compared when implementing one, two or all three of the aforementioned improvements. Knowing which improvement leads to better estimates of site response and less variability would provide some guidance on where future research efforts should focus on: input motion selection protocols, modeling fundamentals of wave propagation in deep profiles or damping characterization.
- When computing new minimum strain damping estimates based on κ_0 values, the added damping to typical laboratory-based values (herein referred to as $\Delta\xi_{min}$) were found by assuming depth-independency and V_s-dependency. A third alternative worth exploring is the depth-dependency of $\Delta\xi_{min}$, considering that both, minimum strain damping and κ, are functions of depth.
- In the case of Japan, it was found that there are two possible estimates of κ_0 associated with hard rock and stiff sites. Further research is necessary to rigorously

investigate some of the hypotheses proposed herein that could explain the observed behavior in the region and explore other potential causes.

- Considering that only linear elastic SRA were conducted when investigating the importance of the EHS assumption, future studies on the effects of soil nonlinear behavior could help expand the recommendations presented herein.
- The applicability of the proposed V_s-κ corrections could be expanded by developing analogous procedures for sites where a V_s profile is not available and only the V_{s30} is known. For example, several recording stations in the NGA-West database only have a site classification based on their V_{s30}. Proposing alternative V_s-κ corrections for these cases would effectively expand the catalog of ground motions that can be used for SRA purposes.
- V_s-κ corrections seem to have varying effects on spectral accelerations at the surface and on amplification functions, depending on the site class. Further investigation including a larger set of site profiles and input ground motions is needed to better understand which parameters control the observed behavior. Such study would be key to clarifying the potential implications of the V_s-κ correction framework on site-specific seismic hazards assessments and dynamic analyses of critical infrastructure.
- The possibility of accounting for κ_0 effects by selecting input ground motions based on their match to a specified spectral shape should be explored. Such practice is already common in current protocols for input motion selection in site response analysis, but only differences in V_{s30} are considered. Interpreting changes in spectral shape due to the attenuation near the surface, as captured by κ_0 values, can

become a useful analysis tool that facilitates the selection of appropriate design motions.

APPENDIX A

Linear Regressions for the Estimation of Site-specific κ Values at the Sixty Selected Sites used in Chapter 3

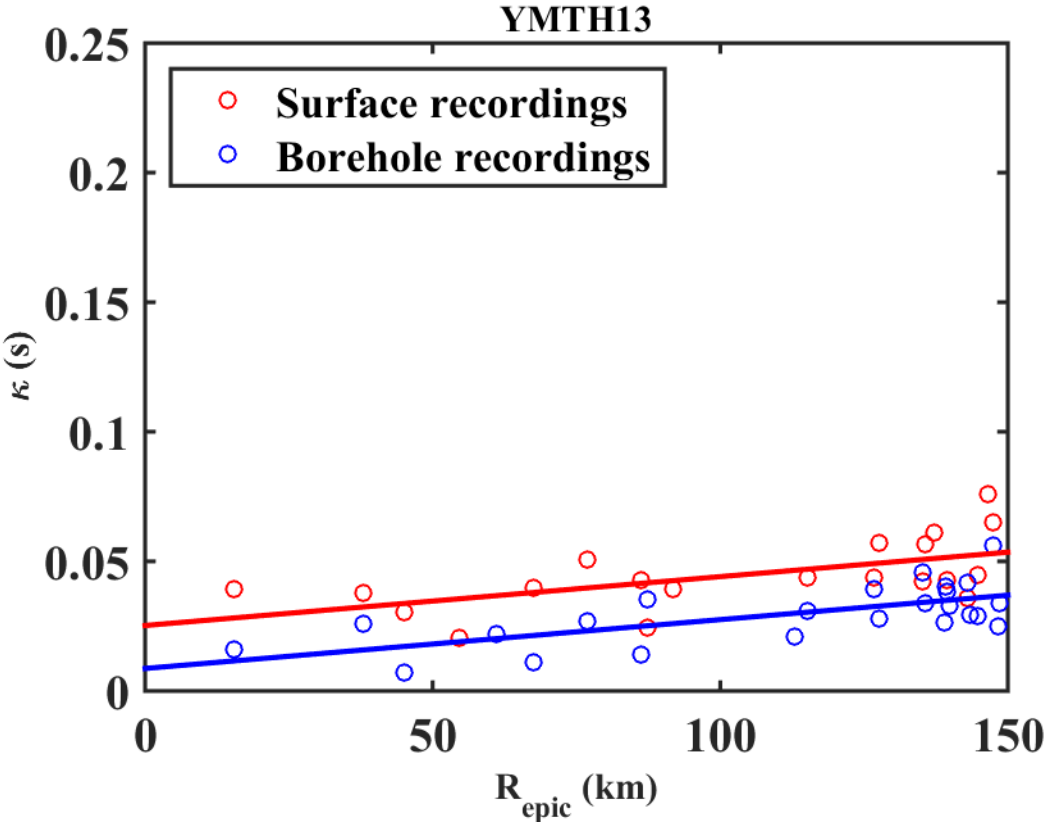
YMTH13
Surface recordings
Borehole recordings
0.25
0.2
0.15
0.1
0.05
0
κ (s)
0
50
100
150
R epic (km)

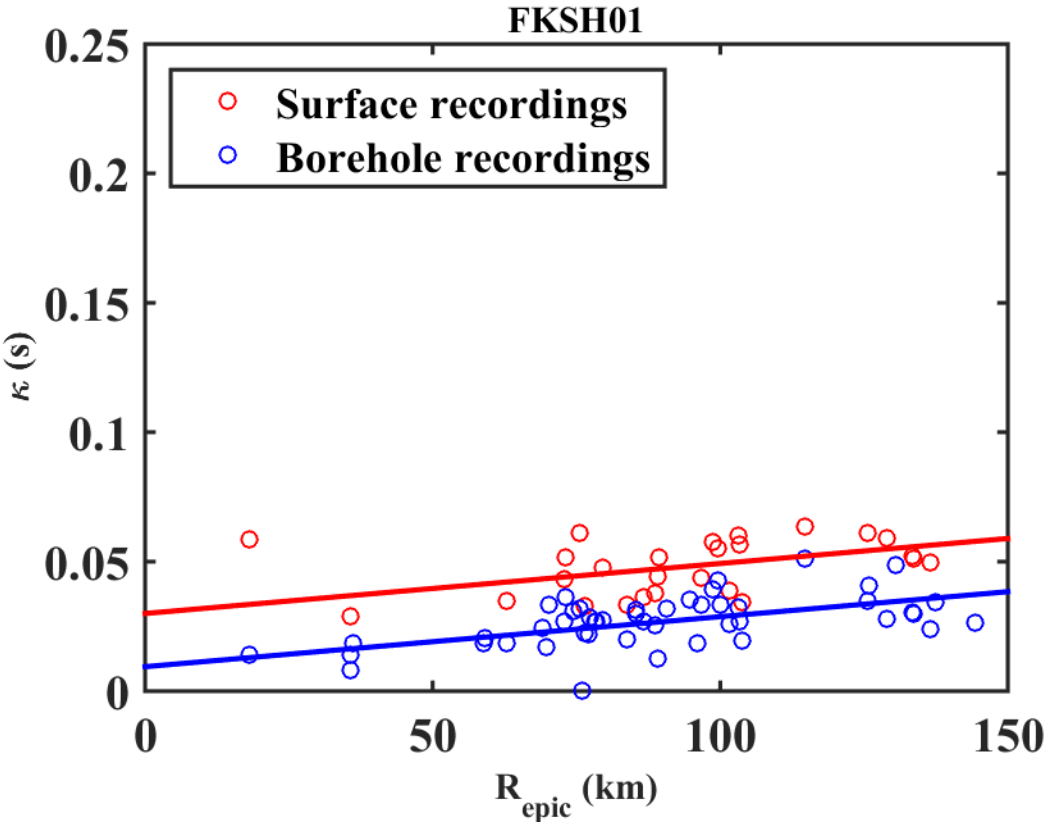
FKSH01
Surface recordings
Borehole recordings
0.25
0.2
0.15
0.1
0.05
0
κ (s)
0
50
100
150
R epic (km)

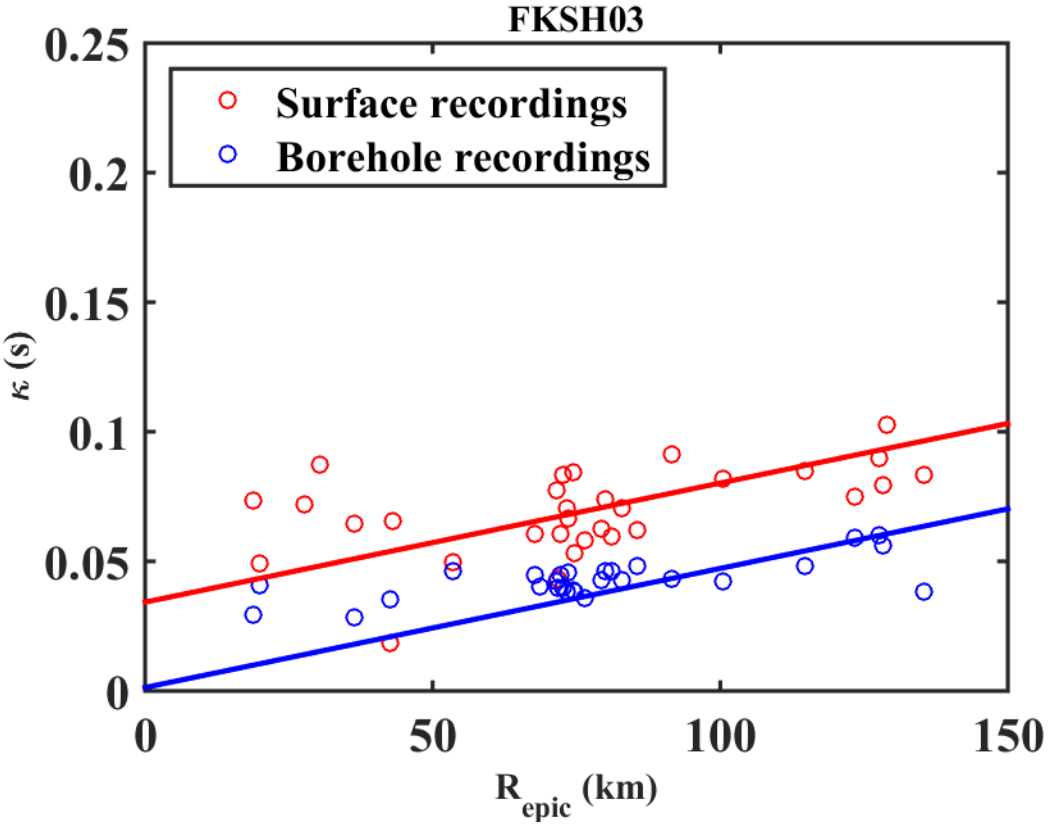
FKSH03
Surface recordings
Borehole recordings
κ (s)
0.25
0.2
0.15
0.1
0.05
0
0
50
100
150
R epic (km)

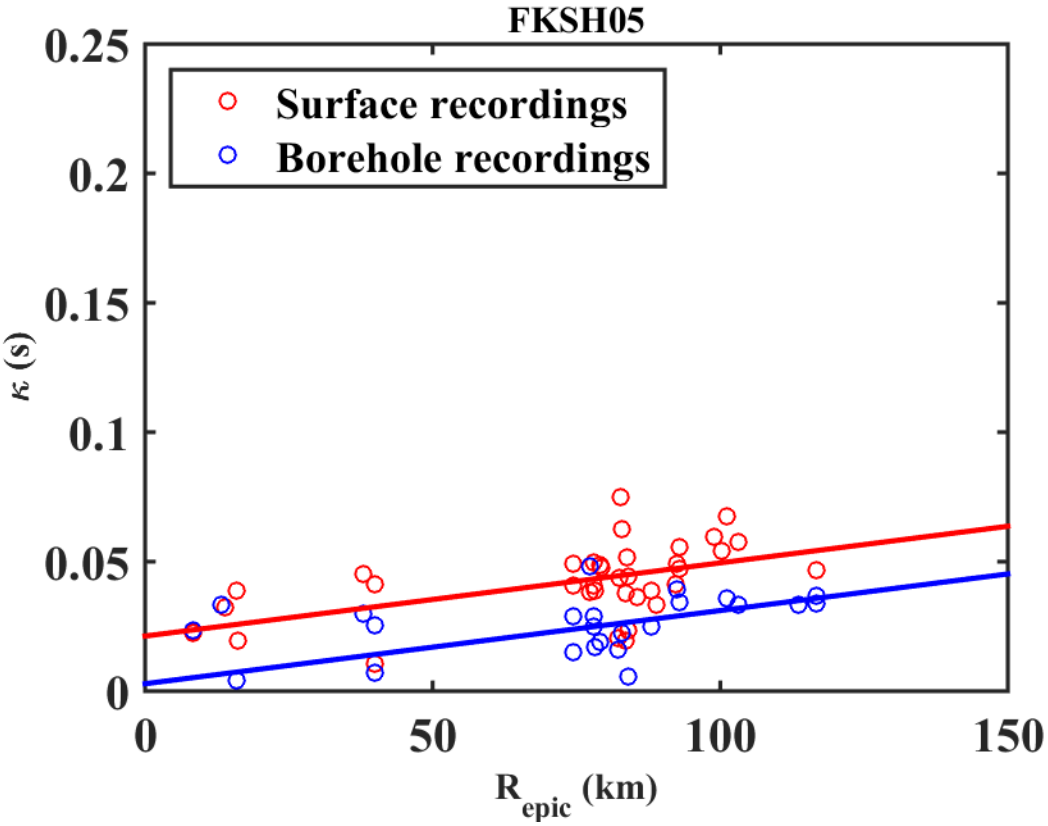
FKSH05
Surface recordings
Borehole recordings
κ (s)
0.25
0.2
0.15
0.1
0.05
0
0
50
100
150
R epic (km)

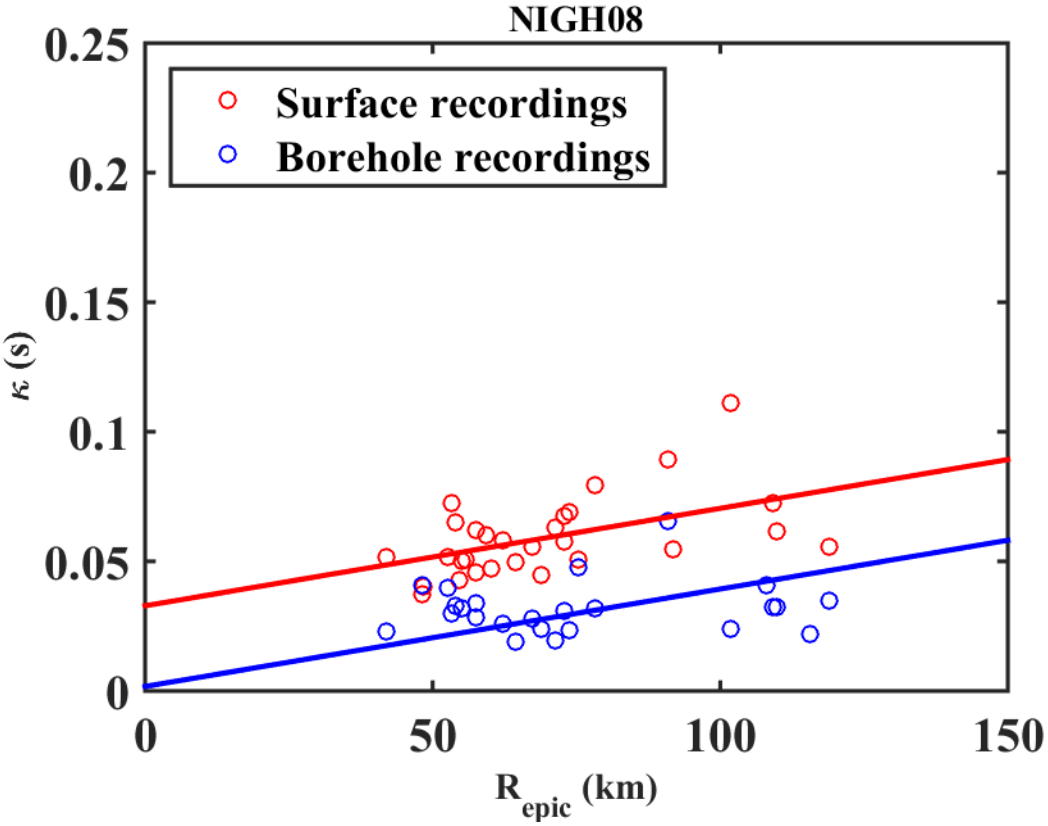
NIGH08
Surface recordings
Borehole recordings
κ (s)
0.25
0.2
0.15
0.1
0.05
0
0
50
100
150
R epic (km)

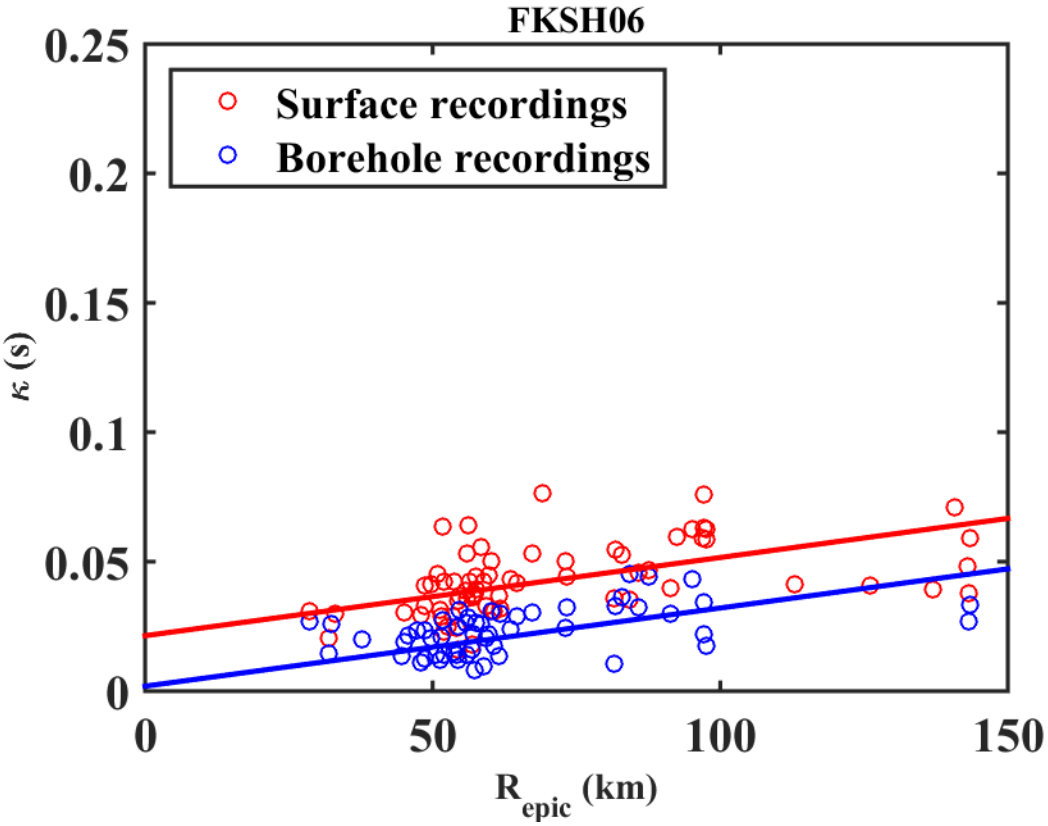
FKSH06
Surface recordings
Borehole recordings
κ (s)
0.25
0.2
0.15
0.1
0.05
0
0
50
100
150
R epic (km)

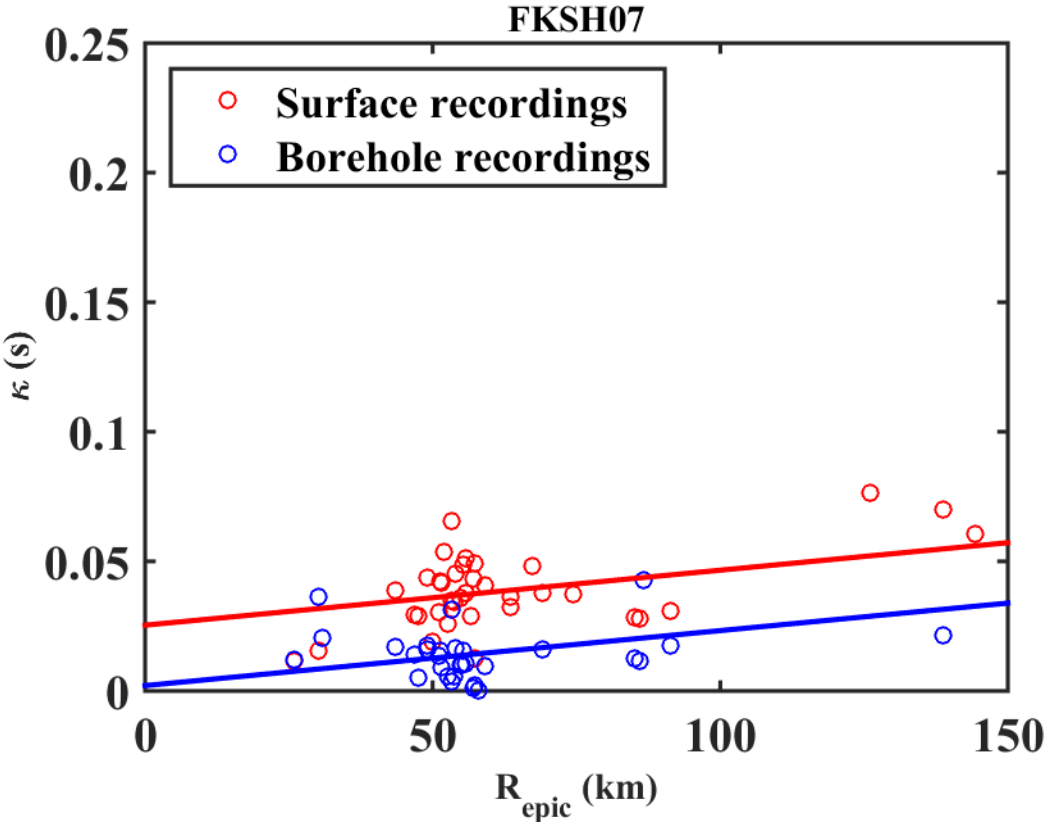
FKSH07
Surface recordings
Borehole recordings
0.25
0.2
0.15
0.1
0.05
0
κ (s)
0
50
100
150
R epic (km)

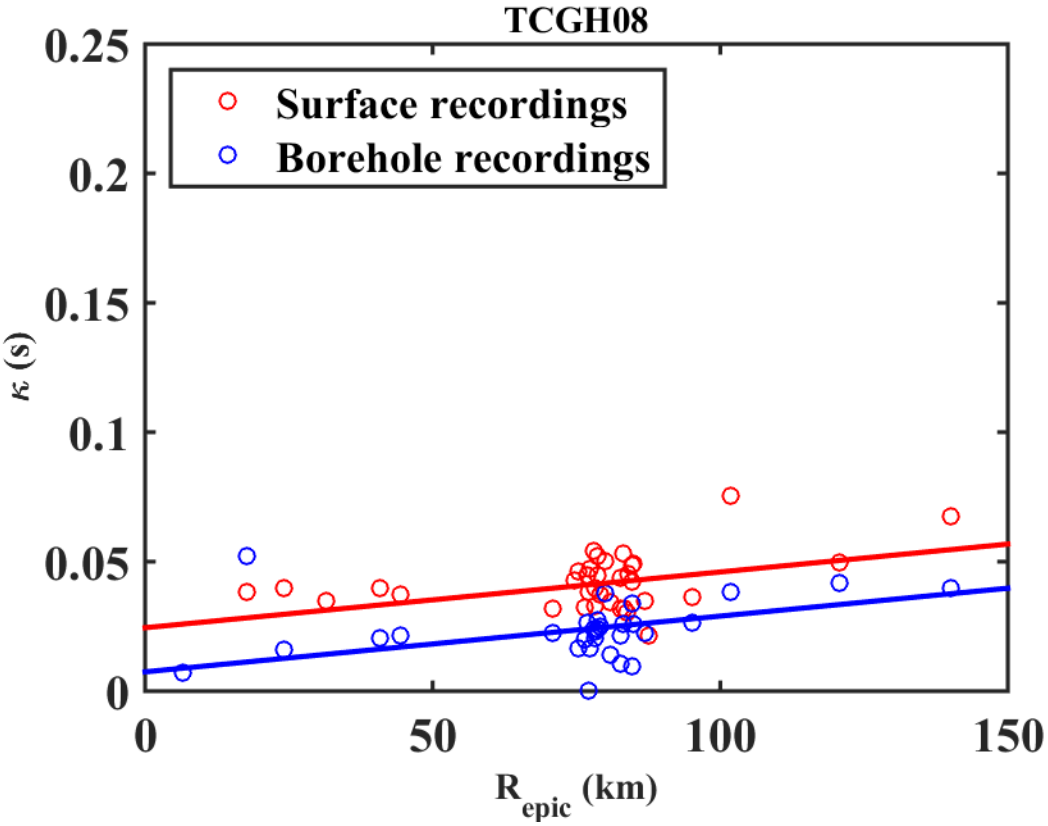
TCGH08
Surface recordings
Borehole recordings
0.25
0.2
0.15
0.1
0.05
0
κ (s)
0
50
100
150
R epic (km)

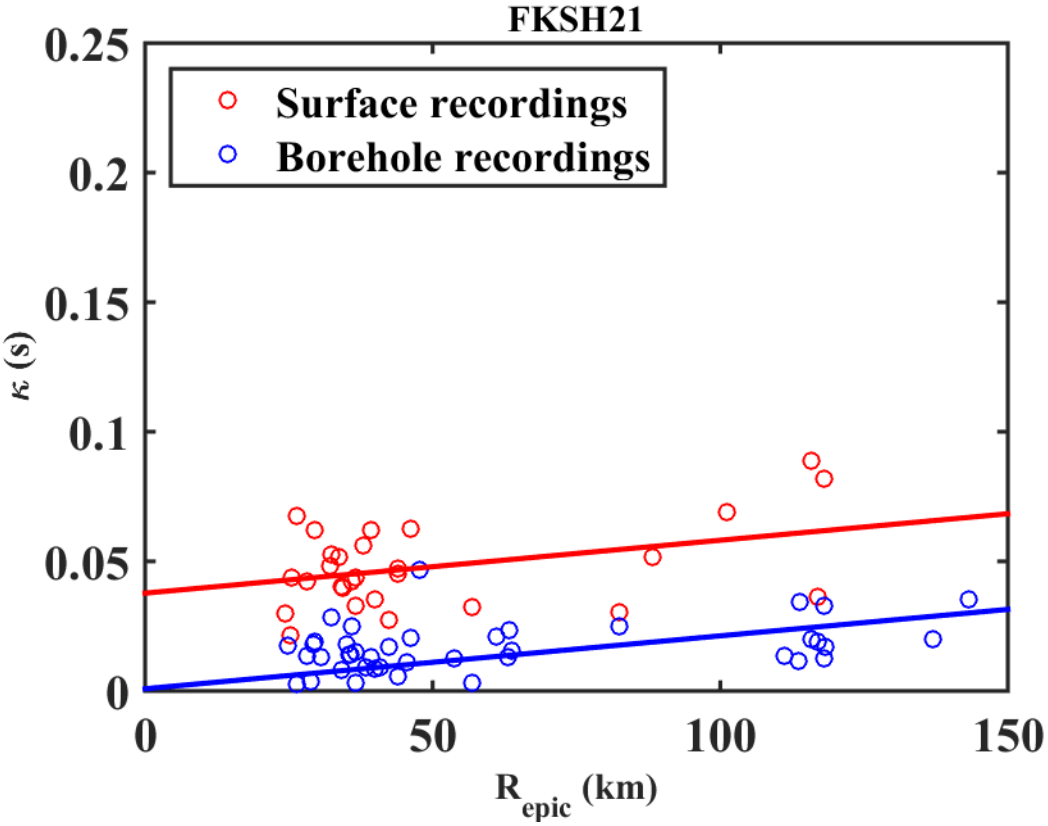
FKSH21
Surface recordings
Borehole recordings
κ (s)
0.25
0.2
0.15
0.1
0.05
0
0
50
100
150
R epic (km)

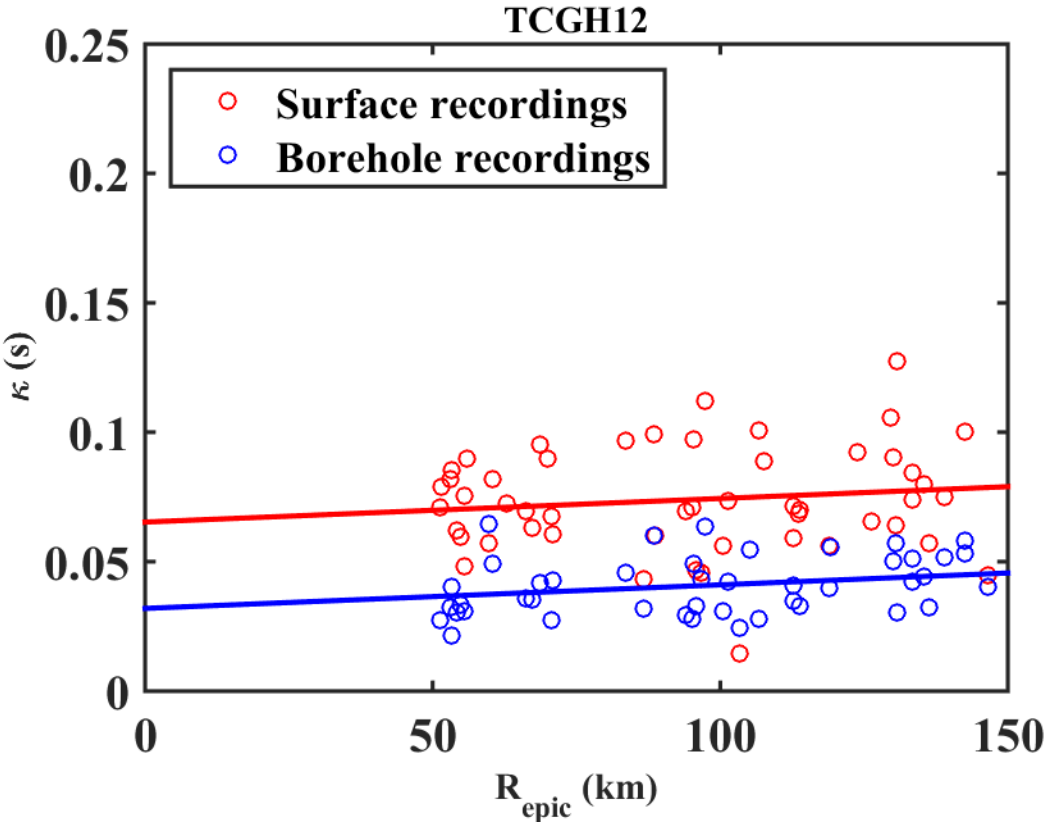
TCGH12
Surface recordings
Borehole recordings
κ (s)
0.25
0.2
0.15
0.1
0.05
0
0
50
100
150
R epic (km)

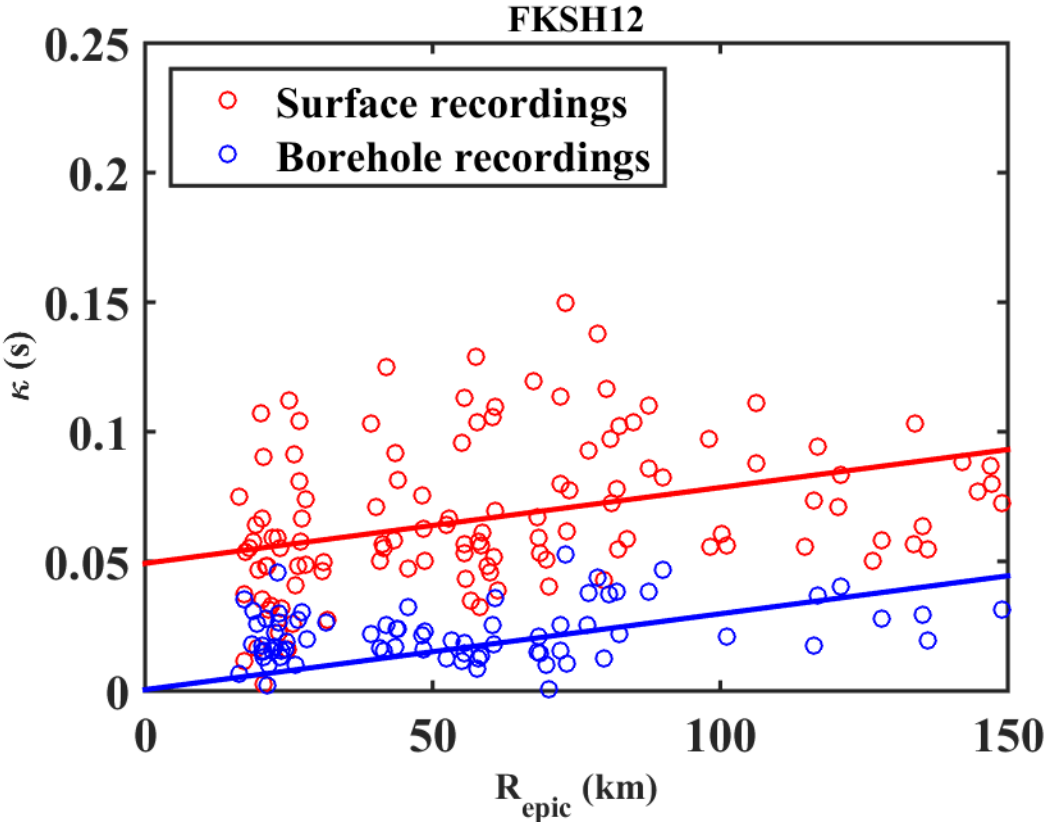
FKSH12
Surface recordings
Borehole recordings
κ (s)
0.25
0.2
0.15
0.1
0.05
0
0
50
100
150
R epic (km)

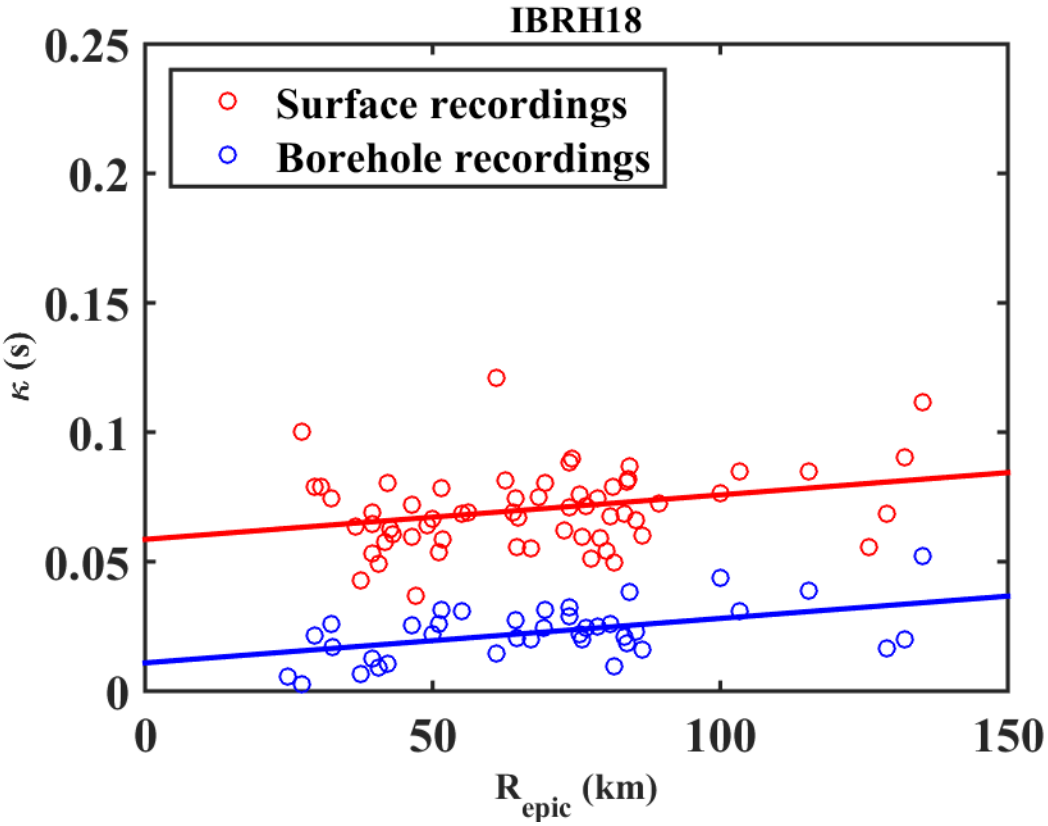
IBRH18
Surface recordings
Borehole recordings
κ (s)
0.25
0.2
0.15
0.1
0.05
0
0
50
100
150
R epic (km)

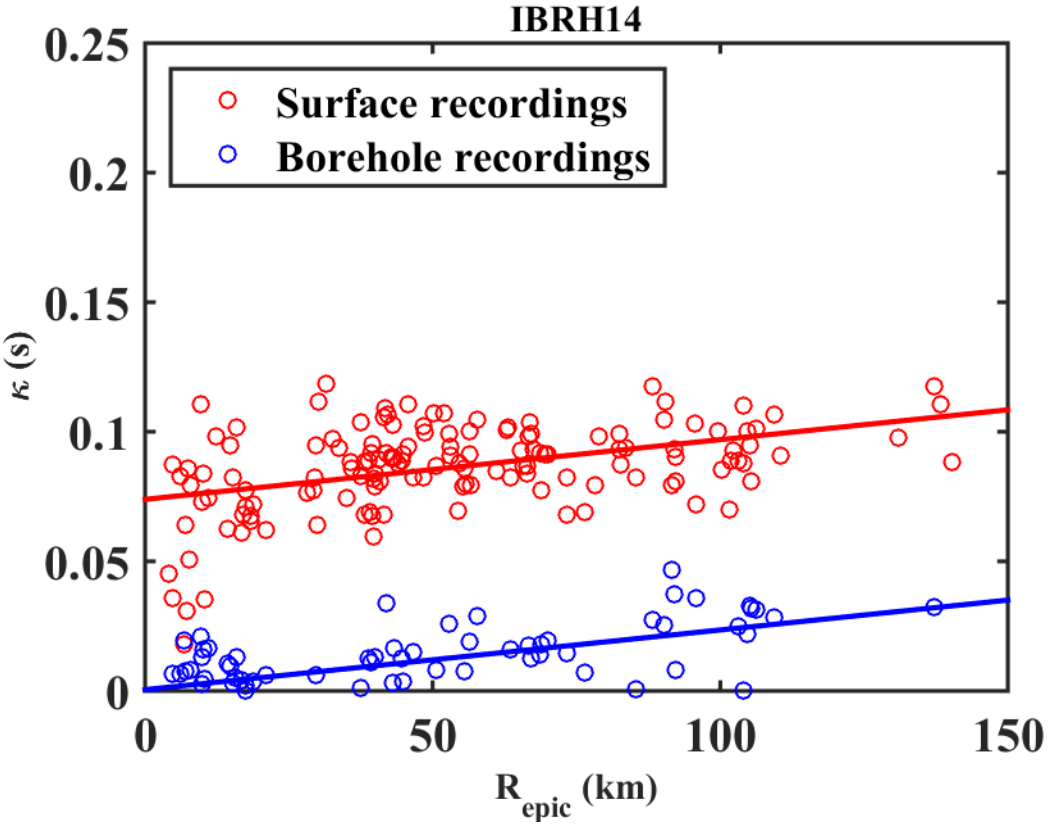
IBRH14
Surface recordings
Borehole recordings
κ (s)
0.25
0.2
0.15
0.1
0.05
0
0
50
100
150
R epic (km)

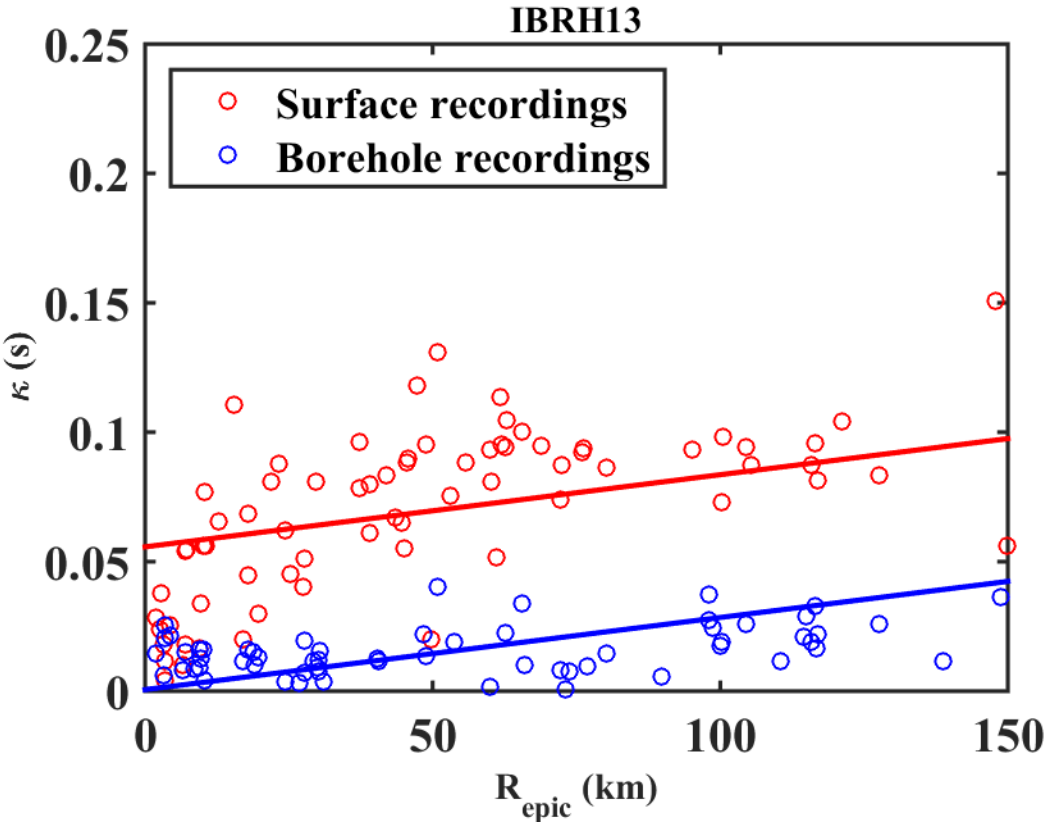
IBRH13
Surface recordings
Borehole recordings
κ (s)
0.25
0.2
0.15
0.1
0.05
0
0
50
100
150
R epic (km)

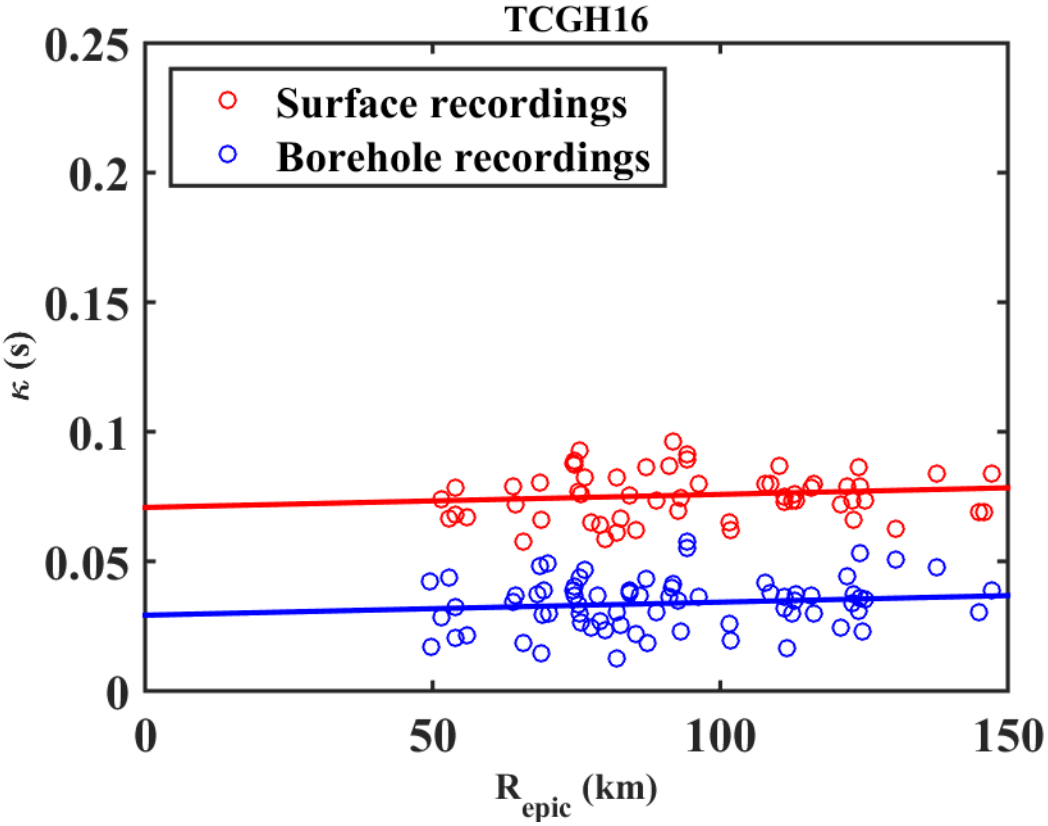
TCGH16
Surface recordings
Borehole recordings
κ (s)
0.25
0.2
0.15
0.1
0.05
0
0
50
100
150
R epic (km)

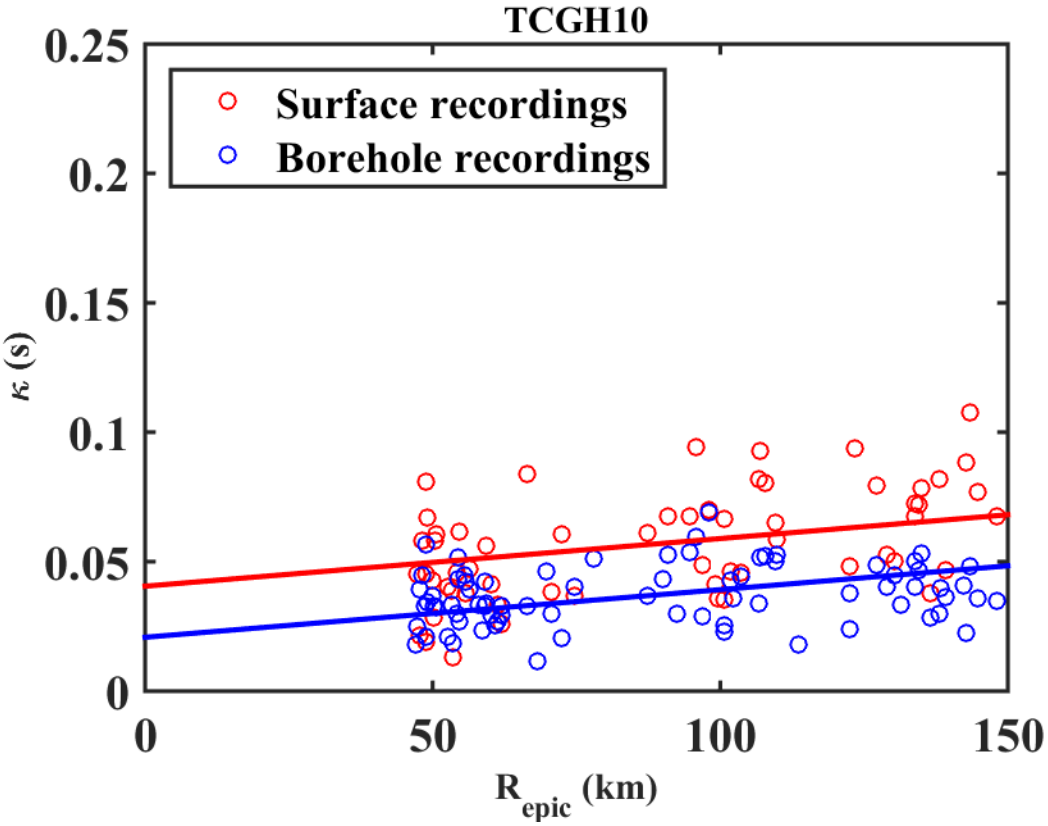
TCGH10
Surface recordings
Borehole recordings
κ (s)
0.25
0.2
0.15
0.1
0.05
0
0
50
100
150
R epic (km)

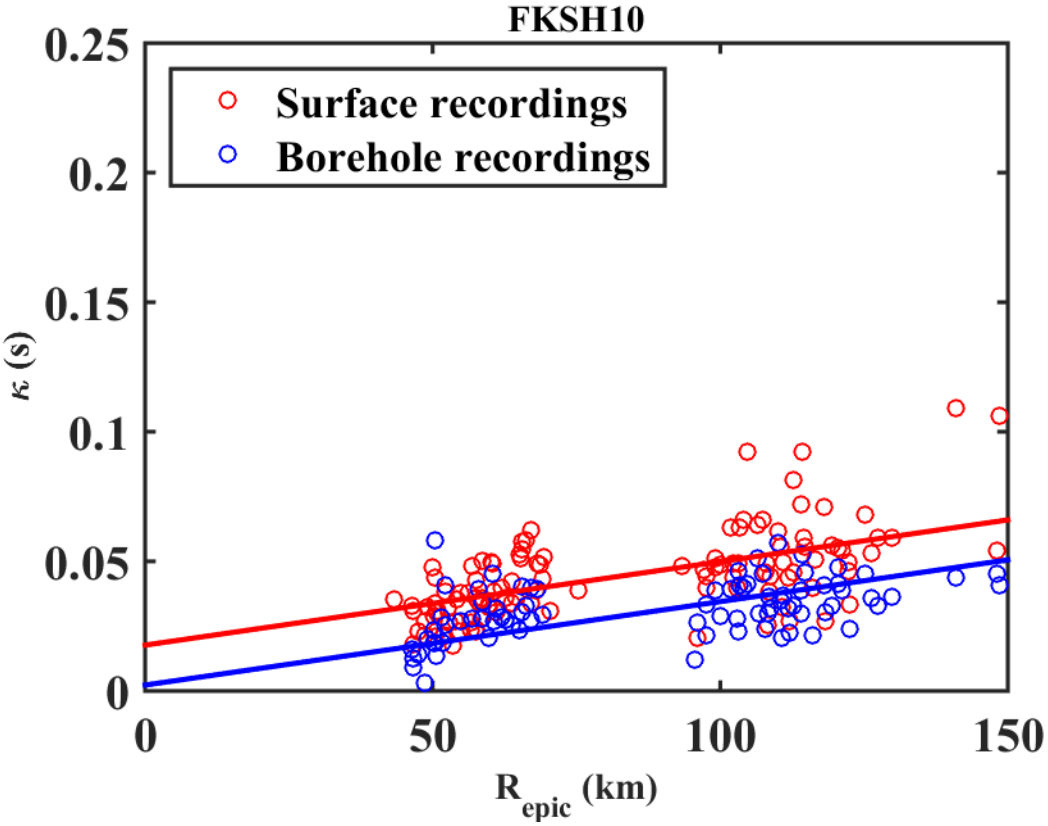
FKSH10
Surface recordings
Borehole recordings
κ (s)
0.25
0.2
0.15
0.1
0.05
0
0
50
100
150
R epic (km)

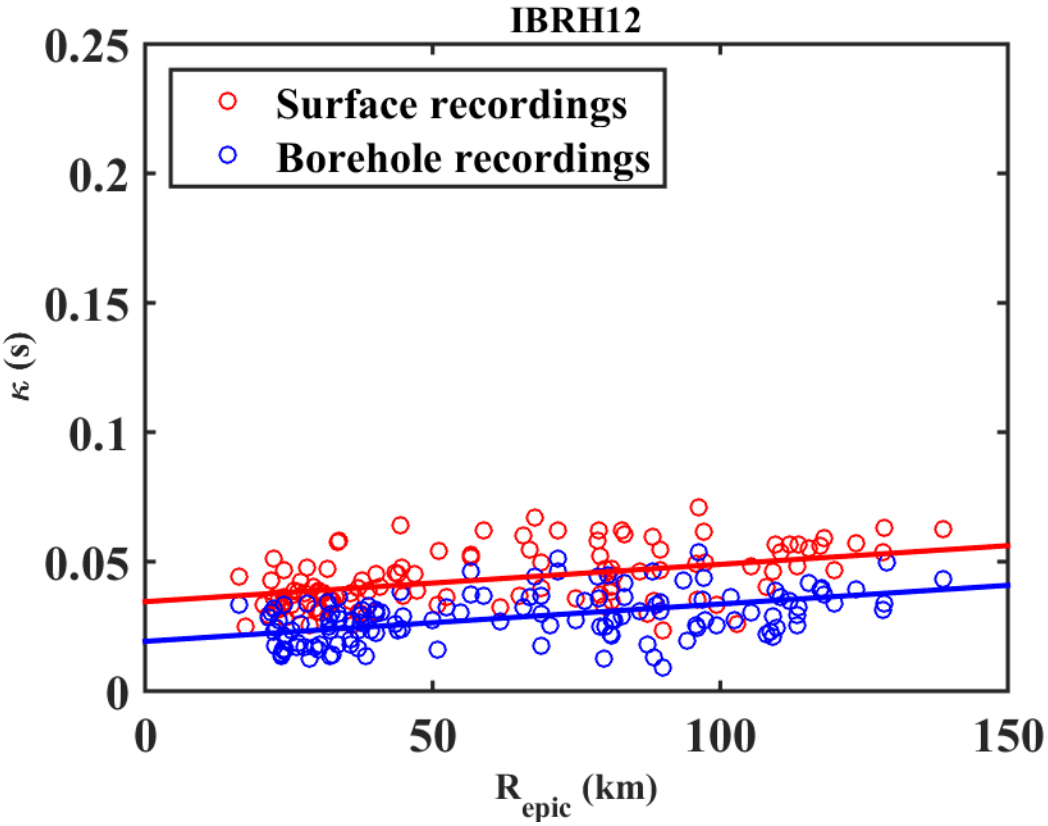
IBRH12
Surface recordings
Borehole recordings
κ (s)
0.25
0.2
0.15
0.1
0.05
0
0
50
100
150
R epic (km)

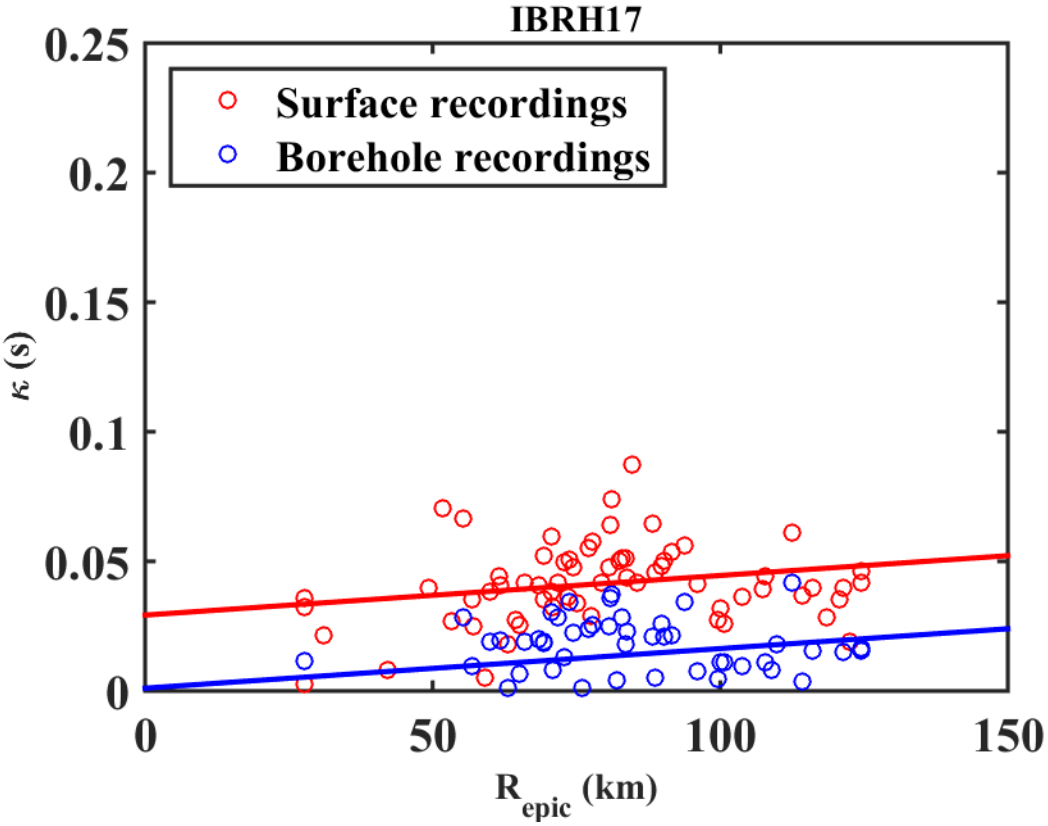
IBRH17
Surface recordings
Borehole recordings
0.25
0.2
0.15
0.1
0.05
0
κ (s)
0
50
100
150
R epic (km)

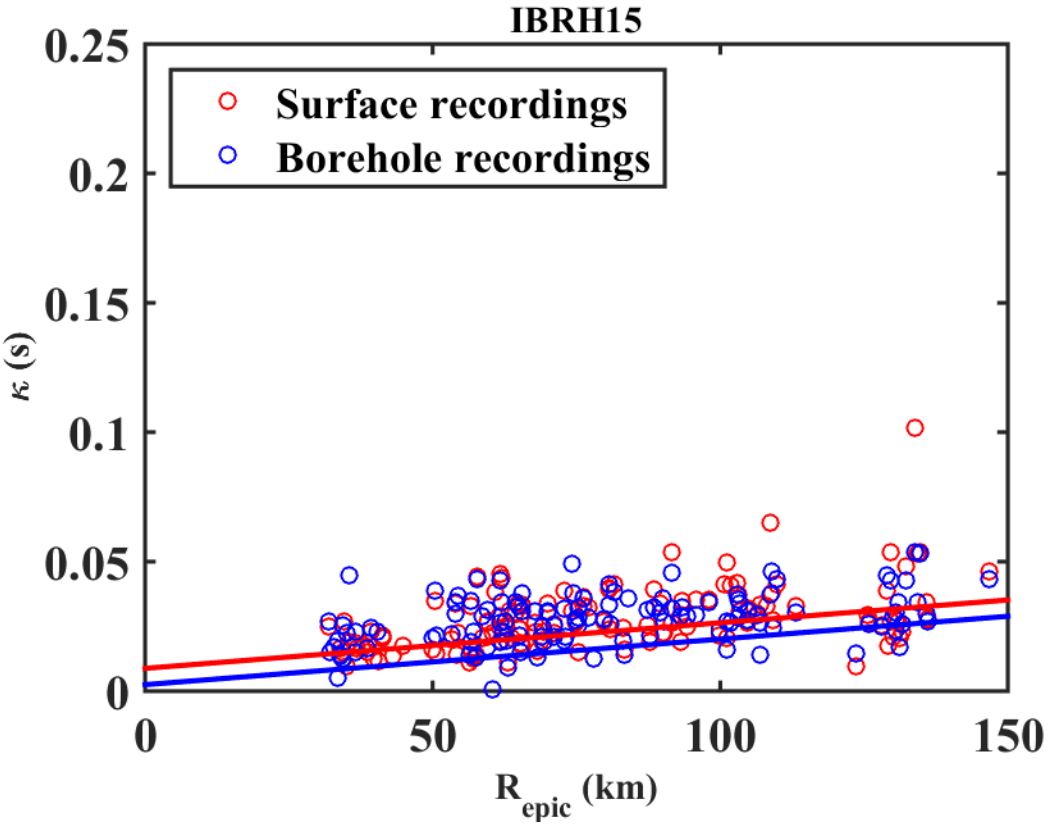
IBRH15
Surface recordings
Borehole recordings
0.25
0.2
0.15
0.1
0.05
0
κ (s)
0
50
100
150
R epic (km)

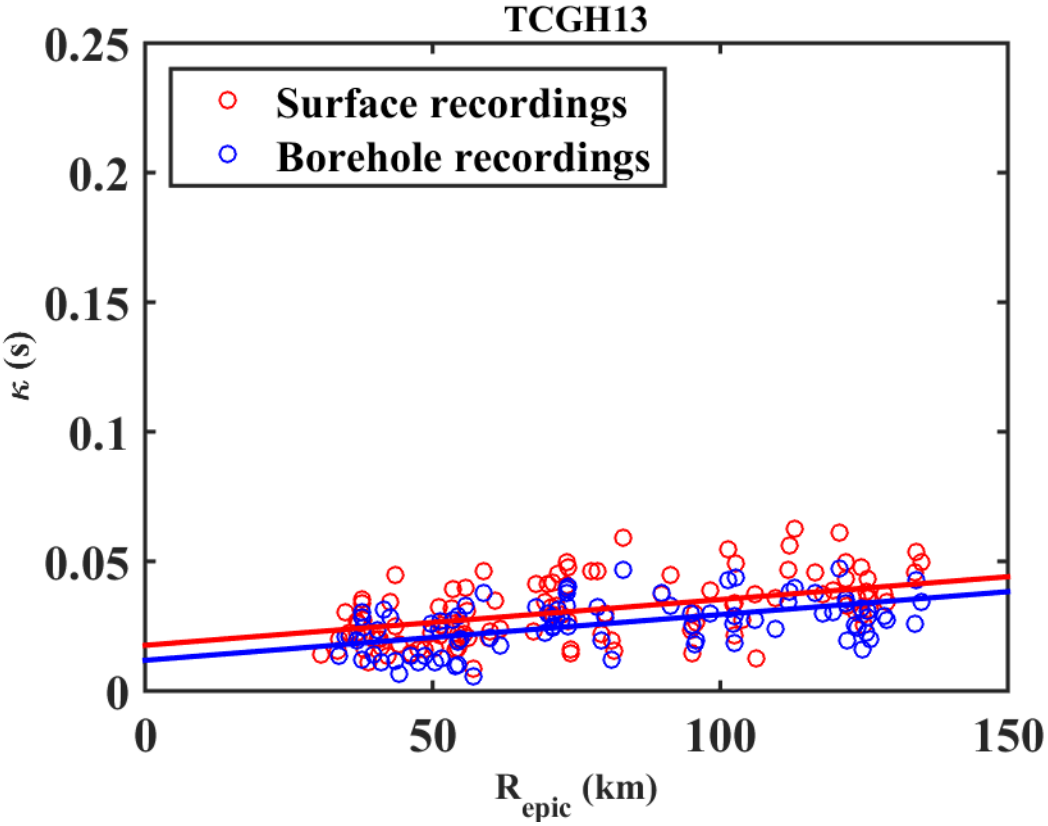
TCGH13
Surface recordings
Borehole recordings
κ (s)
0.25
0.2
0.15
0.1
0.05
0
0
50
100
150
R epic (km)

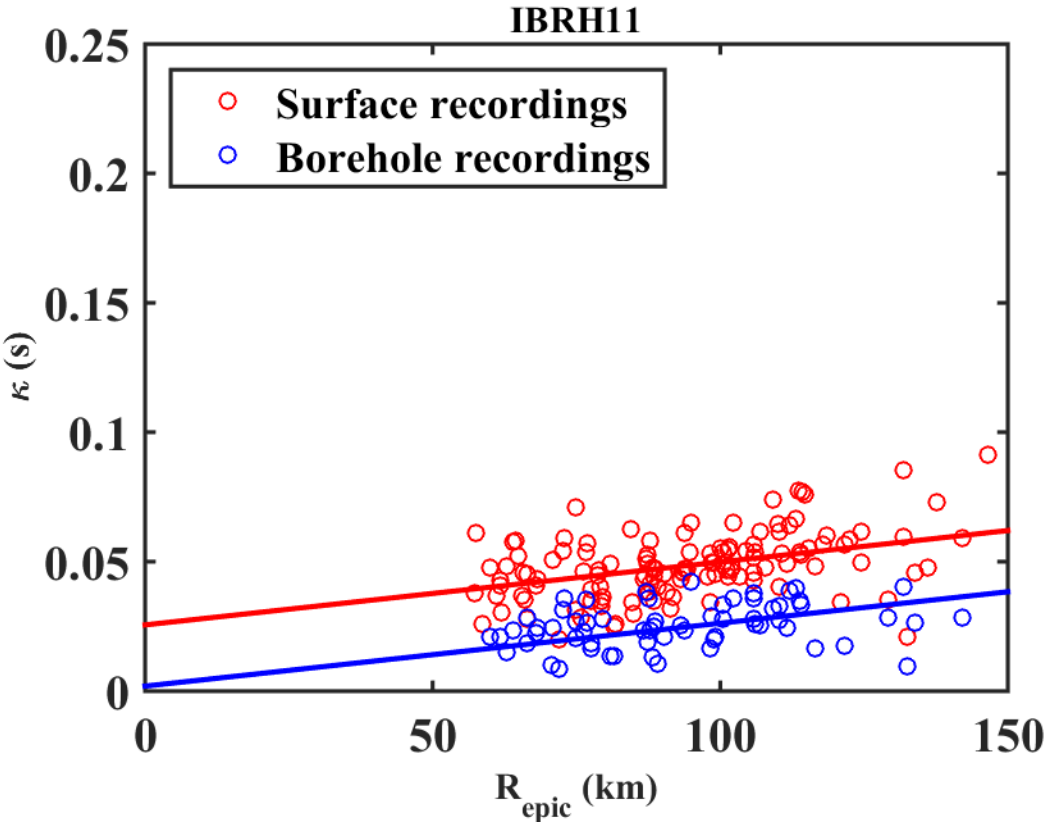
IBRH11
Surface recordings
Borehole recordings
κ (s)
0.25
0.2
0.15
0.1
0.05
0
0
50
100
150
R epic (km)

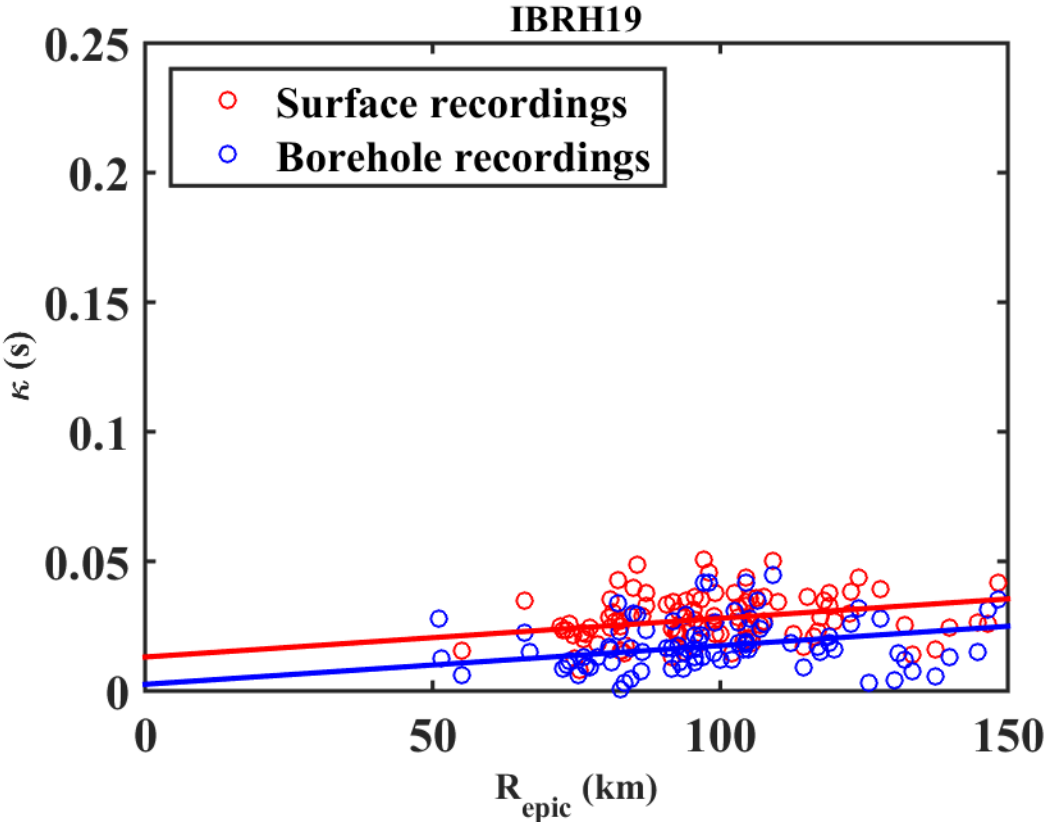
IBRH19
Surface recordings
Borehole recordings
κ (s)
0.25
0.2
0.15
0.1
0.05
0
0
50
100
150
R epic (km)

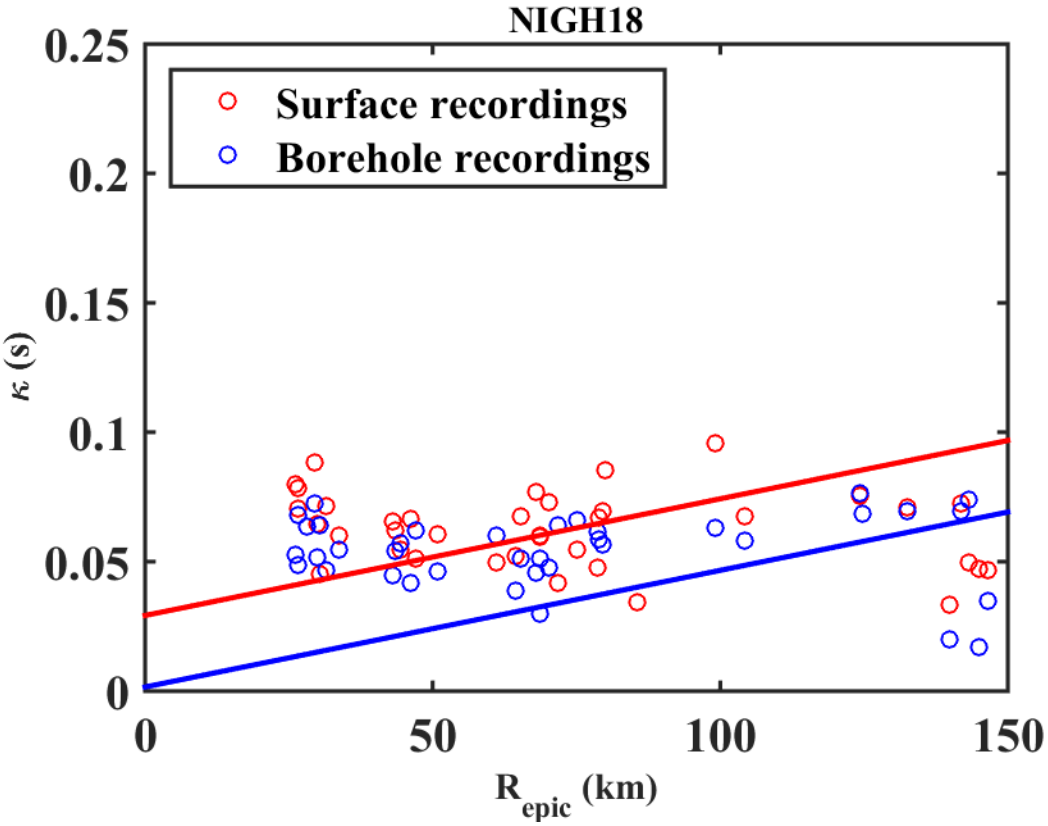
NIGH18
Surface recordings
Borehole recordings
κ (s)
0.25
0.2
0.15
0.1
0.05
0
0
50
100
150
R epic (km)

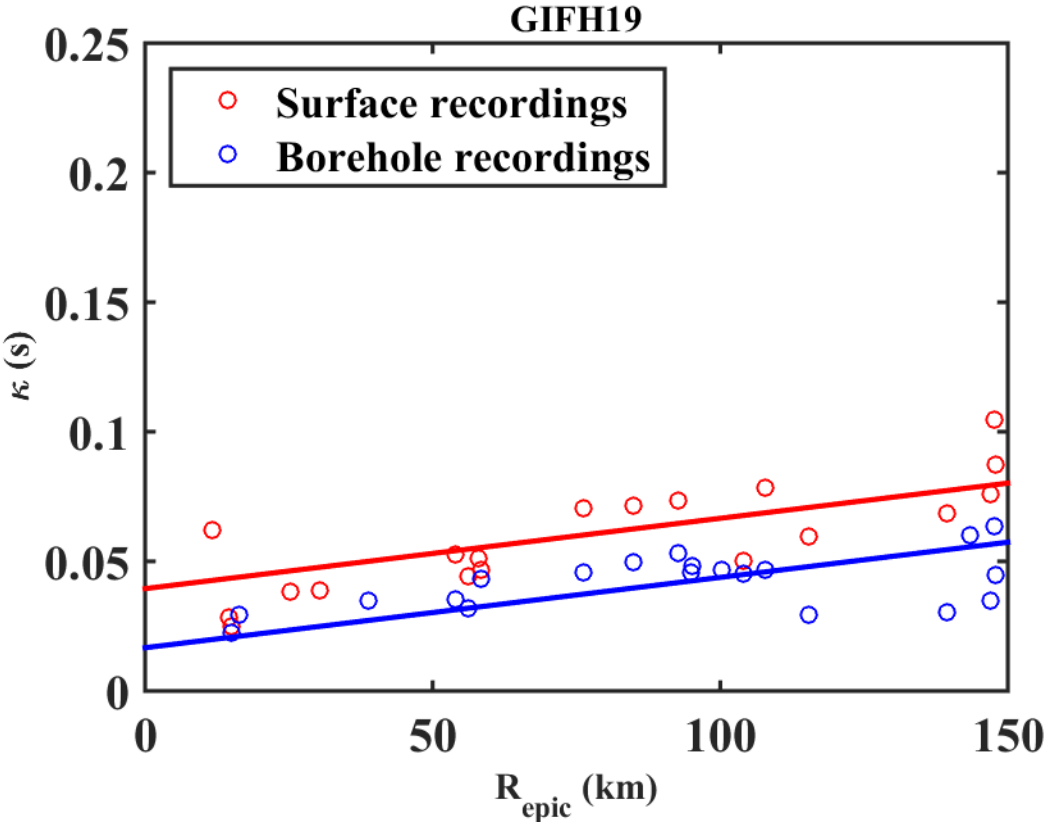
GIFH19
Surface recordings
Borehole recordings
κ (s)
0.25
0.2
0.15
0.1
0.05
0
0
50
100
150
R epic (km)

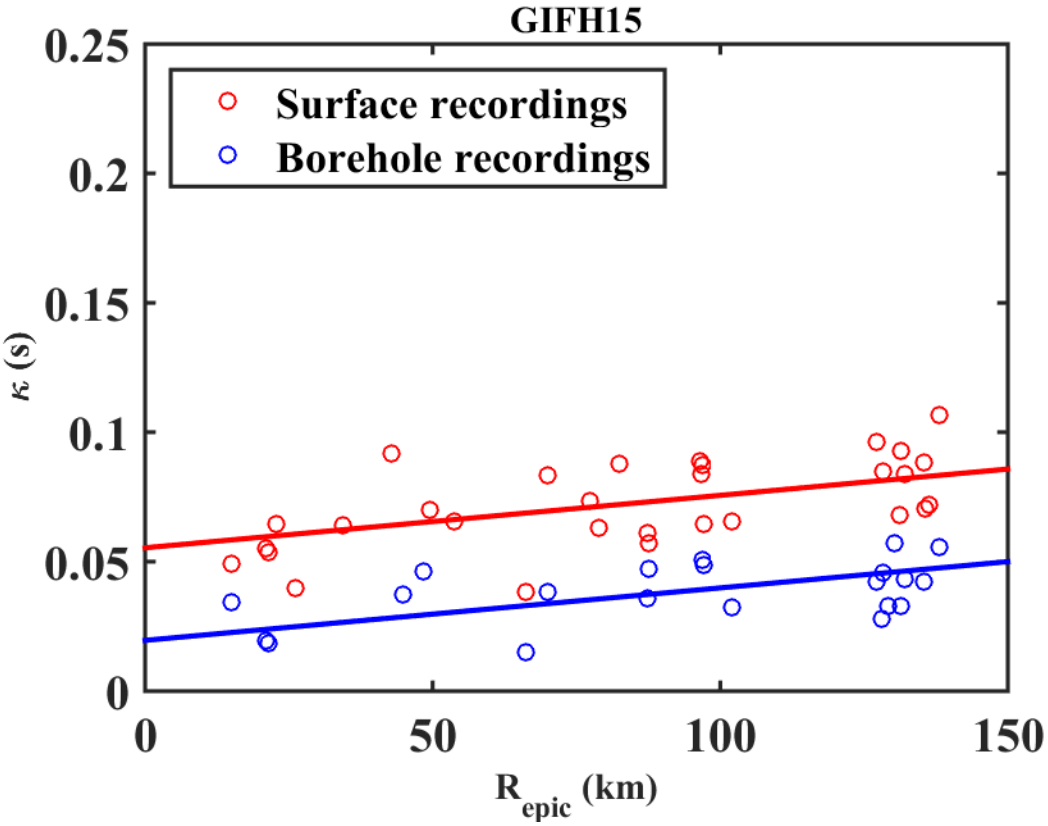
GIFH15
Surface recordings
Borehole recordings
κ (s)
0.25
0.2
0.15
0.1
0.05
0
0
50
100
150
R epic (km)

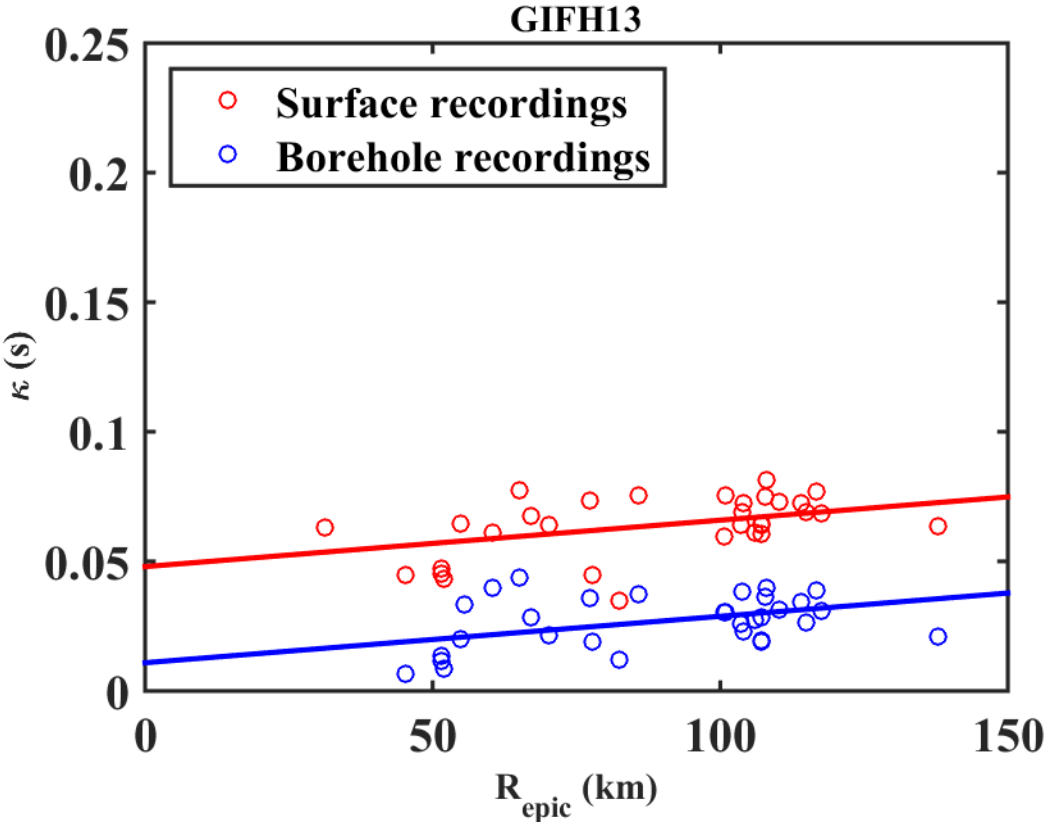
GIFH13
Surface recordings
Borehole recordings
0.25
0.2
0.15
0.1
0.05
0
κ (s)
0
50
100
150
R epic (km)

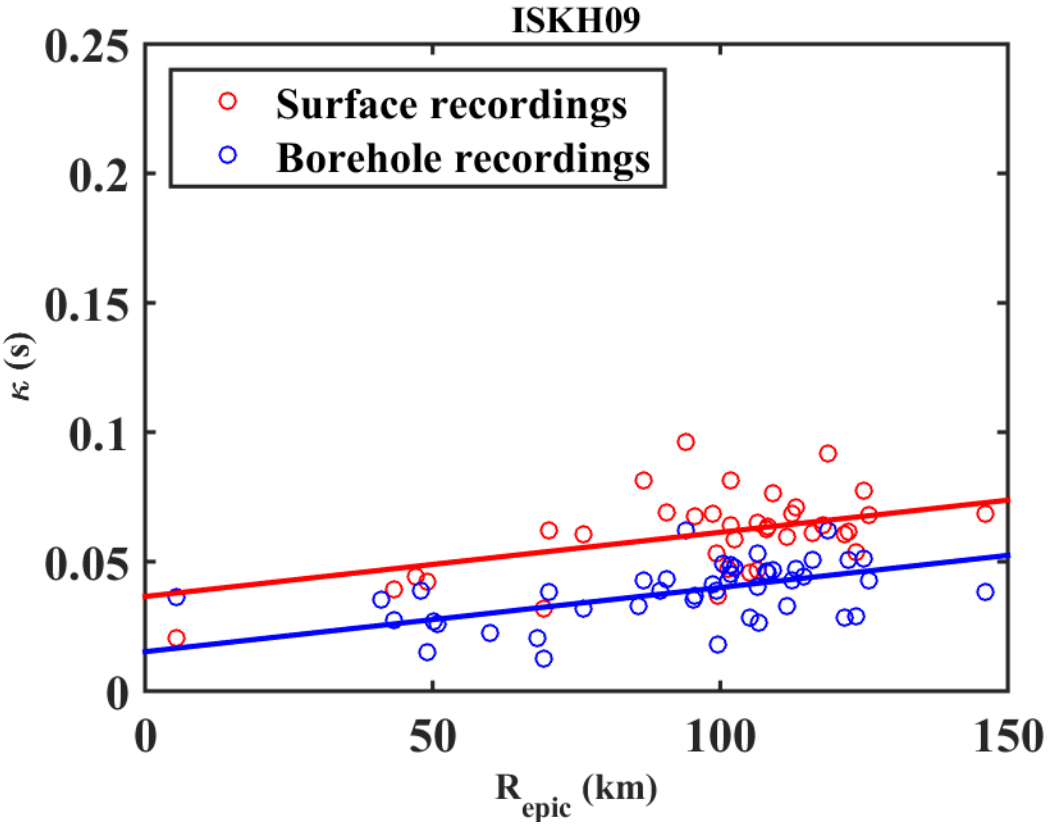
ISKH09
Surface recordings
Borehole recordings
0.25
0.2
0.15
0.1
0.05
0
κ (s)
0
50
100
150
R epic (km)

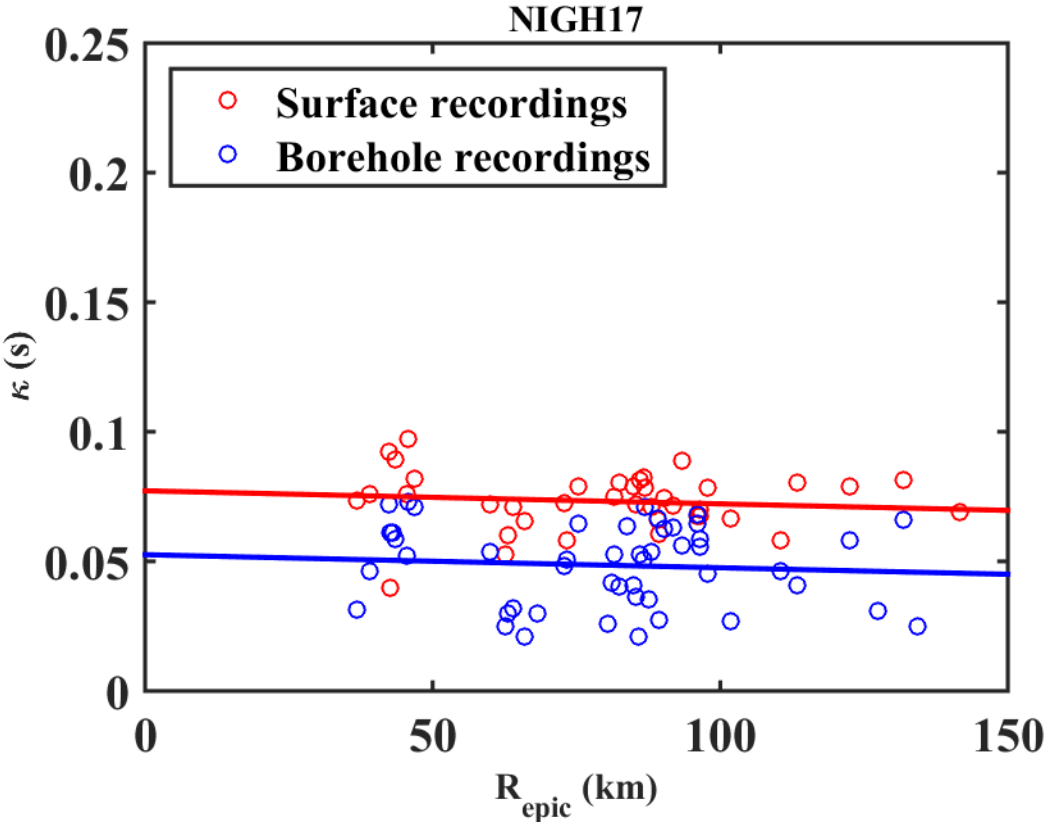
NIGH17
Surface recordings
Borehole recordings
0.25
0.2
0.15
0.1
0.05
0
κ (s)
0
50
100
150
R epic (km)

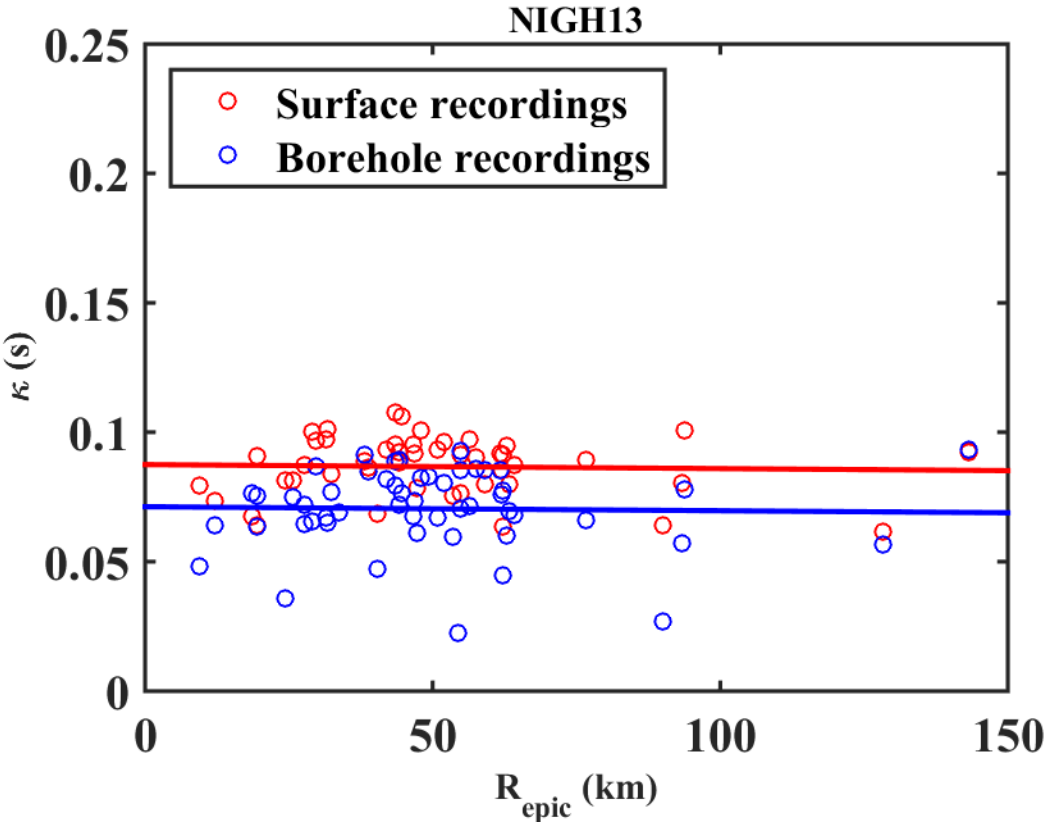
NIGH13
Surface recordings
Borehole recordings
0.25
0.2
0.15
0.1
0.05
0
κ (s)
0
50
100
150
R epic (km)

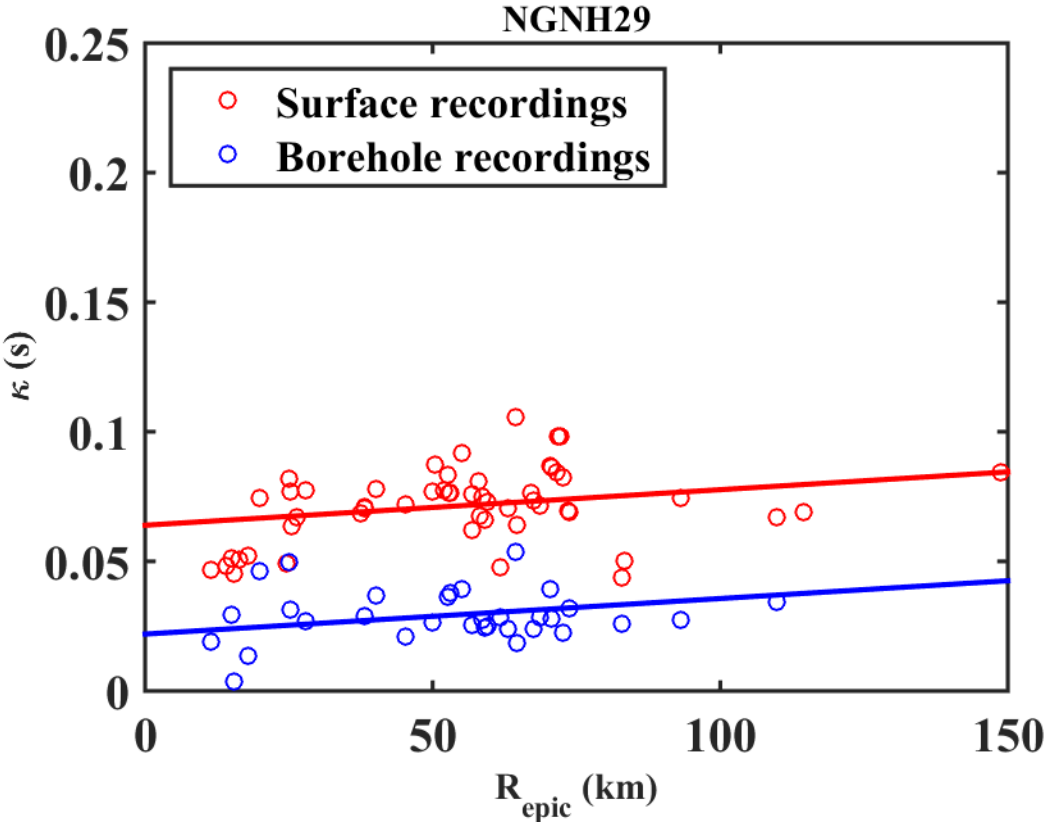
NGNH29
Surface recordings
Borehole recordings
κ (s)
0.25
0.2
0.15
0.1
0.05
0
0
50
100
150
R epic (km)

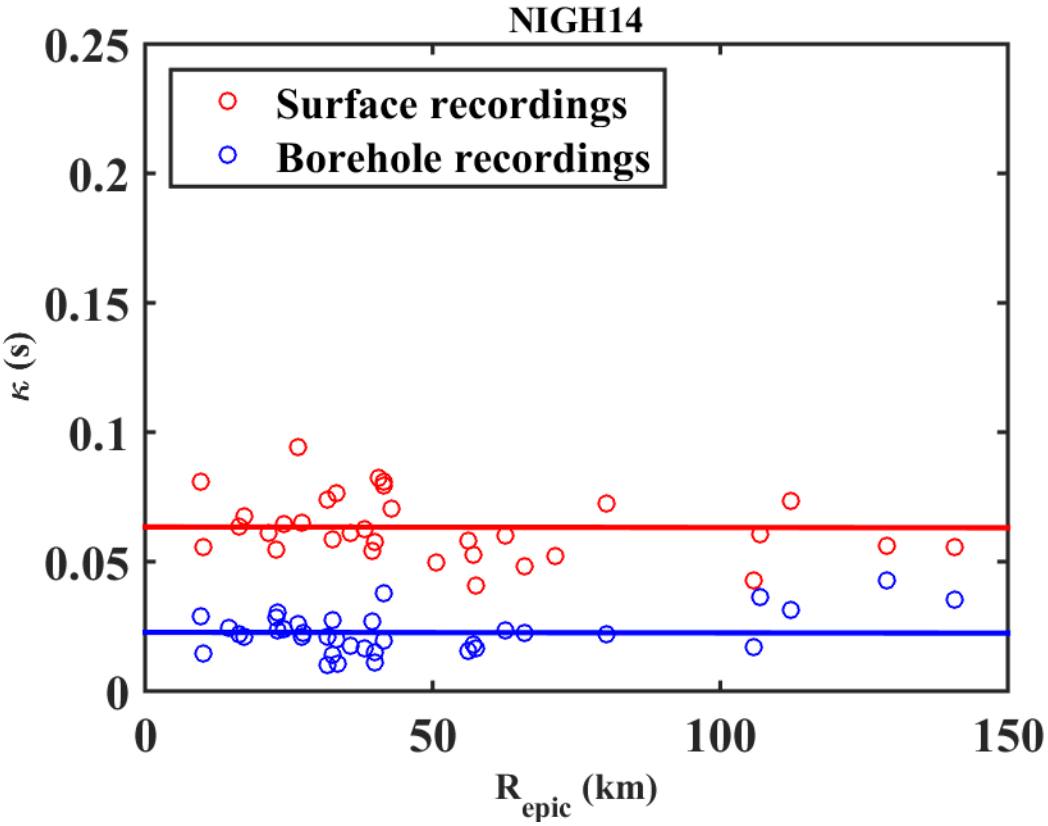
NIGH14
Surface recordings
Borehole recordings
κ (s)
0.25
0.2
0.15
0.1
0.05
0
0
50
100
150
R epic (km)

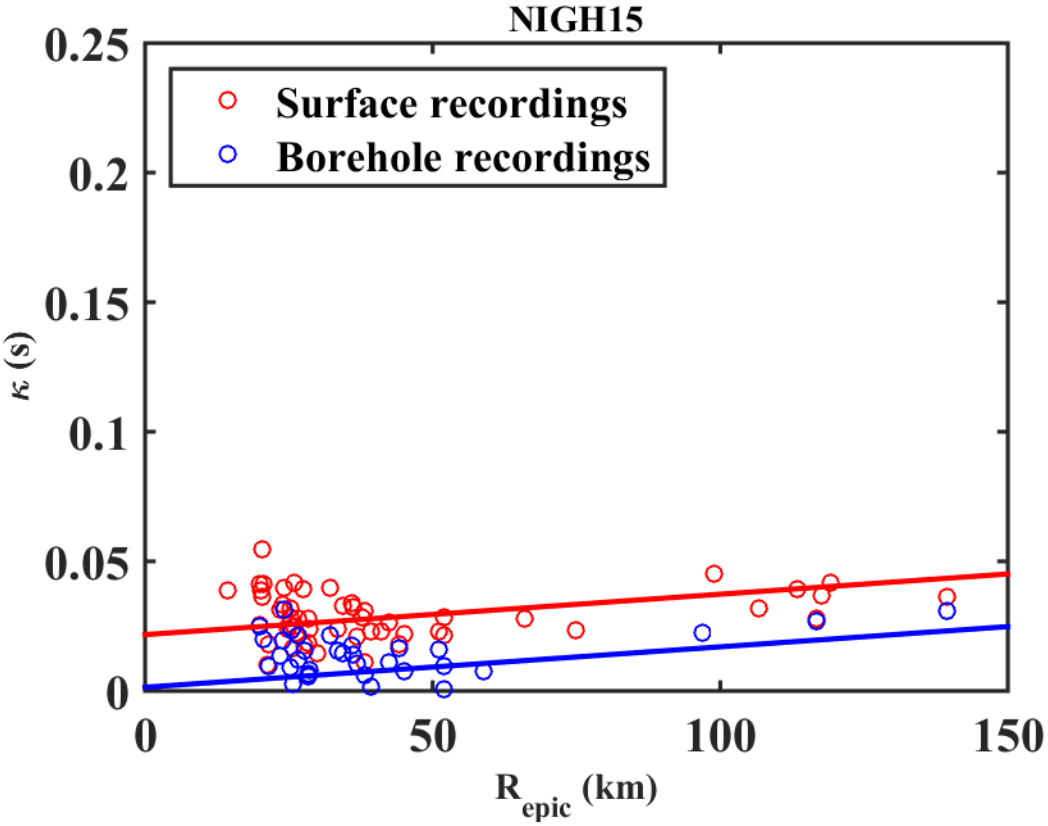
NIGH15
Surface recordings
Borehole recordings
0.25
0.2
0.15
0.1
0.05
0
κ (s)
0
50
100
150
R epic (km)

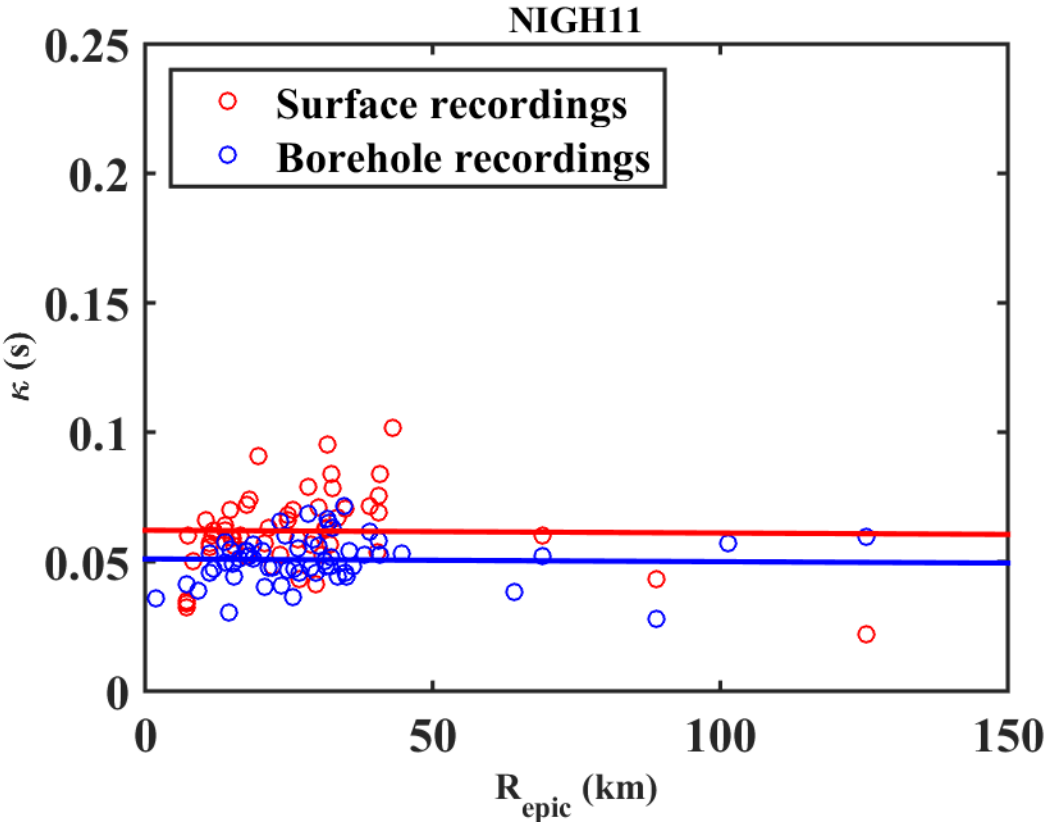
NIGH11
Surface recordings
Borehole recordings
0.25
0.2
0.15
0.1
0.05
0
κ (s)
0
50
100
150
R epic (km)

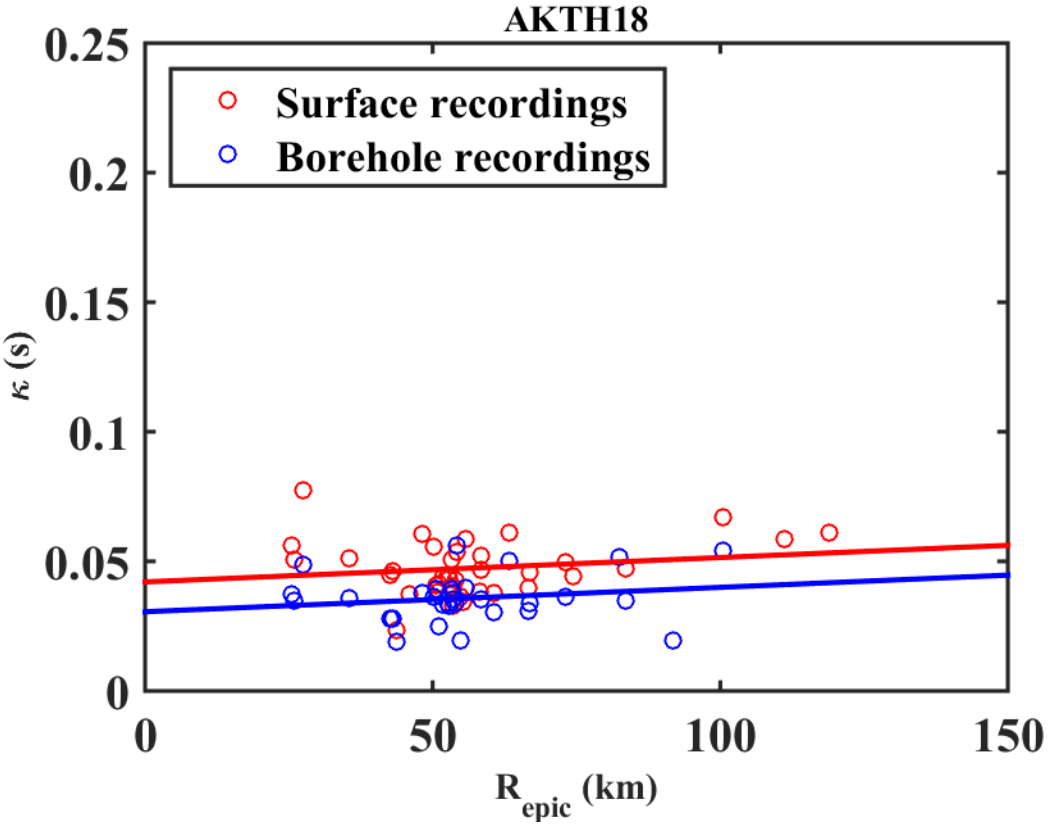
AKTH18
Surface recordings
Borehole recordings
κ (s)
0.25
0.2
0.15
0.1
0.05
0
0
50
100
150
R epic (km)

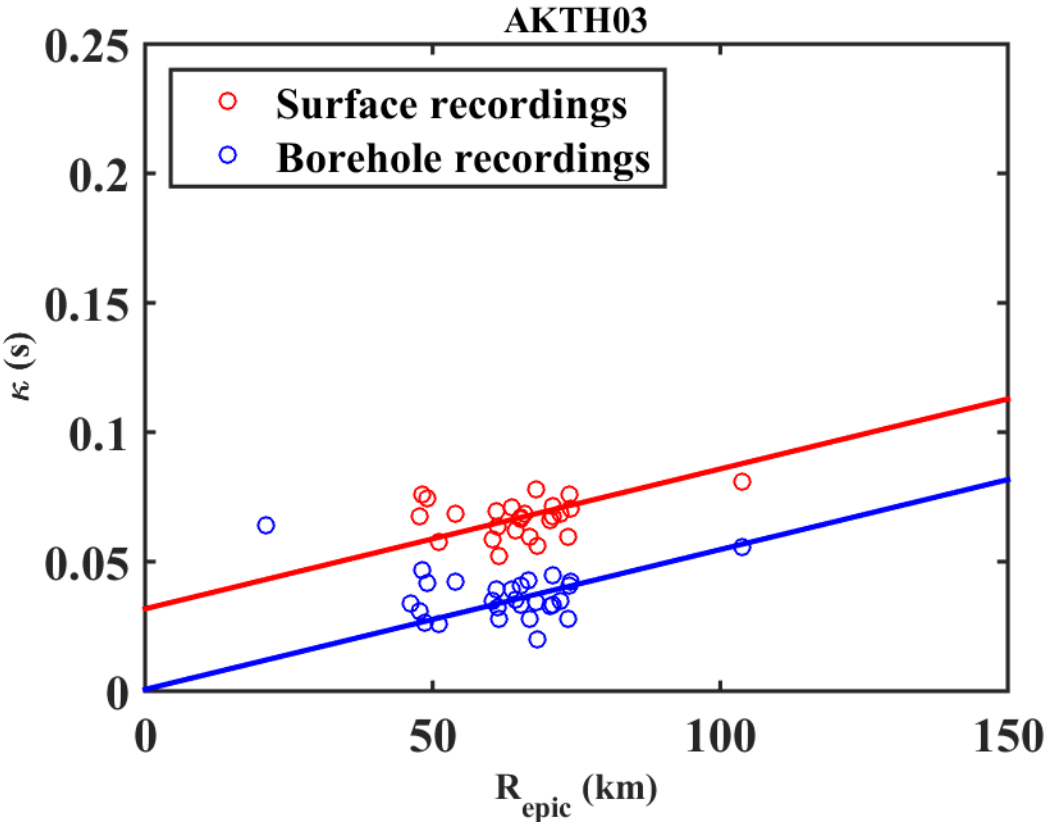
AKTH03
Surface recordings
Borehole recordings
κ (s)
0.25
0.2
0.15
0.1
0.05
0
0
50
100
150
R epic (km)

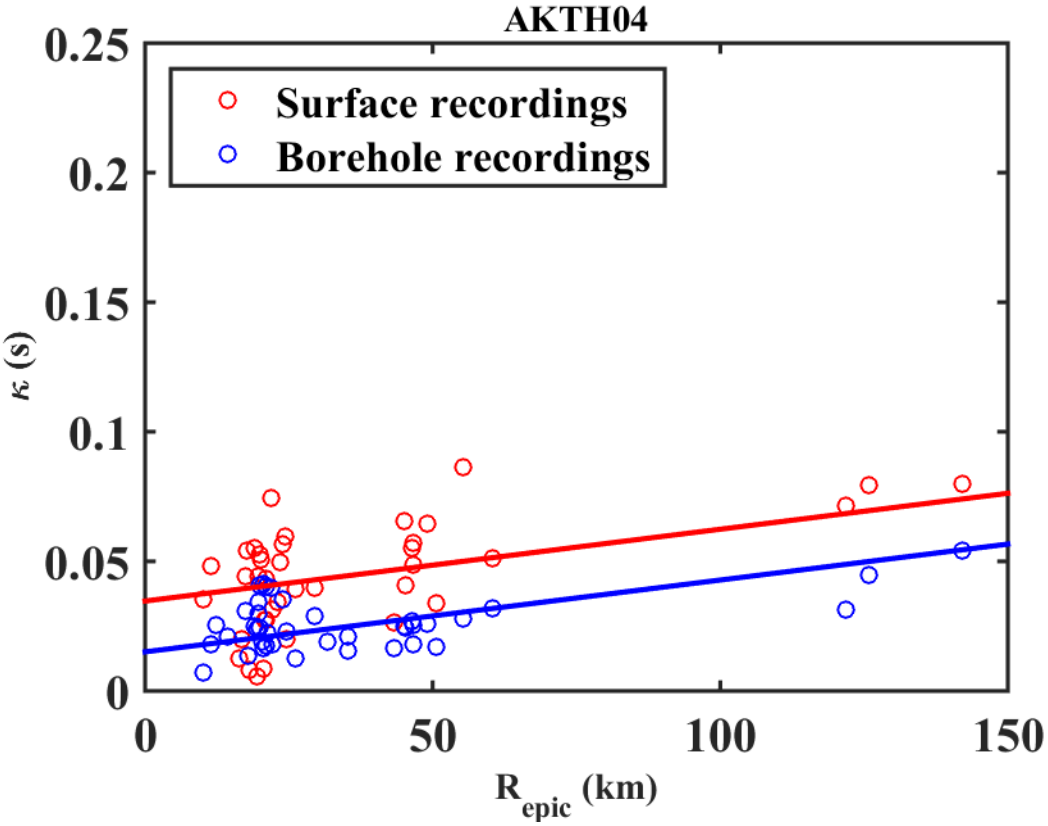
AKTH04
Surface recordings
Borehole recordings
0.25
0.2
0.15
0.1
0.05
0
κ (s)
0
50
100
150
R epic (km)

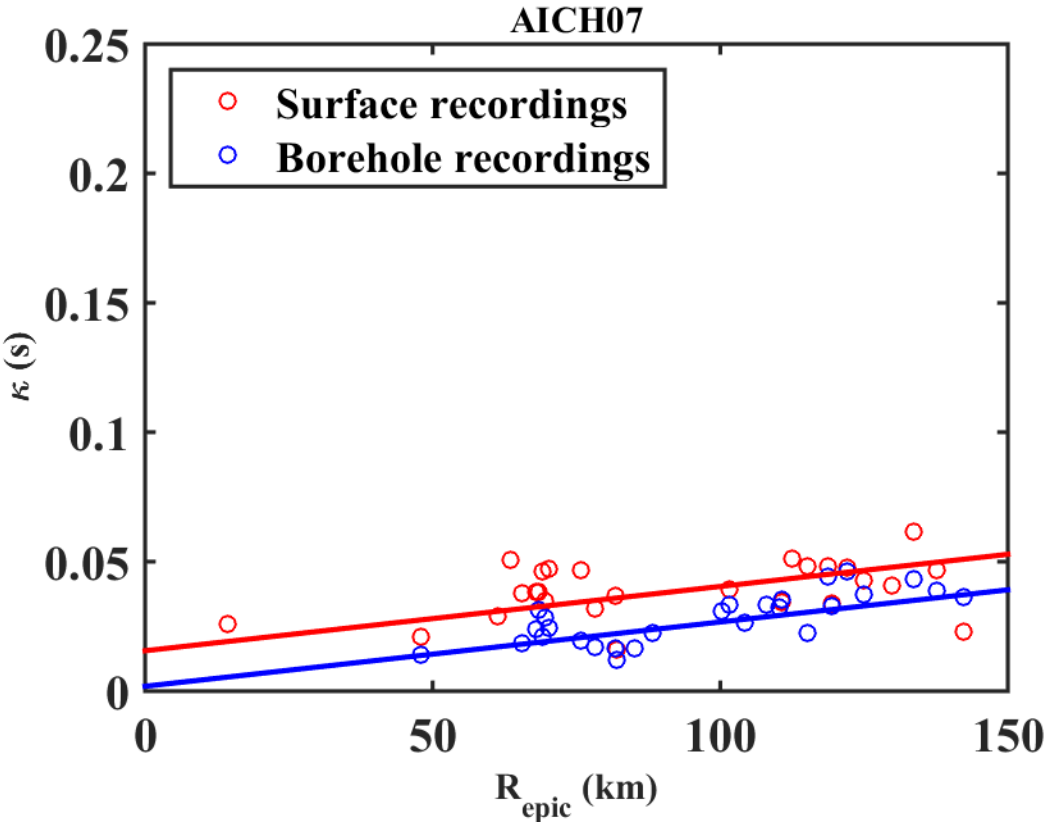
AICH07
Surface recordings
Borehole recordings
0.25
0.2
0.15
0.1
0.05
0
κ (s)
0
50
100
150
R epic (km)

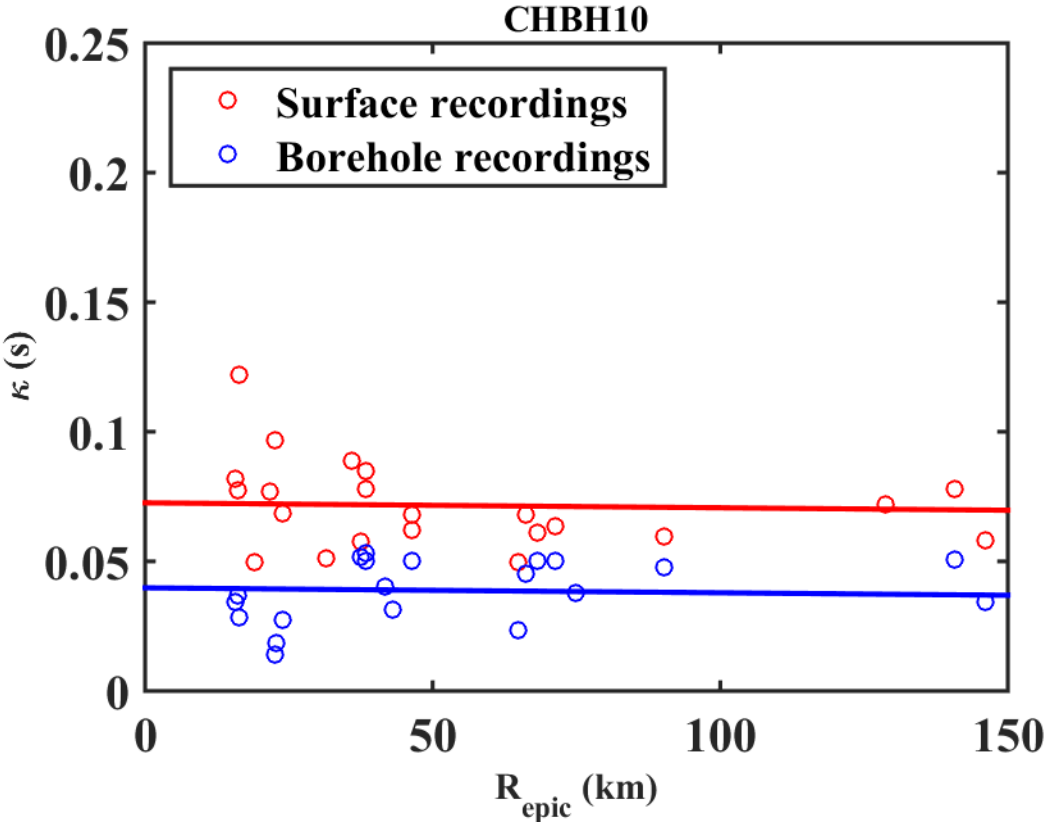
CHBH10
Surface recordings
Borehole recordings
κ (s)
0.25
0.2
0.15
0.1
0.05
0
0
50
100
150
R epic (km)

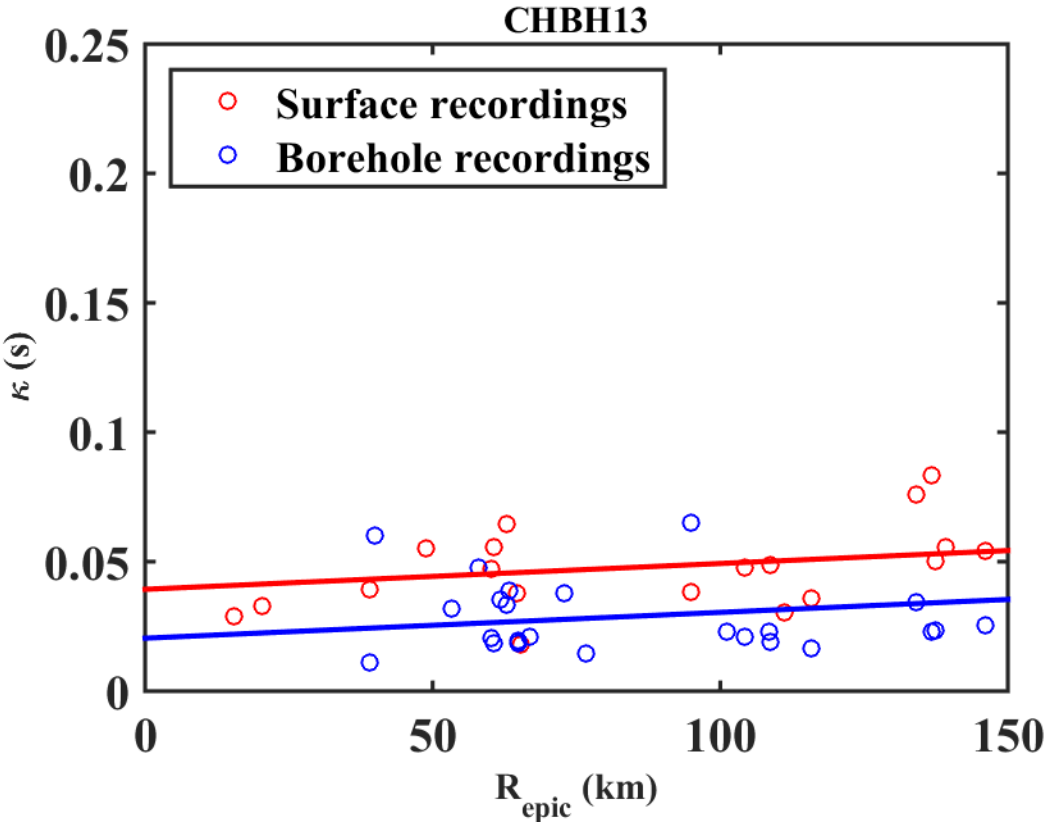
CHBH13
Surface recordings
Borehole recordings
κ (s)
0.25
0.2
0.15
0.1
0.05
0
0
50
100
150
R epic (km)

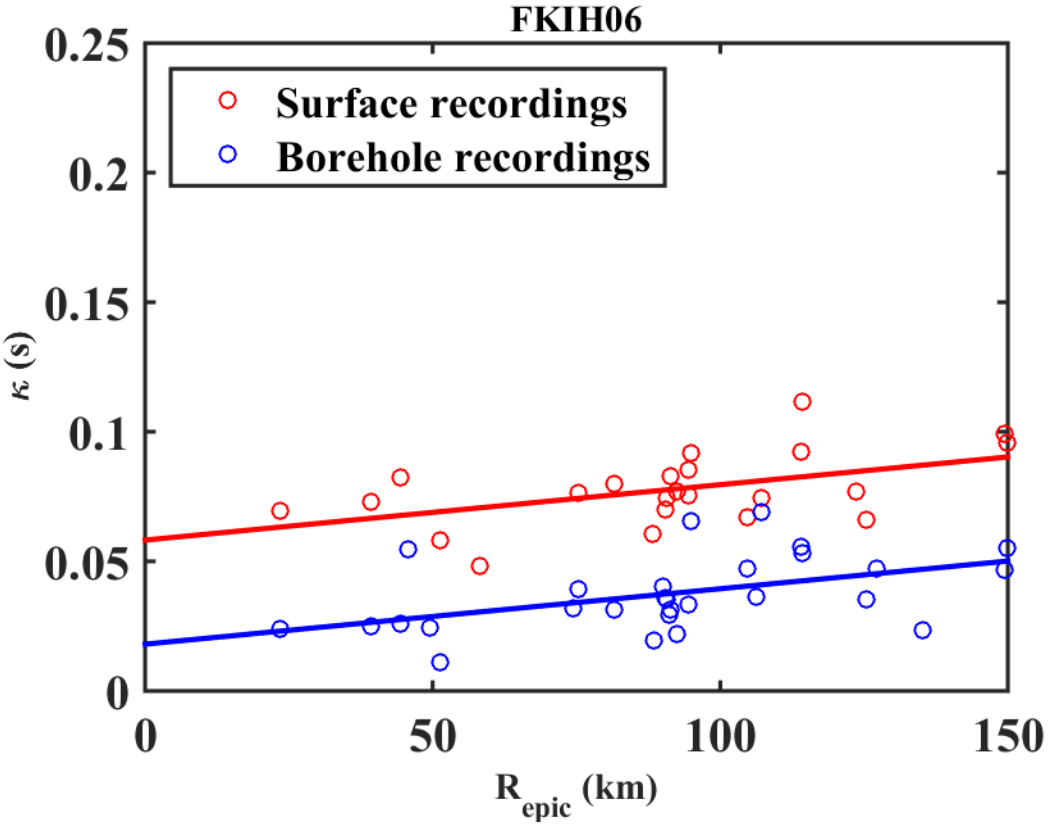
FKIH06
Surface recordings
Borehole recordings
κ (s)
0.25
0.2
0.15
0.1
0.05
0
0
50
100
150
R epic (km)

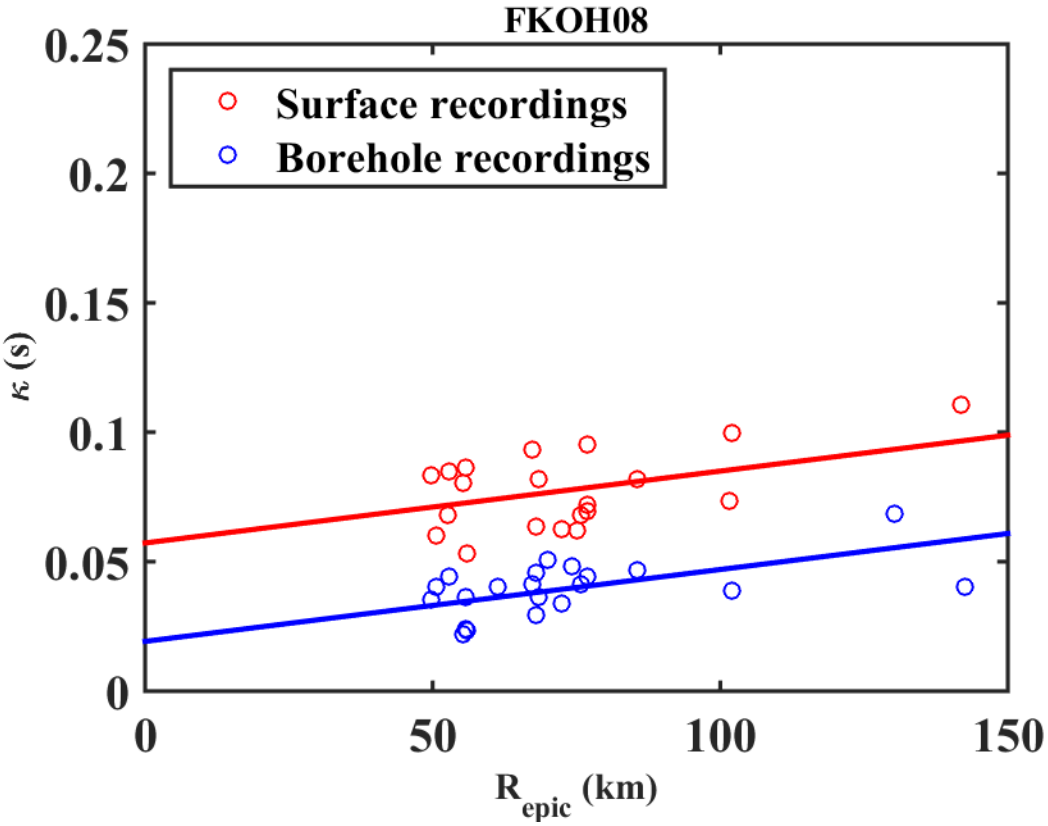
FKOH08
Surface recordings
Borehole recordings
κ (s)
0.25
0.2
0.15
0.1
0.05
0
0
50
100
150
R epic (km)

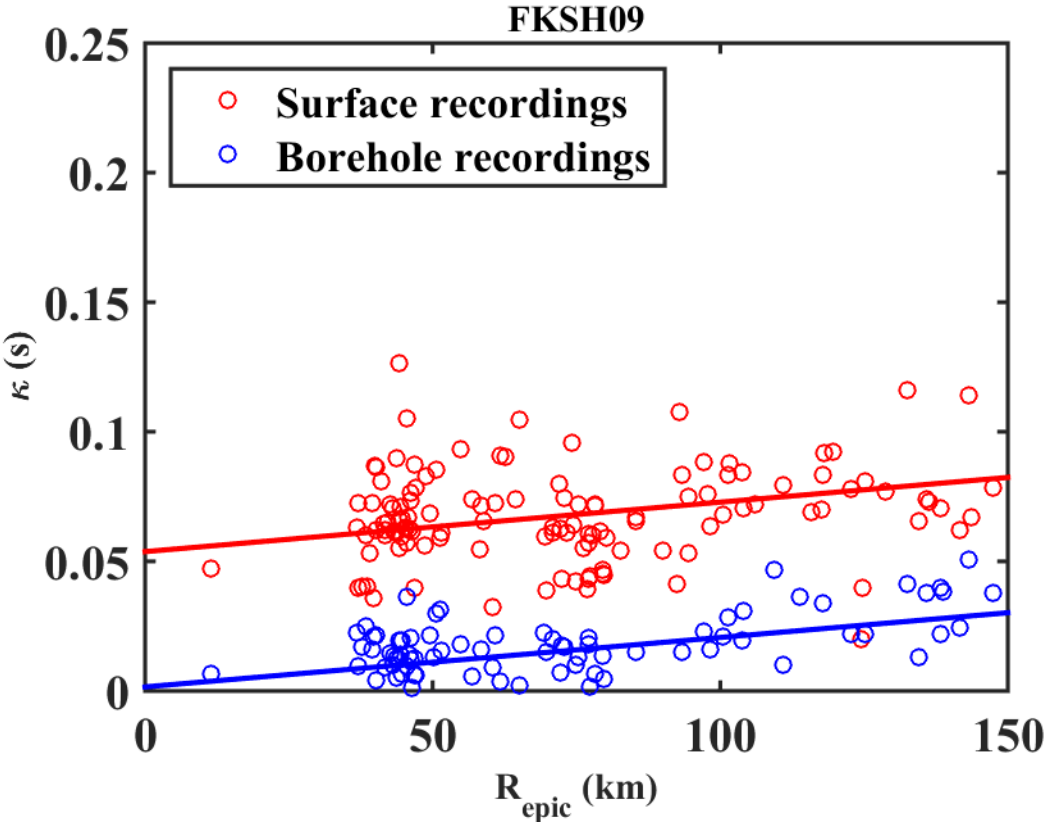
FKSH09
Surface recordings
Borehole recordings
κ (s)
0.25
0.2
0.15
0.1
0.05
0
0
50
100
150
R epic (km)

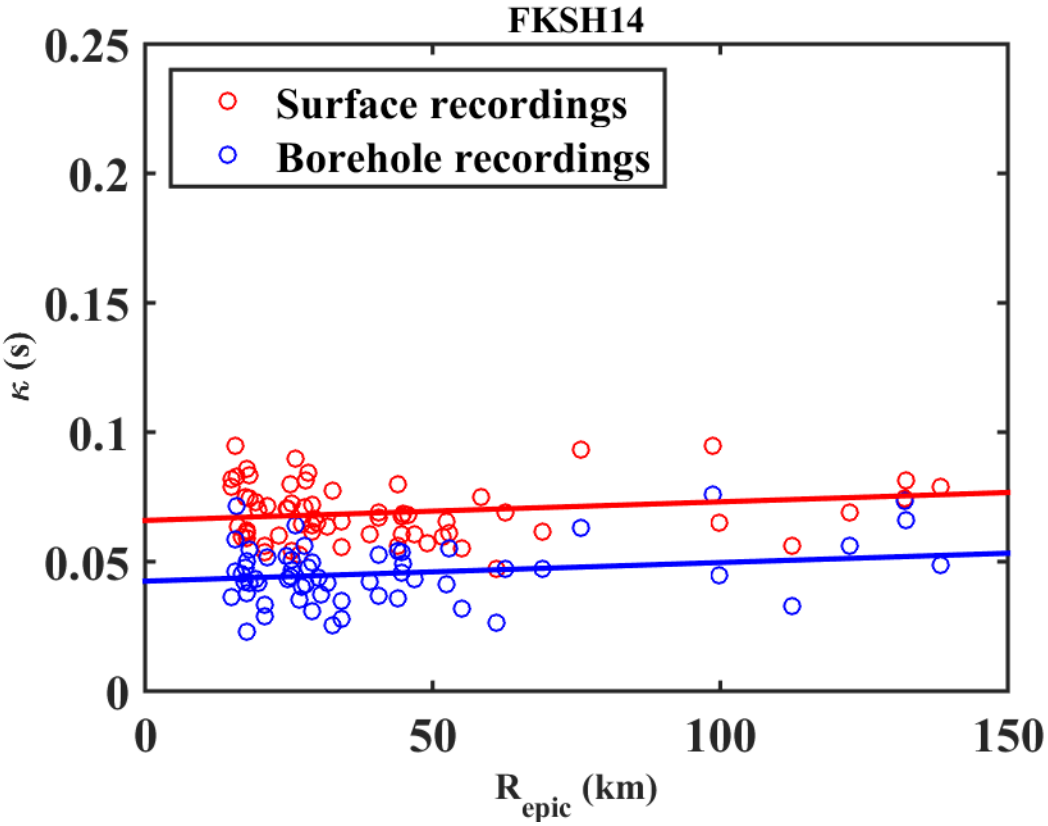
FKSH14
Surface recordings
Borehole recordings
κ (s)
0.25
0.2
0.15
0.1
0.05
0
0
50
100
150
R epic (km)

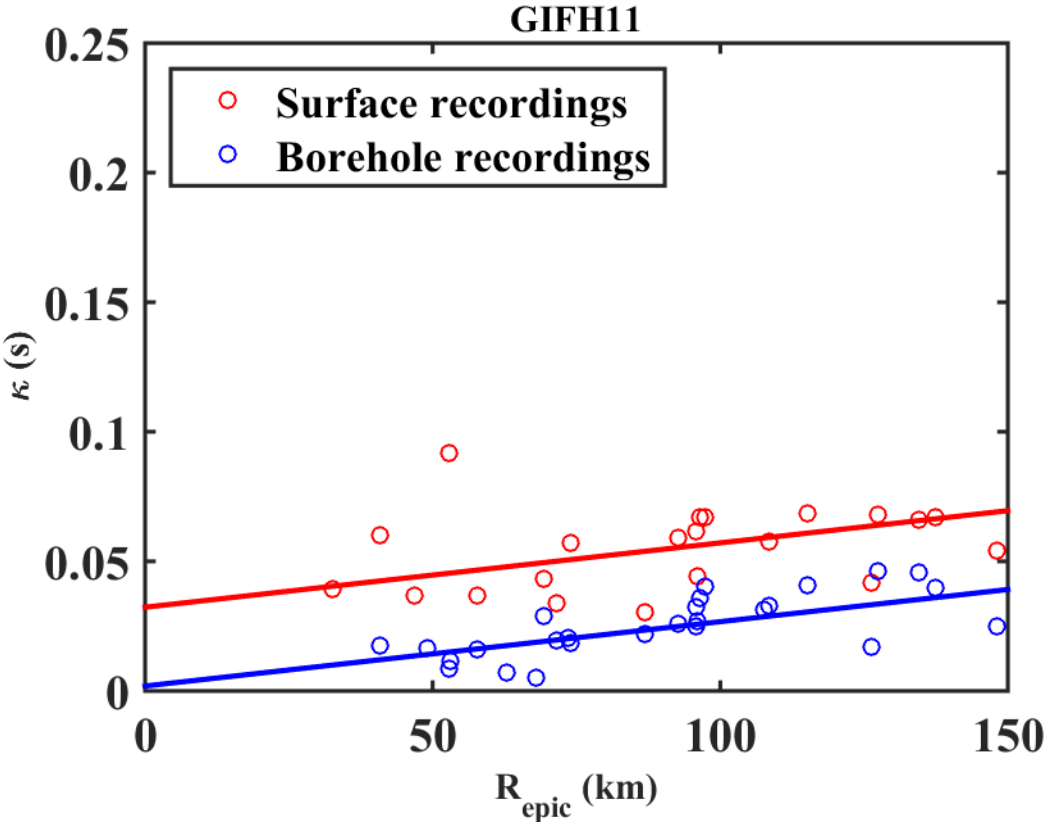
GIFH11
Surface recordings
Borehole recordings
0.25
0.2
0.15
0.1
0.05
0
κ (s)
0
50
100
150
R epic (km)

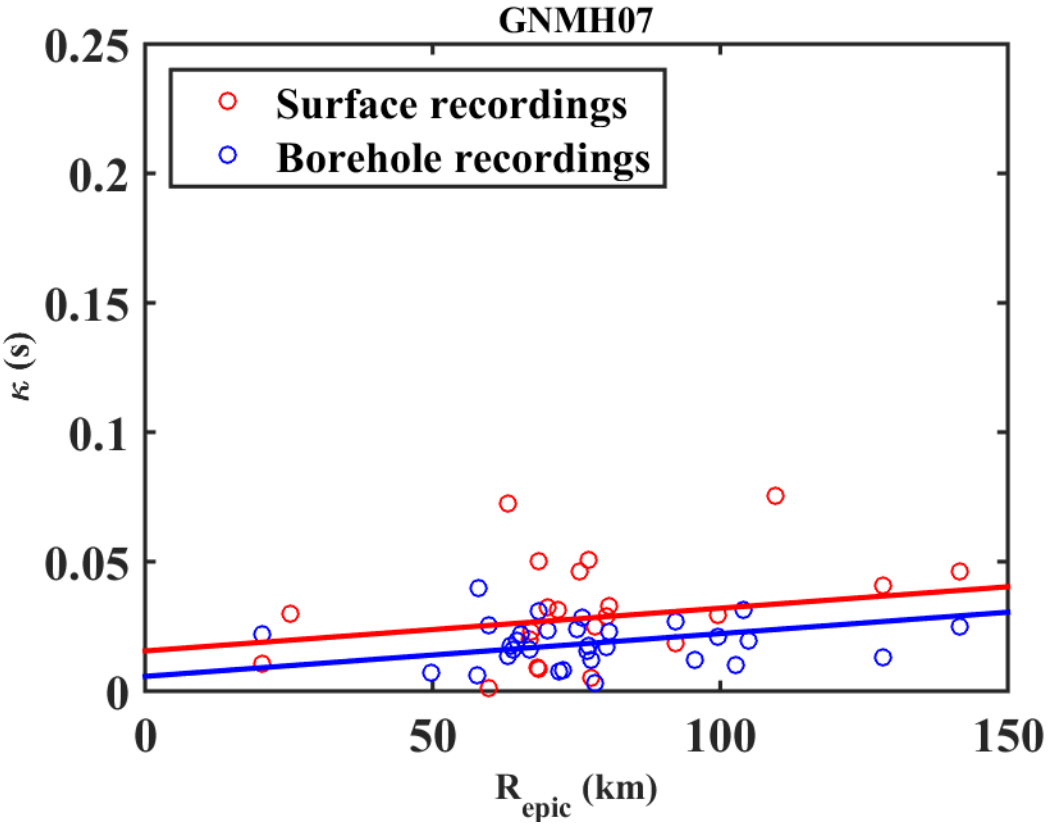
GNMH07
Surface recordings
Borehole recordings
0.25
0.2
0.15
0.1
0.05
0
κ (s)
0
50
100
150
R epic (km)

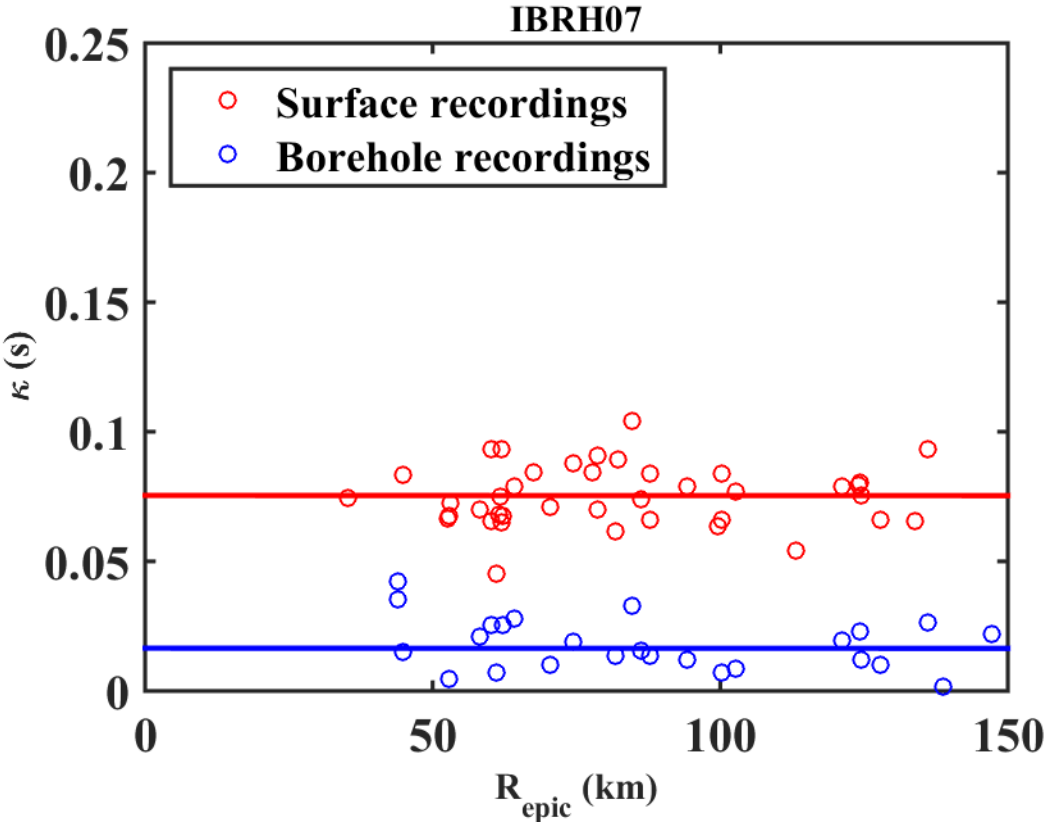
IBRH07
Surface recordings
Borehole recordings
κ (s)
0.25
0.2
0.15
0.1
0.05
0
0
50
100
150
R epic (km)

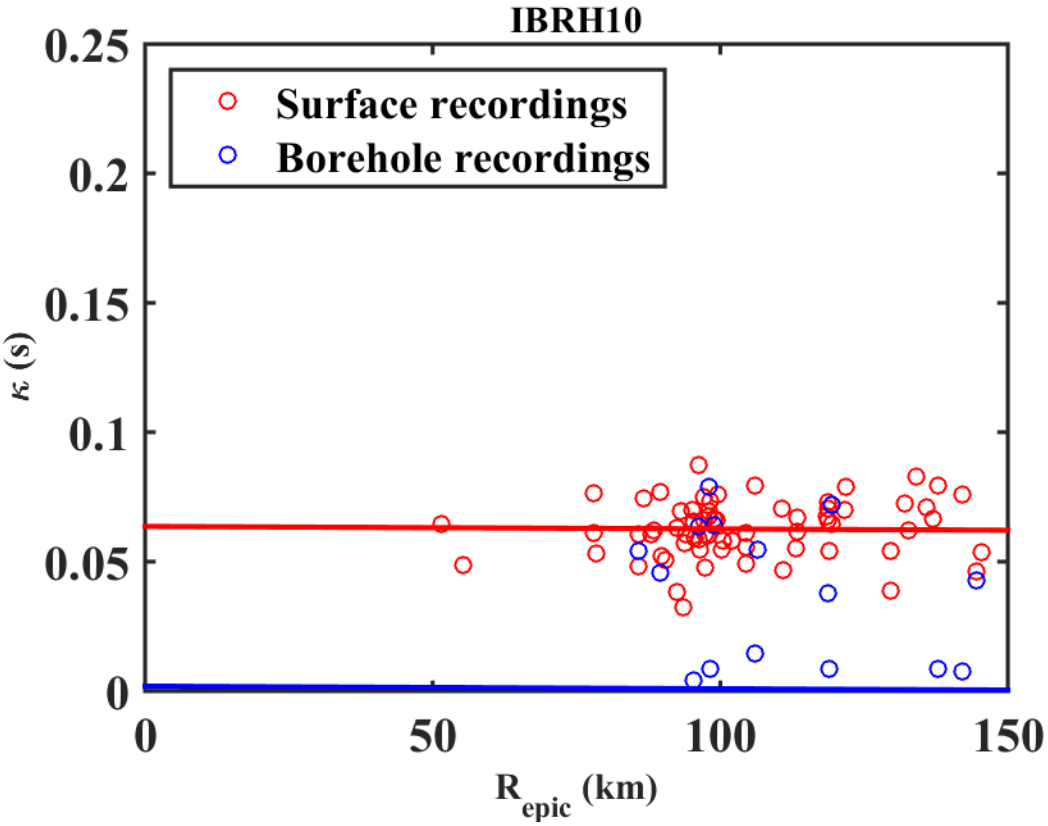
IBRH10
Surface recordings
Borehole recordings
κ (s)
0.25
0.2
0.15
0.1
0.05
0
0
50
100
150
R epic (km)

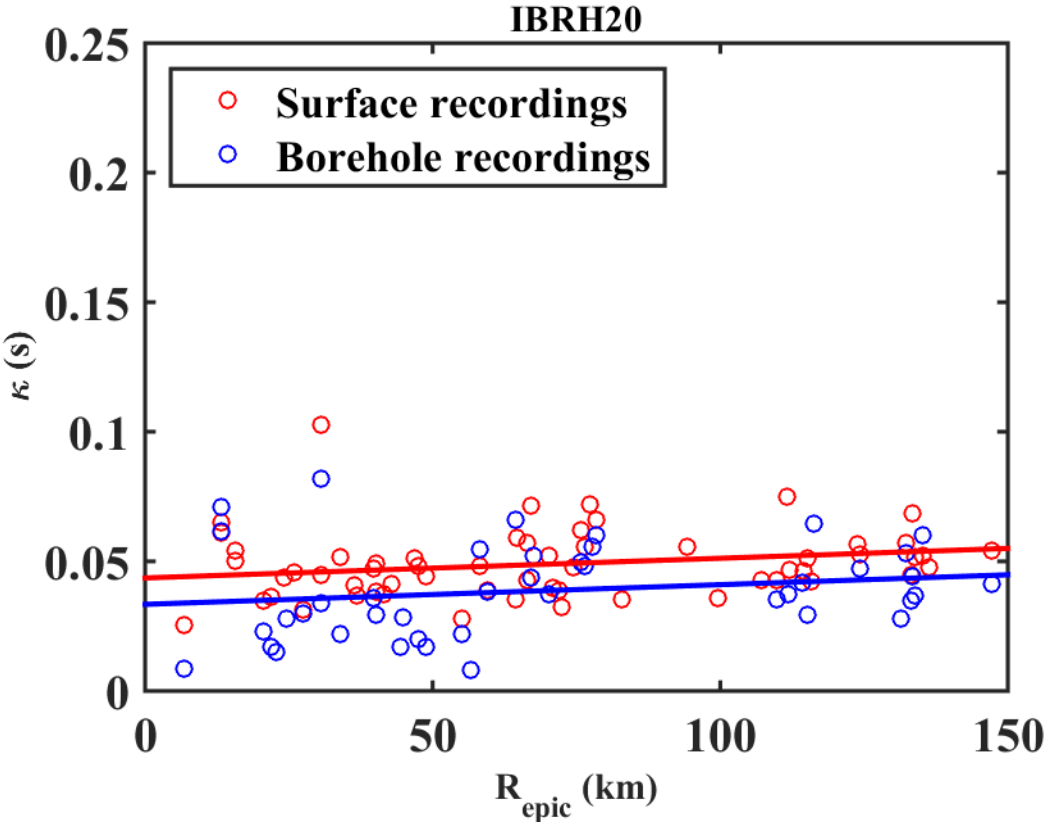
IBRH20
Surface recordings
Borehole recordings
κ (s)
0.25
0.2
0.15
0.1
0.05
0
0
50
100
150
R epic (km)

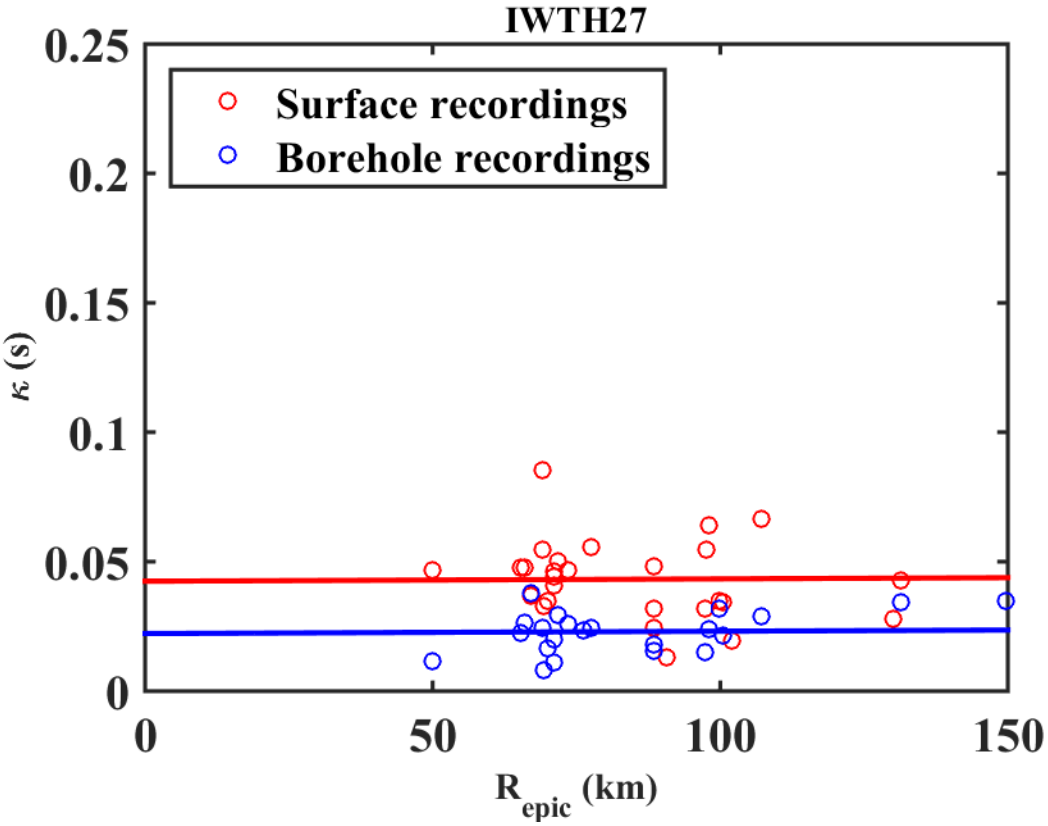
IWTH27
Surface recordings
Borehole recordings
κ (s)
0.25
0.2
0.15
0.1
0.05
0
0
50
100
150
R epic (km)

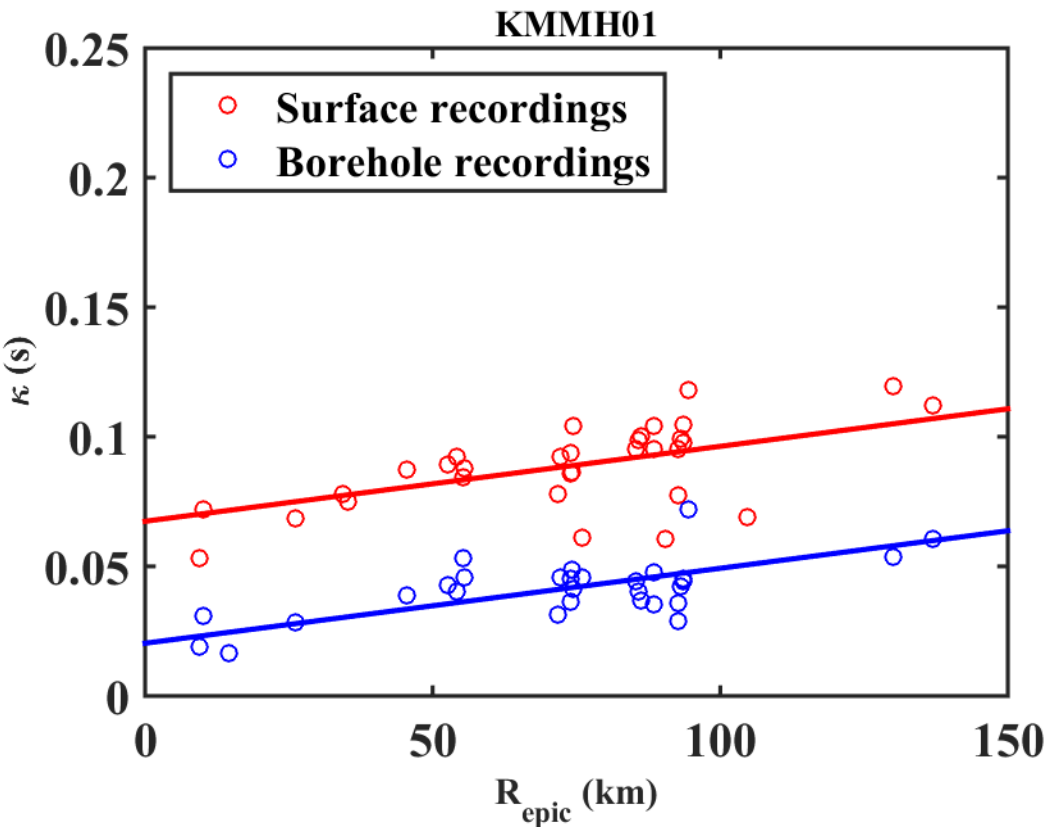
KMMH01
Surface recordings
Borehole recordings
0.25
0.2
0.15
0.1
0.05
0
κ (s)
0
50
100
150
R epic (km)

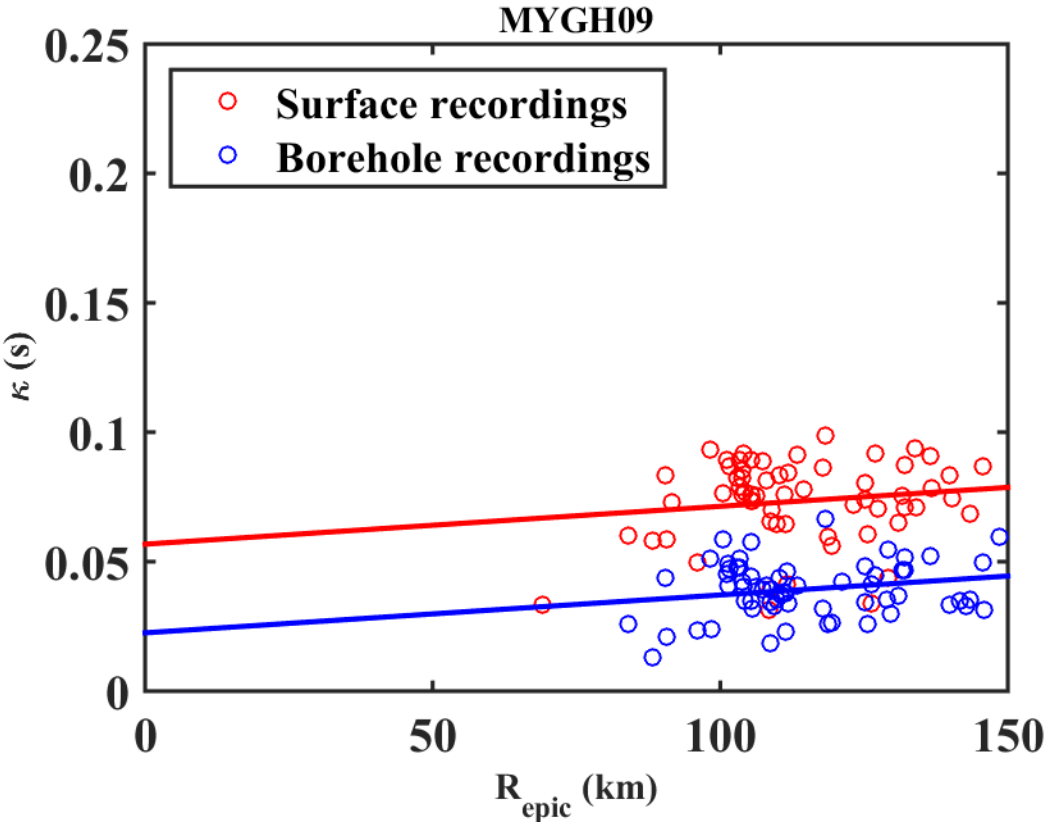
MYGH09
Surface recordings
Borehole recordings
0.25
0.2
0.15
0.1
0.05
0
κ (s)
0
50
100
150
R epic (km)

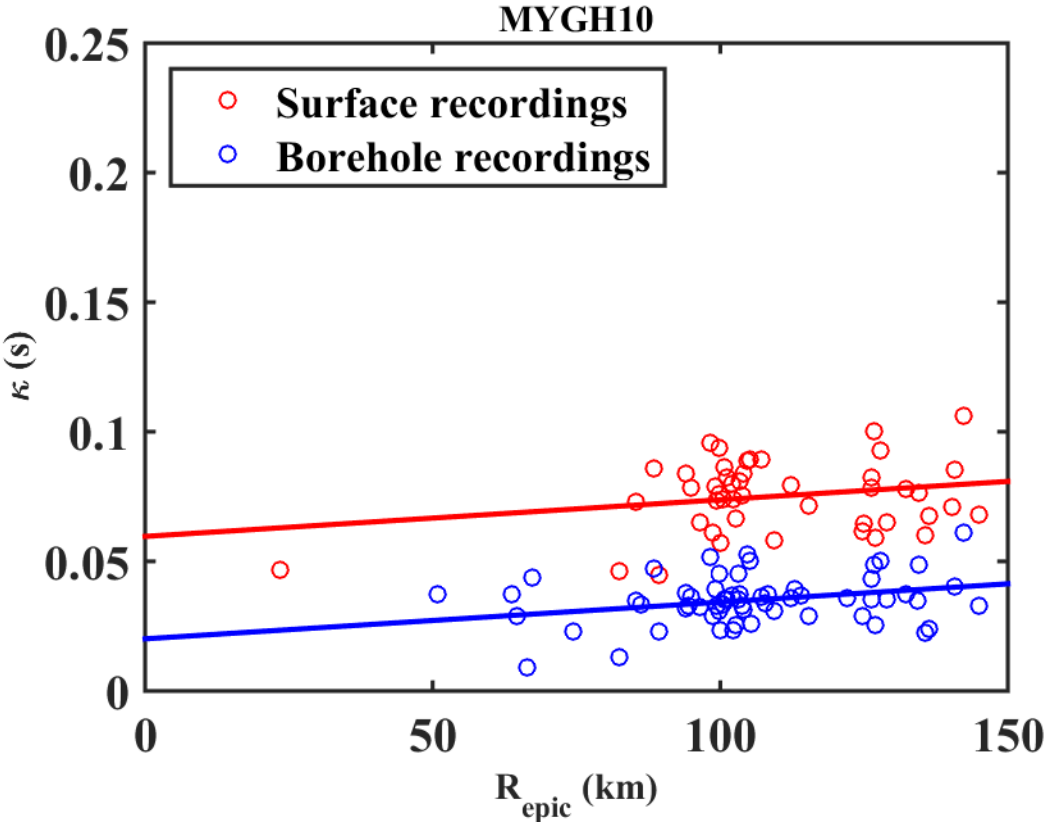
MYGH10
Surface recordings
Borehole recordings
κ (s)
0.25
0.2
0.15
0.1
0.05
0
0
50
100
150
R epic (km)

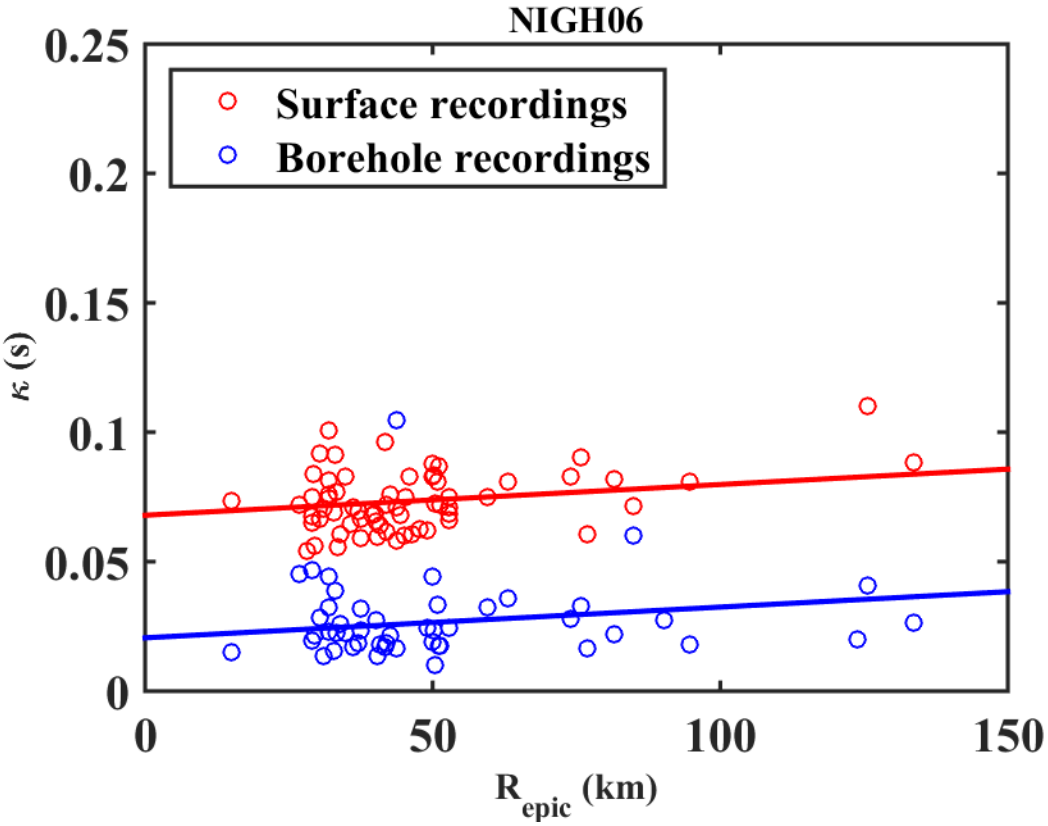
NIGH06
Surface recordings
Borehole recordings
κ (s)
0.25
0.2
0.15
0.1
0.05
0
0
50
100
150
R epic (km)

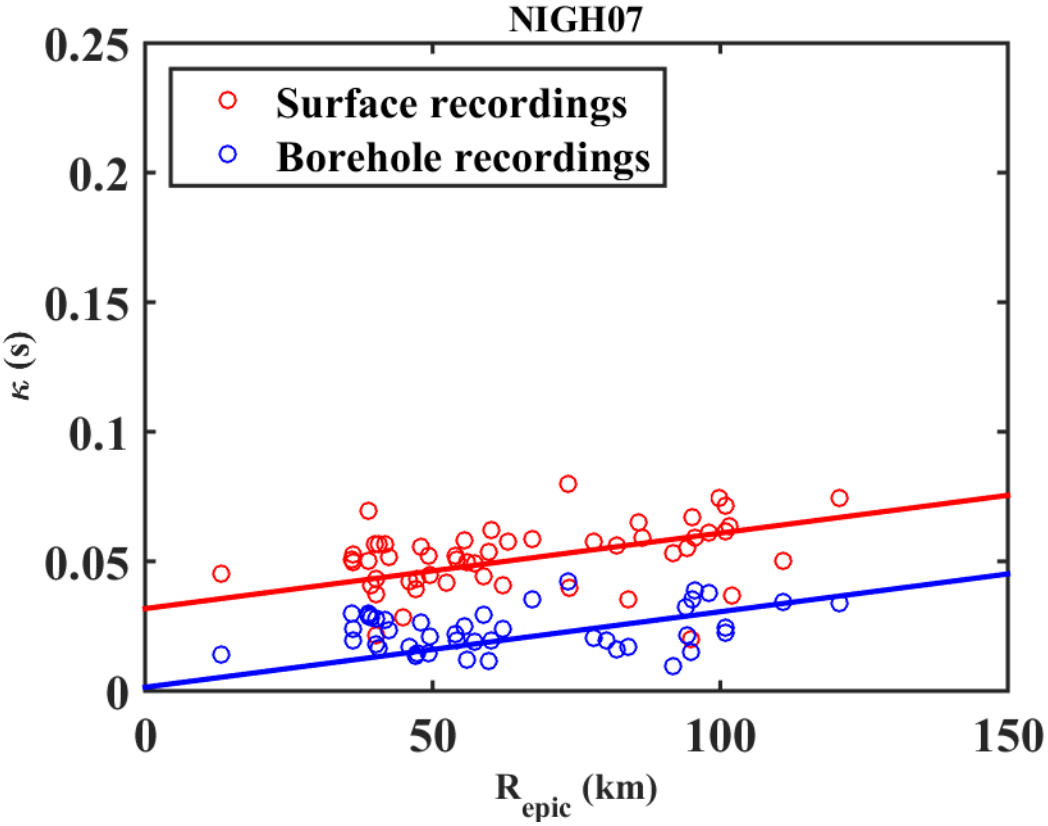
NIGH07
Surface recordings
Borehole recordings
κ (s)
0.25
0.2
0.15
0.1
0.05
0
0
50
100
150
R epic (km)

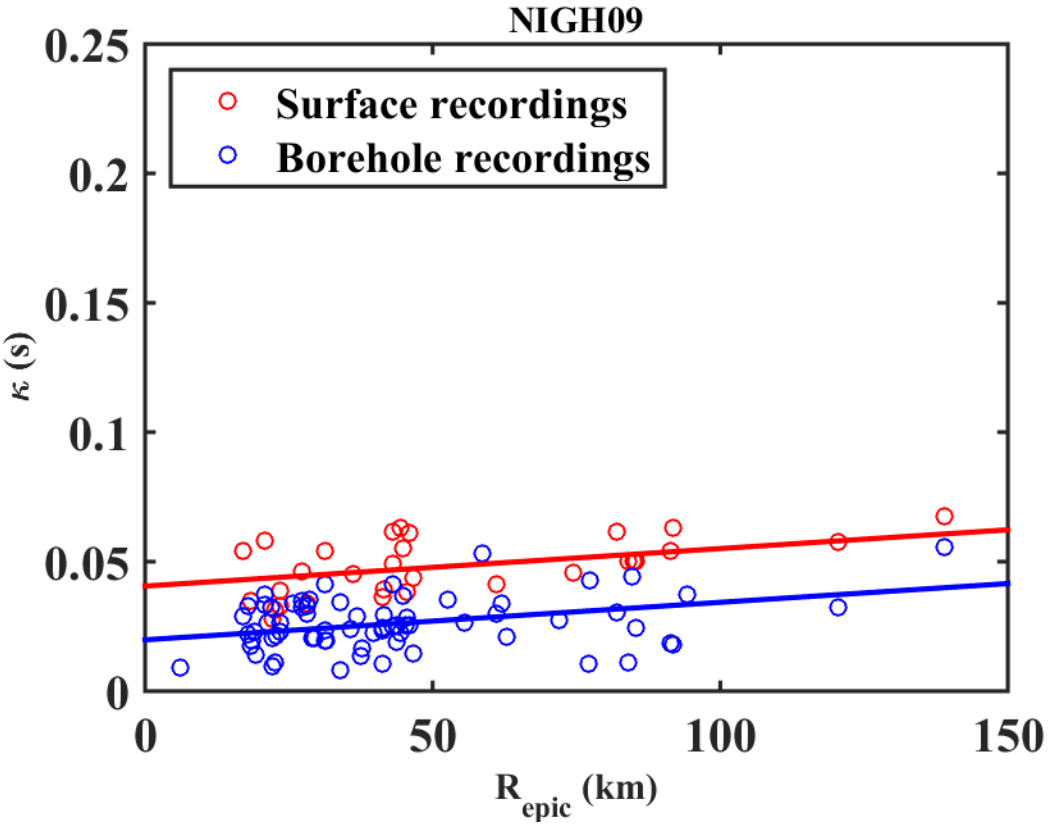
NIGH09
Surface recordings
Borehole recordings
κ (s)
0.25
0.2
0.15
0.1
0.05
0
0
50
100
150
R epic (km)

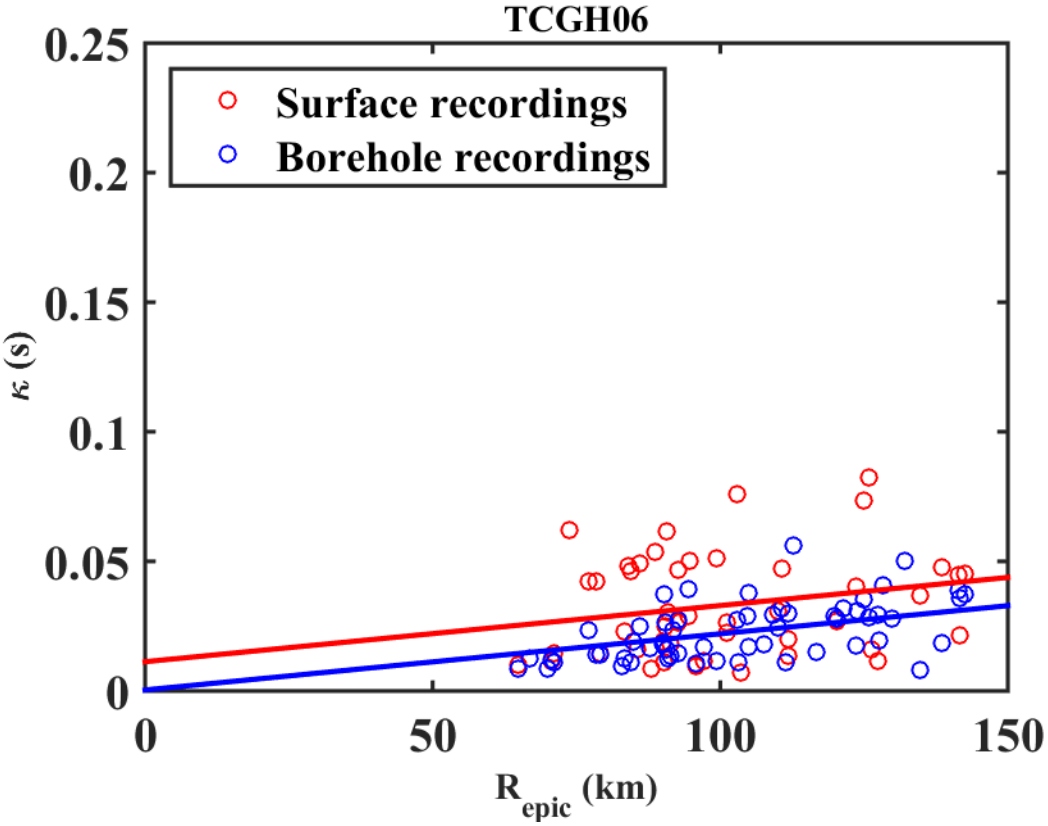
TCGH06
Surface recordings
Borehole recordings
κ (s)
0.25
0.2
0.15
0.1
0.05
0
0
50
100
150
R epic (km)

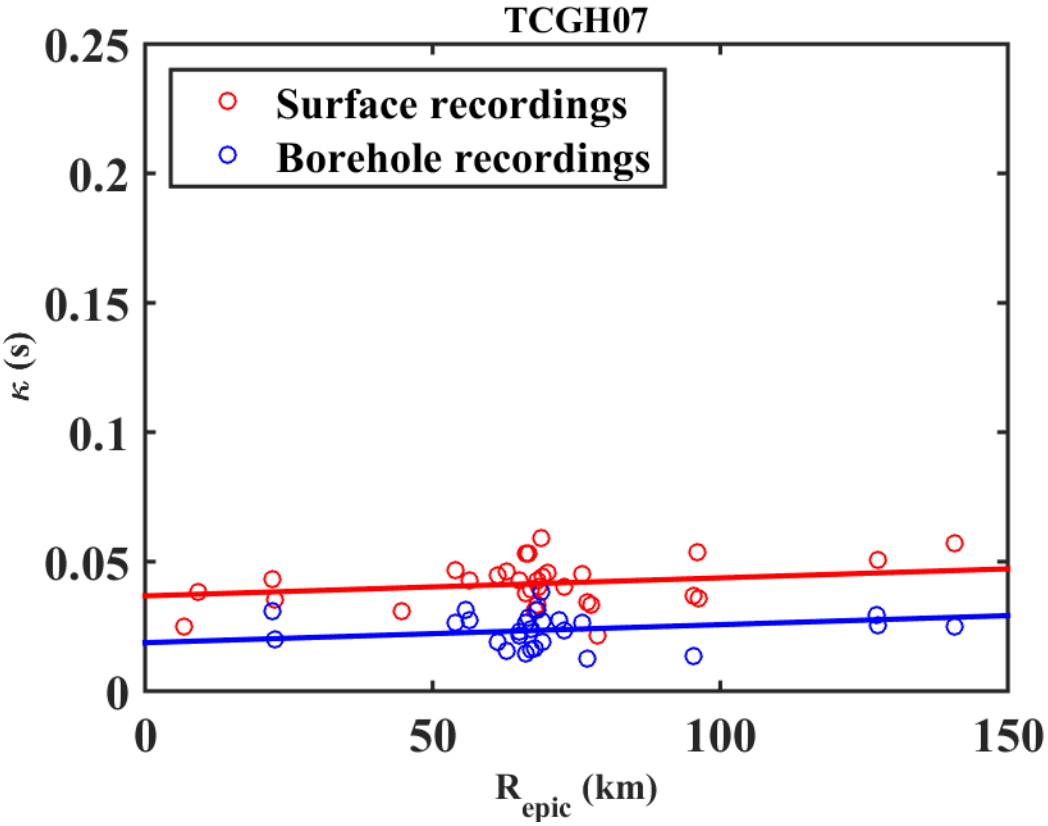
TCGH07
Surface recordings
Borehole recordings
κ (s)
0.25
0.2
0.15
0.1
0.05
0
0
50
100
150
R epic (km)

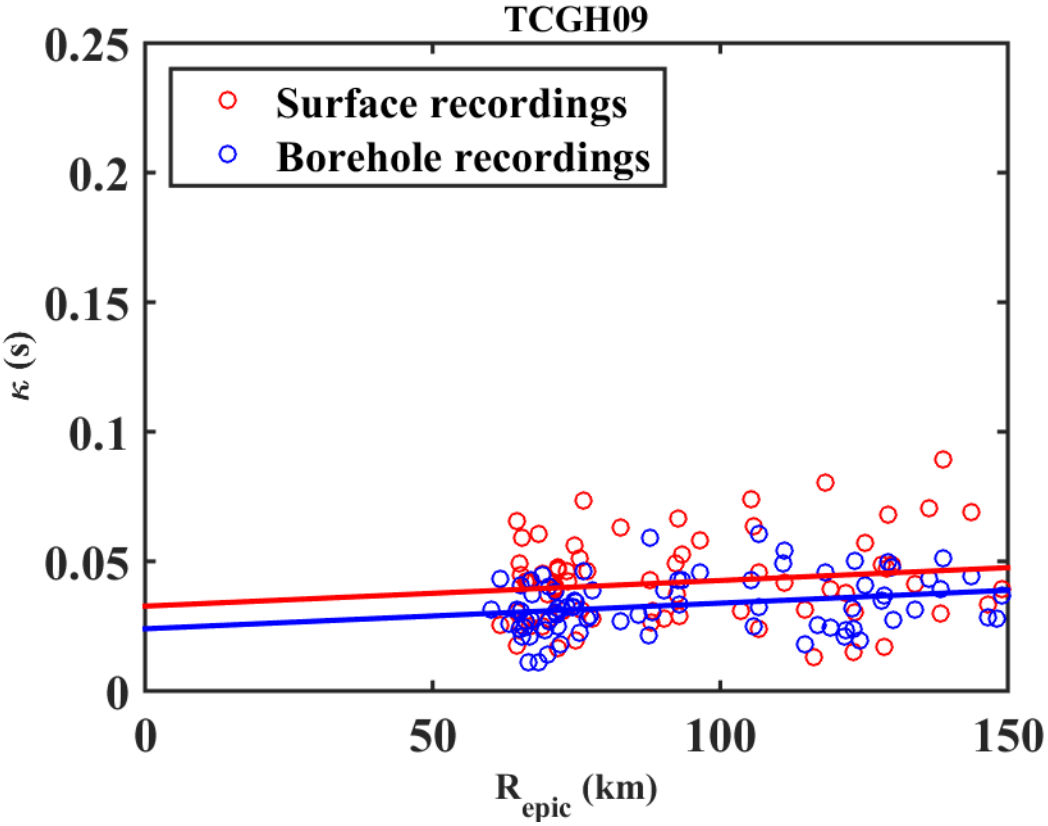
TCGH09
Surface recordings
Borehole recordings
κ (s)
0.25
0.2
0.15
0.1
0.05
0
0
50
100
150
R epic (km)

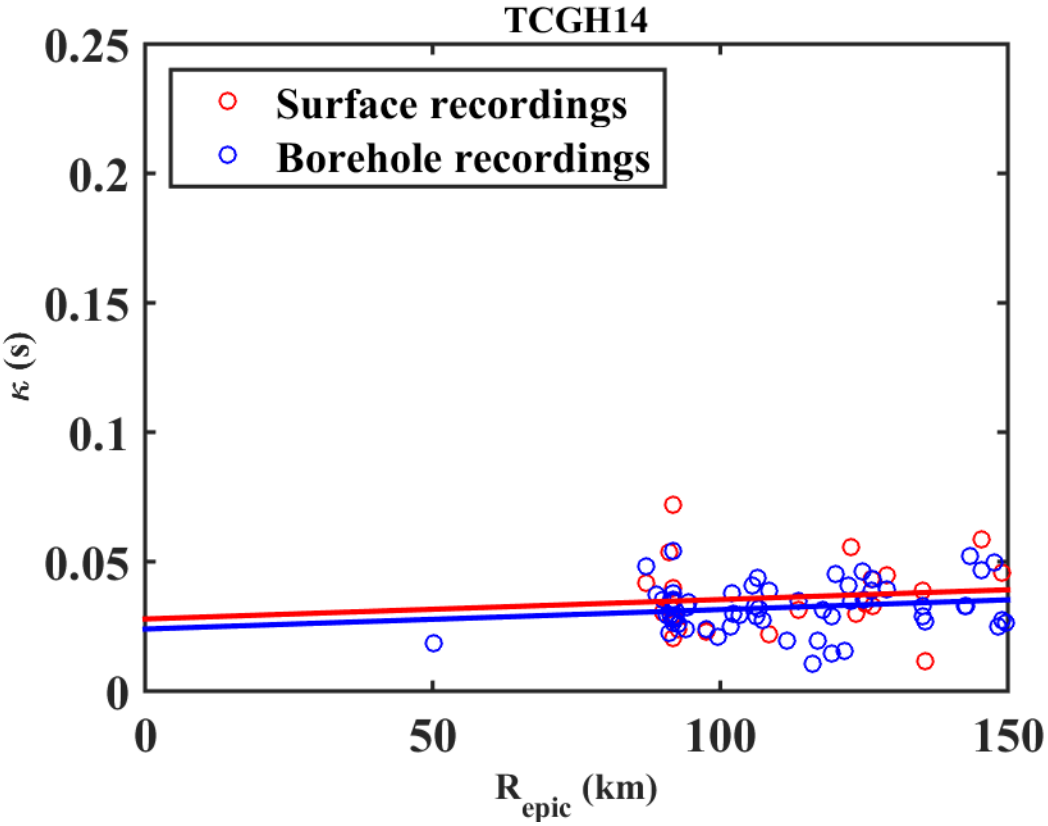
TCGH14
Surface recordings
Borehole recordings
κ (s)
0.25
0.2
0.15
0.1
0.05
0
0
50
100
150
R epic (km)

APPENDIX B

List of KiK-net stations grouped in clusters used in Chapter 3

Cluster #	Station Name	Station Latitude	Station Longitude
1	YMTH13	38.5	139.8
	FKSH01	37.8	139.7
	FKSH03	37.6	139.8
	FKSH05	37.3	139.9
	NIGH08	37.7	139.5
	FKSH06	37.2	139.5
	FKSH07	37.0	139.4
	TCGH08	36.9	139.6
	FKSH21	37.3	139.3
2	TCGH12	36.7	140.0
	FKSH12	37.2	140.6
	IBRH18	36.4	140.6
	IBRH14	36.7	140.6
	IBRH13	36.8	140.6
	TCGH16	36.5	140.1
	TCGH10	36.9	140.0
	FKSH10	37.2	140.1
	IBRH12	36.8	140.3
	IBRH17	36.1	140.3
	IBRH15	36.6	140.3
	TCGH13	36.7	140.2
	IBRH11	36.4	140.1
	IBRH19	36.2	140.1
3	NIGH18	36.9	138.3
	GIFH19	36.0	137.4
	GIFH15	36.1	137.2
	GIFH13	36.3	136.9
	ISKH09	36.3	136.7
	NIGH17	36.9	138.1
	NIGH13	37.1	138.4
	NGNH29	36.9	138.4
	NIGH14	37.0	138.9
	NIGH15	37.1	139.0
	NIGH11	37.2	138.7
4	AKTH18	39.4	140.4
	AKTH03	39.2	140.1
	AKTH04	39.2	140.7

APPENDIX C

Minimum Strain Damping Plots corresponding to the Sixty Selected Sites used in Chapter 3

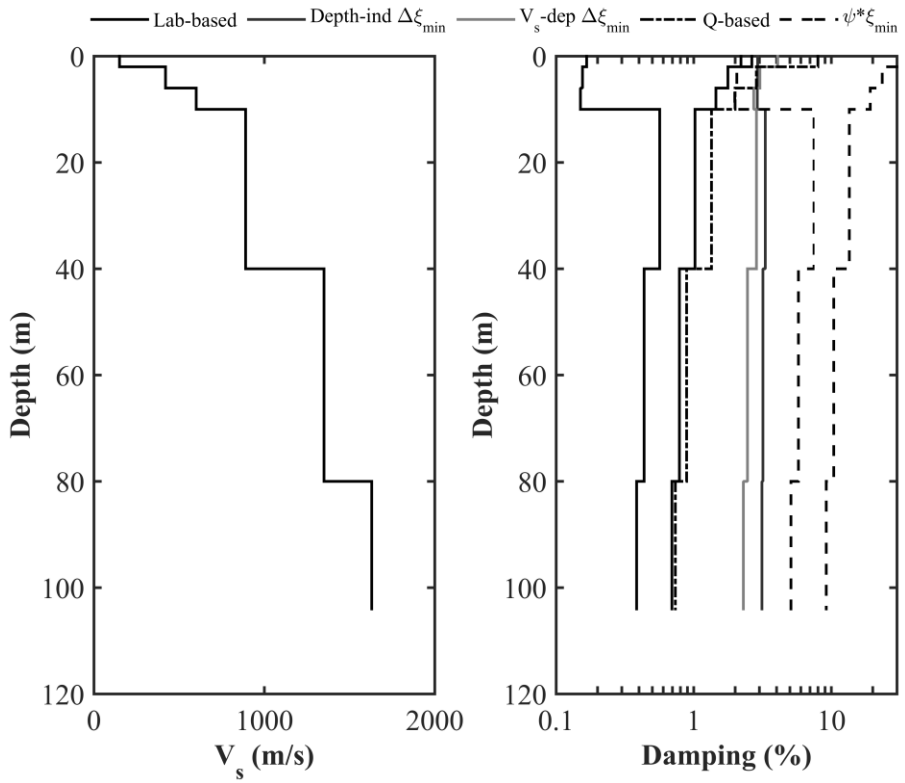

YMTH13

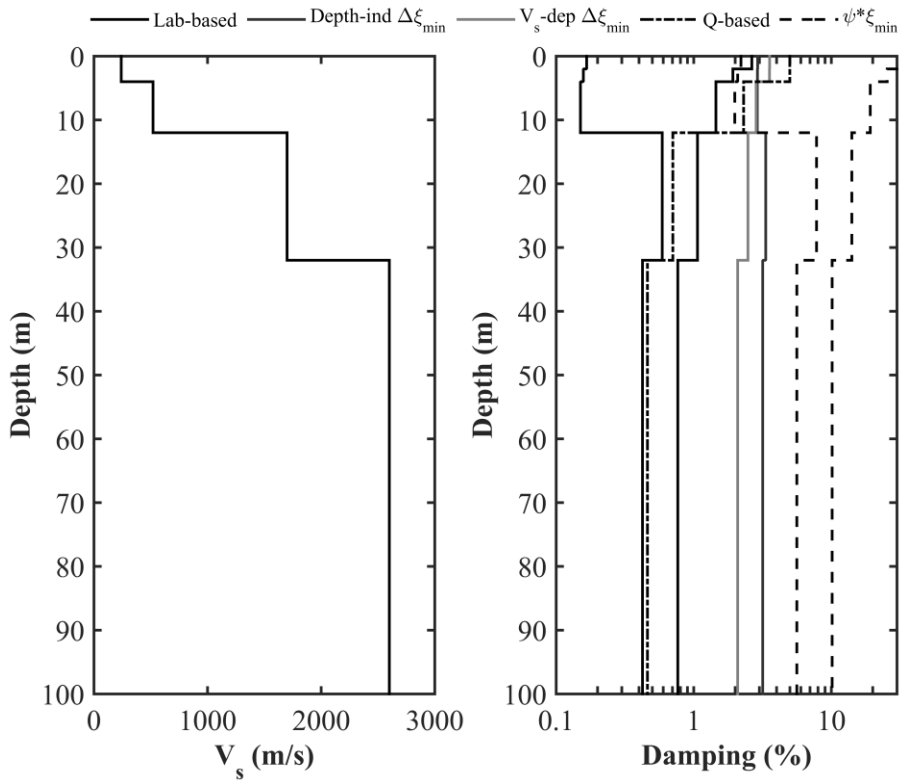

FKSH01

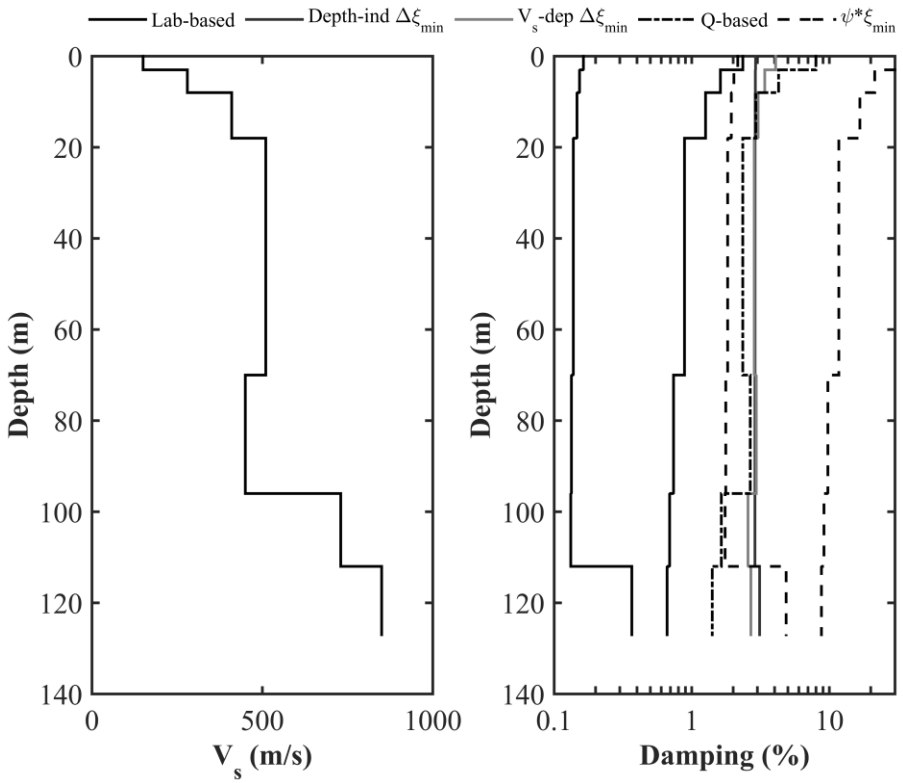

FKSH03

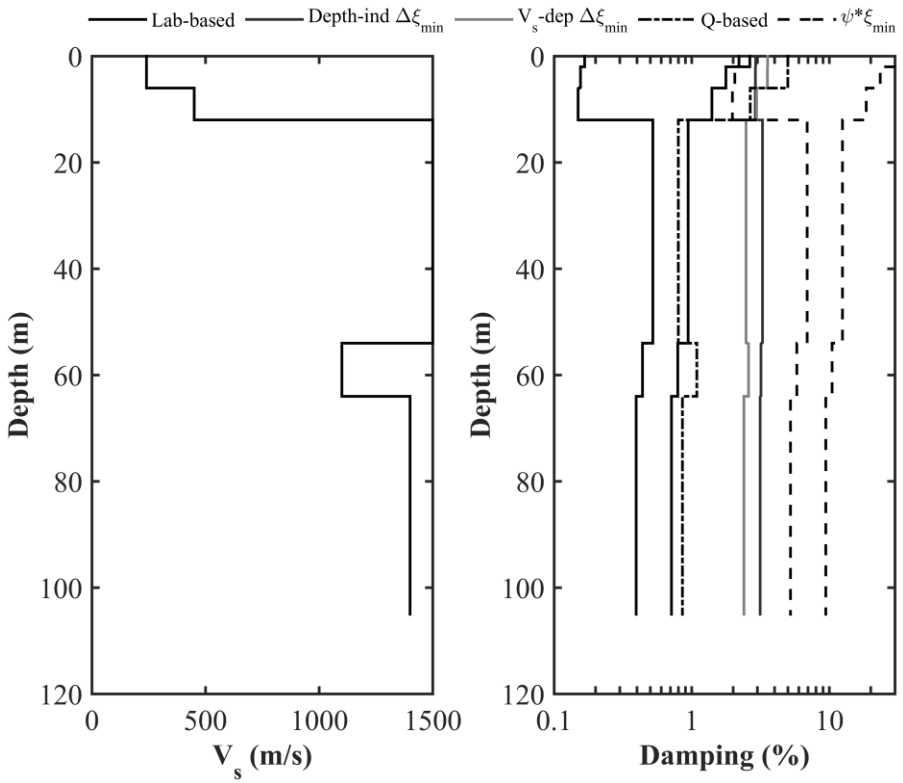

FKSH05

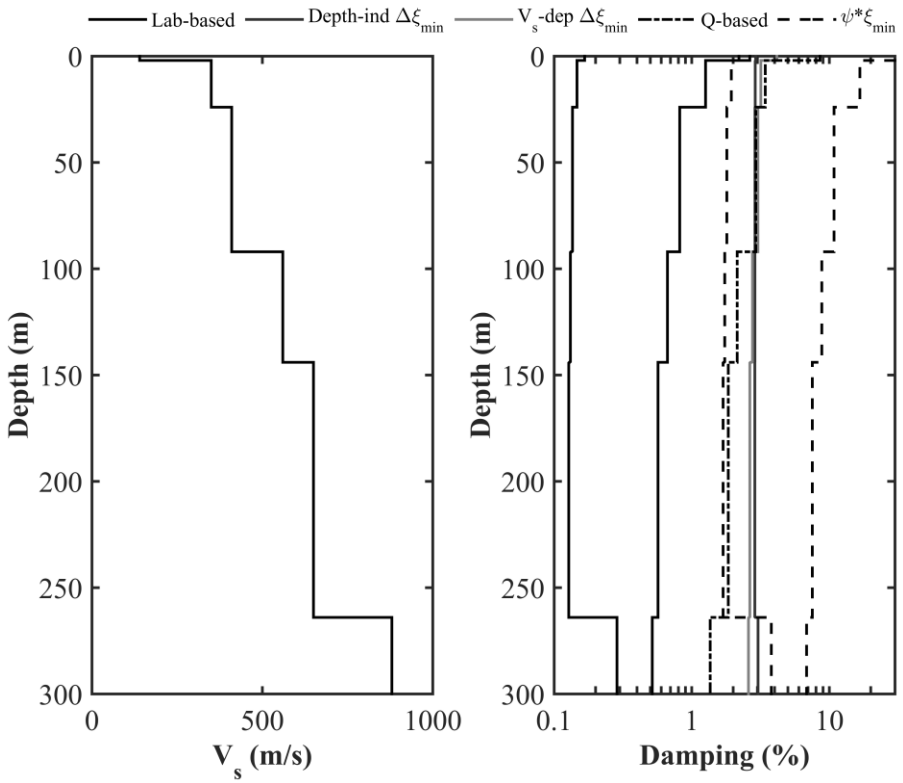

NIGH08

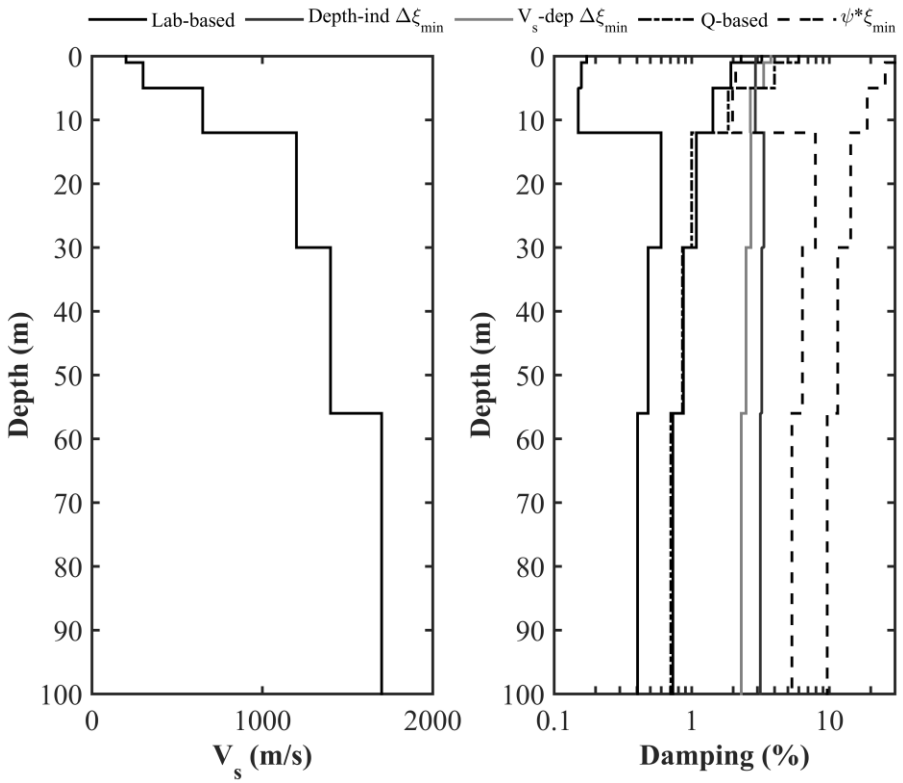

FKSH06

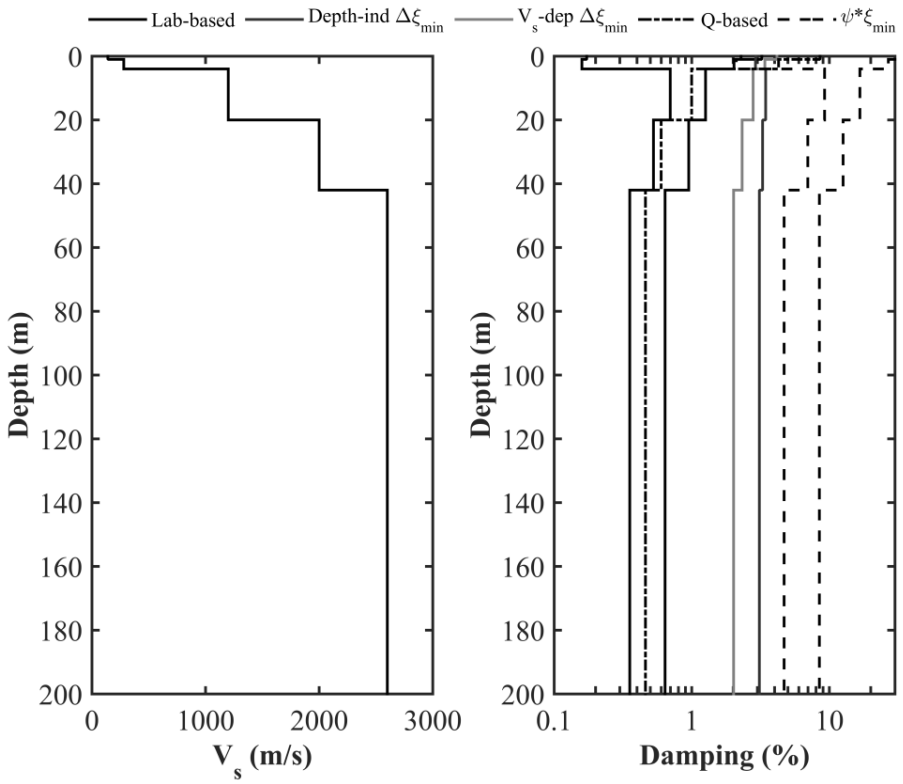

FKSH07

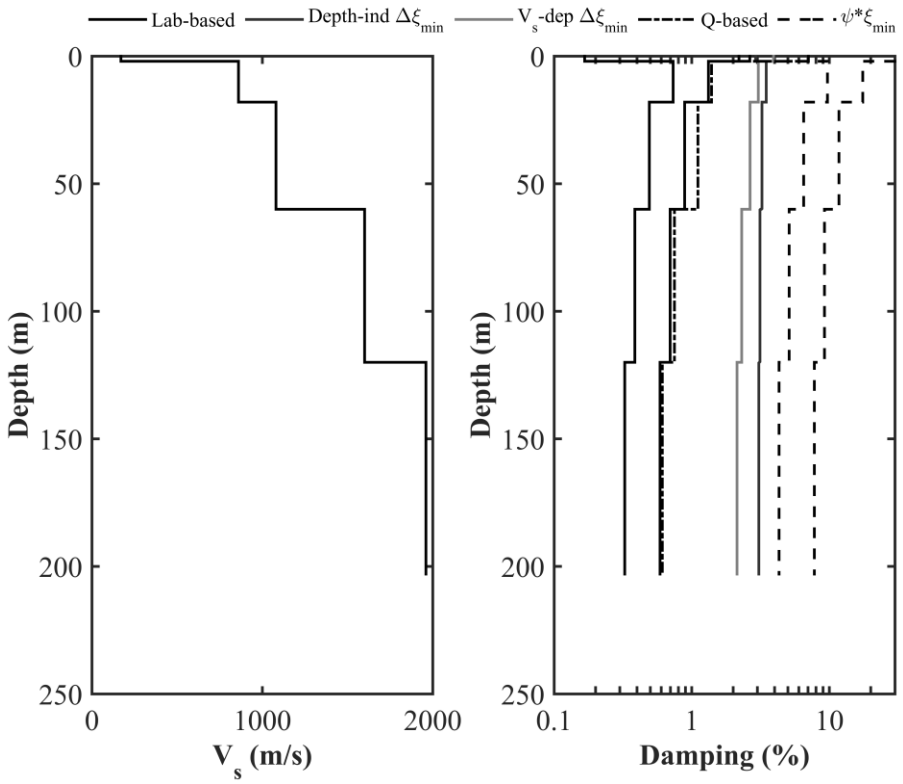

TCGH08

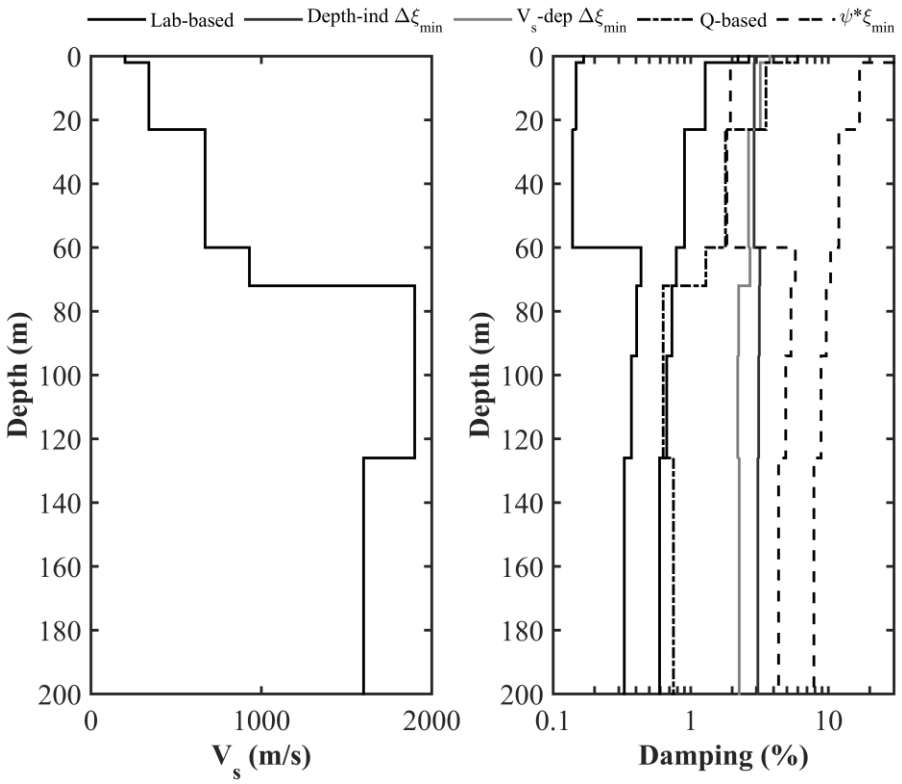

FKSH21

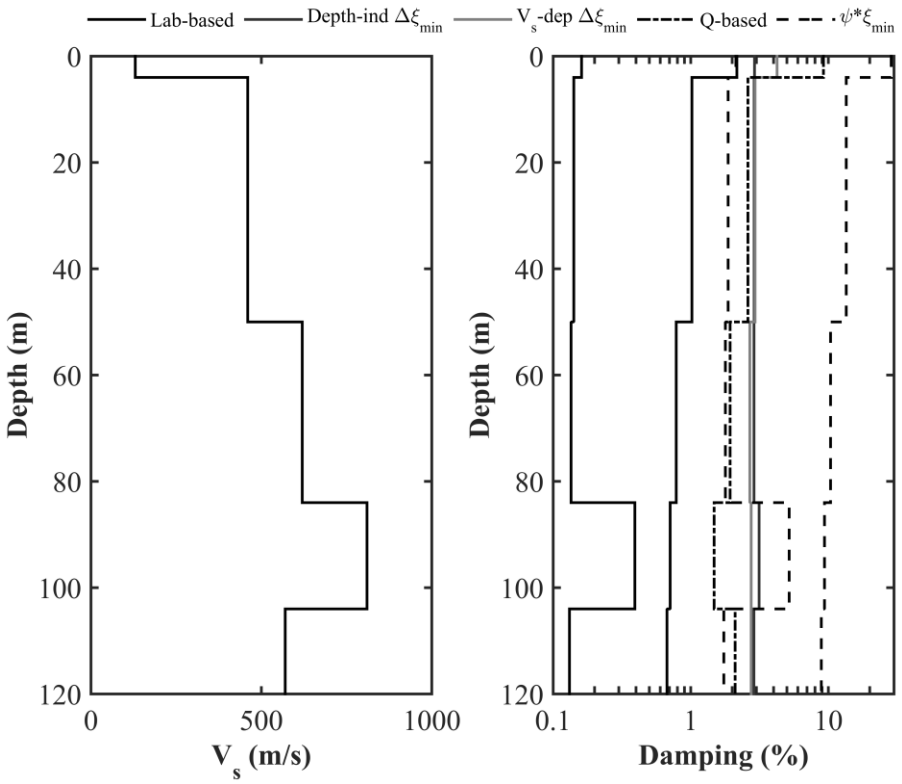

TCGH12

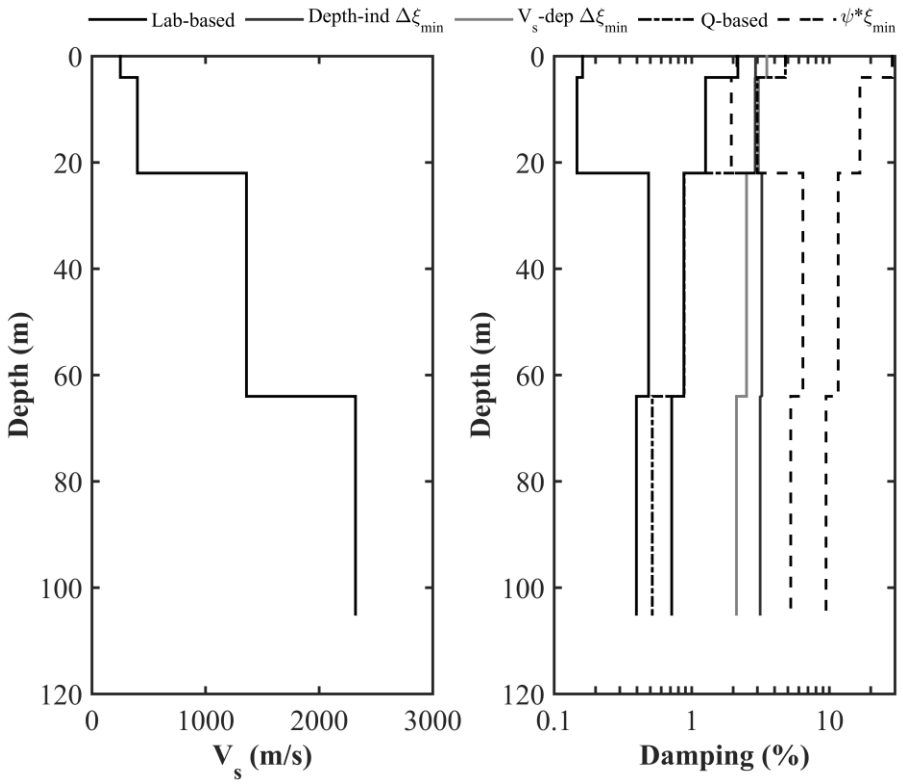

FKSH12

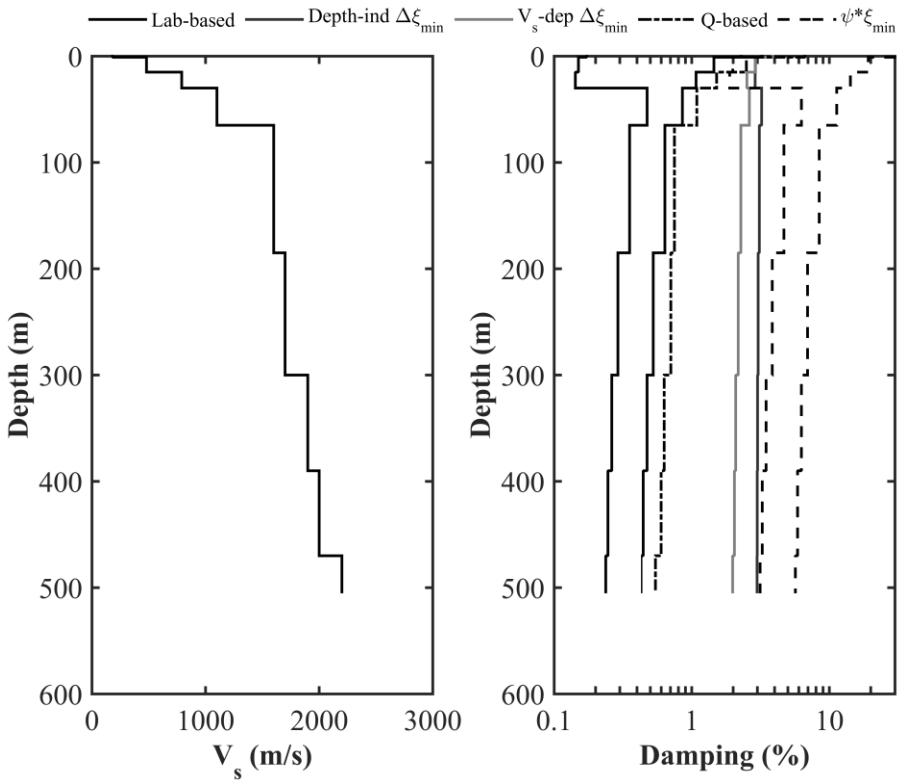

IBRH18

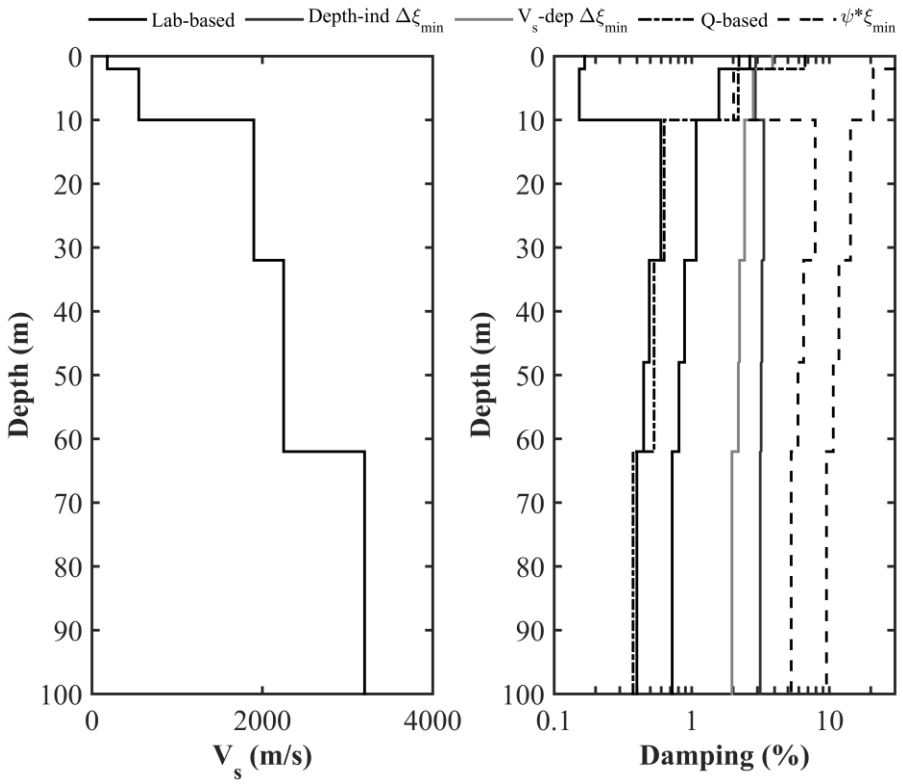

IBRH14

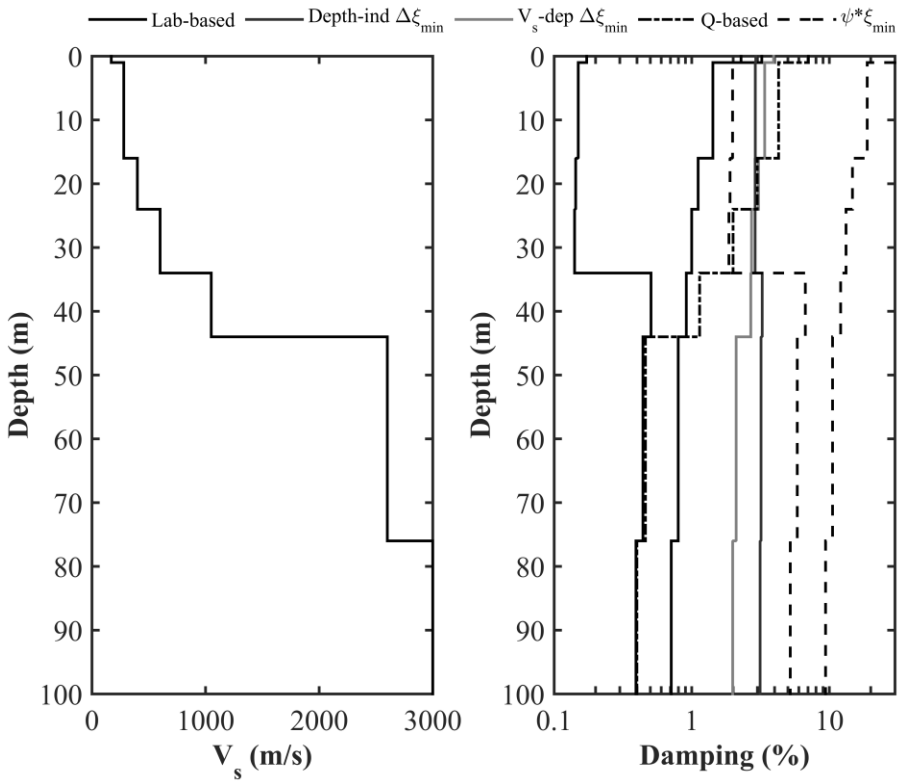

IBRH13

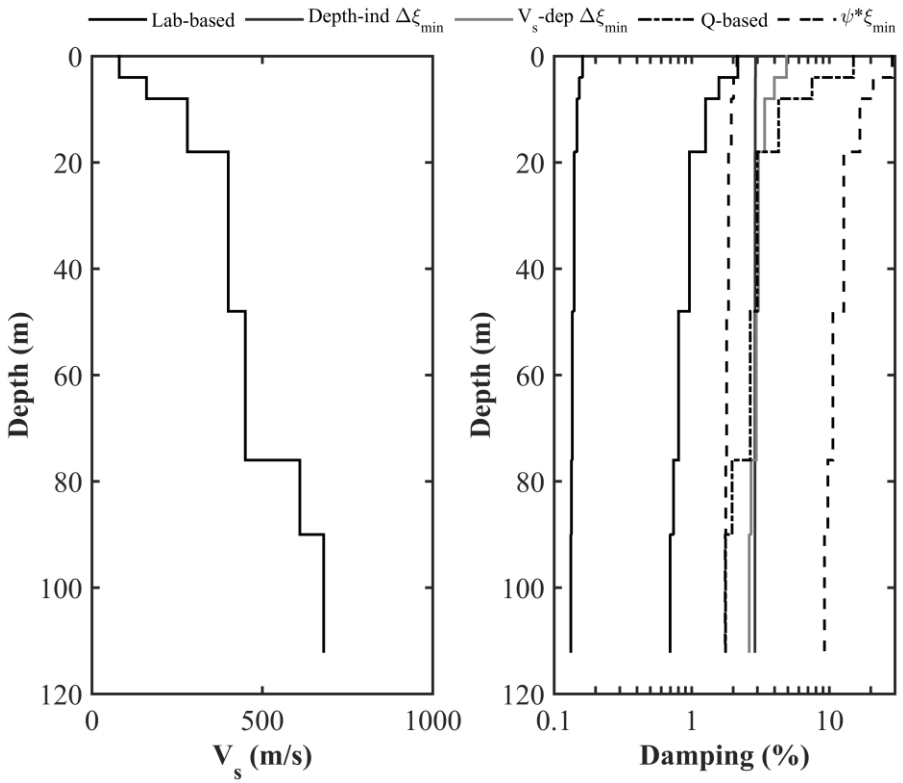

TCGH16

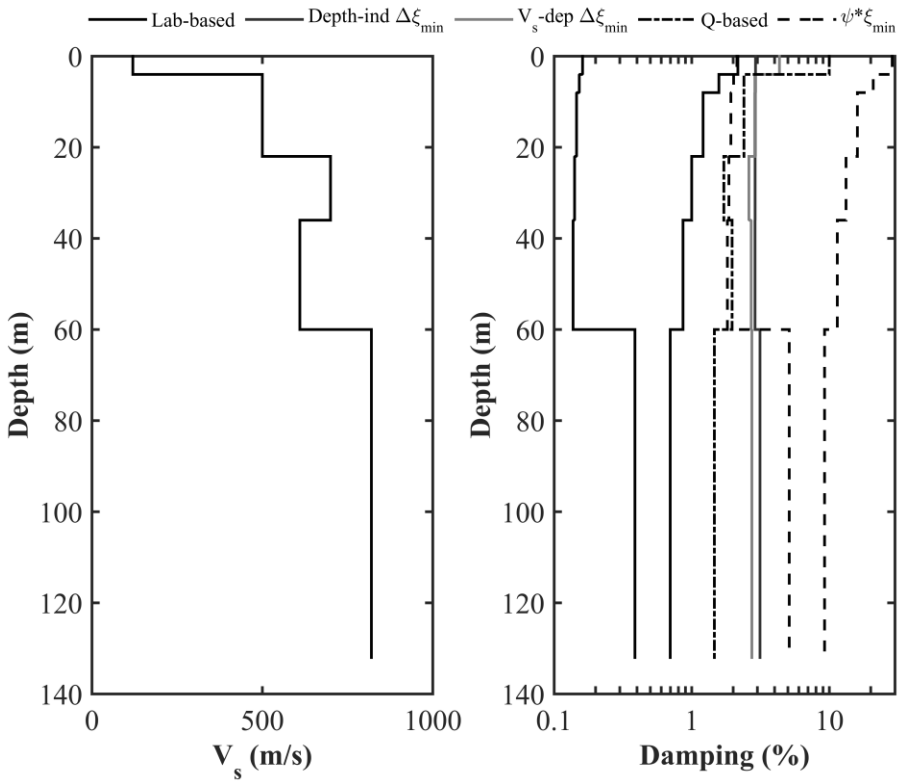

TCGH10

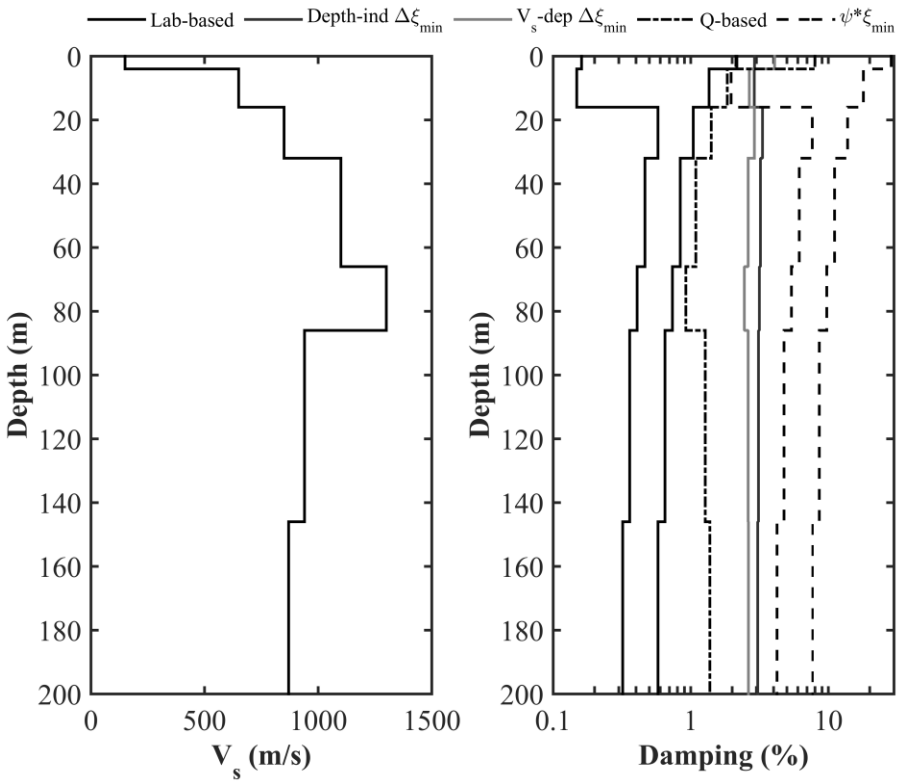

FKSH10

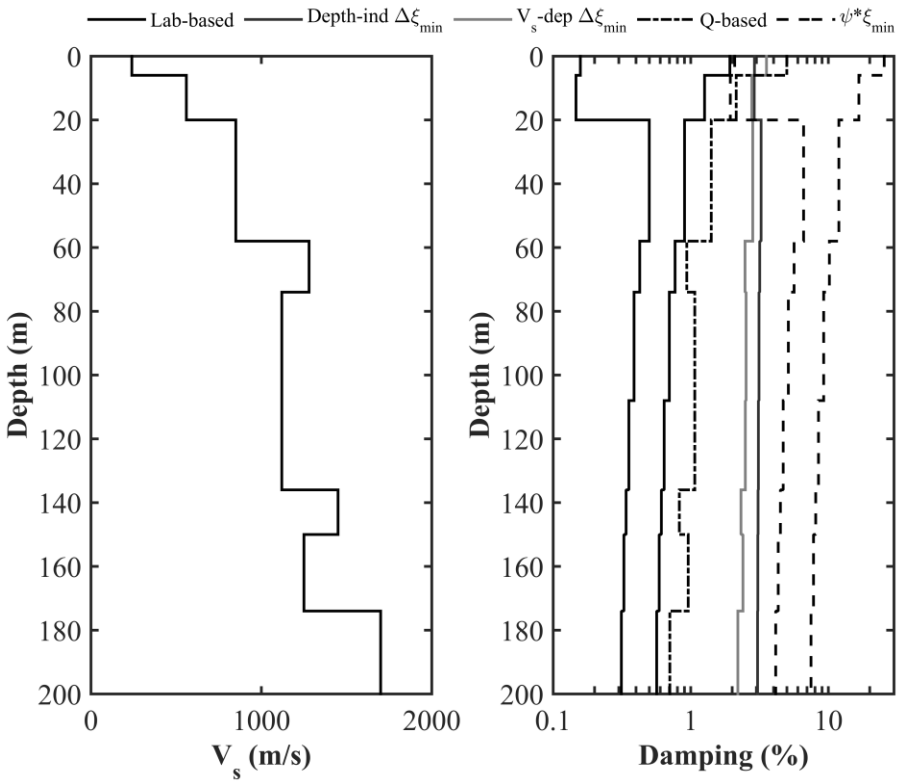

IBRH12

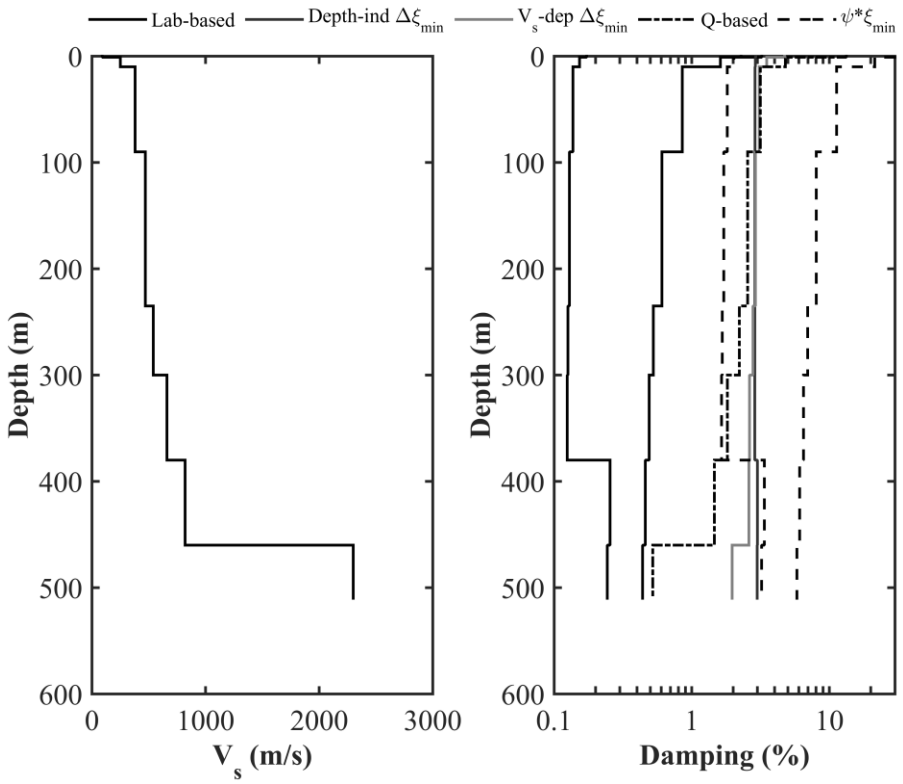

IBRH17

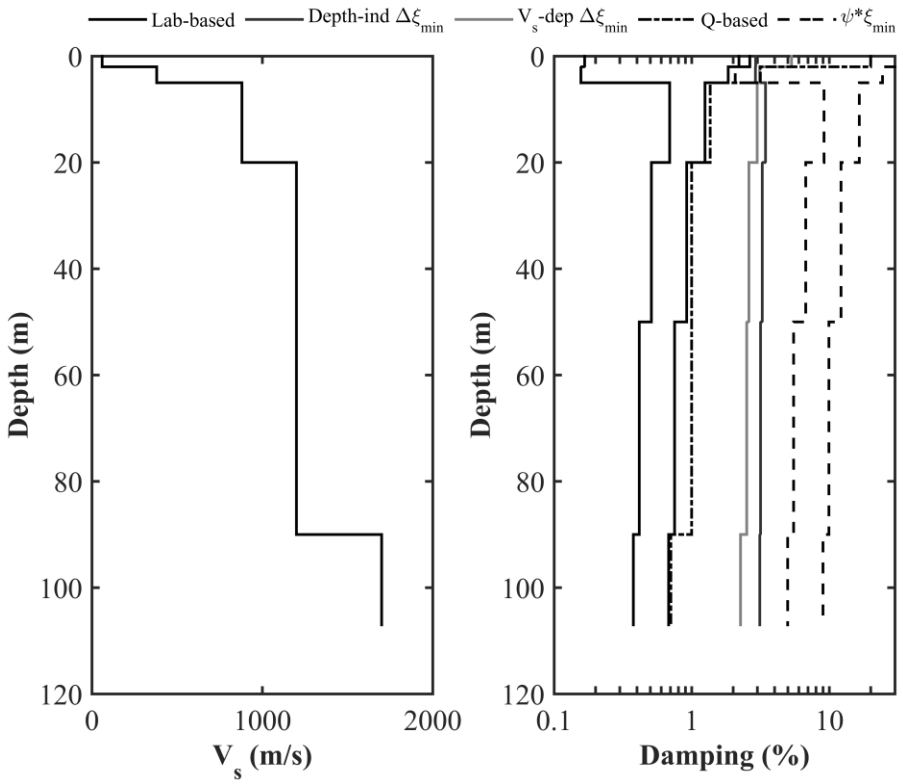

IBRH15

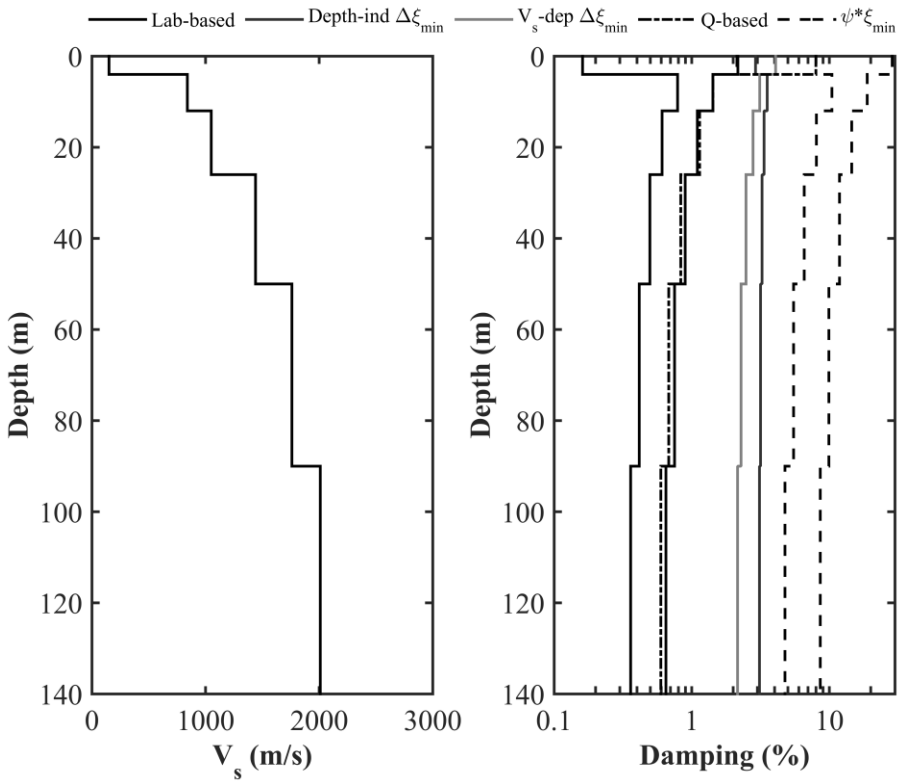

TCGH13

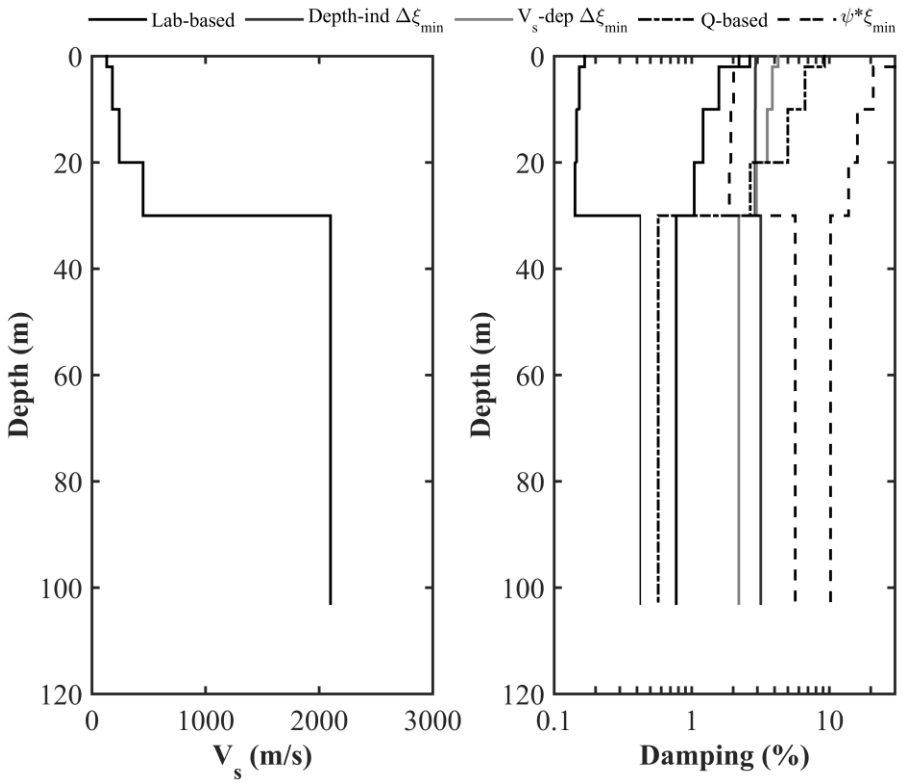

IBRH11

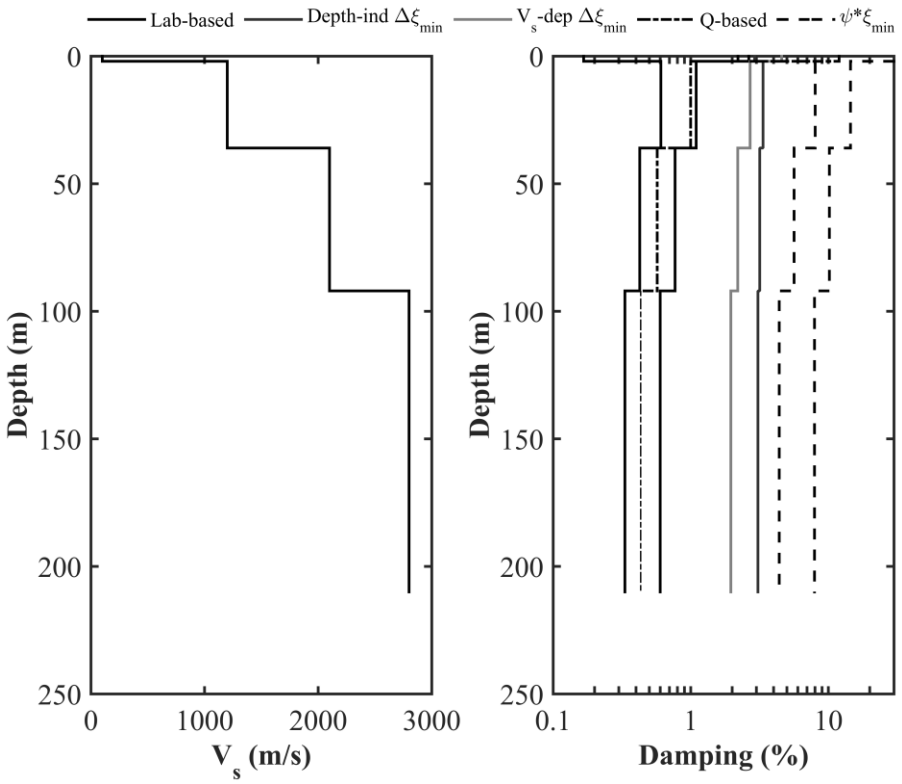

IBRH19

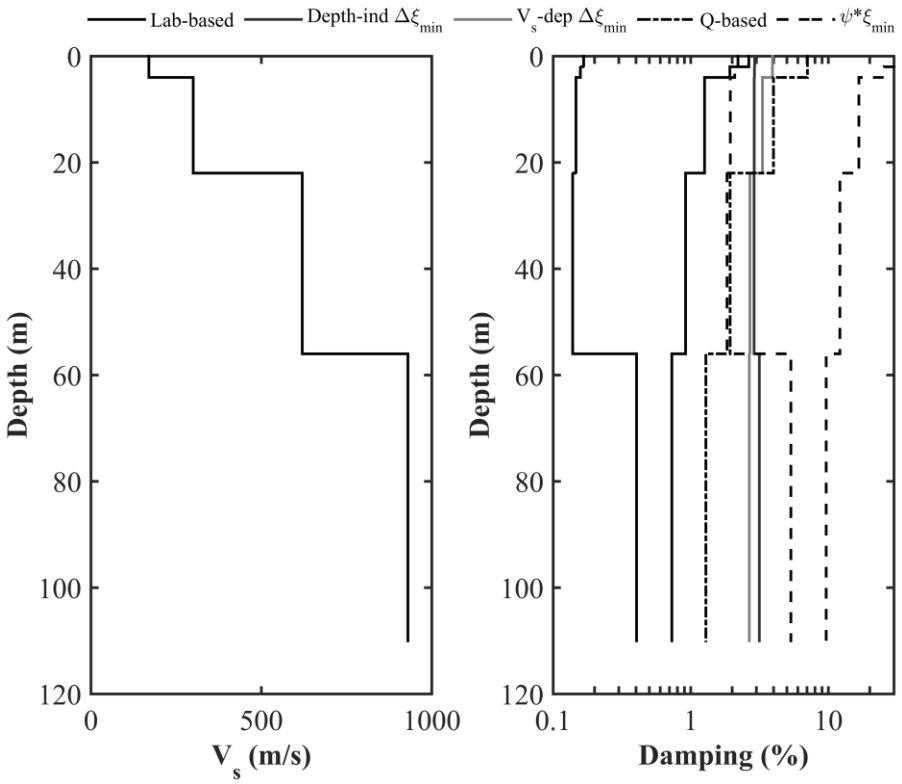

NIGH18

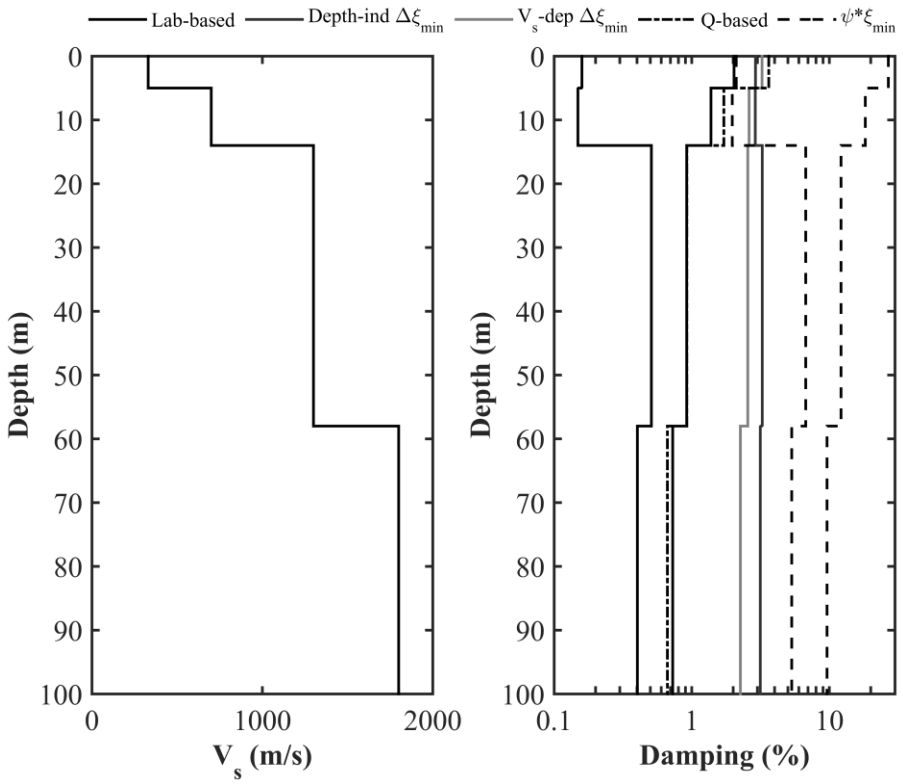

GIFH19

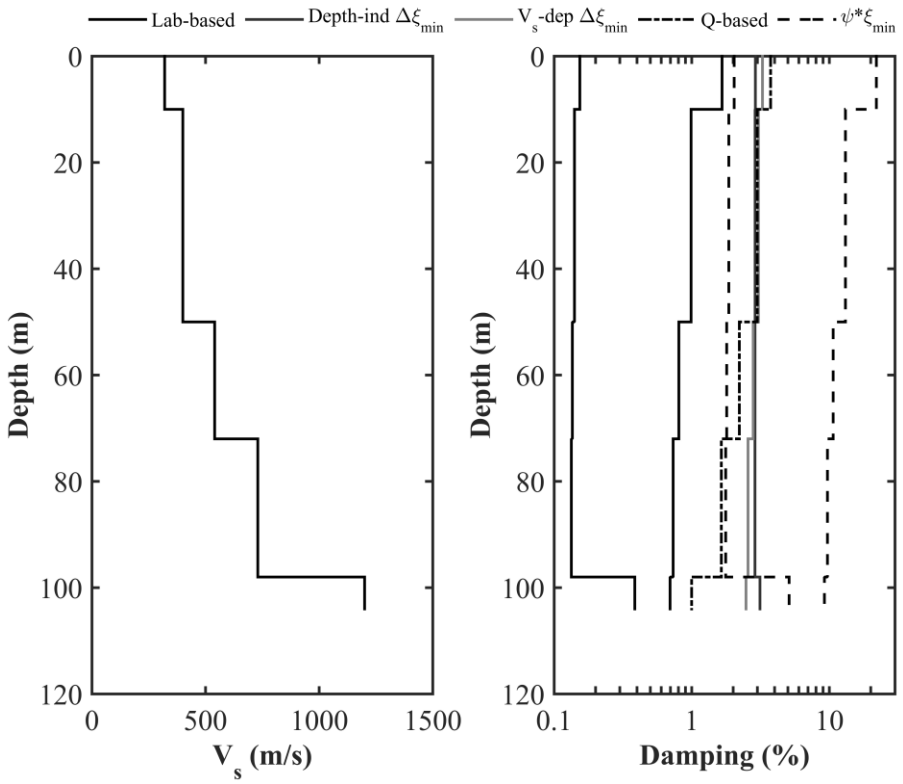

GIFH15

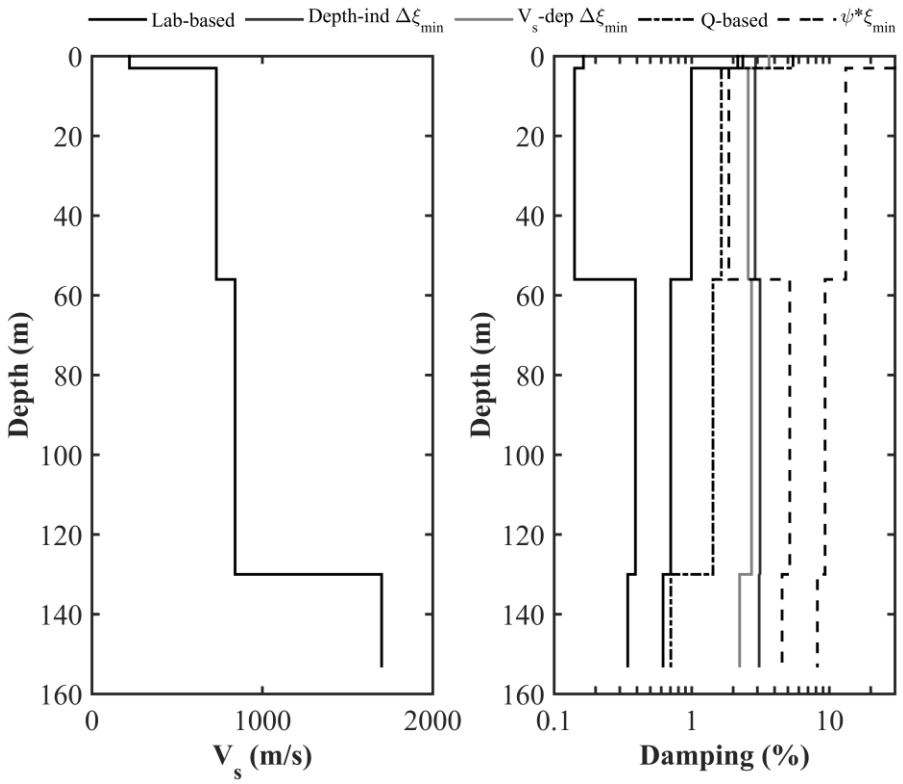

GIFH13

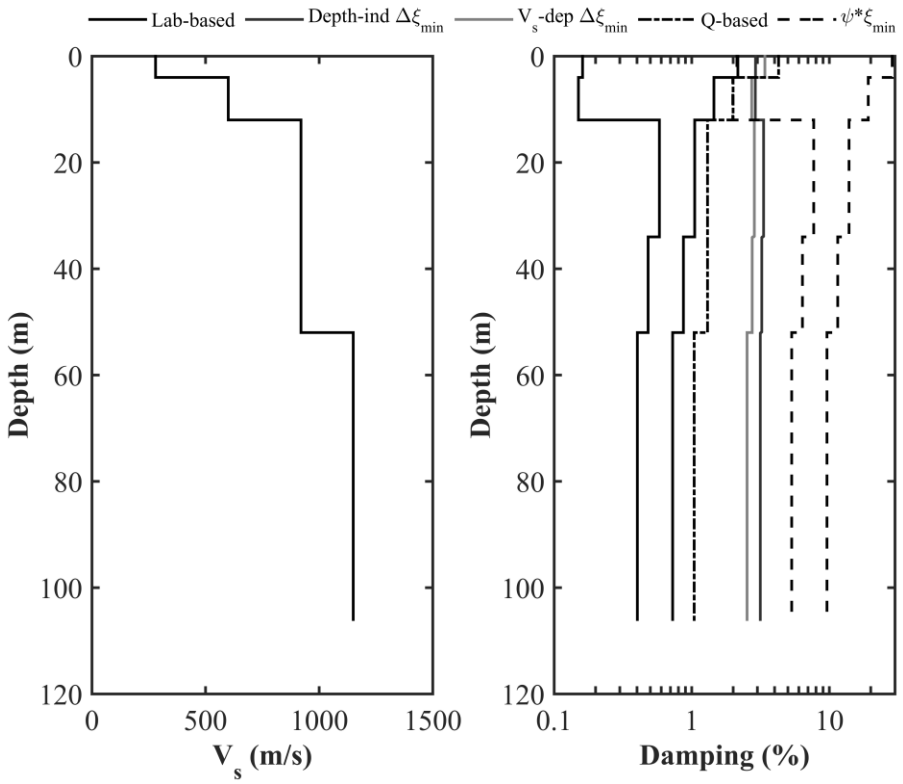

ISKH09

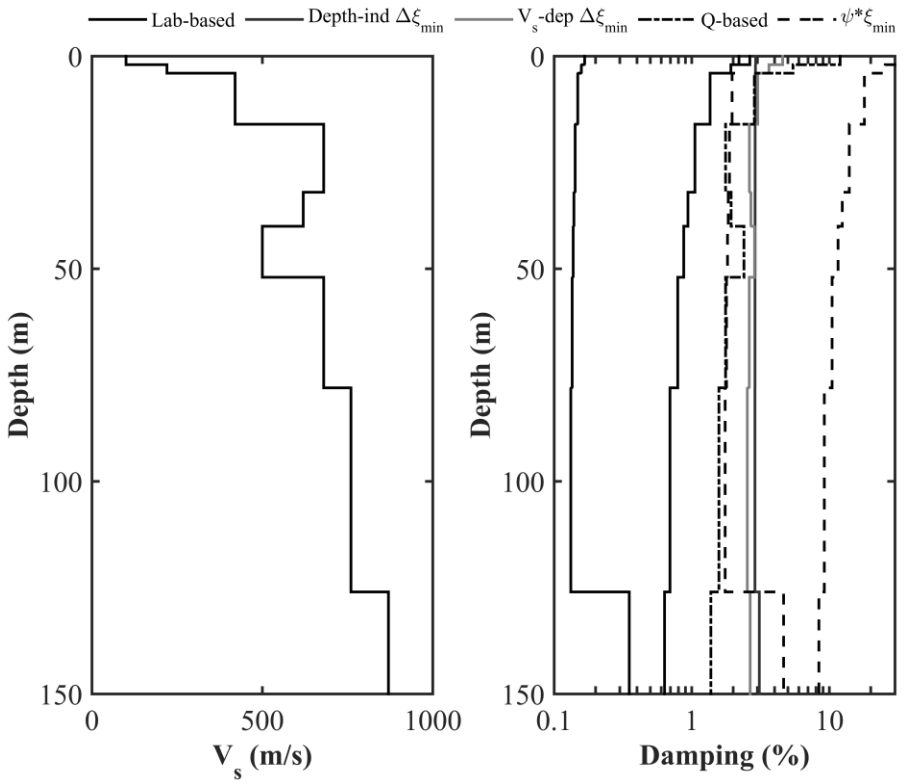

NIGH17

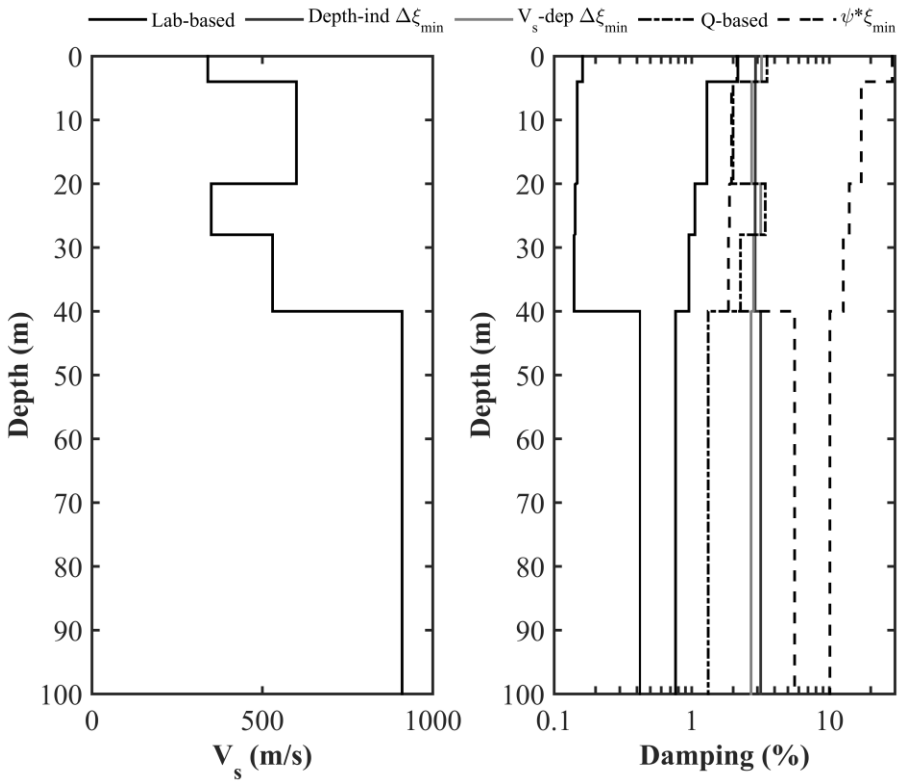

NIGH13

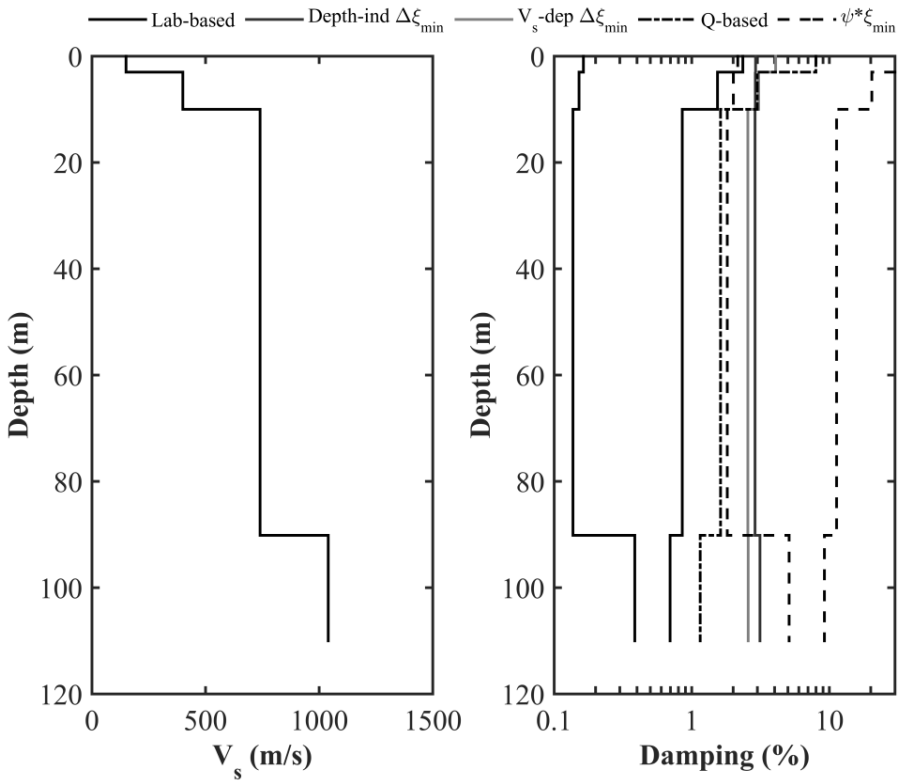

NGNH29

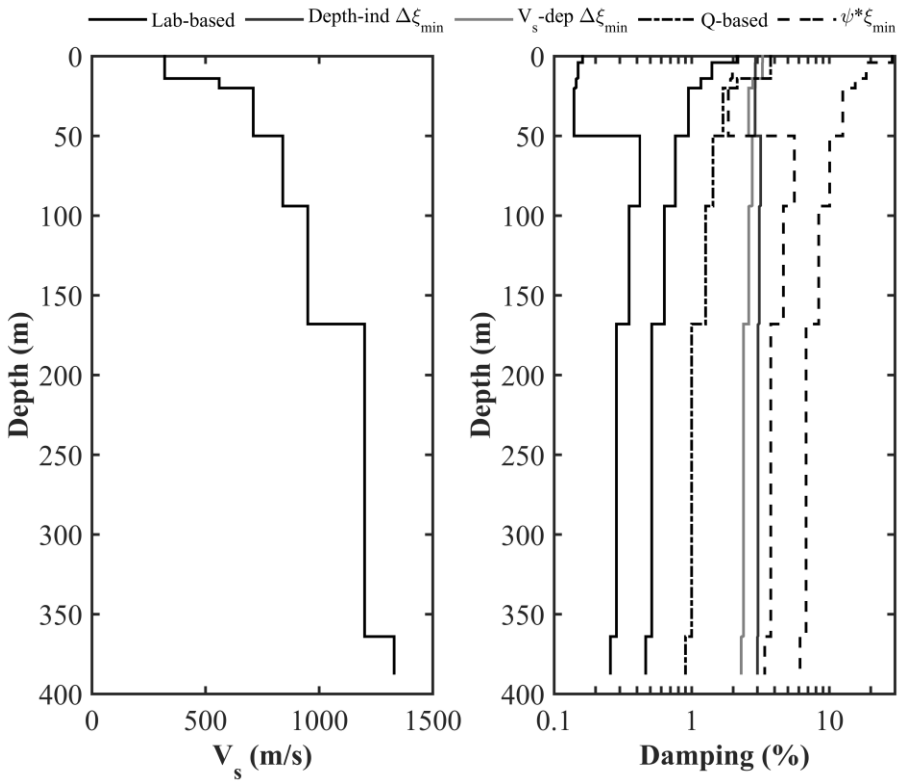

NIGH14

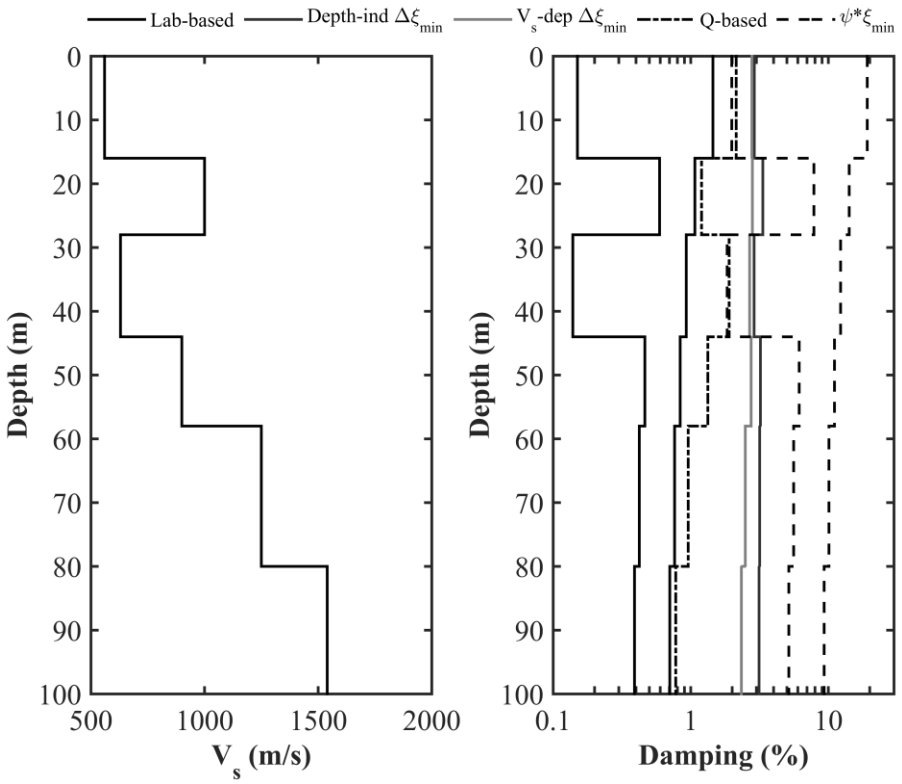

NIGH15

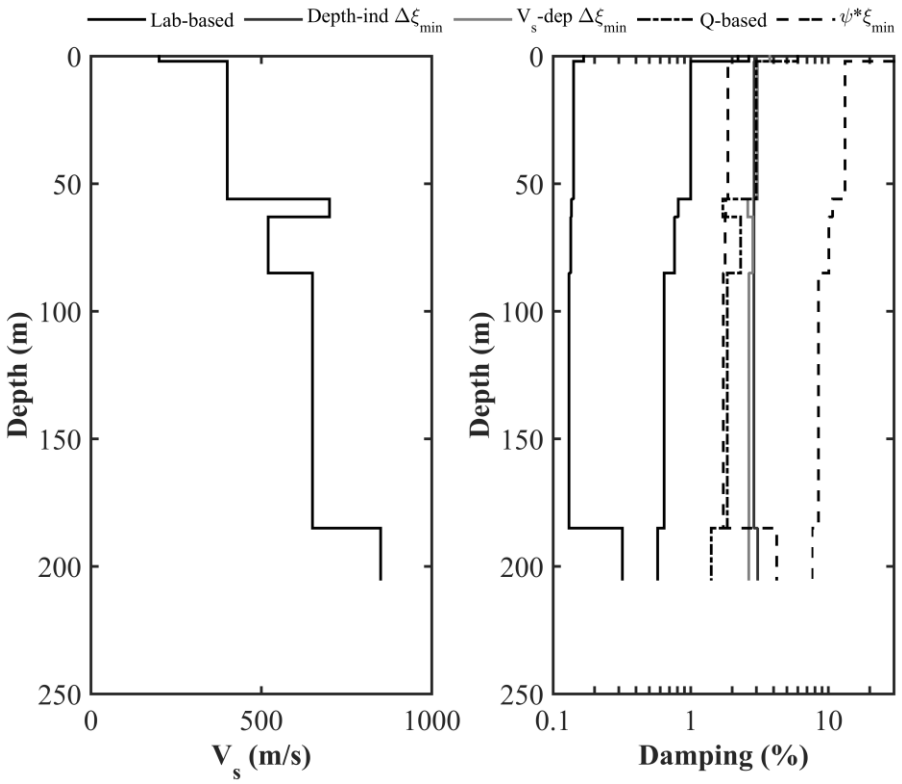

NIGH11

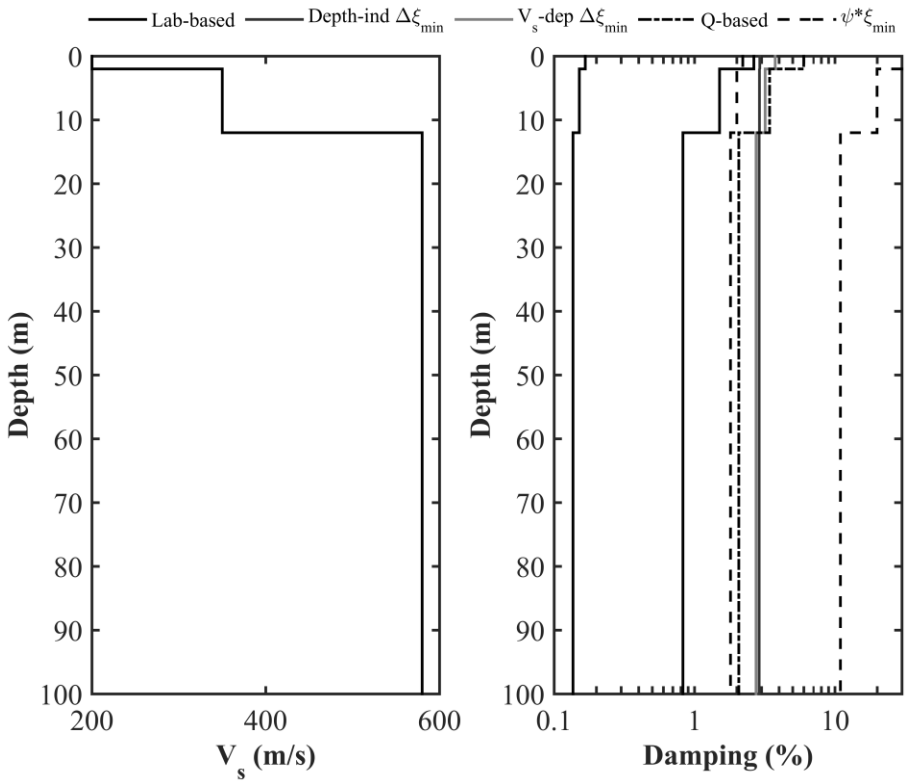

AKTH18

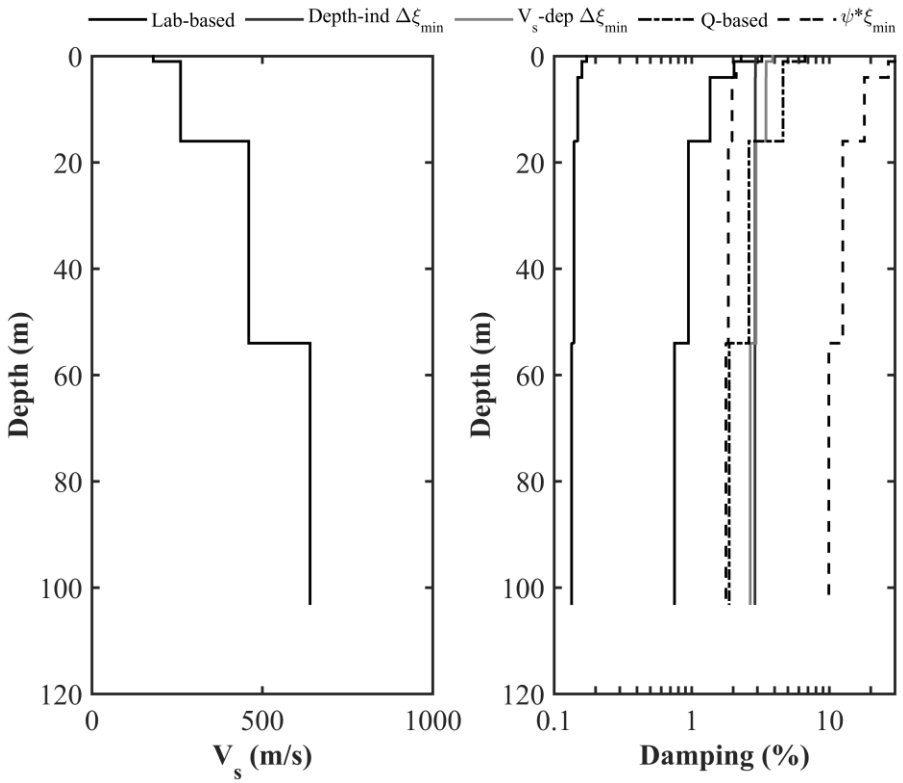

AKTH03

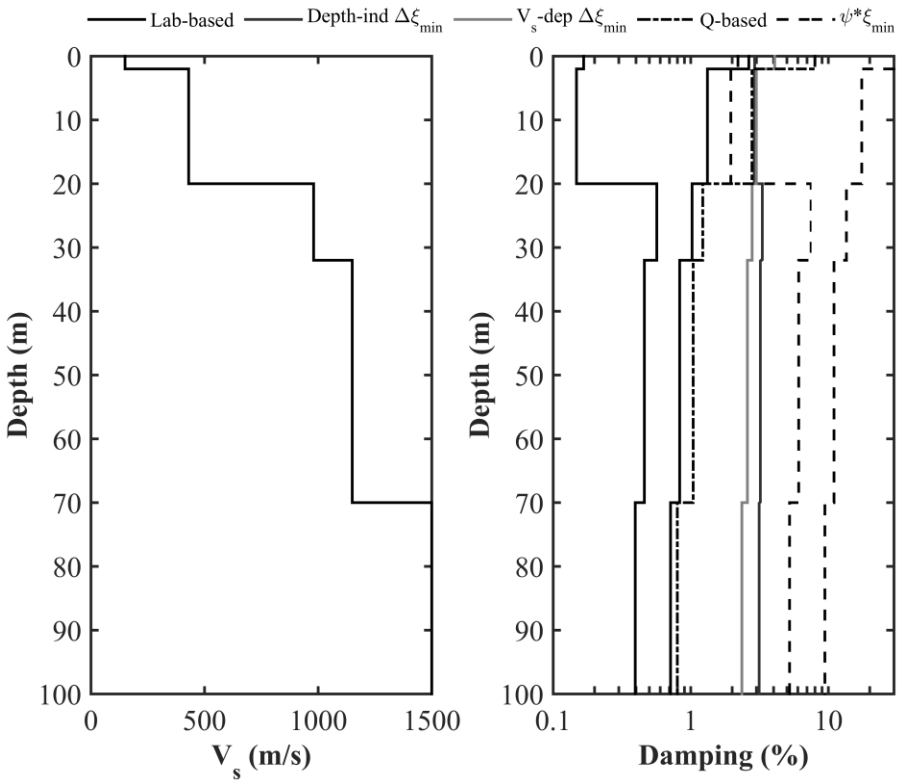

AKTH04

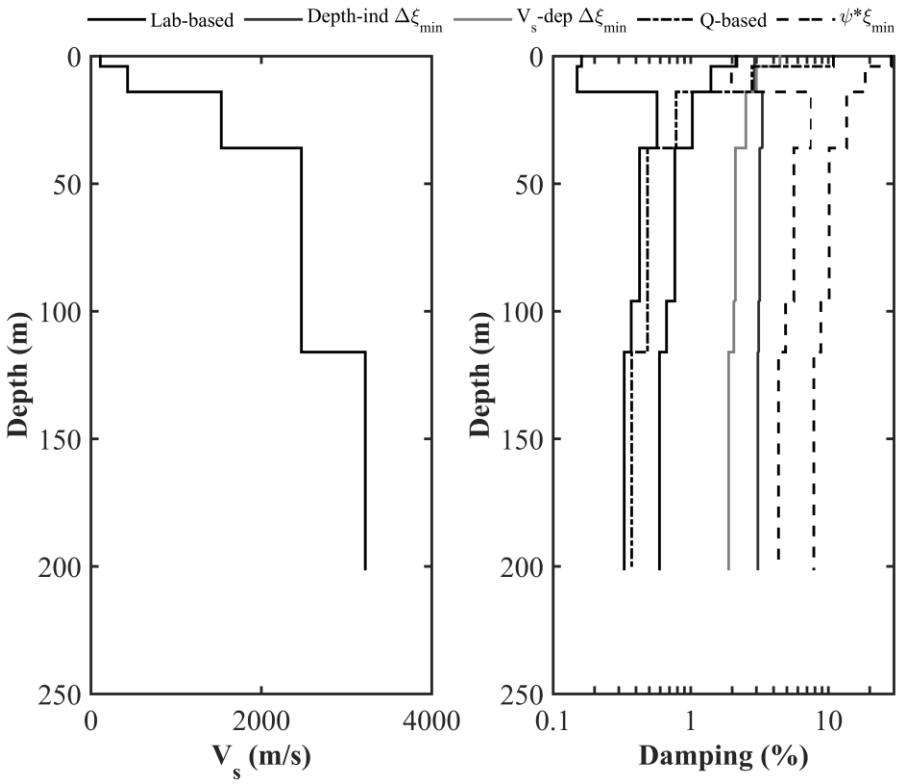

AICH07

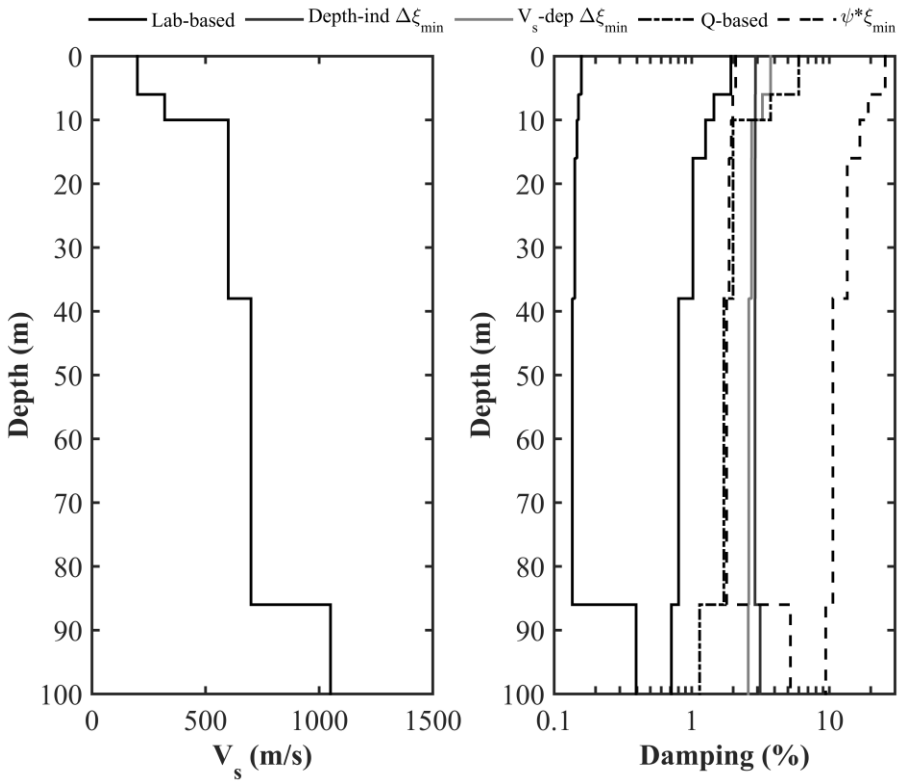

FKIH06

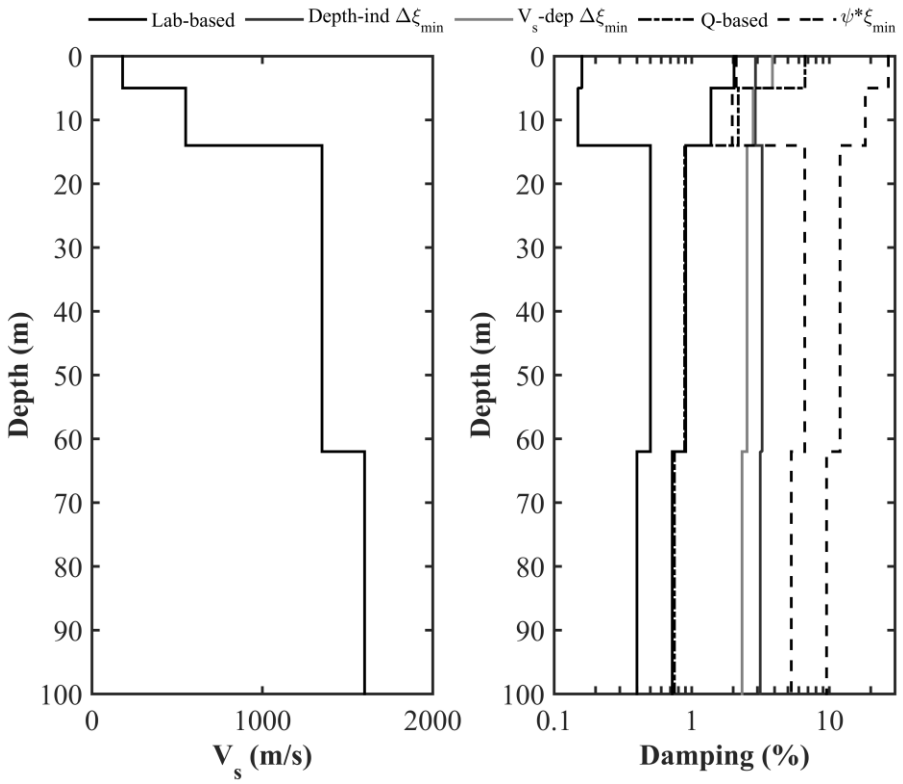

FKOH08

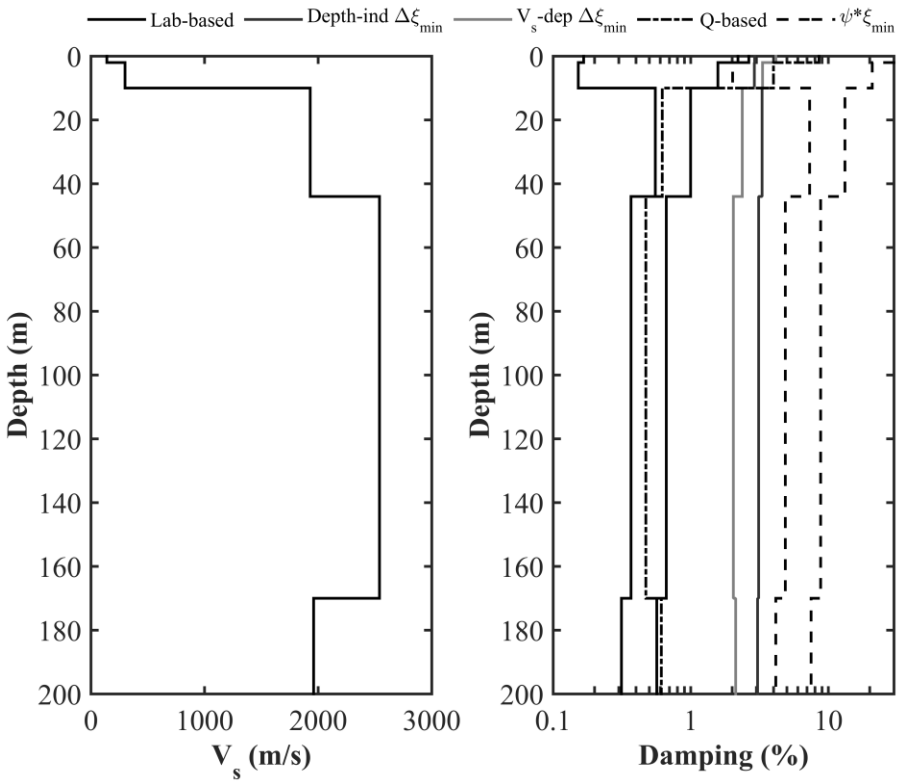

FKSH09

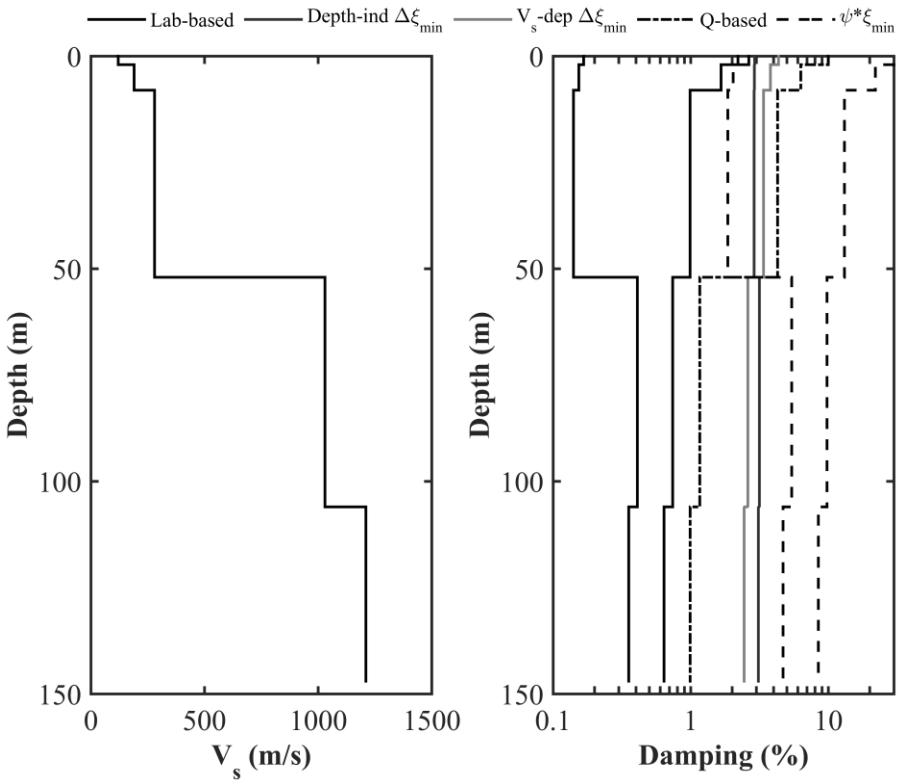

FKSH14

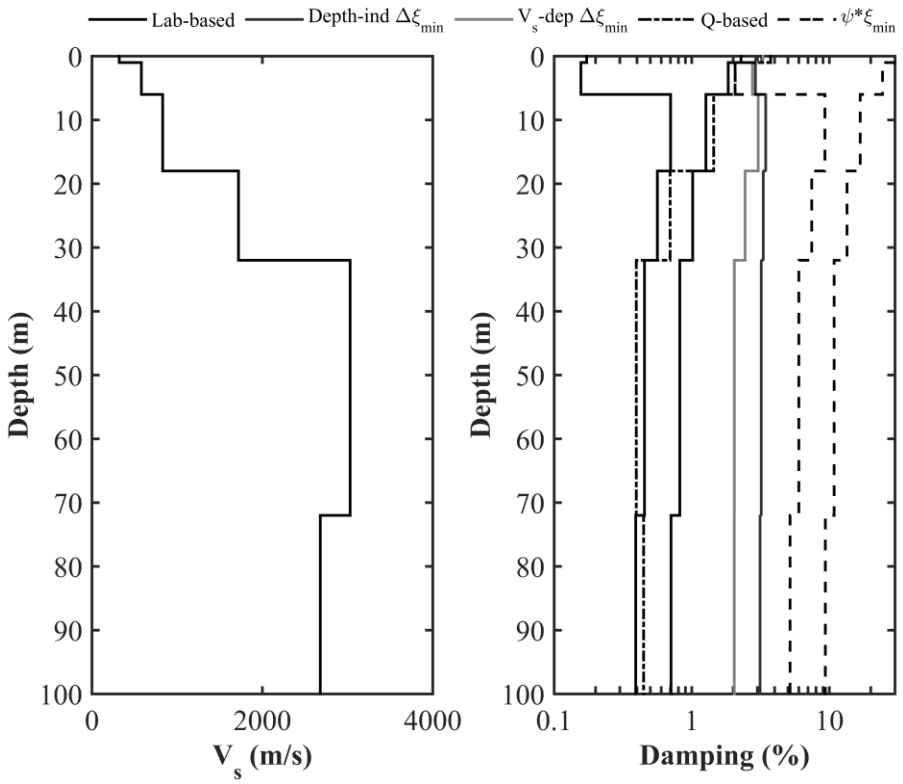

GIFH11

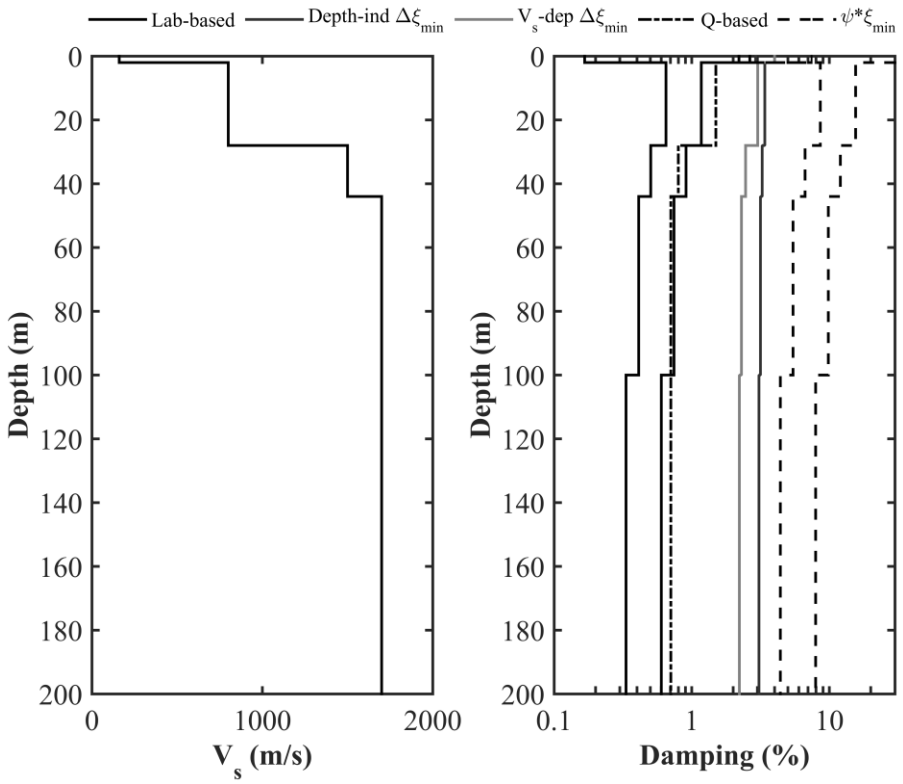

GNMH07

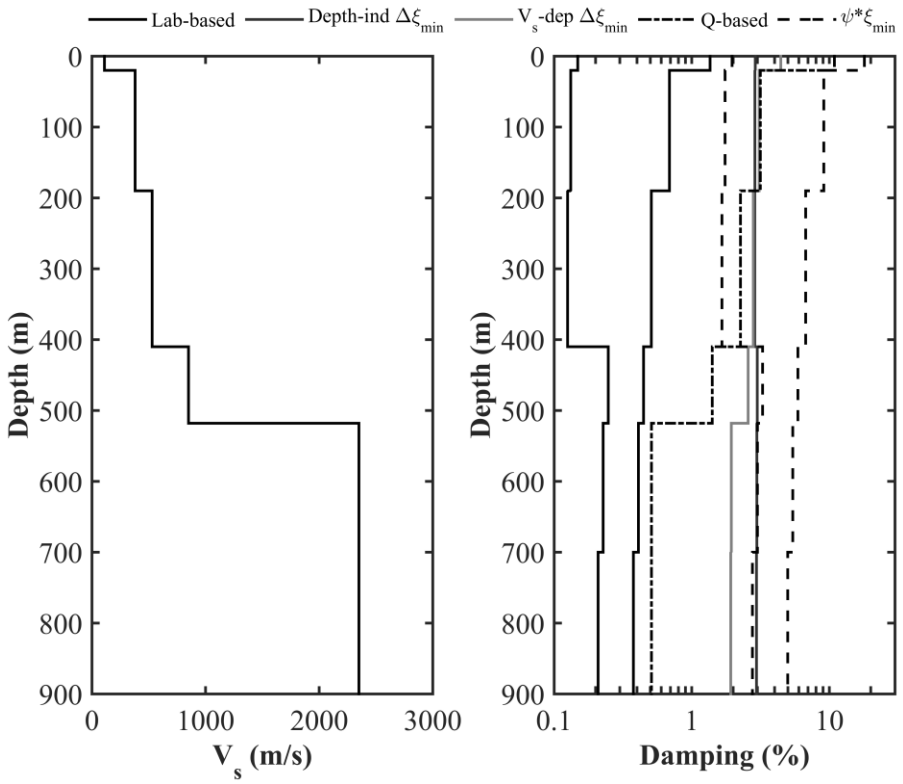

IBRH10

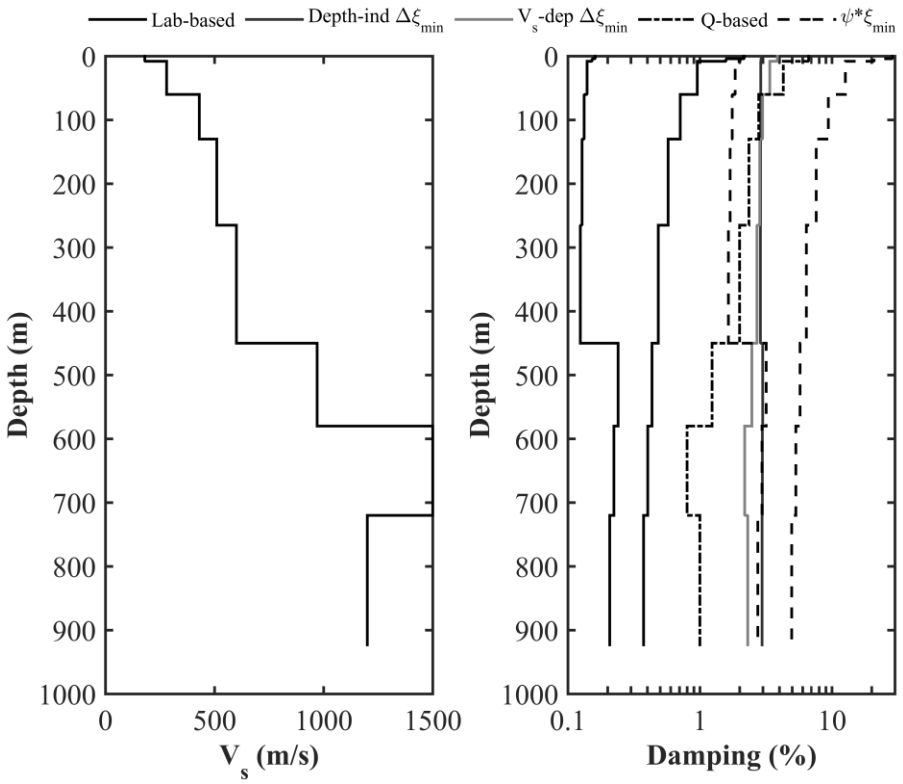

IBRH20

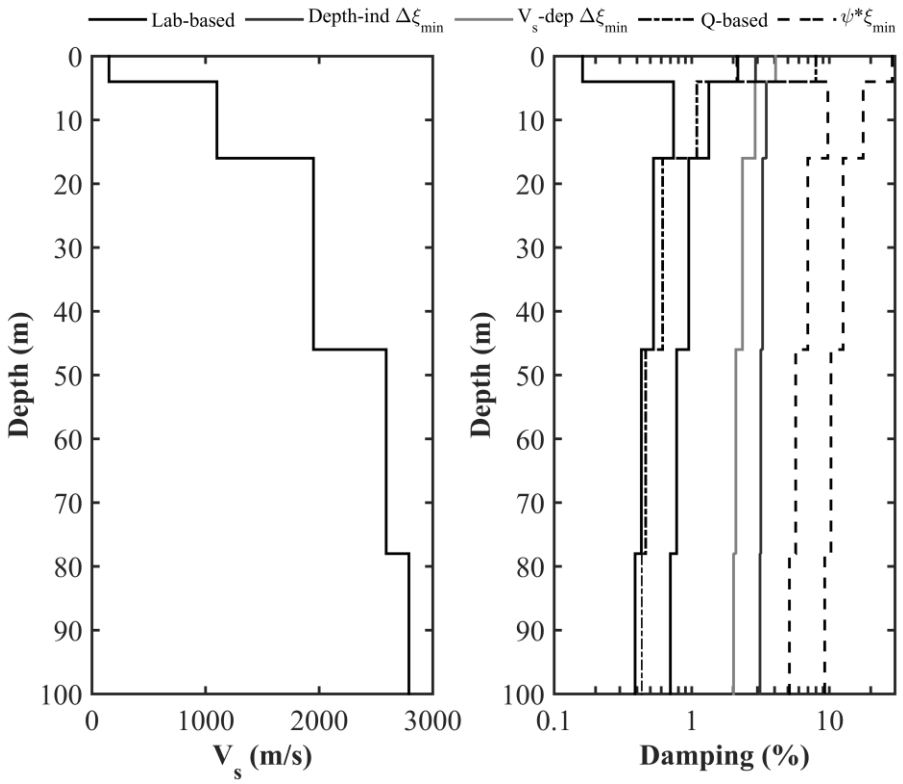

IWTH27

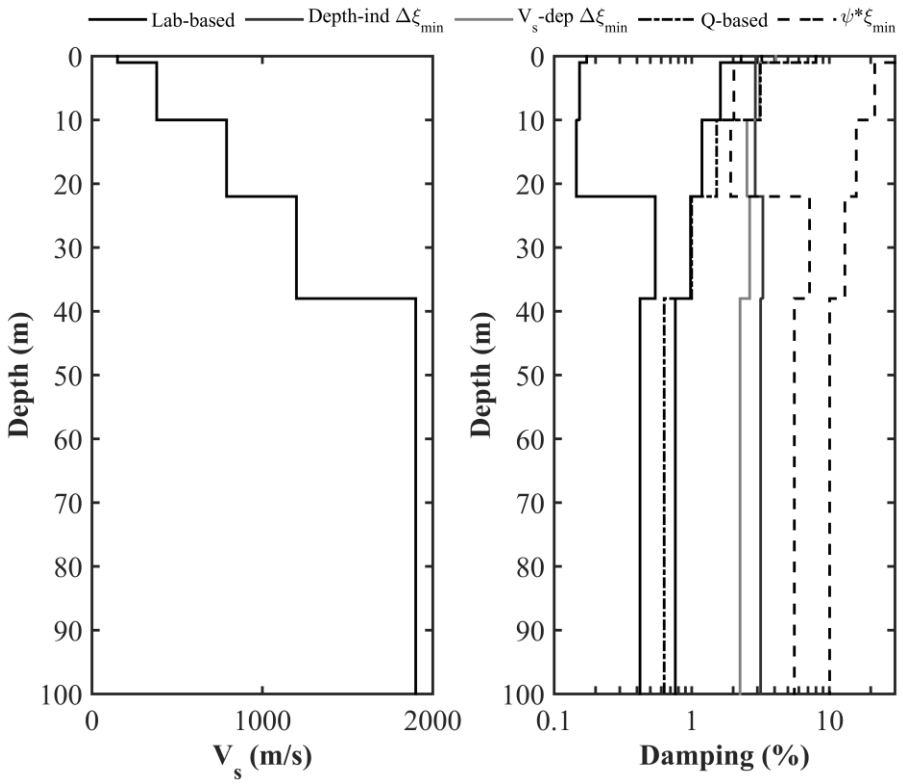

KMMH01

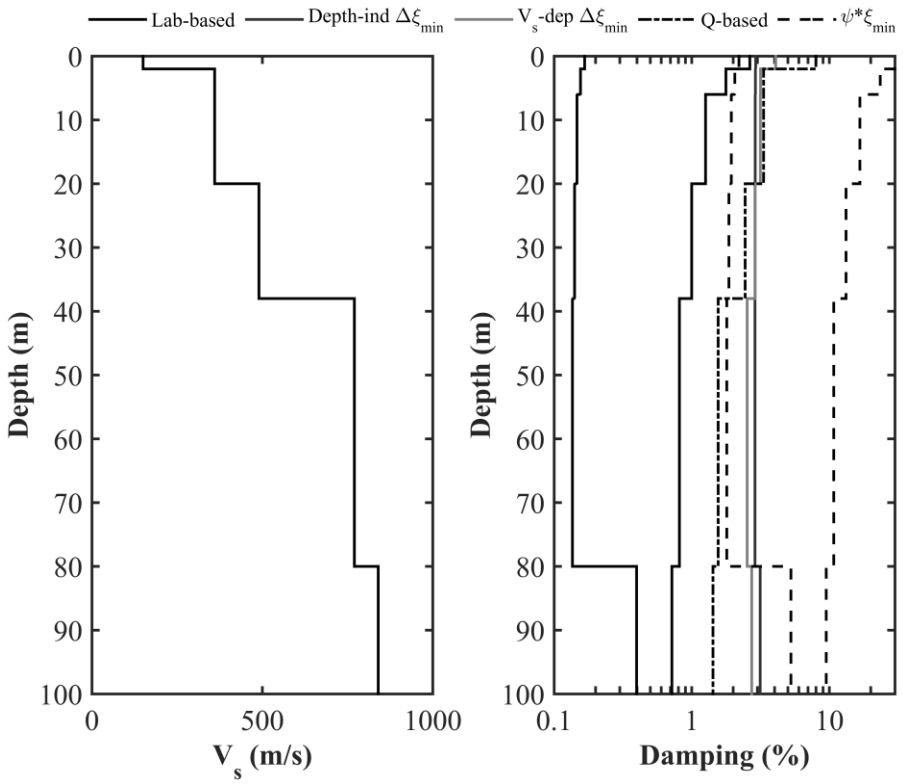

MYGH09

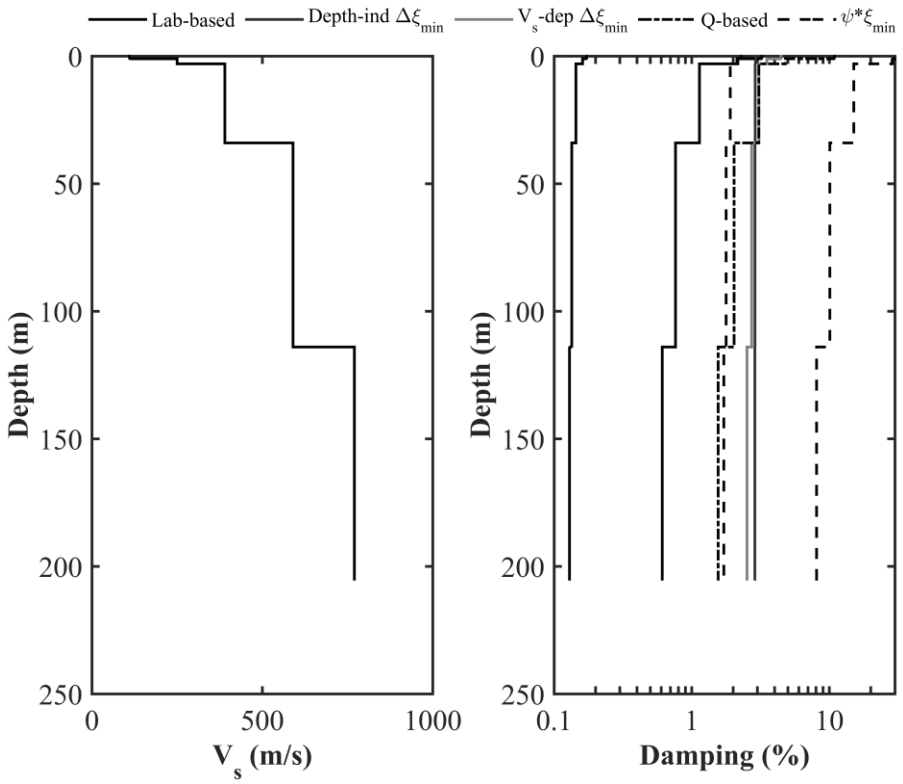

MYGH10

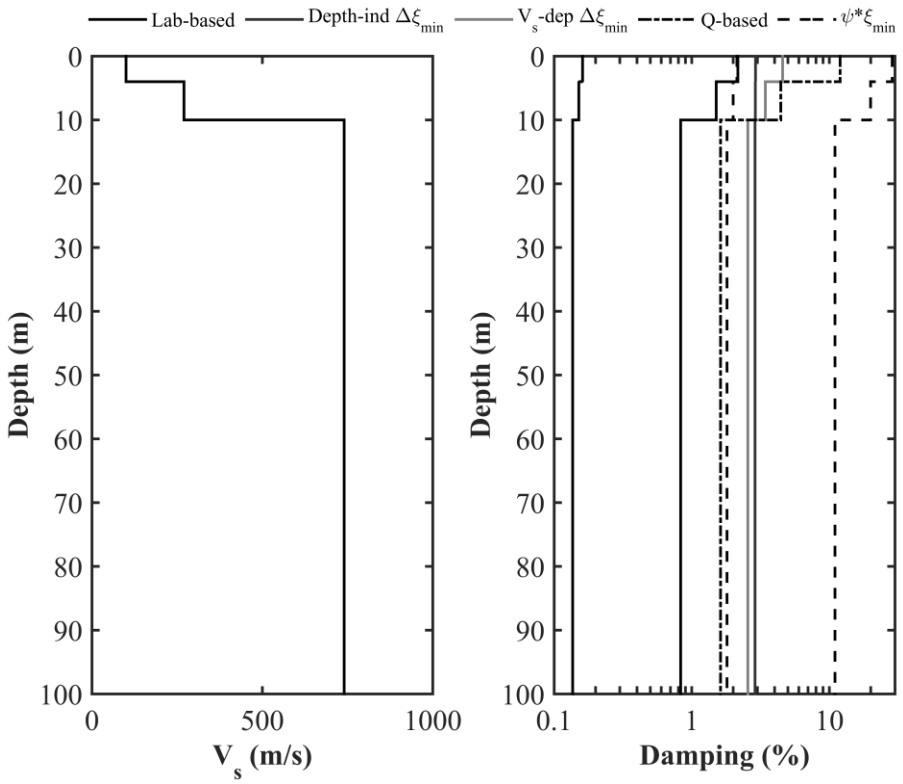

NIGH06

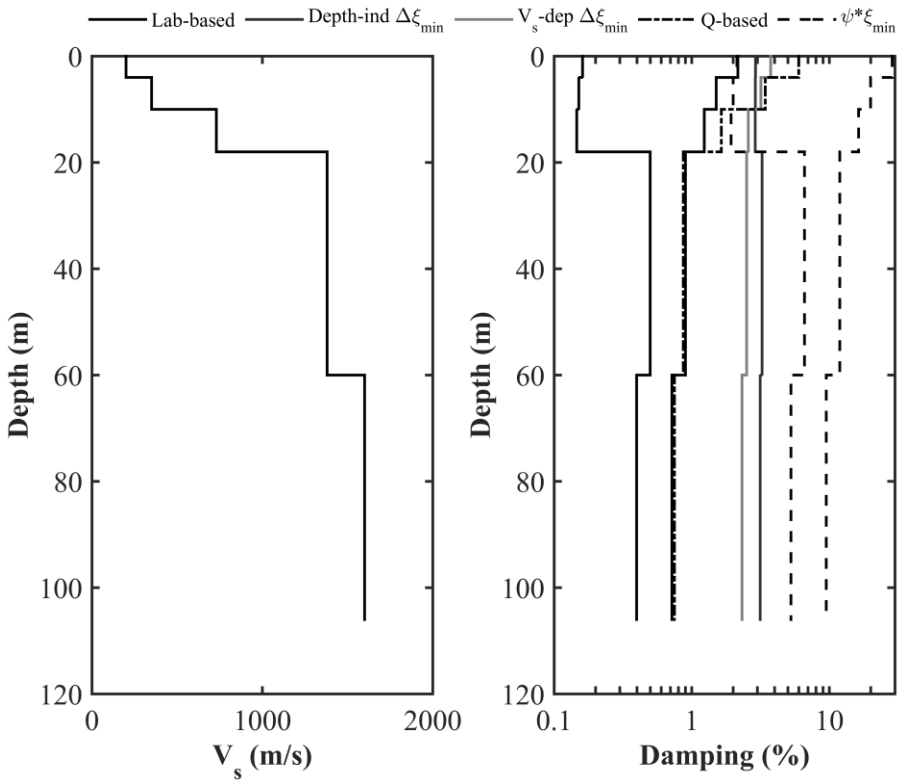

NIGH07

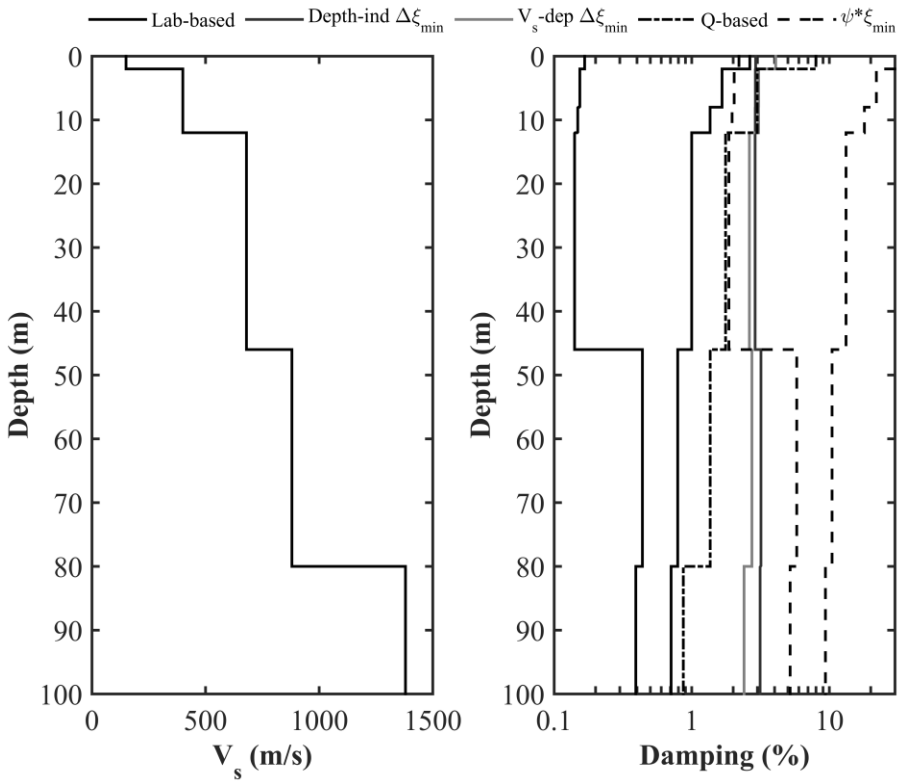

NIGH09

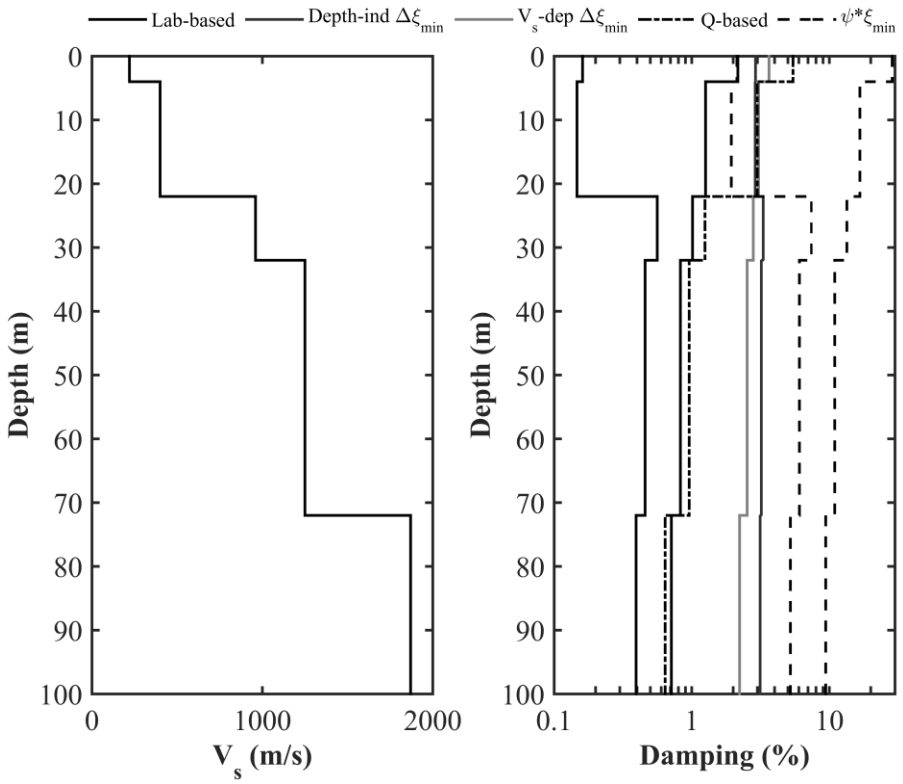

TCGH07

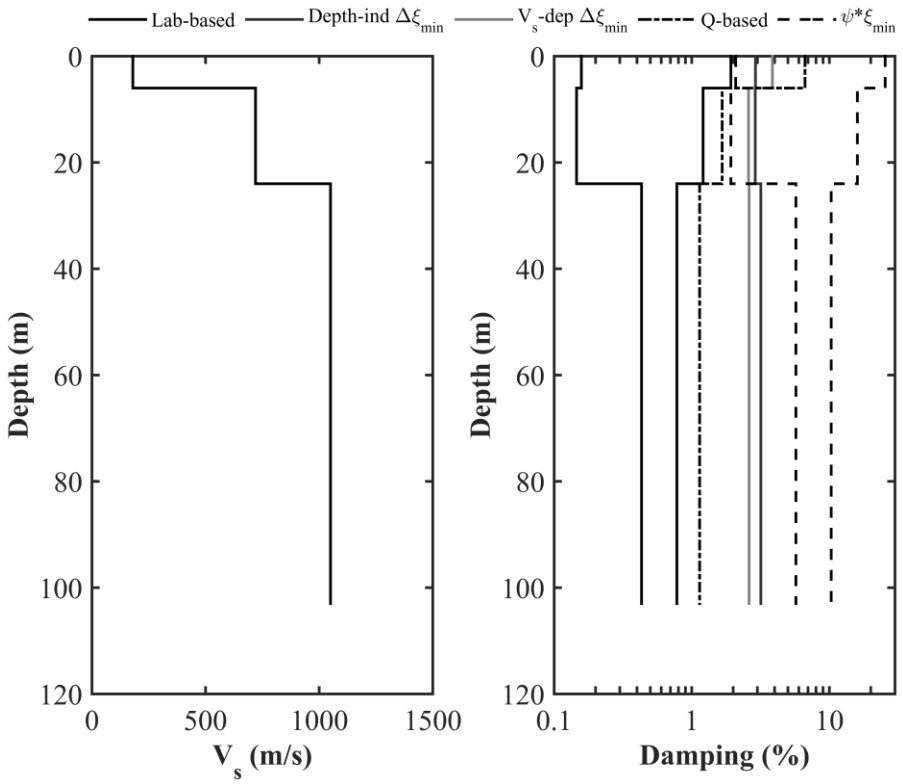

TCGH09

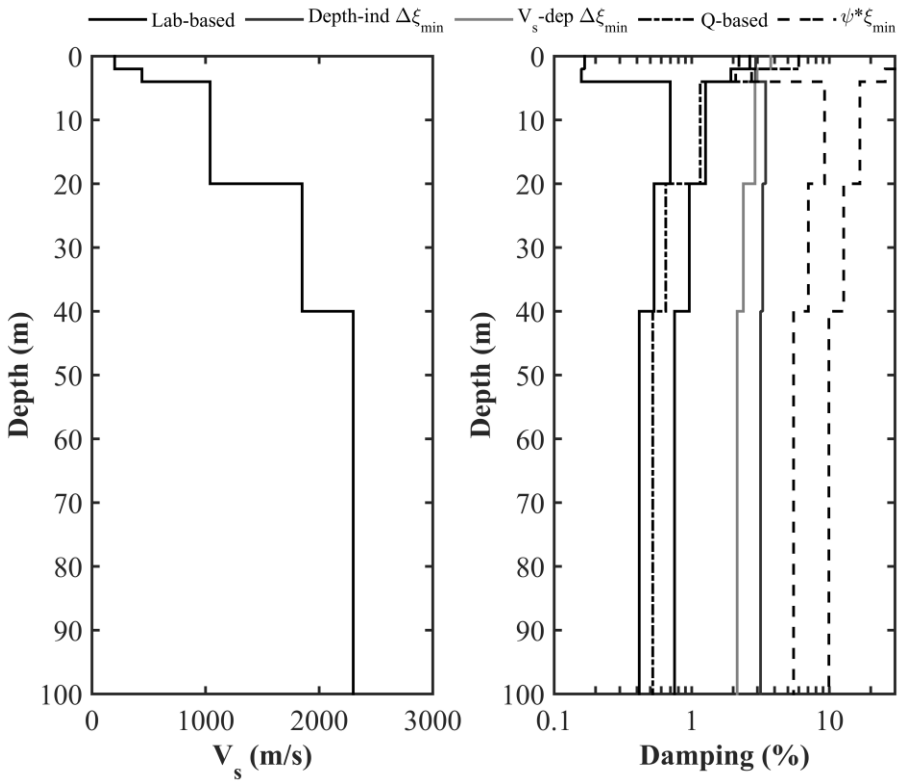

TCGH14